CERN 76-20
8 December 1976

ORGANISATION EUROPÉENNE POUR LA RECHERCHE NUCLÉAIRE
CERN EUROPEAN ORGANIZATION FOR NUCLEAR RESEARCH

PROCEEDINGS OF THE 1976 CERN SCHOOL OF PHYSICS

Wépion, near Namur, Belgium, 6-19 June 1976

G E N E V A
1976

CERN - Service d'information scientifique - RD/193 - 3000 - décembre 1976
1200 - octobre 1978

ABSTRACT

The CERN School of Physics is meant to give young experimental physicists an introduction to the theoretical aspects of recent advances in elementary particle physics. This report contains four sets of lectures dealing with: quarks and partons; recent and future experiments with neutrino beams; the newly discovered J/ψ particles; and an elementary introduction to Yang-Mills theories and their applications to weak and electromagnetic interactions.

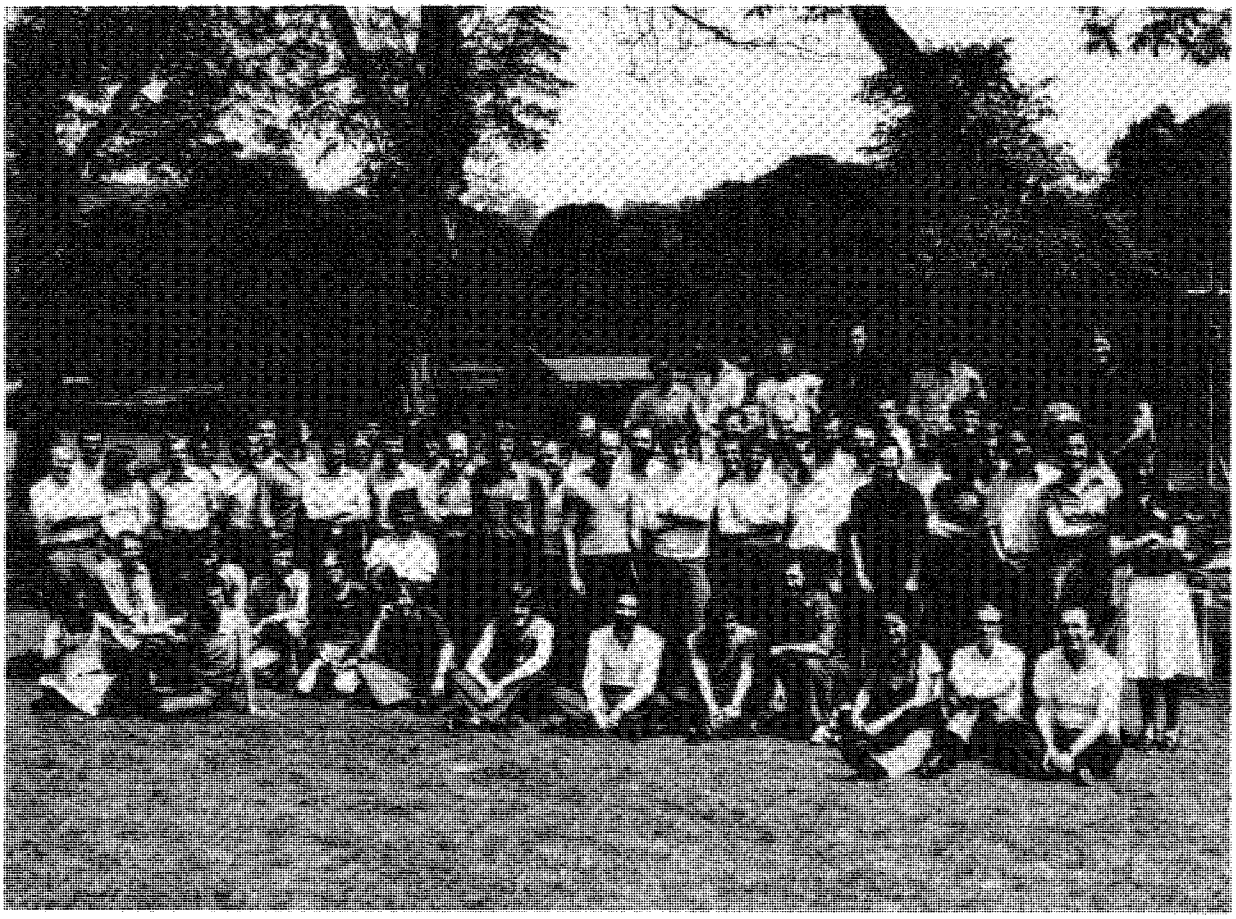

PREFACE

These notes have been written by the lecturers at the 1976 CERN School of Physics and represent the content of the courses they taught on this occasion. Some of the material has been revised and updated in order to be as accurate and complete as possible at the time of publishing.

The CERN School of Physics is meant to give young experimental physicists an introduction to the theoretical aspects of recent advances in elementary particle physics. The subjects we thought most topical in 1976 for this type of audience were those related to the newly discovered J/ψ particles and to the recent and future experiments with neutrino beams.

The lecturers assumed from their students a standard training in particle physics and from there onwards tried to pave as smooth a road as possible to contemporary developments. From the reactions and the discussions at the time of the school I believe this goal has been largely achieved and it is the hope of the organizers that, through these notes, many more students will be enabled to learn, if not without toil at least without tears.

On behalf of them I express appreciation and gratefulness to the lecturers, for their effort to be clear, inspiring and informative.

The school was made possible by a joint financial and organizational effort of CERN and the Belgian National Science Foundation. I think all participants will wish to thank both organizations and their responsible officials Dr. W.O. Lock and Mr. P. Levaux, for this opportunity.

For many of the younger participants it was their first occasion to meet their colleagues from other nations and also as an experiment in international understanding at the basic level, the school was a success.

I would like to thank the authors for providing their typed notes and the CERN Scientific Information Service for their excellent work in reproducing these notes by photo-offset. A final word of appreciation to Miss D.A. Caton (CERN) who acted as an efficient and thoughtful secretary to the School and who was instrumental in putting the texts of many authors (with many other duties...) finally together.

F. Cerulus
Chairman of the Organizing Committee

CONTENTS

	Page
PREFACE *F. Cerulus*	vii
QUARKS AND PARTONS *F.E. Close*	1
AN ELEMENTARY INTRODUCTION TO YANG-MILLS THEORIES AND TO THEIR APPLICATIONS TO THE WEAK AND ELECTROMAGNETIC INTERACTIONS *L. Maiani*	23
NEUTRINO INTERACTIONS *J. Steinberger*	57
THE NEW PARTICLES *B.H. Wiik*	87
ORGANIZING COMMITTEE	125
LIST OF PARTICIPANTS	125

QUARKS AND PARTONS

F.E. CLOSE
Rutherford Laboratory

PART I: QUARKS AND SPECTROSCOPY (Sections 1 and 2)

This material exists in "How high are higher symmetries ...." Rutherford Laboratory report RL-75-091 and is not reproduced here.

PART II: QUARKS IN DEEP INELASTIC PROCESSES

CONTENTS

3. Introduction
4. Inelastic Electron Scattering
5. "Derivation" of scaling in the parton model
   5.1 Electron scattering in Coulomb field
   5.2 Electron-Muon scattering
   5.3 Electron-Parton scattering
6. Partons = Quarks?
   6.1 Electromagnetic Structure Functions
   6.2 Comparison of electromagnetic and Neutrino Interactions
   6.3 Gluon Momentum
   6.4 Sum Rules
   6.5 Neutrino Interactions
7. Charm Production in νN and eN interactions
8. Electron-positron annihilation
9. Inclusive production of hadrons in the quark-parton model
10. Angular distributions of hadron in $e^+e^- \to h$ + anything

3. Introduction

The studies of inelastic electron scattering at SLAC and of neutrino scattering at CERN have been widely interpreted as giving support to the idea that the nucleon is built from elementary constituents, called partons, and that these partons have the same quantum numbers as the quarks that are familiar in spectroscopy. In particular, a very simple regularity in the data, known as scale invariance or just "scaling" was seen at least at moderate energies ($2 \lesssim E \lesssim 20$ GeV, $Q^2 \gtrsim 1$ GeV) which is natural in the parton model.

The data on e^+e^- annihilation also appear to be consistent with scaling when $E_{c.m} \lesssim 3$ GeV. Then after an energy region ($3 \lesssim E \lesssim 5$ GeV) where the new particles and a new production threshold are manifested, one again sees apparently a rescaling when $E \gtrsim 5$ GeV.

These lectures will be concerned with the scaling phenomena. Professor Wiik has discussed the new particles and related effects in e^+e^- annihilation. One may also expect the new hadronic degree of freedom (charm ?) to generate scaling violations in inelastic electron and neutrino scattering. These are mentioned briefly in these lectures and, in neutrino scattering, by Prof. Steinberger.

4. Inelastic Electron Scattering

The inelastic scattering of electrons on nucleons

$$eN \to e + \text{anything} \qquad (4.1)$$

may be represented by fig. 1 in the one-photon exchange approximation. Here k,k' are the initial and final four momenta of the leptons (energy E,E' in the lab.) and W is the mass of the produced hadronic system.

In the lab. the photon energy $\nu = E-E'$ and we can also vary its mass squared

$$q^2 = (k-k')^2 = -4EE'\sin^2\frac{\theta}{2} \qquad (4.2)$$

where θ is the lab. scattering angle of the lepton.

The lepton-photon vertex being known from QED, then the essential dynamics is in the virtual photo-absorption vertex fig. 2, which is a function of two variables ν, q^2.

We see that

$$W^2 \equiv (p+q)^2 = M^2 + 2p\cdot q + q^2 \underset{(lab.)}{=} M^2 + 2M\nu - Q^2 \qquad (4.3)$$

(where $Q^2 \equiv -q^2 \geq 0$).

We will also meet the dimensionless variable

$$\omega \equiv \frac{2M\nu}{Q^2} \qquad (4.4)$$

The region of ν, Q^2 accessible in the electron scattering is shown in fig. 3. Lines of fixed ω radiate from the origin ranging from $\omega = 1$ (elastic scattering) to $\omega = \infty$. Fixed W is also exhibited.

For $Q^2 = 0$ the photon has helicity ± 1 only ("transverse"). For $Q^2 \neq 0$ both transverse and longitudinal (helicity zero) degree of freedom are present. Hence the scattering cross-section involves two structure functions $W_{1,2}(\nu, Q^2)$

$$\frac{d^2\sigma}{dQ^2 d\nu} = \frac{E'}{E}\frac{4\pi\alpha^2}{Q^4}\left\{\cos^2\frac{\theta}{2} W_2(\nu,Q^2) + 2\sin^2\frac{\theta}{2} W_1(\nu,Q^2)\right\} \qquad (4.5)$$

which are related to the two virtual photo-absorption cross sections by

$$W_1(Q^2,\nu) = \frac{K}{4\pi^2\alpha}\sigma_T(Q^2,\nu)$$

$$W_2(Q^2,\nu) = \frac{K}{4\pi^2\alpha}\frac{Q^2}{Q^2+\nu^2}\left(\sigma_T(Q^2,\nu) + \sigma_L(Q^2,\nu)\right) \qquad (4.6)$$

with $K \equiv \nu - Q^2/2M$ the virtual photon flux.

For fixed W (e.g. $\Delta(1236)$)

$$MW_1(Q^2,W) \xrightarrow{Q^2\to\infty} 0$$
$$\nu W_2(Q^2,W)$$

due to the resonance form factors killing the cross-section at large Q^2. However, for fixed $\omega \equiv 2M\nu/Q^2$ we find the remarkable phenomenon that (for $Q^2 \gtrsim 1$ GeV^2)

$$MW_1(\omega,Q^2) \longrightarrow F_1(\omega) \qquad (4.9)$$
$$\nu W_2(\omega,Q^2) \longrightarrow F_2(\omega) \qquad (4.10)$$

independent of Q^2 ("Scaling"). The Q^2 independence of νW_2 for ep → e + anything is seen at $\omega = 4$ in fig. 4. This phenomenon, together with the fact that (fig. 5)

$$\frac{\sigma_L}{\sigma_T} \simeq \frac{\omega F_2 - F_1}{2F_1} \simeq 0 \qquad (4.11)$$

suggests a simple spin $\frac{1}{2}$ parton substructure in the target.

For the basic scattering of the electron being on a parton carrying fraction x of the target four momentum (fig. 6), then if the parton mass and transverse momenta are negligible one has

$$\nu W_2(\nu,Q^2) \to F_2(\omega) = \sum_i \int dx\, e_i^2 x f_i(x)\,\delta\left(x - \frac{1}{\omega}\right) \qquad (4.12)$$

where the sum is over the various species of parton (u,d,s,c ...), $f_i(x)$ is the probability that the parton has momentum in interval $x \to x + dx$. The important structure here is the $xf(x)$ structure from which many relations will be seen to flow. We shall derive this result in a moment. First let us see physically why σ_L/σ_T yields information on the parton spin.

If one sits in a frame where photon and parton momenta are collinear then a spin 0 parton could not absorb a photon with helicity ± 1. Hence for spin zero partons $\frac{\sigma_L}{\sigma_T} \to \infty$. This is not at all like the data so very little, if any, charge of the proton is carried by spin zero objects (at least for the range of $x \gtrsim 0.1$ so far studied). Spin $\frac{1}{2}$ partons give $\sigma_L/\sigma_T \simeq 0$, on the other hand. This agrees well with the data. We shall derive these results in the next paragraphs.

5. "Derivation" of Scaling in the Parton Model

5.1 Electron scattering in a Coulomb field

We shall begin by studying some QED processes. Consider first the simple case of high energy electron scattering in a Coulomb field fig. 7. Then

$$\frac{d\sigma}{dt} = \frac{4\pi\alpha^2}{t^2}\left(\frac{1+\cos\theta}{2}\right)^2 \qquad (5.1)$$

where $t \equiv -Q^2$, θ is the lab. scattering angle, stu are the Mandelstam variables. One can qualitatively understand this result:

i) the dimensions of $\frac{d\sigma}{dt}$ are E^{-4}. Since the photon propagator provides t^{-2} in $\frac{d\sigma}{dt}$ then no further dimensional quantities occur.

ii) the high energy electron-photon vertex conserves helicity. Hence 180° scattering is forbidden and in turn this is the origin of the angular dependence in eq.

5.2 Electron-muon scattering

Now we shall progress to $e^-\mu^+ \to e^-\mu^+$, fig. 8 where $s = (p_e+p_\mu)^2 = 2ME$; $u = (p_{e'}-p_\mu)^2 = -2ME'$

$$-\frac{u}{s} \simeq \frac{1+\cos\theta}{2}$$

Here

$$\frac{d\sigma}{dt} = \frac{1}{2}\,\frac{4\pi\alpha^2}{t^2}\left(\frac{u^2}{s^2}+1\right) \qquad (6.2)$$

i) the factor $\frac{1}{2}$ arises due to the averaging over the two spin states of the "target" muon (contrast the previous example)

ii) when $e^-\mu^+$ have net $J_z = \pm 1$ the 180° scattering is forbidden as before - hence the U^2/S^2. When $J_z = 0$ the 180° scattering can occur (contrast the previous example) - hence the presence of an isotropic term.

Actually we should make explicit the energy-momentum conservation. Let us do this by writing

$$\frac{d^2\sigma}{dt\,du} = \frac{1}{2}\,\frac{4\pi\alpha^2}{t^2}\left(\frac{u^2+s^2}{s^2}\right)\delta(u+t+s) \qquad (5.3)$$

(recall $s + t + u = \Sigma m^2$ and so at high energy, neglecting the masses we have $u = -(s + t)$). Now

$$s = (p_e+p_\mu)^2 \overset{\text{lab.}}{=} 2ME \quad (E = E_{e^-};\ m = m_\mu) \qquad (5.4)$$

$$t = (p_e-p_{e'})^2 = -Q^2 \qquad (5.5)$$

$$u = (p_\mu-p_{e'})^2 = -2ME' \qquad (5.6)$$

so $s + t + u = 2m(E-E') - Q^2 = 2M\nu - Q^2$

It will also be useful, later, to notice that

$$\frac{-t}{s+u} = \frac{Q^2}{2M\nu} = \frac{1}{\omega} \qquad (5.7)$$

5.3 Electron-parton scattering

In the parton model, the inelastic electron-target scattering is hypothesised to be due to the elastic scattering of electrons on the partons in the target. If the partons have spin $\frac{1}{2}$ and couple to the photon just as does the μ^+ of the previous example ("pointlike coupling") then we can easily obtain an expression for the cross-section.

Let us neglect any parton momentum transverse to the target so that

$$p_{parton} = x\,p_{target} \qquad (5.8)$$

Then from the previous example we can write the cross section for elastic scattering on a muon (parton) with momentum Xp as (noting that $s \to Xs$, $u \to Xs$ but t remains untouched since this can be defined involving the electron vertex alone)

$$\left(\frac{d^2\sigma}{dt\,du}\right)_{e\mu(x)\to e\mu(x)} = \frac{1}{2}\,\frac{4\pi\alpha^2}{t^2}\,\frac{u^2+s^2}{s^2} \times \delta\left(t+x(s+u)\right) \qquad (5.9)$$

If the target is built from partons of types (flavours) labelled i, and the probability for a parton i to have momentum fraction x to x + dx is $f_i(x)$ then the inelastic e-target cross-section will be, after summing over all the elastic parton contributions

$$\left(\frac{d^2\sigma}{dtdu}\right)_{eN\to eX} = \frac{1}{2}\frac{4\pi\alpha^2}{t^2}\frac{u^2+s^2}{s^2}\int dx \sum_i x f_i(x)\frac{1}{s+u}\,\delta(x-\tfrac{1}{\omega}) \qquad (5.10)$$

We already see the appearance of the structure in eq. (4.12). To obtain that expression explicitly we must compare the equation (5.10) with the expression for eN → eX which involves $W_{1,2}$ (eq. 4.5).

Noting that

$$\sin^2\frac{\theta}{2} = \frac{tm^2}{su} \quad ; \quad \frac{\epsilon'}{\epsilon} \equiv -\frac{u}{s} \qquad (5.11)$$

$$\nu = \frac{s+u}{2m} \quad ; \quad x \equiv \frac{Q^2}{2M\nu} = \frac{-t}{s+u}$$

we can manipulate eq. (2.5) into the form

$$\left(\frac{d^2\sigma}{dtdu}\right)_{eN\to eX} = \frac{1}{2}\frac{4\pi\alpha^2}{t^2}\frac{1}{s^2(s+u)}\left[2xF_1(s+u)^2 - 2usF_2\right] \qquad (6.12)$$

where $F_1 \equiv MW_1$, $F_2 \equiv \nu W_2$

Since s and u can be independently varied we compare coefficients and immediately see that

$$2xF_1(x) = F_2(x) = \sum_i e_i^2 x f_i(x) \qquad (x \equiv 1/\omega) \qquad (5.13)$$

which is the master formula of the spin ½ parton model.

6. Partons = Quarks?

6.1 Electromagnetic structure functions

We have from eq. (3.13) that

$$F_2(x) = \sum_i e_i^2 x f_i(x) \equiv \sum_i e_i^2 q_i(x) \qquad (6.1)$$

Hence

$$F_2^{\gamma p}(x) = \frac{4}{9}\left(u^p(x)+\bar{u}^p(x)\right) + \frac{1}{9}\left(d^p(x)+\bar{d}^p(x)\right) + \frac{1}{9}\left(s^p(x)+\bar{s}^p(x)\right) \qquad (6.2)$$

$$F_2^{\gamma N}(x) = \frac{4}{9}\left(u^N(x)+\bar{u}^N(x)\right) + \frac{1}{9}\left(d^N(x)+\cdots\right)$$

Now use isospin reflection to note

$$u^p \equiv d^N \text{ (call it simply u)} \qquad (6.3)$$

$$d^p \equiv u^N \text{ (call it d)} \qquad (6.4)$$

$$s^p \equiv s^N \text{ (call it s)} \qquad (6.5)$$

with analogous constraints for the antiquarks.

Consequently

$$F_2^{\gamma p} = \frac{4}{9}\left(u+\bar{u}\right) + \frac{1}{9}\left(d+\bar{d}\right) + \frac{1}{9}\left(s+\bar{s}\right) \qquad (6.6)$$

$$F_2^{\gamma N} = \frac{4}{9}\left(d+\bar{d}\right) + \frac{1}{9}\left(u+\bar{u}\right) + \frac{1}{9}\left(s+\bar{s}\right) \qquad (6.7)$$

and so

$$\frac{1}{4} \le \frac{F_2^{\gamma N}}{F_2^{\gamma p}}(x) \le 4 \qquad (6.8)$$

These bounds are consistent with the data (fig.10).

We can go further by imposing ideas rooted in duality. Separate the quarks (partons) into three "valence" quarks and a sea of quarks and antiquarks along the following lines

3 valence quarks	+	Sea of $q\,\bar{q}$
↕		↕
Resonances	+	Background
↕		↕
Non Diffractive	+	Diffractive

Then (following e.g. Kuti-Weisskopf or Landshoff-Polkinghorne) write

$$q(x) \equiv q_V(x) + q_S(x) \qquad (6.9)$$

The original guess was

$$u_v(x) = 2d_v(x) \qquad (6.10)$$

$$s_v(x) = \bar{u}_v(x) = \bar{d}_v(x) = \bar{s}_v(x) = 0 \qquad (6.11)$$

$$u_s(x) = \bar{u}_s(x) = d_s = \bar{d}_s = s = \bar{s} \equiv K \qquad (6.12)$$

This gives

$$F_2^{\gamma N} = \frac{1}{9}\left(u_v + 4d_v\right) + \frac{12}{9}K \qquad (6.13)$$

$$F_2^{\gamma P} = \frac{1}{9}\left(d_v + 4u_v\right) + \frac{12}{9}K \qquad (6.14)$$

so that if K(x) dominates

$$\frac{F_2^{\gamma N}}{F_2^{\gamma P}}(x) \to 1 \quad (x \to 0\ ?) \qquad (6.15)$$

whereas for dominance of the valence quarks (and if $u_v \geq 2d_v$)

$$\frac{F_2^{\gamma N}}{F_2^{\gamma P}}(x) \to \frac{2}{3} \text{ to } \frac{1}{4} \quad (x \gtrsim 0.2\ ?) \qquad (6.16)$$

Hence we begin to have the first hints that maybe the valence quarks are dominantly at large X while the sea is near X ≃ 0. This will be reinforced in our subsequent data analyses, but first let us give an intuitive picture of why this picture is not unreasonable.

In QED the bare electron becomes dressed by diagrams such as fig. 11. The analogue for the partons will be that vector (?) gluons (something has to hold the target together) will play the role of the photons in QED. Then a three valence quark system will be dressed in fig. 12, where the wiggly lines denote gluons and the solid lines are quark-partons. The bremmstrahlung probability for momentum k in the gluon behaves as $\frac{dk}{k}$ and hence like $\frac{dx}{x}$. This means that the gluon emission, and hence the $q\bar{q}$ structure or sea, tends to like small x. So we can view the target as three valence quarks carrying most of the momentum bound by gluons which will also carry momentum and radiating and absorbing soft gluons which dress the valence quarks with a soft cloud of $q\bar{q}$ pairs.

6.2 Comparison of electromagnetic and neutrino interactions

The charged weak interaction couples to the isospin of the partons and in the limit of zero Cabibbo angle the reaction is triggered by

$$\nu\begin{bmatrix} d \\ \bar{u} \end{bmatrix} \to \mu^-\begin{bmatrix} u \\ \bar{d} \end{bmatrix} \qquad (6.17)$$

we have

$$F_2^{\nu P}(x) = 2\left[d(x) + \bar{u}(x)\right] \qquad (6.18)$$

$$F_2^{\nu N}(x) = 2\left[u(x) + \bar{d}(x)\right] \qquad (6.19)$$

where in (6.19) we have used $d^N = u^P$ = u etc. The factor of 2 arises from the presence of axial as well as vector currents coupling and in the parton model the weak current is taken to be V - A as for leptons, hence the axial coupling magnitude is the same as that of the vector.

Comparing (6.18, 6.19) with (6.6, 6.7) yields

$$\left[\frac{F_2^{\gamma N} + F_2^{\gamma P}}{F_2^{\nu N} + F_2^{\nu P}}\right](x) = \frac{\frac{5}{9}(u+\bar{u}+d+\bar{d}) + \frac{2}{9}(s+\bar{s})}{2(u+\bar{u}+d+\bar{d})} \geq \frac{5}{18} \qquad (6.20)$$

(the rather mysterious $5/18$ is of course just the average squared charge of the u, d quarks).

In fig. 13 we see the data from CERN-Gargamelle where $F_2^{\nu N+\nu P}(x)$ is compared with $\frac{18}{5}F_2^{eP+eN}$ from SLAC. The agreement supports the quark quantum numbers and the saturation of the inequality at large x suggest that $s, \bar{s}$ $(x \gtrsim 0.2) \simeq 0$ (which is in line with our picture that strange quarks are in the $q\bar{q}$ sea which in turn is confined to small x values).

6.3 Gluon momentum

Since $F_2(x) \sim xf(x) \sim q(x)$ then $q(x)$ is proportional to the fractional momentum distribution of the quarks. Momentum conservation then yields

$$\int_0^1 dx \left(u+\bar{u}+d+\bar{d}+s+\bar{s}\right)(x) = 1-\epsilon \qquad (6.21)$$

where ϵ will be the fraction of momentum carried by target constituents other than the quarks, e.g. the gluons.

From equations (6.6), (6.7) and (6.18, 6.19) we see that (6.21) can be rewritten as

$$\int_0^1 dx \left(\frac{9}{2}F_2^{\gamma p+\gamma n} - \frac{3}{4}F_2^{\nu p+\nu n}\right) = 1-\epsilon \qquad (6.22)$$

Inserting the data on the left hand side we find $\epsilon \simeq \frac{1}{2}$, i.e. about half the momentum is carried by the gluons.

6.4 Sum rules

Since a nucleon has no strangeness then

$$0 = \int_0^1 \frac{dx}{x}\left(s(x) - \bar{s}(x)\right) \qquad (6.23)$$

The charges of proton and neutron give

$$1 = \int \frac{dx}{x}\left(\frac{2}{3}(u-\bar{u}) - \frac{1}{3}(d-\bar{d})\right)(x)$$

$$0 = \int \frac{dx}{x}\left(\frac{2}{3}(d-\bar{d}) - \frac{1}{3}(u-\bar{u})\right)(x)$$

and so

$$2 = \int \frac{dx}{x}\left(u(x) - \bar{u}(x)\right) \qquad (6.24)$$

$$1 = \int \frac{dx}{x}\left(d(x) - \bar{d}(x)\right) \qquad (6.25)$$

These state the net number of s, d, u quarks in the proton are 0, 1, 2 respectively.

These sum rules for the quark distributions can now be combined with the structure functions relations (6.6, 6.7, 6.18, 6.19) to yield sum rules for the targets.

First, since $F_2^{\nu N}(x) - F_2^{\nu P}(x) \equiv 2\{u - \bar{u} - d + \bar{d}\}(x)$ we find the "Adler Sum Rule"

$$\int \frac{dx}{x}\left(F_2^{\nu N}(x) - F_2^{\nu P}(x)\right) = 2 \qquad (6.26)$$

Another interesting quantity is

$$F_2^{eP}(x) - F_2^{eN}(x) \equiv \frac{1}{3}\left\{u+\bar{u}-d-\bar{d}\right\}(x) \qquad (6.27)$$

If we impose duality (i.e. $u = u_v + u_s$ etc.) then the sum rules (4.24) and (4.25) become

$$1 = \int \frac{dx}{x} d_v(x) \qquad (6.28)$$

$$2 = \int \frac{dx}{x} u_v(x) \qquad (6.29)$$

and so eq. (4.27) yields

$$\left(F_2^{eP} - F_2^{eN}\right)(x) \equiv \frac{1}{3}\left\{u_v(x) - d_v(x)\right\} \qquad (6.30)$$

which gives

$$\int \frac{dx}{x}\left(F_2^{eP}(x) - F_2^{eN}(x)\right) = \frac{1}{3}\left(\equiv \sum e_p^2 - e_N^2\right) \qquad (6.31)$$

The data are consistent with this and yield $0.28 \pm ?$. The ? is the contribution from large (small x). If we believe that $F^{eP} - F^{eN} \sim X^{\frac{1}{2}}$ as $X \to 10$ (Regge like) then the data are consistent with the predicted value of $\frac{1}{3}$.

6.5 Neutrino interactions

Defining $x \equiv Q^2/2M\nu$ and $y = \nu/E$ then it is a straightforward exercise to rewrite eq. (4.24) in the form

$$\frac{d^2\sigma}{dx\,dy} = \frac{4\pi\alpha^2 s}{t^2}\left\{F_2(x)(1-y) + F_1(x)xy^2\right\} \qquad (6.32)$$

For the process $\nu(\bar{\nu})p \to \mu^{\pm} X$ one has a similar formula

$$\frac{d^2\sigma^{\nu,\bar{\nu}}}{dxdy} = \frac{G^2}{2\pi} s\left\{F_2(x)(1-y) + F_1(x)xy^2 \mp y\left(1-\frac{y}{2}\right)xF_3(x)\right\} \qquad (6.33)$$

in which, for spin $\frac{1}{2}$ partons, inserting $xF_1(x) = F_2(x)$ yields

$$\frac{d^2\sigma^{(\bar{\nu})}}{dxdy} = \frac{G^2}{2\pi} sF_2(x)\left\{\frac{1+(1-y)^2}{2} \mp \frac{1-(1-y)^2}{2}\frac{xF_3(x)}{F_2(x)}\right\} \qquad (6.34)$$

In comparison with the electromagnetic case, eq. (6.32), we see the absence of t^{-2} due to the assumed pointlike (no photon exchanged) nature of the neutrino interaction. Also there is the new structure function F_3 which is due to the violation of parity in the weak interactions. Its role will be transparent after we discuss the quark parton model for this process.

In the quark parton model the basic interaction is a weak coupling of lepton with the weak quark current. If the quark weak current is V - A ((like $\nu \to \mu$) then the y dependence of neutrino - quark cross-sections are as follows

$$\frac{d\sigma}{dy}\left[\nu\bar{q}_L;\ \bar{\nu}q_L\right] \sim (1-y)^2 \qquad (6.35)$$

$$\frac{d\sigma}{dy}\left[\nu q_L;\ \bar{\nu}\bar{q}_L\right] \sim 1 \text{ (isotropic)} \qquad (6.36)$$

Qualitatively this can be understood as follows. For an interaction at a point one is in S wave; all the angular momentum information of the νq interaction will therefore be contained in the spin structure. A neutrino-quark interaction will have $J_z = 0$ in the c.m. system since both are carrying helicity minus one. The pointlike interaction will therefore carry no memory of direction and hence an isotropic distribution can ensue. For neutrino interacting with an antiquark, whose helicity will be plus one, the total $J_z = -1$. The emerging $\bar{q}$ and μ are right handed and left handed respectively and so $J_{z'} = -1$ along the z' axis (oriented at θ with respect to the initial z axis). The 180° scattering is clearly supressed and so one can appreciate the $(1-y)^2$ as against isotropic behaviour in the νq case.

For the case of an isoscalar target, writing $q(x)$ and $\bar{q}(x)$ for the probabilities to find quarks or antiquarks at given x, then

$$\frac{d^2\sigma^{\nu}}{dxdy} \sim x\left\{q(x) + (1-y)^2\bar{q}(x)\right\} \qquad (6.37)$$

$$\frac{d^2\sigma^{\bar{\nu}}}{dxdy} \sim x\left\{\bar{q}(x) + (1-y)^2 q(x)\right\} \qquad (6.38)$$

where we have used (6.35 and (6.36). Comparing with (6.34) then we have

$$\frac{xF_3(x)}{F_2(x)} = \frac{q(x) - \bar{q}(x)}{q(x) + \bar{q}(x)} \qquad (6.39)$$

and so the x distribution of quarks and antiquarks can be compared (more correctly, the distribution of V ± A elementary currents). The eq. (6.39) also helps us to appreciate why the extra structure function F_3 appears in the weak interaction as compared to the electromagnetic case. The parity violation causes the left and right handed couplings to be independent (hence F_3) in the weak interaction, and hence the difference in q and $\bar{q}$ couplings.

The data on F_3 and xF_3 from Gargamelle ($Q^2 > 1$ GeV^2, $W^2 > 4$ GeV^2) are shown in fig. 16. We see that for $x \gtrsim 0.4$ $F_2(x) \simeq xF_3(x)$ and so from eq. (4.39) we have

$$x \gtrsim 0.4 \qquad \frac{\bar{q}(x)}{q(x)} \to 0 \qquad (6.40)$$

whereas for $x \to 0$ $xF_3(x) \to 0$ and hence

$$x \to 0 \qquad \bar{q}(x) \to q(x) \qquad (6.41)$$

This fits in with our previous guess from the electromagnetic case, namely that the (valence) quarks dominate as $x \gtrsim 0.4$ while antiquarks are all in the sea with $x \to 0$.

We can look at this in more detail by studying the y distributions for various regions of x. The data for $E\nu \lesssim 30$ GeV from Gargamelle and Fermilab are all consistent with $(1-y)^2$ distributions for $\bar{\nu}$ induced reactions and isotropy for ν interactions at large X.

A best fit to the Gargamelle data on y distributions yields

$$\mathcal{B} \equiv \frac{\langle xF_3 \rangle}{\langle F_2 \rangle} \sim 0.180 \qquad (6.42)$$

and hence

$$\frac{\langle \bar{q} \rangle}{\langle q+\bar{q} \rangle} = 0.10 \pm 0.03 \qquad (6.43)$$

So far we have just assumed that the $\nu(\bar{\nu})$ data scale analogously to their electromagnetic cousin. This we should really check. If we integrate (6.34) over dx and dy then, assuming scaling (i.e. $F_2(x,Q^2) \to F_2(x)$) we have for the total cross section

$$\sigma_\nu^{\bar{\nu}}(S) = \frac{G^2 S}{2\pi} \int dx\, F_2(x) \left\{ \frac{2}{3} \mp \frac{1}{3} \frac{xF_3(x)}{F_2(x)} \right\} \qquad (6.44)$$

and hence would have a linear rise with energy ($S \equiv 2$ ME). This is indeed consistent with the Gargamelle data as shown in Steinberger's lectures.

Furthermore, from (6.44) and (6.39) we have

$$\frac{\sigma^{\bar{\nu}}}{\sigma^{\nu}} = \frac{\frac{1}{3} + \frac{2}{3}\left\langle \frac{\bar{q}}{q+\bar{q}} \right\rangle}{1 - \frac{2}{3}\left\langle \frac{\bar{q}}{q+\bar{q}} \right\rangle} \qquad (6.45)$$

and hence is bounded to lie between $\frac{1}{3}$ and 3. The Gargamelle data (all Q^2, W) have this ratio $\simeq 0.37$ which again fits with the dominance of quarks over antiquarks (or, rather, of left handed parton currents).

If one makes the cut $Q^2 > 1$ GeV^2, $W^2 > 4$ GeV^2 then from fitting the x,y distributions one had (eq. 4.43)

$$\left\langle \bar{q}/q+\bar{q} \right\rangle = 0.10 \pm 0.03$$

and so in eq. (4.45)

$$\frac{\sigma^{\bar{\nu}}}{\sigma^{\nu}} \simeq 0.43$$

This is slightly larger than without the Q^2,W cut and while insignificant for our present discussion may be worth bearing in mind in connection with the possible increase of $\sigma^{\nu}/\sigma^{\nu}$ at higher energies in Fermilab. (See Steinberger's lectures).

7. Charm Production in νN and eN

In view of the possibility that a new heavy hadronic degree of freedom exists associated with a charmed quark (see Prof. Wiik and Maiani's Lectures) and that this charmed quark is believed to have weak interaction

$$\bar{\nu} c \to \mu^+ \left(d \sin\theta_c + s \cos\theta_c \right) \qquad (7.1)$$

then it is interesting to see what effect it will have on the parton model predictions.

Below threshold and for $X \gtrsim 0.1$ we have

$$\frac{d\sigma^{\nu N}}{dy} \sim \text{constant} \; ; \; \frac{d\sigma^{\bar{\nu} N}}{dy} \sim (1-y)^2 \qquad (7.2)$$

due to the absence of antiquarks. This is realised in the data, whereas at $X \lesssim 0.1$ the data is consistent with isotropy for both ν and $\bar{\nu}$.

A new threshold appears at some fixed hadronic mass W and since

$$W^2 = M^2 + 2M\nu - Q^2$$

then

$$W^2 - M^2 = 2ME y (1-x) \qquad (7.3)$$

Hence a threshold at W_{th} first appears in the x and y distributions at small x and large y. Since at large y the $\bar{\nu}$N cross section was small below threshold $|(1-y)^2$ distribution$|$ then the threshold contributions will be more immediately apprent in $\bar{\nu}$N than νN. However, since we do not precisely

know how the antiquark distributions behave it may be hard to separate the threshold behaviour from possible antiquark contributions filling in the large y cross-section.

The data from HPWF do appear to show some hints that something anomalous is happening in the y distributions.

Above the threshold for exciting charmed particle final states the new contributions to the cross sections arising from the GIM charm-changing current are ($\cos\theta_c \simeq 0$)

$$\Delta\sigma^{\nu N} \sim s(x) + \bar{c}(x)(1-y)^2$$
$$\Delta\sigma^{\bar{\nu}N} \sim \bar{s}(x) + c(x)(1-y)^2 \qquad (7.4)$$

and so the contributions arise entirely from quarks in the sea. The actual magnitude of $\Delta\sigma/\sigma$ below threshold will of course depend upon the distribution of the u,d,s,c quarks in the sea and of the relative importance of sea and valence quarks. Particular assumptions (SU_4 symmetric sea, SU_3 symmetric sea etc.) lead to particular predictions. There is quite an industry in this direction at present.

Another interesting idea is that there may exist right handed currents involving the quarks. In particular one idea was that there might exist (in $\cos\theta_c = 0$ approximation)

$$\bar{\nu}\bar{s} \xrightarrow{R.H.} \mu^+\bar{c} \qquad (7.5)$$

This would have an isotropic distribution and be very significant in filling in the large y domain of $\sigma^{\bar{\nu}N}(x,y)$.

The possibility that $\nu d \xrightarrow{RH} \mu^- c$ is unlikely since it involves the valence quark d and so we would naively expect a doubling of $\sigma^{\nu N}/E$ on crossing charm threshold. Any such behaviour is not apparent in the data.

In deep inelastic electroproduction (or muon production) the charm production threshold should be seen at small x where

$$\frac{\Delta\sigma}{\sigma} = \frac{\frac{4}{9}\left(c(x) + \bar{c}(x)\right)}{\frac{4}{9}\left(u(x)+\bar{u}(x)\right) + \frac{1}{9}\left(d(x)+\bar{d}(x)\right) + \frac{1}{9}\left(s(x)+\bar{s}(x)\right)} \qquad (7.6)$$

In the case of an SU_4 symmetric sea one therefore would expect that $\frac{\Delta\sigma}{\sigma} = \frac{2}{3}$. While this may be true as $Q^2 \to \infty$ (where all mass scales are probably irrelevant) presumably at finite Q^2 the charm quark will be less important (being associated typically with heavier mass scales). Hence

$$\frac{\Delta\sigma}{\sigma}(x\to 0; Q^2) = \frac{2}{3}\epsilon(Q^2) \qquad (7.7)$$
$$\epsilon \equiv \frac{c(x\to 0; Q^2)}{u,d,s(x\to 0; Q^2)} \leq 1$$

A guess for the relative importance of charm to uncharmed quarks as a function of Q^2 might be something like

$$\epsilon = \frac{M_\rho^2 + Q^2}{M_\psi^2 + Q^2}$$

which is about 5% at $Q^2 = 0$ (like estimates from VMD) rising through 50% by $Q^2 = 10$ GeV^2.

The violation of scaling reported by the Chen-Hand inelastic muon scattering experiment at Fermilab. is consistent with being above charm threshold and ϵ having a Q^2 dependence similar to eq.7.8. An explicit calculation is given in ref.CSS and comparison between it and the data shown in fig. 17.

The best place for seeing the immediate effects of a new heavy, charm, threshold is in e^+e^- annihilation, to which we now turn.

8. Electron-Positron Annihilation

Production of muon pairs via a single photon in electron-positron annihilation has cross section (where $m \equiv m_\mu$)

$$\sigma(e^+e^- \to \mu^+\mu^-)(Q^2) = \frac{4\pi\alpha^2}{3Q^2}\left(1-\frac{4m^2}{Q^2}\right)^{1/2}\left(1+\frac{2m^2}{Q^2}\right) \qquad (8.1)$$
$$\xrightarrow{Q^2 \gg m^2} \frac{4\pi\alpha^2}{3Q^2} \qquad (8.2)$$

This simple expression is a nice illustration of the pointlike nature of the interaction, the dimensions are carried entirely by the large Q^2 photon mass and no scale of length associated with the muon appears. Compare this with $e^+e^- \to p\bar{p}$ which is again production of a pair of spin ½ particles we have (where M = proton mass)

$$\sigma(e^+e^- \to p\bar{p})(Q^2) = \frac{4\pi\alpha^2}{3Q^2}\left(1-\frac{4M^2}{Q^2}\right)^{1/2}\left(G_M^2(Q^2) + \frac{2M^2}{Q^2}G_E^2(Q^2)\right) \quad (8.3)$$

$$\xrightarrow{Q^2 \gg M^2} \frac{4\pi\alpha^2}{3Q^2}G_M^2(Q^2) \quad (8.4)$$

$$\sim \frac{4\pi\alpha^2}{3Q^2}\left(1+\frac{Q^2}{0.71\,GeV^2}\right)^{-4} \quad (8.5)$$

where the finite size of the proton is always present in the form factor dependence.

The two form factors $G_{E,M}$ ("electric and magnetic") could be thought of as the longitudinal and transverse form factors since G_E couples only to the longitudinal ($J_Z = 0$) photon while G_M couples only to the transverse ($J_z = \pm 1$). Hence for pair production of spin ½ particles

$$\frac{\sigma_L}{\sigma_T}(Q^2) = \frac{2M^2}{Q^2}\left|\frac{G_E(Q^2)}{G_M(Q^2)}\right|^2 \xrightarrow{\text{pointlike}} \frac{2M^2}{Q^2} \quad (8.6)$$

In the parton model we expect that $e^+e^- \to$ hadrons takes place by $e^+e^- \to$ parton - antiparton and the partons then fragment into the observed hadrons by some unknown mechanism. Then at large Q^2

$$\sigma(e^+e^- \to \text{hadrons}) = \sum_{i=udsc} \sigma(e^+e^- \to q_i\bar{q}_i) \quad (8.7)$$

$$= \sum_i e_i^2\,\sigma(e^+e^- \to \mu^+\mu^-)_{QED} \quad (8.8)$$

and hence

$$R \equiv \frac{\sigma(e^+e^- \to \text{hadrons})}{\sigma(e^+e^- \to \mu^+\mu^-)_{QED}} = \sum_i e_i^2 \quad (8.9)$$

so we expect to find this quantity <u>constant</u> in Q^2 and its magnitude measures <u>directly</u> the sum of the the squared charges of the fundamental fermion fields. Hence below charm theshold, the u.ds degrees of freedom are operative and as they come in three colours (e.g. spectroscopy) we have

$$R_{uds} = 3\left(\frac{4}{9}+\frac{1}{9}+\frac{1}{9}\right) = 2 \quad (8.10)$$

At higher Q^2 we will cross the threshold for production of charmed mesons. The first feature in the data will be the appearance of narrow vector mesons in the e^+e^- channel (identified with the ψ at 3.1 GeV and 3.7 GeV) followed by charm production threshold where R will rise and show complicated structure (around 4 GeV?). At higher Q^2 one anticipates that R will again show scaling (become constant) with value

$$R = 2 + e_{charm}^2 \quad (8.11)$$

$$\text{If } e_c = {}^2/_3 \text{ then } R \quad 3\tfrac{1}{3} \quad (8.12)$$

The data do indeed show scaling behaviour (fig.18). Frascati data at $\sqrt{Q^2} < 3$ GeV is unclear but not inconsistent with constant ~2 to 3 in magnitude. Better data from SPEAR below 3.5 GeV suggest R ~ 2.5 to 3 with no <u>obvious</u> structures. After the 4 GeV structures R appears to have settled down again to a value around 5½. One unit of this is believed to be due to pair production of a new heavy lepton. Is the remaining 4½ consistent with uds and c or are more quarks needed?

In non-abelian gauge theories with asymptotic freedom one expects the asymptotic value of R to be approached slowly from above. Hence I would regard the e^+e^- annihilation data as being a remarkable manifestation of the scaling idea and maybe even of the simple quark-parton model.

If the partons have spin ½ we expect $\sigma_T >> \sigma_L$ at large Q^2 and the partons to be produced with a $1 + \cos^2\theta$ angular distribution (relative to the e^+e^- axis). The hadron fragments from the partons will, at high energies, be produced in a cone along the direction of motion of the parent parton. Hence we expect to see jets of hadrons with a $1 + \cos^2\theta$ distribution. This remarkably appears to be manifested by the high energy data. We will show this in section 10 but first will prepare the scene by discussing the general features of quark fragmentation into hadrons and with particular reference to the inclusive hadron production in $ep \to eh \ldots$, $\nu p \to \mu h \ldots$ $e^+e^- \to h \ldots$ etc.

9. Inclusive production of hadrons and the quark-parton model.

Interesting tests of the quark-parton model arise from inclusive hadron production experiments like $e^+e^- \to h$ + anything, and $e(\nu)N \to e(\mu^-)h$ + anything. In particular the production of detected hadrons h in the current fragmentation region* of the $e(\nu)$ scattering experiments is intimately related with the production in e^+e^- annihilation, and there is some support that this correlation is in fact realised in the data.

1) $\ell N \to \ell' h \ldots . (\ell \equiv e, \mu, \nu)$

This process is illustrated in figure 18. The hadron and nucleon momenta are p_h, p_N respectively and $X \equiv Q^2/2M\nu$ as usual. There is great similarity with the ℓN inclusive process discussed earlier, but now we have an extra kinematical degree of freedom associated with p_h, the momentum of the hadron h detected. We will work in the centre of mass system of the current (γ or W) and nucleon, and will define the positive Z axis to be the γ-direction. Then we choose variables to characterise the problem:

$$Q^2,\ X(\equiv Q^2/2M\nu),\ p_T^h,\ Z(\equiv p_z^h/p_{z(\max)}^h)^+ \qquad (9.1)$$

We will concentrate on the current fragmentation region ($Z > 0$). The parton model analysis of this process is illustrated in the Breit frame of the current and the parton with which it interacts (fig. 19). The nucleon carries a large longitudinal momentum P and is treated as a collection of independent pointlike constituents (partons). The current, with momentum

$$q = (0;\ 0\ 0\ -2\ x\ P) \qquad (9.2)$$

interacts incoherently with a parton whose momentum vector is

$$p = (xP;\ 0\ 0\ xP) \qquad (9.3)$$

and so its momentum is reversed. This is analogous to the total cross-section description of section 3 (fig. 6), and this part of the process is described by the quark-parton distribution functions $u(x)\,dx$ etc. (the average number of u quarks in an interval dx of x) that we met in section 3-5.

In fig. 19a we exhibit the fragmentation of the quark-parton into hadrons, one of which, h, is observed.

*Defined later

+One often meets rapidity $\eta \equiv \tfrac{1}{2}\ell n \dfrac{E^h + p_z^h}{E^h - p_z^h}$ where E^h is the hadron's energy.

Technical Aside

There are two rather different regions, $Z \lesssim 0$. In both of these $q.p_h \sim O(Q^2)$ while $p_N.p_h$ is finite for $Z < 0$ but grows as $O(Q^2)$ for $Z > 0$. The former is intuitively the target fragmentation region and, for the reader familiar with parton model diagrams, can be represented by

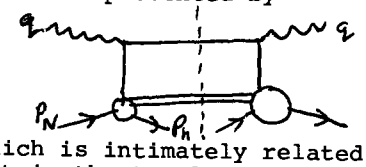

which is intimately related to the diagram met in the total cross-section at large Q

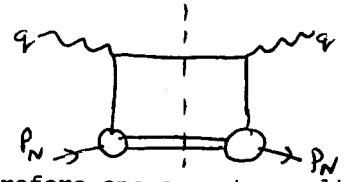

Therefore one expects scaling in this region (technically, one can argue that the light-cone dominates here).

The natural picture for $Z > 0$ is

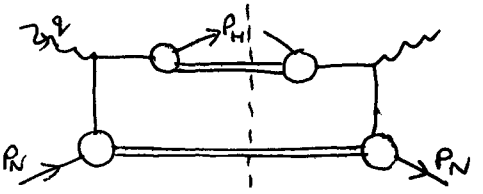

with p^h emerging along the direction of q and $p^h - q \sim O(Q^2)$. In the light-cone formalism one can say very little about this region since it is not light cone dominated (the fragmentation takes place between the two currents in the figure). Hence the parton model has extra power here if we define functions $D_i^h(Z, Q^2, p_T)$ to represent the fragmentation probabilities for (quark)-parton of flavour i to produce hadron h. See text.

The struck parton is separated by a large momentum from the nucleon fragments and so we shall assume that the fragmentation is independent of the earlier current interaction. Hence we shall assume it to be independent of and only dependent upon z, the fraction of the parton's momentum that is carried off by the observed hadron (fig. 19)

$$p^h = (zxP,\ 0,0,\ -zxP) \qquad (9.4)$$

and so we introduce a set of "parton fragmentation functions" $D_i^f(z)dz$ which represent the probability that parton type i produces hadron f in an interval dz about z.

2. The quark fragmentation functions

In terms of the known quark distribution functions U(X)... and the unknown $D_i^f(z)$ fragmentation functions, we can discuss hadron inclusive production in a variety of current induced processes e.g. $e^+e^- \to h..$, $ep(n) \to eh...$, $\nu p(n) \to \mu^- h...$ etc. We can obtain relations among these various processes due to the $\sum_q q(x)D_q^f(z)$ structure and constrain the relative production rates of various hadrons by limiting the number of independent $D_i^f(z)$ using isospin and charge-conjugation invariance. This yields, for π production,

$$D_u^{\pi^+} = D_d^{\pi^-} = D_{\bar{d}}^{\pi^+} = D_{\bar{u}}^{\pi^-} \qquad (9.5)$$

$$D_d^{\pi^+} = D_u^{\pi^-} = D_{\bar{u}}^{\pi^+} = D_{\bar{d}}^{\pi^-} \qquad (9.6)$$

$$D_s^{\pi^+} = D_s^{\pi^-} = D_{\bar{s}}^{\pi^+} = D_{\bar{s}}^{\pi^-} \qquad (9.7)$$

(where for simplicity we have ignored any contributions from new heavy quarks. These will in general be necessary when discussing very high energy data, but for our present introduction we will restrict our attention to data that is believed to be below threshold for production of heavy hadronic degrees of freedom such as charm).

The way these fragmentation functions enter in comparison with data depends upon the process under study. We list these below; their derivation is obvious.

i) $e^+e^- \to h...$

$$\frac{1}{\sigma_{TOT}}\frac{d\sigma}{dz}(e^+e^- \to h..) = \frac{\sum_i e_i^2 \{D_i^h(z) + D_{\bar{i}}^h(z)\}}{\sum_i e_i^2} \qquad (9.8)$$

(i = quark flavors)

(note here that the photon produces a parton-antiparton pair, either of which could have produced the observed hadron, hence the D_i and $D_{\bar{i}}$ appear, in distinction to the next examples).

ii) $ep \to eh...$

$$\frac{1}{\sigma_{TOT}}\frac{d\sigma}{dz}(ep \to eh..) = \frac{\sum_i e_i^2 f_i(x) D_i^h(z)}{\sum_i e_i^2 f_i(x)} \qquad (9.9)$$

(i = quark and antiquark flavors)

(where $f_i(x)$ are the quark-parton distribution functions of section

iii) $\nu p \to \mu^- h...$

$$\frac{1}{\sigma_{TOT}}\frac{d\sigma}{dz}(\nu p \to \mu^- h..) = \frac{d(x)D_u^h(z) + \frac{1}{3}\bar{u}(x)D_{\bar{d}}^h(z)}{d(x) + \frac{1}{3}\bar{u}(x)} \qquad (9.10)$$

(where we have approximated $\theta_c = 0$ and ignored charm).

Note that the d quark turns into a u quark before fragmenting. The 1/3 is due to the left handed current coupling to antiquarks (integration over dy having been performed as in section 6).

A. $\nu p \to \mu^- h...$

From the nature of these expressions we see that the neutrino data are a direct measurement of the fragmentation functions for pions since from eq. 9.5, 9.6

$$D_u^{\pi^+} \equiv D_{\bar{d}}^{\pi^+} \qquad (9.11)$$

and so the $d(x) + \bar{u}(x)$ cancels in numerator and denominator of eq. 9.10 yielding

$$\frac{1}{\sigma_{TOT}}\frac{d\sigma}{dz}(\nu p \to \mu^- \pi^{\pm} ..) = D_u^{\pi^{\pm}}(z) \qquad (9.12)$$

Also $$\frac{1}{\sigma_{TOT}}\frac{d\sigma}{dz}(\bar{\nu} p \to \mu^+ \pi^{\pm} ..) = D_d^{\pi^{\pm}}(z) = D_u^{\pi^{\mp}}(z) \qquad (9.13)$$

Data from Gargamelle on the ratio of π^+/π^- production with ν/beams (and equivalently π^-/π^+ with $\bar{\nu}$) are shewn in fig. 20. These directly yield

$$\eta(z) \equiv D_u^{\pi^+}(z) \Big/ D_u^{\pi^-}(z) \qquad (9.14)$$

and we see this is of order 3 for $0.3 \leq z \leq 0.7$ rising as $z > 0.7$. That this ratio is greater than 1 is intuitively reasonable since π^+ is $u\bar{d}$ in the simplest configuration. It has been widely argued that, as $z \to 1$, $\eta(z) \to \infty$ due to the presence of u valence quark in π^+ whereas U in π^- is in the sea. Whether or not these data support this is unclear since at any finite energy, $\eta(z \to 1) \to \infty$ due to the fact that $\nu p \to \mu^-$ + (charge 2) in the quasi exclusive limit. What is of immediate interest is that

$$\eta(z)_{0.3 \leq z \leq 0.7} \simeq 2 \text{ to } 3 \qquad (9.15)$$

is consistent with the inelastic electroproduction data (discussed in a moment) and also that the data support the implication of eq. 9.12 viz

$$\frac{\frac{d\sigma}{dz}(\nu p \to \mu^- \pi^{\pm} ..)}{\frac{d\sigma}{dz}(\nu p \to \mu^- \pi^- ..)} = \text{independent of } x \qquad (9.16)$$

The data with $0.3 < z < 0.7$ are shown as a function of x in fig. 21 and are indeed consistent with this prediction.

Very recent data from the 15' Hydrogen bubble chamber at Fermilab yield information on the production of positives and negatives separately. (fig. 22). The ratio of +/- production is qualitatively in agreement with the lower energy Gargamelle data, namely +/- > 1 and rising as z increases, though the difference between positive and negative production appears to be rather larger at Fermilab than the Gargamelle data at a comparable z. one reason may be due to the Fermi lab experiment being <u>all</u> positive (negative) charges whereas Gargamelle is explicitly $\pi^{\pm}$, also there may be some contamination from quasi exclusive channels that have a $Q^2(E_\nu)$ dependence that has to be taken into account before a proper comparison can be made.

If the hadrons are dominantly π and K then

$$\frac{\langle n^+\rangle}{\langle n^-\rangle} = \frac{D_u^{\pi^+}(z) + \dfrac{d(x)D_u^{K^+}(z) + \frac{1}{3}\bar{u}(x)D_{\bar{d}}^{K^+}(z)}{d(x) + \frac{1}{3}\bar{u}(x)}}{D_u^{\pi^-}(z) + \dfrac{d(x)D_U^{K^-}(z) + \frac{1}{3}\bar{u}(x)D_{\bar{d}}^{K^-}(z)}{d(x) + \frac{1}{3}\bar{u}(x)}} \qquad (9.17)$$

The contribution from antiquarks is believed to be very small (section so let's neglect them for simplicity so that we have

$$\frac{\langle n^+\rangle}{\langle n^-\rangle} = \frac{D_u^{\pi^+}(z) + D_U^{K^+}(z)}{D_u^{\pi^-}(z) + D_u^{K^-}(z)} \qquad (9.18)$$

Hence

$$\frac{\langle n^+\rangle}{\langle n^-\rangle} > \frac{\langle n^{\pi^+}\rangle}{\langle n^{\pi^-}\rangle} \quad \text{if} \quad \frac{D_U^{K^+}}{D_U^{K^-}} > \frac{D_U^{\pi^+}}{D_U^{\pi^-}} \qquad (9.19)$$

B. <u>ep(n) → eh...</u>

The analysis of inelastic electron scattering is slightly more involved than for neutrinos due to the contributions from all the charged quarks:

$$\frac{1}{\sigma_{TOT}}\frac{d\sigma}{dz}(eN \to eh..) = \frac{\sum_i e_i^2 f_i(x) D_i^h(z)}{\sum_i e_i^2 f_i(x)} \qquad (9.20)$$

For ease of notation I shall normalise to the total cross section (W_1) and write

$$N_i^h(x,z) = \sum_i e_i^2 f_i(x) D_i^h(z) \qquad (9.21)$$

(this quantity is $L_i^h(x2)$ in Feynmans book ref. F1)

In their original analysis of the data of Bebek et al ($Q^2 = 2$ GeV^2, $\omega = 4$) Cleymans and Rodenberg (CR) ignored the contribution from all but the valence quarks which is reasonable for $\omega \simeq 4$. Hence in $ep \to e\pi^{\pm}...$ they have (writing $u(x) \equiv f_u(x)$ etc.)

$$\frac{N^{\pi^+}(x,z)}{N^{\pi^-}(x,z)} = \frac{\frac{4}{9}u(x)D_U^{\pi^+}(z) + \frac{1}{9}d(x)D_d^{\pi^+}(z)}{\frac{4}{9}u(x)D_U^{\pi^-}(z) + \frac{1}{9}d(x)D_d^{\pi^-}(z)} \qquad (9.22)$$

$$= \frac{4u(x)\eta(z) + d(x)}{4u(x) + d(x)\eta(z)} \qquad (9.23)$$

where in the final step we utilised the relations eq. 9.5-9.7 and, as before, defined

$$\eta(z) = D_U^{\pi^+}(z) \Big/ D_U^{\pi^-}(z) \qquad (9.24)$$

The Bebek data are consistent with scaling in the range $0.2 \leq z \leq 0.7$ and so the analysis was limited to this region for which $\langle n^{\pi^+}\rangle/\langle n_{\pi^-}\rangle \simeq 2$ independent of z. For $\omega \simeq 4$ approximately $u(x) = 2d(x)$ and so

$$2 \simeq \frac{8\eta(z) + 1}{8 + \eta(z)} \qquad (9.24)$$

which yields $\eta(z) \simeq 2.5$ $0.2 \leq z \leq 0.7$. This is in perfect agreement with the Gargamelle data on $\pi^{\pm}$ production by neutrino beams (eq. 9.15) and so we have strong support here for the quark-parton picture of the semi-inclusive hadron production.

Dakin and Feldman (DF) refined and extended the above analysis by incorporating later data in the range $0.5 < Q^2 < 2.5$ GeV^2 and $3 \leq \omega \leq 60$ and allowing for the contribution of valence <u>and</u> sea quarks. They parametrised the longitudinal momentum distributions of the quarks as follows

$$\begin{aligned} u(x) &= u_v(x) + K(x) \\ d(x) &= d_v(x) + K(x) \\ s(x) &= \bar{s}(x) = \bar{u}(x) = \bar{d}(x) = K(x) \end{aligned} \qquad (9.25)$$

where $u_v(x)$, $d_v(x)$ represent the distribution functions for valence quarks and the sea was hypothesised to be SU(3) symmetric (this is not a very crucial assumption for their analysis it turns out).

These functions u(x), K(x) etc. were taken from the McElheney and Tuan fits to the total cross-section data (this is essentially the Kuti Weisskopf model modified to take account of the fact that

$\nu W_2^{en}/\nu W_2^{ep} < 2/3$ as $x \to 1$).

Then one has, in place of eq. 9.23

$$\frac{N^{\pi^+}(x,z)}{N^{\pi^-}(x,z)} = \frac{4u_v(x)\eta(z)+d_v(x)+(S\eta(z)+7)K(x)}{4u_v(x)+\eta(z)d_v(x)+(S\eta(z)+7)K(x)} \qquad (9.26)$$

The Cleymans-Rodenberg formula, eq. 9.23, is obtained when $K(x) \to 0$ (and hence $u_v \equiv u$ etc.). The effect is to raise $\eta(z)$ slightly as compared to $K(x) = 0$:

$$\eta(z) \simeq 3.0 \pm 0.6 \qquad (9.27)$$

(compare $\eta(z) \simeq 2.5$ when $K(x) = 0$ as in Cleymans-Rodenberg). Qualitatively it is obvious that this should be so since the sea populates π^+ and π^- equally, hence tends to dilute the ratio. To have the same ratio as in the data then $\eta(z)$ must be larger than in the analysis where the sea was ignored.

Having determined $\eta(z)$ and knowing the $f_i(x)$ from the McElhaney-Tuan parametrisation of the total cross-section data then one can predict the $x(\omega)$ dependence of the π^+/π^- production ratio using eq. 9.26. This quantity is compared with the data in fig. 23.

Due to the dominance of $u(x)$ as $x \to 1$, more positive charge is predicted to be forward produced.

The production from neutron targets is immediately obtained by interchanging U_v and d_v in eq. 9.26 while $K(x)$ is the same as before (the sea has $I = 0$)

Hence

$$\left[\frac{N^{\pi^+}}{N^{\pi^-}}(x,z)\right]^{en} = \frac{4d_v(x)\eta(z)+u_v(x)+(S\eta(z)+7)K(x)}{4d_v(x)+\eta(z)u_v(x)+(S\eta(z)+7)K(x)} \qquad (9.28)$$

So that with $\eta(z) \simeq 3$ we immediately predict the curve of fig. 23 which is compared with the data

Note the general feature that as $\omega \to \infty$ ($x \to 0$) the π^+/π^- ratio tends to unity (sea dominance). Coming to smaller ω the ratio rises and then as $\omega \to 1$ falls below 1 due to dominance of the U_T quark. In general with U quark dominance

$$\frac{\pi^+}{\pi^-}(x \to 1) \longrightarrow \frac{1}{\eta} \text{ in en} \qquad (9.29)$$

$$\longrightarrow \eta \text{ in ep} \qquad (9.30)$$

Footnote A cautionary note is provided by Hanson at the Stanford Symposium. Plotting the π^+/π^- ratios against x and also W for various Q^2 (N the mass of hadronic system) one cannot yet tell if i) π^+/π^- is a function only of ω i.e. scales in $\omega(x)$ or ii) function only of W. The variation of π^+/π^- with W or x over the measured range of parameters is too small to see a significant difference between the two.

Further oritentation on the significance of these production ratios is obtained by noting that in the photon fragmentation region at $Q^2 = 0$ $\pi^+/\pi^- = 0.8$ This is quite different from the values 1.2 to 1.3 predicted at moderate ω in the present model for $Q^2 \neq 0$.

Sum Rules in eN → eh...

Normalising to $F_1^{eN}(x)$, the number of hadrons i in the current fragmentation region, with momentum z in an experiment done at fixed x reads

$$N^i(z,x) = \frac{4}{9}\left(u(x)D_u^i(z) + \bar{u}(x)D_{\bar{u}}^i(z)\right) + \frac{1}{9}\left(d(x)D_d^i(z) + \bar{d}(x)D_{\bar{d}}^i(z)\right) + \frac{1}{9}\left(s(x)D_s^i(z) + \bar{s}(x)D_{\bar{s}}^i(z)\right) \qquad (9.31)$$

plus further possible contributions from charmed quarks etc. We can simplify this messy expression by studying, for example, the excess of π^+ over π^-

$$N^{\pi^+}(z,x) - N^{\pi^-}(z,x) = \left[D_u^{\pi^+}(z) - D_u^{\pi^-}(z)\right]\left[\frac{4}{9}(u-\bar{u}) - \frac{1}{9}(d-\bar{d})\right](x) \qquad (9.32)$$

where we used relations like $D_s^{\pi^+} = D_s^{\pi^-}$ etc. (eq. 9.7). (This exression is true in general since further quarks with I = 0 will not contribute to the $\pi^+\pi^-$ difference).

Since we know from the proton a neutron charge sum rules (eq. 4.24-4.26)

$$\int[u(x) - \bar{u}(x)]\,dx = \int[d(x) - \bar{d}(x)]\,dx = 2 \qquad (9.33)$$

then

$$\int dx\,(N_{ep}^{\pi^+} - N_{ep}^{\pi^-})(z,x) = \left[D_u^{\pi^+}(z) - D_u^{\pi^-}(z)\right]\frac{7}{9} \qquad (9.34)$$

Similarly on neutron targets one derives (interchanging u, d in eq. 9.32)

$$N_{en}^{\pi^+}(z,x) - N_{en}^{\pi^-}(z,x) = \left[D_u^{\pi^+}(z) - D_u^{\pi^-}(z)\right]\left(\frac{4}{9}(d-\bar{d}) - \frac{1}{9}(u-\bar{u})\right)(x) \qquad (9.35)$$

and so

$$\int_0^1 dx\,(N_{en}^{\pi^+} - N_{en}^{\pi^-})(z,x) = \left[D_u^{\pi^+}(z) - D_u^{\pi^-}(z)\right]\frac{2}{9} \qquad (9.36)$$

Consequently, independent of z or $P_{n,t}^2$,

$$\frac{\int dx\,(N^{\pi^+}(z,x) - N^{\pi^-}(z,x))^{en}}{\int dx\,(N^{\pi^+}(z,x) - N^{\pi^-}(z,x))^{ep}} = \frac{2}{7} \qquad (9.37)$$

Experimentally it is more useful to integrate over all z and since

$$\frac{\int dz\, N_{en}^{\pi^+}(z,x)}{\int dz\, N_{ep}^{\pi^+}(z)} \equiv \frac{\int dz \left(\frac{d\sigma}{dz}\right)_{en}^{\pi^+}}{\int dz \left(\frac{d\sigma}{dz}\right)_{ep}^{\pi^+}} \qquad (9.38)$$

then

$$\frac{\int_0^1 dx\, F_1^{en}(x)\left(\langle n_{\pi^+}\rangle_{en} - \langle n_{\pi^-}\rangle_{en}\right)}{\int_0^1 dx\, F_1^{ep}(x)\left(\langle n_{\pi^+}\rangle_{ep} - \langle n_{\pi^-}\rangle_{ep}\right)} = \frac{2}{7} \qquad (9.39)$$

where $\langle n_i \rangle$ is the average multiplicity of particle i as a function of x. This sum rule was derived by Gronau et al. but is not yet well tested by data.

c. $e^+e^- \to h\ldots$

In equation 9.8 we have

$$\frac{1}{\sigma_{TOT}}\frac{d\sigma}{dz}(e^+e^- \to h\ldots) = \frac{\sum_i e_i^2 \{D_i^h(z) + D_{\bar{i}}^h(z)\}}{\sum_i e_i^2} \qquad (9.40)$$

or, since*

$$\sigma_{TOT}/\sigma_{\mu\mu} \equiv R = 3\sum_i e_i^2 \quad \text{then}$$

$$\frac{1}{\sigma_{\mu\mu}}\frac{d\sigma}{dz}(e^+e^- \to h\ldots) = 3\sum_i e_i^2 \{D_i^h(z) + D_{\bar{i}}^h(z)\} \qquad (9.41)$$

If for small z $D(z) \sim 1/z$ (e.g. by analogy with the $f(x) \sim 1/x$ for the probability of finding given quarks in the hadron) then a logarithmic rise in multiplicity is predicted since on integrating over z

$$R\langle n_h \rangle = \int_{z_{min}}^1 \frac{1}{\sigma_{\mu\mu}}\frac{d\sigma}{dz}\,dz = 3\sum_i e_i^2 \int_{\frac{2m}{\sqrt{q^2}}}^1 [D_i^h + D_{\bar{i}}^h]\,dz \qquad (9.42)$$

and the lower limit on the z integral generates the logarithmic growth in Q^2. We have already seen (fig. 22) some evidence that $D(z) \sim 1/z$ as $z \to 0$ and so it is interesting to find that there may be a logarithmic growth of the multiplicity in $e^+e^- \to h\ldots$ (fig. 24).

Since $\sigma_{\mu\mu} = \frac{4\pi\alpha^2}{3s}$ then we can rewrite eq. 9.41 to read

$$s\frac{d\sigma}{dz}(e^+e^- \to h\ldots) = \frac{4\pi\alpha^2}{3} 3\sum_i e_i^2 \{D_i^h(z) + D_{\bar{i}}^h(z)\} \qquad (9.43)$$

$$\simeq 88 \times 3 \sum_i e_i^2 \{D_i^h(z) + D_{\bar{i}}^h(z)\}\ \text{nb-GeV}^2$$

*Footnote: The factor 3 is for three colours of quarks.

The distributions in $s\frac{d\sigma}{dz}$ are shown in fig. 25 and do show the possibility of scaling for $z > 0.5$. We dont expect scaling for all s here because R is rising as one passes through this complicated region. It does, however, appear that the data scale for all s when $z \geq 0.5$. This, and the z, s dependence of the scaling violation are nicely seen in fig. 2 which plots $s\,d\sigma/dz$ versus $E_{c.m.}$ for various z intervals. Scaling would imply that $s\frac{d\sigma}{dz}$ should be independent of $E_{c.m.}$ for any fixed z.

If the entire rise in R is due to pair production of new particles $e^+e^- \to U^+U^-$ which decay immediately into the observed hadrons then the final decay products at threshold should be limited to $z < 0.5$ since each new U is carrying half the energy. If each of these then decays, clearly half the momentum of any single decay product cannot exceed ½ of the total energy and hence $z < 0.5$. For U production slightly above threshold a few decay products can have $z > 0.5$ but their effect will be negligible so the argument holds true.

Bearing this is mind, look again at the figure 26. For $z > 0.5$ we see scaling (independence of $s\frac{d\sigma}{dz}$) for the full range of $3 \leq E_{c.m.} \leq 8$ GeV. For $z < 0.5$ the data have rescaled above 4 GeV except at the smallest values of z. Here the finite energy means that we are still seeing threshold effects and so we dont expect scaling to set in until PEP/PETRA energies. Hence, semi-quantitatively we can understand the observed behaviour as a combination of threshold and scaling phenomena.

Consequently we may suppose that the $s\frac{d\sigma}{dz}$ distribution is a superposition of "old" and "new".

If this is indeed true, then the data at 3 GeV is due entirely to "old" physics and moreover is exhibiting (for $z \geq 0.2$) the scaling behaviour of the uds quark degrees of freedom. Hence we might analyse this data in terms of the relation

$$\frac{1}{\sigma_{\mu\mu}}\frac{d\sigma}{dz}(e^+e^- \to h\ldots) = 3\sum_{i=uds} e_i^2 \{D_i^h(z) + D_{\bar{i}}^h(z)\} \qquad (9.44)$$

and compare with the analogous data on inclusive hadron production in lepto-induced reactions as discussed previously.

As orientation and to simplify matters let us just make the approximation that only the u quark is important (it is the most probable quark in the proton and also has the biggest squared charge by a factor of four). Then for ep → eh...

$$\frac{1}{\sigma_{TOT}}\frac{d\sigma}{dz} = \sum_i e_i^2 f_i(x) D_i^h(z) \Big/ \sum_i e_i^2 f_i(x) \to D_u^h(z) \qquad (9.45)$$

and hence

$$\frac{1}{\sigma_{tot}}\left[\frac{d\sigma}{dz}(ep\to eh^{+}..) + \frac{d\sigma}{dz}(ep\to eh^{-}..)\right] \simeq D_u^{h^+}(z) + D_u^{h^-}(z) \qquad (9.45)$$

For e^+e^- annihilation at $\sqrt{Q^2} \lesssim 3.5$ GeV (where by hypothesis only the uds degrees of freedom contributes), taking $u\bar{u}$ as the largest contributor to R then

$$\frac{1}{2\sigma_T}\left[\frac{d\sigma}{dz}(e^+e^-\to h^+..) + \frac{d\sigma}{dz}(e^+e^-\to h^-..)\right] \qquad (9.46)$$

$$\simeq \frac{1}{2}\left[D_u^{h^+}(z) + D_{\bar{u}}^{h^-}(z) + D_{\bar{u}}^{h^+}(z) + D_u^{h^-}(z)\right] = D_u^{h^+}(z) + D_u^{h^-}(z)$$

and so finally one has the immediate comparison

$$\frac{1}{\sigma_T}\left(\frac{d\sigma}{dz}\right)(ep\to eh^{\pm}..) = \frac{1}{2\sigma_T}\left(\frac{d\sigma}{dz}\right)(e^+e^-\to h^{\pm}..) \qquad (9.47)$$

This comparison is shown in fig. 27 and agreement is excellent at large z where different choices for the comparison variable are less important.*

Ultimately it will be nice to see if π, K, p production separately satisfy this relation since at present $h^{\pm}$ means <u>all</u> hadrons of the relevant charge. Also one will attempt to separate each quark's individual contribution using ν and e data; one might already think of doing this using the data in figs. ignoring any q^2 dependence and assuming that only uds quarks are important. Then as one crosses charm (?) threshold and rescaling is seen (?) the role of the c quark fragmentation can be examined. This is in principle a straightforward extension of the present discussion which should provide enough material for the interested reader to perform the exercise for her or himself.

10. <u>Angular distributions of hadrons in $e^+e^- \to h$ anything</u>

The stored $e^{\pm}$ beams circulate in a magnetic field whose direction ($\hat{y}$) is perpendicular to the plane ($x\hat{z}$) of the storage ring. After a period of time the positrons (electrons) tend to populate the state where their spins are parallel (antiparallel) to the guide magnetic field, this state having lower energy than the opposite spin orientation. Consequently the storage ring beams are polarised in the $\hat{y}$ direction. If the polarisation is 100% then the photon created by the e^+e^- annihilation has zero helicity along the $\hat{y}$ direction,

$$J_y^{\gamma} = 0 \qquad (10.1)$$

we will calculate the angular distribution of a hadron h produced by such a polarised photon in

$$e^+e^- \to \gamma \to h + \text{anything}$$

If the hadron emerges at angle θ relative to the $\hat{z}$ axis (the e^+ direction) and ϕ relative to the $x\hat{z}$ plane of the ring then the direction of its momentum vector is

$$\hat{p}_h = (\sin\theta\cos\phi,\ \sin\theta\sin\phi,\ \cos\theta) \qquad (10.2)$$

illustrated in the figure 28, so that the angle β between the hadron momentum vector and the $\hat{y}$ axis is given by

$$\cos\beta = \sin\theta\sin\phi \qquad (10.3)$$

The expression for the angle β enables us to immediately calculate

$$\frac{d\sigma}{d\Omega}(e^+e^-\to h..)$$

If λ = helicity of the photon along h (i.e. spin projection along $\hat{p}_h$)

then since

β = angle between $\hat{p}_h$ and $\hat{y}$

and

photon spin projection = 0 along $\hat{y}$

we have

$$\left(\frac{d\sigma}{d\Omega}\right) \propto \sum_{\lambda=\pm1,0} |A_\lambda|^2 \left|d^1_{\lambda 0}(\beta)\right|^2 \qquad (10.4)$$

($d^1_{MM'}$, because J = 1 for e^+e^- annihilation through a single photon). Parity forces

$$|A_1| = |A_{-1}| \qquad (10.5)$$

and so

$$\left(\frac{d\sigma}{d\Omega}\right) \propto |A_1|^2\sin^2\beta + |A_0|^2\cos^2\beta \qquad (10.6)$$

*<u>Footnote</u>: Gilman[2p] here used $X_{c.m.}$ for $ep \to eh..$ and $x = \frac{2p}{\sqrt{Q^2}}z$ for $e^+e^- \to h..$ As $Q^2 \to \infty$, $X, X_{c.m.} \to z$. At present energies the choice of variables can make a significant difference at small z but differences are less important at large z since all particles are relativistic there.

We define the transverse and longitudinal cross-sections proportional to $|A_1|^2$ and $|A_0|^2$ respectively, and these are functions of Q^2 (the photon squared mass) and p_h (the momentum of the produced hadron)*. These functional dependences are implicit in all the following equations. We can therefore write

$$\left(\frac{d\sigma}{d\Omega}\right)_{pol.} = \sigma_T \sin^2\beta + \sigma_L \cos^2\beta = \sigma_T + (\sigma_L - \sigma_T)\sin^2\theta\sin^2\phi \qquad (10.7)$$

The subscript "pol." is to remind us that this is the cross-section arising from a completely polarised photon (e^+e^- beams). If instead we had unpolarised beams then

$$\left(\frac{d\sigma}{d\Omega}\right)_{unpol} = \sigma_T + (\sigma_L - \sigma_T)\sin^2\theta \cdot \frac{1}{2} \qquad (10.8)$$

since $\langle\sin^2\phi\rangle = \frac{1}{2}$. Consequently in general, for a degree of polarisation P

$$\left(\frac{d\sigma}{d\Omega}\right) = (1-P^2)\left(\frac{d\sigma}{d\Omega}\right)_{unpol.} + P^2\left(\frac{d\sigma}{d\Omega}\right)_{pol.} \qquad (10.9)$$

and so

$$\left(\frac{d\sigma}{d\Omega}\right) = \frac{1}{2}(\sigma_T+\sigma_L)\left[1 + \alpha\left(\cos^2\theta + P^2\sin^2\theta\cos 2\phi\right)\right] \qquad (10.10)$$

with

$$\alpha \equiv \frac{\sigma_T - \sigma_L}{\sigma_T + \sigma_L} \qquad (10.11)$$

Equation 10.10 is the general angular distribution for the inclusive hadron production in electron positron annihilation through one photon. From the observed angular distributions of h one can determine $\sigma_L/\sigma_T(z,Q^2)$ which contains the interesting dynamical information (in the model where the hadrons are the fragmentation products of spin ½ partons then $\sigma_L/\sigma_T \sim 1/Q^2$).

In <u>principle</u> one can determine σ_L/σ_T, or equivalently α, from the θ distribution alone and so the polarisation P gives no additional information. In <u>practice</u> since the SPEAR detector has rather limited acceptance in θ, $|\cos\theta| \lesssim 0.6$, (due to the open ends of the cylindrical detector which allow the beams to enter and depart) while there is complete acceptance in ϕ, then it is easier to separate σ_L/σ_T from the ϕ dependence, i.e. exploiting the polarised beams. This is illustrated clearly in the data (Schwitters, Stanford Conference 1975). Integrating over ϕ one has

$$\frac{d\sigma}{d\Omega} = \frac{1}{2}(\sigma_T+\sigma_L)(1+\alpha\cos^2\theta) \qquad (10.12)$$

*<u>Footnote</u>: More usually chosen as Q^2 and $z = 2P/\sqrt{Q^2}$, see section 9.

and the θ distributions very poorly determine α (fig. 29).

The inclusive azimuthal distributions for particles with $z > 0.3$ and $|\cos\theta| \lesssim 0.6$ are exhibited in figs. 27 for two energies 7.4 GeV and 6.2 GeV in the c.m. There is a very clear $\cos 2\phi$ dependence in the data sample taken at $E_{c.m.} = 7.4$ GeV. At 6.2 GeV there happens to be a depolarising resonance in the SPEAR ring (a matching of the machine parameters and the g_e-2 such that the spins of $e^\pm$ process by an exact integer number of turns per orbit). Hence at 6.2 GeV the beams are "accidentally" unpolarised and an isotropic ϕ distribution emerges.

Using the $E_{c.m.} = 7.4$ GeV data with its clear $\cos 2\phi$ dependence we can determine α by making a best fit to the form of $d\sigma/d\Omega$ (eq. 10.10) once we have obtained the magnitude of ρ^2. This quantity is found by fitting the distributions for $e^+e^- \to \mu^+\mu^-$ data which are collected at the same time as the hadronic production data and as $(\sigma_L/\sigma_T)_{\mu^+\mu^-} \simeq 0$ then

$$\left(\frac{d\sigma}{d\Omega}\right)^{\cdot}_{e^+e^-\to\mu^+\mu^-} = \frac{1}{2}\sigma_T\left(1+\cos^2\theta+P^2\sin^2\theta\cos 2\phi\right) \qquad (10.13)$$

Hence P^2 is determined and found to be 0.46 ± 0.05 at this energy. One now uses this information in fitting the hadronic sample and α (or σ_L/σ_T) is obtained for $e^+e^- \to h$...

The results for σ_L/σ_T (and α) as functions of z at $E_{c.m.} = 7.4$ GeV are shown in fig. 30. At low z where the hadron h is recoiling against a high mass system near to threshold (it is produced nearly at rest) σ_L and σ_T are almost equiprobable. At $z \gtrsim 0.2$, where Bjorken scaling was observed (section 9), σ_T dominates, characteristic of production of pairs of spin ½ particles (c.f. $\mu^+\mu^-$).

Hence the data are consistent with the model where the observed hadrons are emitted by spin ½ partons.

Further support for the idea that the hadrons are parton fragments comes from a study of the multiprong hadronic events, where it is found that these have a "jet" structure (limited momentum transverse to some axis). This phenomenon is familiar in hadron physics and is a natural consequence of the parton model. The picture is that at high $E_{c.m.}$ the spin ½ partons are produced with angular distribution typical of $\alpha = 1$ and that the final state observed hadrons will limit momenta transverse to the direction θ in which the partons were produced. Hence two jets of particles will be expected, the jet axis being the memory of the original parton direction.

In those events with ≥ 3 hadrons a search was made for an axis which minimised the sum of the squares of the momenta perpendicular to it. For any event, having found this axis, then a quantity S called the "sphericity" is defined.

$$S \equiv 3\sum_i p_{T_i}^2 \Big/ 2\sum_i p_i^2 \; ; \; 0 \le S \le 1 \qquad (10.14)$$

where p_i, p_{T_i} are the i-th particle's momenta and its momenta transverse to the jet axis. Events with $S \to 0$ are jetlike while $S \to 1$ are spherical. The sphericity distributions at three different energies are shown in fig.I9 of Scwitter's talk on page 20 of the Stanford conference. The mean sphericity plotted versus $E_{c.m.}$ is shown in fig31 and as the energy increases the increasingly jetlike character of the events is apparent.

While much work still remains to be done here these effects do appear to b e more than j ust correlations arisisng from energy-momentum conservation and are genuine multiparticle effects. A comparison with a Monte Carlo jet model with $\langle p_T \rangle \simeq 350 \text{MeV}/c$ is an excellent description of the data whereas the Monte Carlo phase space model is poor. The inclusive angular distribution is also well fitted by the jet model and for $E_{c.m} \simeq 7.4\text{GeV}$ the display is shown in fig32with

$$\alpha_{jet} = 0.78 \pm 0.12$$

The momenta of the hadrons relative to the jet produce the range of values in the shaded part of the figure.

BIBLIOGRAPHY

FI. R.P.Feynman "Ph oton-Hadron interactions (Benjamin,N.Y. I972)

Proceedings of the Stanford Conference I975 In particular the talks by Gilman,Harari, Scwitters,Llewellyn Smith and as cited in the list by chapters below.

C.H.Llewellyn Smith,Physics Repts3C,264(72)

P.Landshoff,CERN-Rept-74-22,(I974 Summer School in this series)

J.Kuti and V.Weisskopf,Phys RevD4,34I8(7I)
P.Landshoff and J.Polkinghorne,Nucl.Phys B28,240(7I)

Chapter 6-7

HPWF collaboration:Gargamelle collaboration I5'bubble chamber : pp5II-57I of Stanford Conference,op cit

Inelastic electron and muon scattering: L.Mo and also R.Taylor in P65I-670 of Stanford conference op cit.

CSS: F.E.Close,D.M.Scott and D.Sivers, Phys.Letters62B,2I3(76)

Chapter9

J.Cleymans and R.Rodenberg,Phys RevD9,I55(74)
J.Dakin and G.Feldman,Phys.RevD8,2862(73)

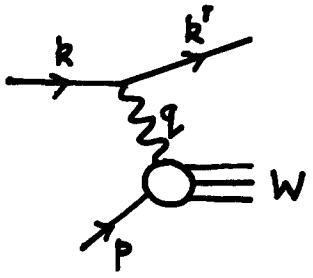

Fig. 1 Inelastic electron scattering

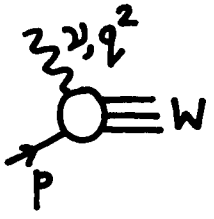

Fig. 2 Virtual photoabsorption

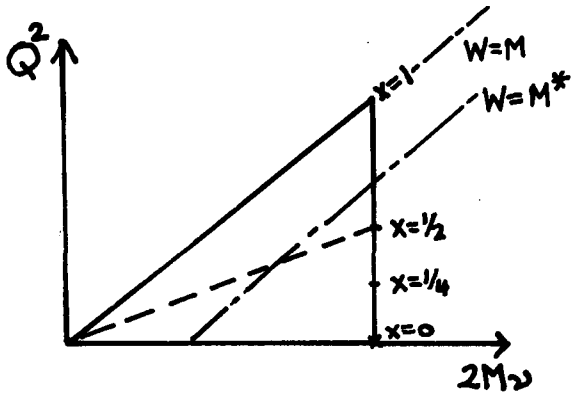

Fig. 3 ν, Q^2 kinematic region

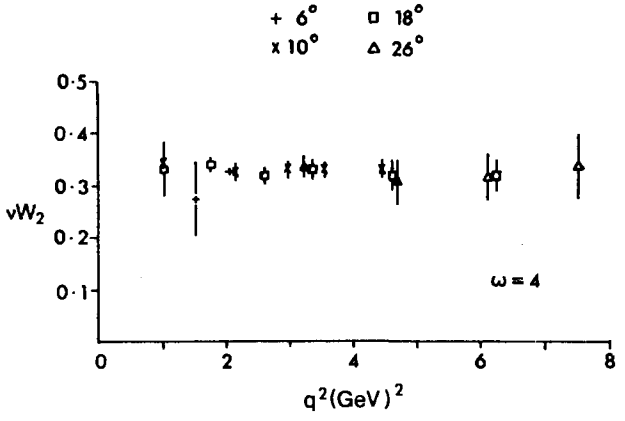

Fig. 4 $\nu W_2(\omega=4)$-Q^2 independence

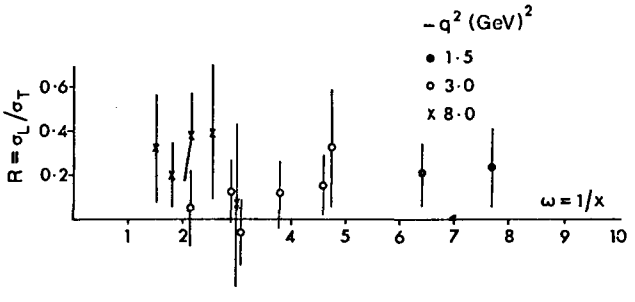

Fig. 5 $R(\sigma_L/\sigma_T)$

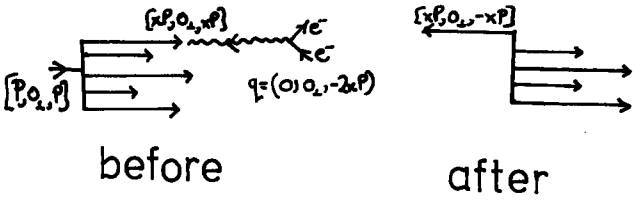

Fig. 6 Current-nucleon scattering in the current-parton Breit frame

Fig. 7 Electron scattering in a Coulomb field

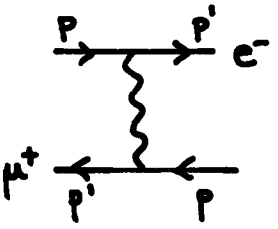

Fig. 8 Electron-muon scattering

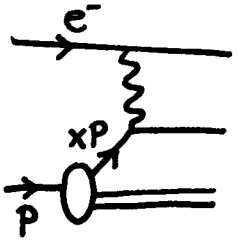

Fig. 9 Electron-parton scattering

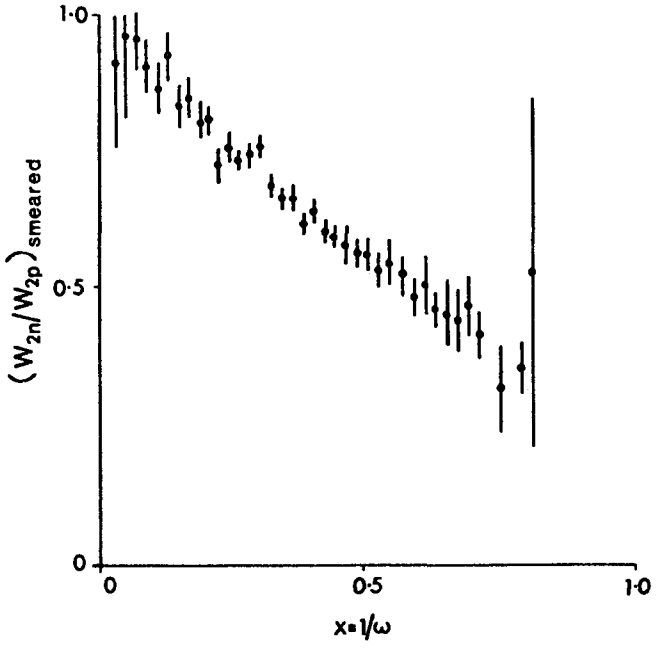

Fig. 10 Neutron to proton structure function ratio for electron scattering

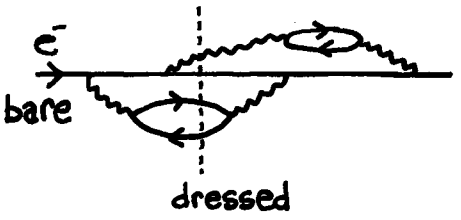

Fig. 11 Dressing a bare electron in QED

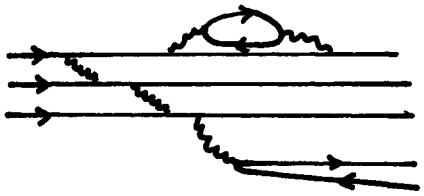

Fig. 12 Dressing a bare quark with gluons

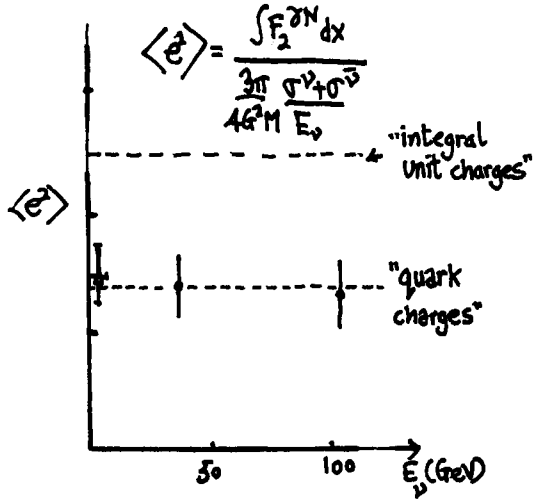

Fig. 13 CERN-GGM data comparing inelastic neutrino and SLAC data

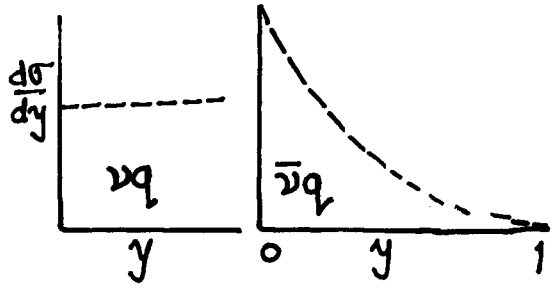

Fig. 14 y dependence of neutrino-quark and antiquark scattering

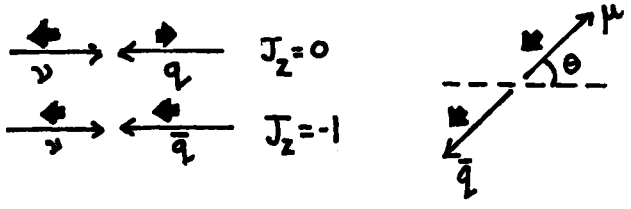

Fig. 15 Neutrino-quark and antiquark angular distributions

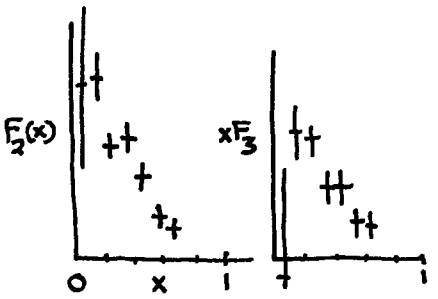

Fig. 16 F_2 and xF_3 from Gargamelle

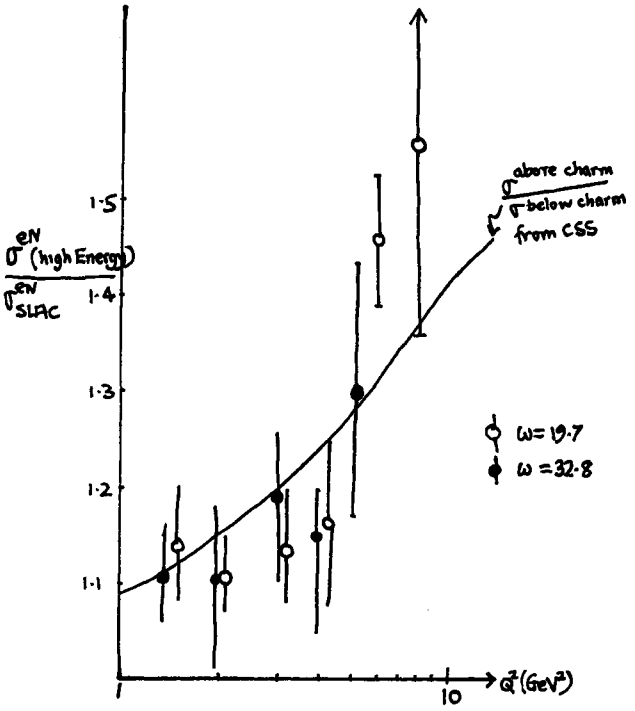

Fig. 17 Violation of scaling in inelastic muon scattering above charm production threshold and comparison with data from the Chen-Hand experiment (from CSS)

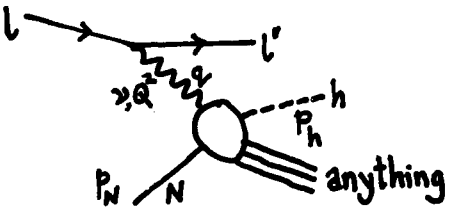

Fig. 18 Inclusive hadron production in the parton model

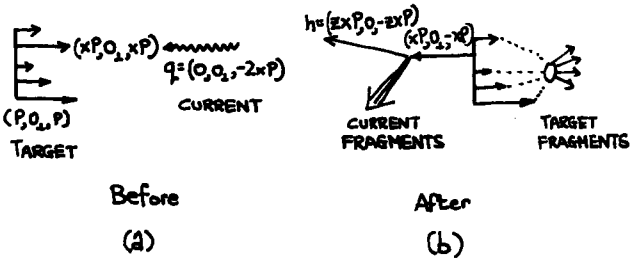

Fig. 19 Quark fragmentation into hadrons

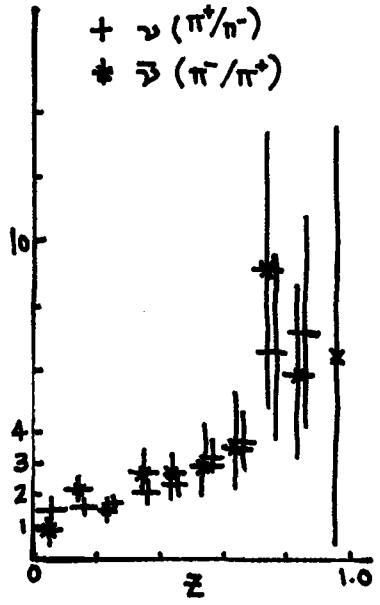

Fig. 20 Gargamelle data on pion production by neutrino and antineutrino beams

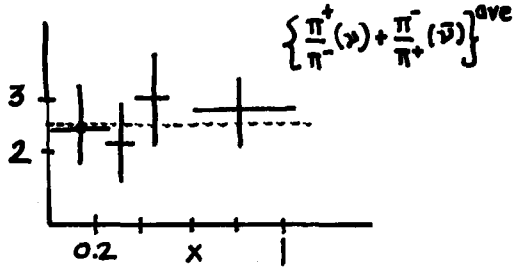

Fig. 21 x independence of pion production in neutrino experiments (π^+/π^- ratio) for $0.3 \leq z \leq 0.7$

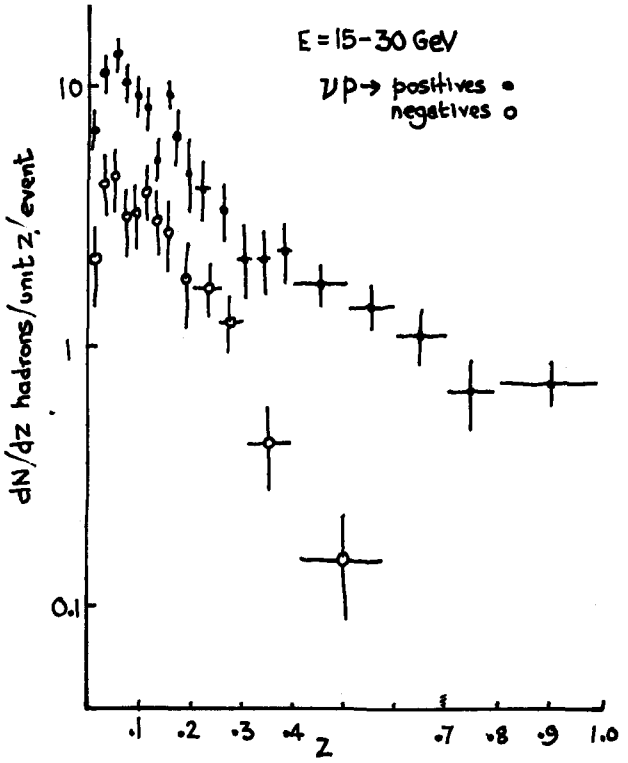

Fig. 22 Positive and negative hadron production by neutrinos in the Fermilab 15' bubble chamber

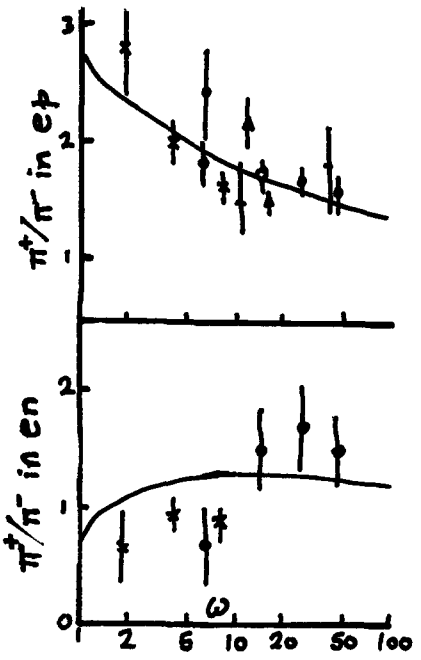

Fig. 23 ep, en → π^+/π^-

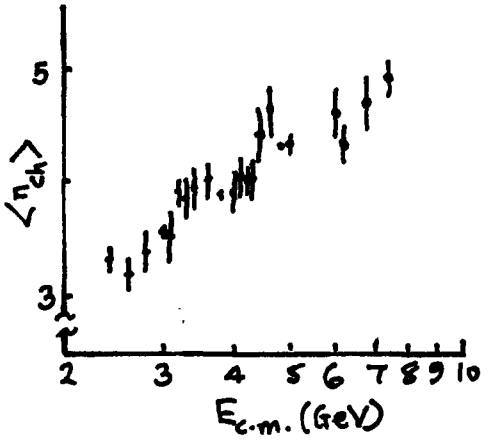

Fig. 24 Logarithmic growth in hadron multiplicity in e^+e^- annihilation

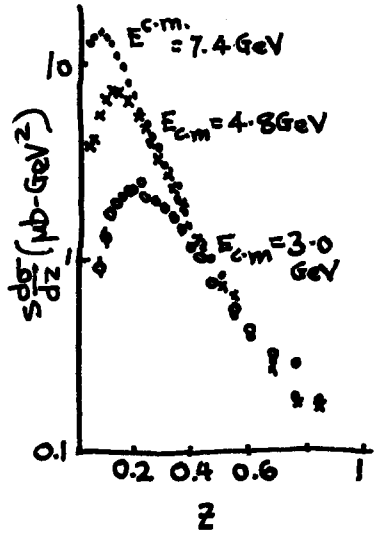

Fig. 25 $s(d\sigma/dz)$ for $e^+e^- \rightarrow h$ ...

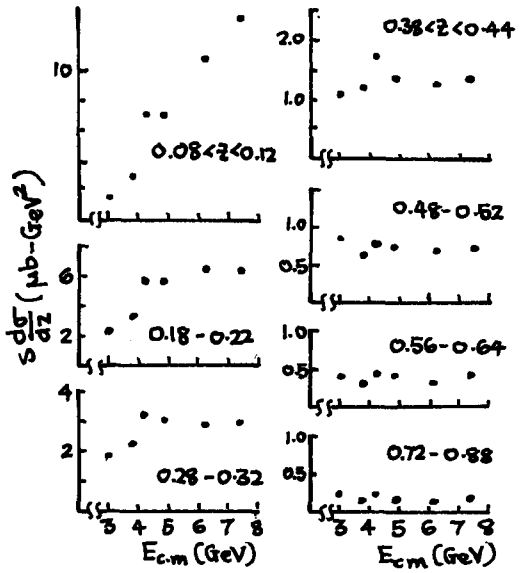

Fig. 26 As fig. 25, plotted against $E_{c.m.}$

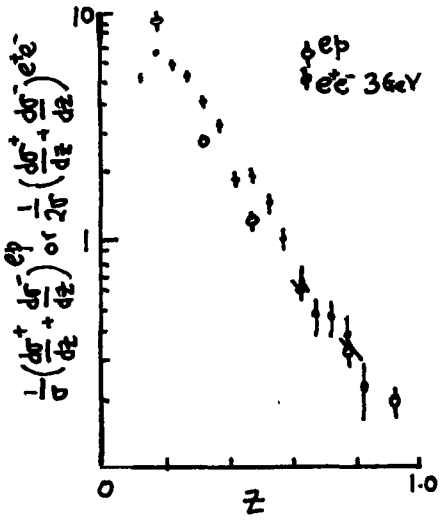

Fig. 27 Comparison of hadron production in ep and $e^+e^- \to h$ ...

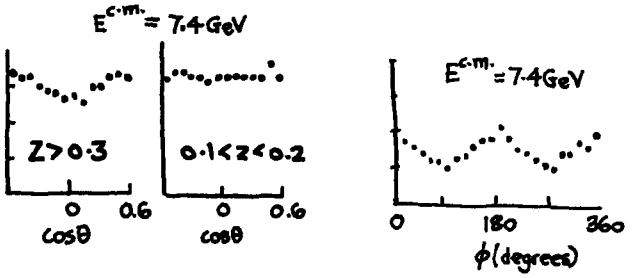

Fig. 29 Angular distribution of $e^+e^- \to h$ ...

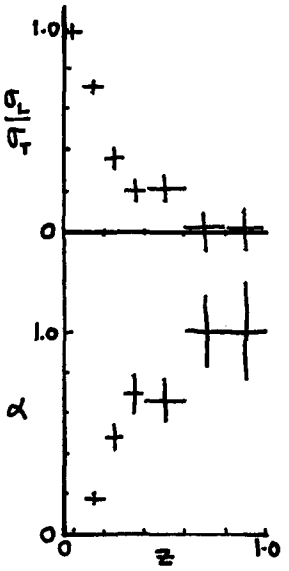

Fig. 30 (σ_L/σ_T) and α at 7.4 GeV

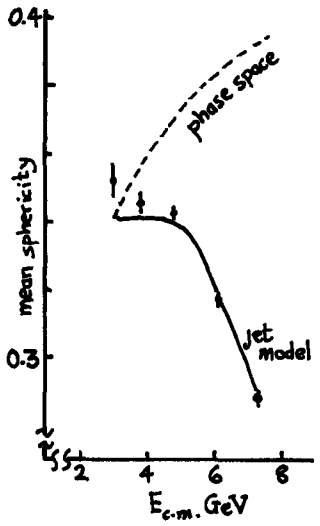

Fig. 31 Mean sphericity versus $E_{c.m.}$

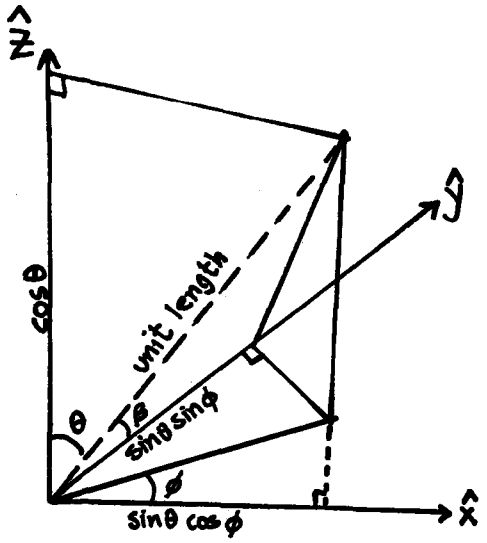

Fig. 28 $\hat{p}_h$ vector

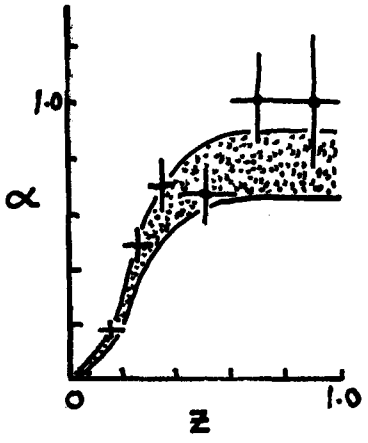

Fig. 32 Jet model and data at 7.4 GeV

AN ELEMENTARY INTRODUCTION TO YANG-MILLS THEORIES AND TO THEIR APPLICATIONS TO THE WEAK AND ELECTROMAGNETIC INTERACTIONS

L. Maiani (*)
Laboratori di Fisica, Istituto Superiore di Sanita, Roma, Italy.
and
Istituto Nazionale di Fisica Nucleare, Roma, Italy

Introduction

Gauge theories have been first considered by Yang and Mills more than twenty years ago. Their aim was to construct a theory where the global isospin symmetry of strong interactions could be extended into a local symmetry, so that one could be allowed to perform independent isospin transformations in different space-time regions.

Invariance under space time dependent symmetry transformations is, in fact, so intimately related to the very notion of a local field theory, that it was apparent from the outset that, if a local field theory had to be relevant at all in describing the fundamental interactions, the Yang-Mills concept had to play a fundamental role.

This explains why gauge theories have appeared, from time to time, in different parts of particle physics.

In strong interactions, the original Yang-Mills theory led to the concept of universal vector meson couplings, ρ dominance etc., and played an important role in the discovery of the SU(3) symmetry. Consideration of unified gauge theories for weak and e.m. interactions was started by Schwinger as early as in 1957.

Progress has been slow, however, and difficult, for various reasons. Invariance under local gauge transformations leads to massless gauge fields. One had to reconcile this fact with the remarkable absence of massless vector mesons both in strong and in weak interactions. Furthermore, to get a consistent perturbative treatment of gauge theories proved to be a formidable problem, which took a long while to be solved.

In the middle sixties, the introduction into Yang-Mills theories of the notion of spontaneous symmetry breaking provided an appealing way of giving gauge fields a mass (the Higgs mechanism). This opened the way to the construction of concrete unified theories for the weak and e.m. interactions of the known leptons, accomplished by Weinberg and Salam. Consideration of hadronic weak interactions had to wait a little longer, however, until in 1970 it was realized by Glashow, Iliopoulos and Maiani that a new hadronic quantum number (charm) was needed.

On the more formal side, investigations on the quantization and the perturbative expansion of gauge theories, associated, among others, to the names of De Witt, Feynman, Faddeev and Popov, Veltman, culminated in 1971 in the work of 't Hooft, whereby the complete renormalization program for a spontaneously broken gauge theory was accomplished.

This and the subsequent works in this field, put the Yang-Mills theories of weak and e.m. interactions at the same theoretical level as quantum electrodynamics. The experimental discovery of weak neutral currents and the most recent evidence for charmed particles gave them the concrete support of real facts.

The success of the quark model, and the idea of an unbroken color symmetry for strong interactions has led to further developments. Asymptotically free gauge theories have been proposed, where the observed strong interactions arise from a more fundamental, Yang-Mills, interaction of quarks with the colored gluons. Prompted by the observed scaling in deep inelastic processes, the elaboration of such theories has been made possible by the spectacular progress achieved in field theory in recent years (K. Wilson works on renormalization group, the Callan-Szymanzik equation, etc.).

It is conceivable, though by no means proved, that all the fundamental interactions (except gravity) are indeed Yang-Mills interactions. In this connection, it is interesting to point out a change which has taken place, in going from the original Yang-Mills theory to the most recent ones.

In the former, strong interactions were associated to the observed isospin symmetry. In the color gauge theories, strong interactions are associated to the hidden color symmetry, while isospin, SU(3) and all other flavor related broken symmetries are to be associated to the gauge group of the weak and e.m. interactions.

(*) Address after Nov. 1, 1976. Istituto di Fisica dell'Universita, Roma, Italy.

In these lecture notes, we shall deal exclusively with a gauge theory of weak and e.m. processes. The aim is to give an elementary introduction to the subject by discussing the general underlying ideas, and the way these ideas can be put to work in a concrete theory, based on the gauge group $SU(2) \otimes U(1)$.

All our arguments will be carried on at a classical level, or, equivalently, at a level where only tree Feynman diagrams (no internal loops) are considered. This limitation has excluded from the outset any reference to strong interaction gauge theories, where e.g. renormalization effects are essential. Finally, while I tried to indicate as clearly as possible where theory makes contact to experiments, no detailed comparison is carried out of the theoretical predictions with the presently available experimental results. For many topics, this is done in the other courses.

The plan of these lectures is as follows. In Section 1 we review the notion of a global symmetry and introduce the associated conserved currents. In Sections 2 and 3 we discuss the general idea of local gauge symmetry, the construction of the Yang-Mills lagrangian, and work out the elementary properties of the resulting interaction. The connection to observed weak interactions is considered in Section 4, where a mass is given to the gauge fields by adding an ad hoc term to the lagrangian. Spontaneous symmetry breaking is discussed in Section 5, and the Higgs mechanism in Section 6, using as a working example the bosonic sector of the Weinberg-Salam model. The weak interactions of leptons are considered in Section 7, where contact is first made to experimentally testable predictions. In Section 8 we discuss the e.m. interaction of the charged intermediate bosons. The way one can give a mass to elementary fermions is discussed in Section 9, with reference to the leptons. The general formalism is worked out in detail, and the possible arising of electron and muon number violation is discussed. Hadronic weak interactions are discussed in Section 10, with reference to the four quark model, and the possibility of still more quark types is considered in Section 11. Finally, Section 12 contains a few conclusive remarks, and some comments on the open problems.

Given the pedagogical character of these lectures, very few references are made to original papers. Reference to the original contributions can be found in the general references listed at the end.

1. Global Symmetries

We shall work in the framework of lagrangian field theory. The dynamics is therefore specified by the lagrangian $\mathcal{L}$, which is a function of the various fields (collectively denoted by ψ) and of their 4-space derivatives ($\partial_\mu \psi$). The action, S, is the integral over 4-space of the lagrangian and the equations of motion are obtained by equating to zero the variation of S , resulting from infinitesimal, arbitrary variations of the fields. In formulae :

$$\mathcal{L} = \mathcal{L}(\psi, \partial_\mu \psi) \tag{1.1}$$

$$S = \int d^4x \, \mathcal{L} \tag{1.2}$$

$$0 = \delta S = \int \left[\frac{\partial \mathcal{L}}{\partial \psi} \delta\psi + \frac{\partial \mathcal{L}}{\partial \partial_\mu \psi} \partial_\mu \delta\psi \right] \tag{1.3}$$

Partially integrating the term with the derivative in eq. (1.3), discarding integrals of 4-divergences, and setting to zero the coefficient of $\delta\psi$, we get from (1.3) the equation of motion :

$$\frac{\partial \mathcal{L}}{\partial \psi} - \partial_\mu \frac{\partial \mathcal{L}}{\partial \partial_\mu \psi} = 0 \tag{1.4}$$

If we have many fields ψ_i , we get an equation like (1.4) for each field component.

We have a global symmetry whenever it is possible to perform an infinitesimal transformation :

$$\psi \to \psi' = \psi + \delta\psi \tag{1.5}$$

such that : i) it leaves $\mathcal{L}$ invariant : $\mathcal{L}(\psi') = \mathcal{L}(\psi)$
ii) it is the same at all space-time points.

Furthermore, we speak of an <u>internal</u> symmetry when the transformation (1.5) does not mix fields with different space-time properties. Stated differently, internal symmetries correspond to transformations which commute with the space-time transformations (Lorentz transformations and 4-dimensional translations). We will restrict, in the following, to internal symmetries, choosing as a working example the isospin symmetry.

Suppose we have a doublet of fields, which can have either spin 1/2 (e.g. proton and neutron, or u and d quarks) or spin zero (e.g. K^+ and K^0). We collect these two fields in a single isospinor :

$$\psi = \begin{pmatrix} p \\ n \end{pmatrix} \quad \text{or} \quad \begin{pmatrix} K^+ \\ K^0 \end{pmatrix}$$

Consider now the infinitesimal transformations :

$$\psi' = \psi + \delta\psi$$

$$\delta\psi = i \varepsilon^a \frac{\tau^a}{2} \psi(x) \qquad a = 1, 2, 3 \tag{1.6}$$

where τ_a are the 2×2 Pauli matrices and ε^a are three infinitesimal parameters. Here and in the following we understand to sum over repeated indices. The τ_a matrices obey the commutation rules :

$$\left[\frac{\tau_a}{2}, \frac{\tau_b}{2}\right] = i\,\varepsilon_{abc}\,\frac{\tau_c}{2} \qquad (1.7)$$

(ε_{abc} is the totally antisymmetric tensor, $\varepsilon_{123} = 1$).

We say that $\mathcal{L}$ is isospin-invariant if :

$$\mathcal{L}(\psi') = \mathcal{L}(\psi) \qquad \text{i.e.}$$
$$\delta\mathcal{L} = 0$$

An important consequence of this is the existence of a triplet of conserved currents (Noether's theorem):

$$0 = \delta\mathcal{L} = \frac{\partial\mathcal{L}}{\partial\psi_\alpha}\,\delta\psi_\alpha + \frac{\partial\mathcal{L}}{\partial\partial_\mu\psi_\alpha}\,\partial_\mu(\delta\psi_\alpha) =$$
$$= i\varepsilon^a\left(\frac{\partial\mathcal{L}}{\partial\psi_\alpha} - \partial_\mu\frac{\partial\mathcal{L}}{\partial\partial_\mu\psi_\alpha}\right)\left(\frac{\tau^a}{2}\right)_{\alpha\beta}\psi_\beta +$$
$$+ i\varepsilon^a\,\partial_\mu\left[\frac{\partial\mathcal{L}}{\partial\partial_\mu\psi_\alpha}\left(\frac{\tau^a}{2}\right)_{\alpha\beta}\psi_\beta\right]$$

Since the first term in the last formula vanishes by (1.4), we see that the currents :

$$J^a_\mu = -i\,\frac{\partial\mathcal{L}}{\partial\partial_\mu\psi_\alpha}\left(\frac{\tau^a}{2}\right)_{\alpha\beta}\psi_\beta \qquad (1.8)$$

are conserved :

$$\partial^\mu J^a_\mu = 0 \qquad (1.9)$$

A well known consequence of (1.9) is the existence of conserved "charges". We set :

$$I^a = \int d^3x\; J^a_0(\underline{x}, t) \qquad (1.10)$$

then :

$$\frac{d}{dt}\,I^a = \int d^3x\left[\partial^\mu J^a_\mu + \vec{\nabla}\cdot\vec{J}^a\right] =$$
$$= \int d^3x\;\vec{\nabla}\cdot\vec{J}^a = 0 \qquad (1.11)$$

If we quantize the theory by canonical quantization, I^a become operators whose equal time commutation relations can be easily computed to be :

$$\left[I^a(t), I^b(t)\right] = i\,\varepsilon_{abc}\,I^c(t) \qquad (1.12)$$

The operators I^a give a realization (or representation) of the commutation rules (1.7) which, in turn, correspond to the algebra of the infinitesimal rotations in a 3-dimensional abstract space, the isospin-space. Furthermore eq. (1.11) becomes :

$$\dot{I}^a = i\left[H, I^a\right] = 0 \qquad (1.13)$$

The operators I^a commute with the hamiltonian H ; therefore they connect states with the same energy. All states will thus appear in isospin-multiplets. For example, $\psi\,\bar{\psi}$ bound states will form families of isospin multiplets (with I = 1 or 0) mass being equal for members of the same multiplet.

We usually split $\mathcal{L}$ into a free and an interaction part :

$$\mathcal{L} = \mathcal{L}_{free} + \mathcal{L}_{int}$$

where

$\mathcal{L}_{free} = \bar{\psi}(i\not{\partial} - m)\psi$ (for spin 1/2 fields)

$\mathcal{L}_{free} = (\partial_\mu\varphi^+)(\partial^\mu\varphi) - m^2\varphi^+\varphi$ (for spin 0 complex fields)

(We set $\not{\partial}\psi = \partial_\mu\gamma^\mu\psi$, γ^μ being the Dirac matrices). If $\mathcal{L}_{int}$ does not contain derivative couplings (as is frequently, but not always, the case), the explicit form of J^a_μ can be directly computed from $\mathcal{L}_{free}$, since $\partial\mathcal{L}/\partial\partial_\mu\psi_\alpha = \partial\mathcal{L}_{free}/\partial\partial_\mu\psi_\alpha$.

We obtain

$$J^a_\mu = \bar{\psi}\gamma_\mu\frac{\tau^a}{2}\psi \qquad \text{(spin 1/2 case)}$$
$$J^a_\mu = -i\left[\partial_\mu\varphi^+\frac{\tau^a}{2}\varphi - \varphi^+\frac{\tau^a}{2}\partial_\mu\varphi\right] \equiv \qquad (1.14)$$
$$\equiv -i\,\varphi^+\frac{\tau^a}{2}\overleftrightarrow{\partial_\mu}\varphi \qquad \text{(spin 0 case)}$$

An internal symmetry transformation for Fermi fields could involve, besides matrices acting on "internal" indices (like the Pauli matrices), also the Dirac γ_5 matrix ($\gamma_5 = i\gamma_0\gamma_1\gamma_2\gamma_3$, $\gamma_5^+ = \gamma_5$, $\gamma_5^2 = +1$). This is because γ_5 transforms as a pseudoscalar under Lorentz transformations. Thus we may enlarge the set of transformations (1.6), adding the so-called "chiral isospin" transformations :

$$\delta_5\psi = i\eta^a\frac{\tau^a}{2}\gamma_5\psi \qquad a = 1.2.3 \qquad (1.15)$$

η^a being again three infinitesimal parameters. Eqs. (1.6) and (1.15) form a new group of infinitesimal transformations, whose generators obey the commutation rules

$$\left[\frac{\tau_a}{2}, \frac{\tau_b}{2}\right] = i\,\varepsilon_{abc}\,\frac{\tau_c}{2}$$
$$\left[\frac{\tau_a}{2}, \frac{\tau_b}{2}\gamma_5\right] = i\,\varepsilon_{abc}\,\frac{\tau_c}{2}\gamma_5 \qquad (1.16)$$
$$\left[\frac{\tau_a}{2}\gamma_5, \frac{\tau_b}{2}\gamma_5\right] = i\,\varepsilon_{abc}\,\frac{\tau_c}{2}$$

The chiral algebra commutators can be set into a simpler form, if we express the infinitesimal generators in terms of the so-called left and righthanded generators :

$$L^a = \frac{1-\gamma_5}{2}\,\frac{\tau_a}{2}$$
$$R^a = \frac{1+\gamma_5}{2}\,\frac{\tau_a}{2} \qquad (1.17)$$

We get :

$$\left[L^a, L^b\right] = i\,\varepsilon_{abc}\,L^c$$
$$\left[R^a, R^b\right] = i\,\varepsilon_{abc}\,R^c \qquad (1.18)$$
$$\left[L^a, R^b\right] = 0$$

For mass-less Fermi fields (see Appendix I)

$\gamma_5 = 2 \times$ (helicity), so that L^a acts only on helicity = - 1/2 states, while R^a acts on helicity = + 1/2 states. Eq. (1.18) show that chiral transformations are nothing but independent (hence commuting) isospin rotations performed over the two helicity states of the fermion field. (Recall that for massless particles the helicity is a Lorentz invariant quantity). The group structure of eqs. (1.16) or (1.18) is usually referred to as chiral $SU(2) \otimes SU(2)$.

Chiral transformations can be a symmetry of $\mathcal{L}$ only in the case of massless fermions. We can in fact compute the variation of $\mathcal{L}_{free}$ under chiral transformations. Recalling that γ_5 anticommutes with γ_μ, one finds :

$$\delta_5 (\mathcal{L}_{free}) = -2i \eta^a \bar{\psi} \gamma_5 \frac{\tau^a}{2} m \psi$$

so that $\delta_5 \mathcal{L}_{free} = 0$ only when $m = 0$.

2. Gauge Transformations

The existence of a symmetry expresses the fact that certain choices are purely conventional and have no effect on the dynamics. Isospin symmetry, for example, implies that we can choose as we please the orientation of the axes in isospin space. Consequently, the definition of the fields to be associated to the proton (isospin "up") and to the neutron (isospin "down") is entirely conventional.

A global symmetry implies however that once we have fixed what we define to be isospin "up" at a given point in space-time, we must maintain the same definition at all other points. This seems to be rather unnatural and not in line with the general ideas underlying the concept of a local field theory, where it is meaningful to compare different quantities only at the same point, and not at distant points. It seems therefore desirable and legitimate to investigate theories where the invariance under the global transformations (1.6) is extended to include transformations which can be different at different space-time points, e.g. transformations of the form :

$$\delta\psi = i \varepsilon^a(x) \frac{\tau^a}{2} \psi(x) \qquad (2.1)$$

$\varepsilon^a(x)$ being now infinitesimal, arbitrary functions of the four coordinates, x . In such theories the orientation of the isospin axes, besides being conventional as before, can be choosen at will at any spacetime point x , irrespectively of the orientation we have choosen at any other space time point $x' \neq x$.

Requiring invariance under spacetime dependent transformations is by no means a trivial constraint. On the contrary, such a "geometrical" principle will force us to restrict to a particular class of field theories, gauge theories, where a set of vector fields (gauge fields), interact with the other fields in a perfectly prescribed manner. A similar situation is encountered in general relativity, where a "geometrical" invariance principle (namely invariance under general coordinate transformations) leads to a prescribed form of the interaction of matter with the gravitational field.

To understand the problems which arise in enlarging a global symmetry into the symmetry under space-time dependent transformations, let us consider the case of a free, spin 1/2, isodoublet, whose lagrangian is :

$$\mathcal{L}_{free} = i \bar{\psi} \partial\!\!\!/ \psi - m \bar{\psi} \psi$$

While $\mathcal{L}_{free}$ is invariant under (1.6), it is not invariant under (2.1), the reason being that $\partial_\mu \psi$ transforms quite differently from ψ itself, so that the term $\bar{\psi} \partial\!\!\!/ \psi$ is not invariant. In fact :

$$\delta \partial_\mu \psi = i \varepsilon^a(x) \frac{\tau^a}{2} \partial_\mu \psi + i (\partial_\mu \varepsilon^a) \frac{\tau^a}{2} \psi$$

$$\delta(\bar{\psi} \partial\!\!\!/ \psi) = i \partial_\mu \varepsilon^a \bar{\psi} \gamma_\mu \frac{\tau^a}{2} \psi \neq 0 \qquad (2.2)$$

A similar situation is found in classical electrodynamics. There, we describe a charged particle by a complex field ψ, charge conservation being related, by the Noether's theorem, to the invariance under global phase transformations :

$$\psi \to \psi' + \delta\psi$$
$$\delta\psi = i \alpha \psi$$

(α is an infinitesimal constant). As is well known, however, the electrodynamics lagrangian is also invariant under space-time dependent transformations. This is because when we subject ψ to space-time dependent phase transformations, $\alpha = \alpha(x)$, the terms analogous to the dangerous terms in (2.2), namely the terms proportional to $\partial_\mu \alpha$ arising from the variation of $\partial_\mu \psi$, are exactly compensated if we subject, at the same time, the e.m. field A_μ to a gauge transformation :

$$A_\mu \to A'_\mu = A_\mu + \delta A_\mu$$
$$\delta A_\mu = -\frac{1}{e} \partial_\mu \alpha$$

(e = electric charge). This compensation, in turn, can be traced back to the fact that the e.m. field A_μ is introduced in the lagrangian either through the "minimal prescription" : $\partial_\mu \psi \to (\partial_\mu + ie A_\mu)\psi$

or through the gauge invariant quantity :

$$F_{\mu\nu} = \partial_\mu A_\nu - \partial_\nu A_\mu .$$

Similarly to electrodynamics, to enforce the symmetry under (2.1), we are therefore led to introduce a set of vector fields A^a_μ (one for each group generator), which will be assumed to transform in such a way that the field combination :

$$\nabla_\mu \psi \equiv \left(\partial_\mu + ig A_\mu^a \frac{\tau^a}{2}\right)\psi \qquad (2.3)$$

transforms precisely like ψ :

$$\delta(\nabla_\mu \psi) = i \varepsilon^a(x) \frac{\tau^a}{2} \nabla_\mu \psi \qquad (2.4)$$

In eq. (2.3), g is a coupling constant (analogous to the electric charge e) which describes the interaction of A^a_μ with the field ψ . The requirement that (2.3) transforms according to (2.4) can then be easily shown (See Appendix II) to lead uniquely to :

$$\delta A_\mu^a = - \varepsilon_{abc} \varepsilon^b(x) A_\mu^c - \frac{1}{g} \partial_\mu \varepsilon^a(x) \qquad (2.5)$$

In the following we will refer to A^a_μ and $\nabla_\mu \psi$ with the words "gauge fields" and "covariant derivative", respectively. Also, in analogy to electrodynamics, we will call the transformations (2.1) and (2.5) "gauge transformations".

The usefulness of the covariant derivative lies in the fact that, due to (2.4), any function of ψ and $\nabla_\mu \psi$ which is invariant under the global transformations (1.6) is also invariant under (2.1). This is clear from the fact that neither (2.1) nor (2.4) depend upon $\partial_\mu \varepsilon^a(x)$, and therefore any function of ψ and $\nabla_\mu \psi$ will behave precisely in the same way for constant or space-time dependent transformations.

This observation gives us the clue to the construction of lagrangians invariant under space-time dependent transformations.

Consider a lagrangian $\mathcal{L}(\psi, \partial_\mu \psi)$ describing all the interactions of ψ , except for the interaction with the gauge fields A^a_μ , and assume $\mathcal{L}$ to be invariant under (1.6). Then, by the above observation, the new lagrangian obtained by the "minimal prescription"

$$\partial_\mu \psi \rightarrow \nabla_\mu \psi$$

namely, the lagrangian :

$$\mathcal{L}(\psi, \nabla_\mu \psi) \qquad (2.6)$$

is invariant if we subject ψ to the transformations (2.1) and A^a_μ to (2.5). Note that (2.6) contains in a perfectly prescribed way the interaction of ψ with A^a_μ .

The lagrangian (2.6) cannot still be the total lagrangian. In fact, since $\mathcal{L}(\psi, \nabla_\mu \psi)$ is at most quadratic in $\partial_\mu \psi$, $\mathcal{L}(\psi, \nabla_\mu \psi)$ will be at most linear in the first derivatives of A^a_μ , while we need terms quadratic in $\partial_\nu A^a_\mu$, in order to obtain meaningful (i.e. 2nd order) equations of motion for the fields A^a_μ .

To accomplish this, we have to construct a gauge invariant lagrangian for the fields A^a_μ alone. Following again electrodynamics, one defines the gauge covariant curl:

$$F^a_{\mu\nu} = \partial_\mu A^a_\nu - \partial_\nu A^a_\mu - g \varepsilon_{abc} A^b_\mu A^c_\nu \qquad (2.7)$$

A straightforward, if not simple, algebra (see Appendix II) shows that $F^a_{\mu\nu}$ transforms linearly, if we subject A^a_μ to (2.5); namely :

$$\delta F^a_{\mu\nu} = - \varepsilon_{abc} \varepsilon^b(x) F^c_{\mu\nu} \qquad (2.8)$$

Hence :

$$\mathcal{L}_{YM} = -\frac{1}{4} F^a_{\mu\nu} (F^a)^{\mu\nu} \qquad (2.9)$$

is gauge invariant and it is the required lagrangian for the Yang-Mills gauge fields alone.

We close this section with a number of observations on the properties of the covariant derivatives and on the extension of the Yang-Mills idea to symmetry groups other than the isospin group, $SU(2)$.

First note that, by eqs. (1.6) and (2.3), the covariant derivative of ψ can also be expressed as :

$$\nabla_\mu \psi = \partial_\mu \psi + g A^a_\mu \frac{\delta \psi}{\delta \varepsilon^a} \qquad (2.10)$$

where $\delta\psi$ is the variation of ψ under the global transformation (1.6). Eq. (2.10) allows us to write down the covariant derivative of any field or function of fields, provided we know how do they transform under (1.6). Examples :

i) consider an invariant field or function of fields, $\mathcal{L}(x)$.

$$\delta \mathcal{L}(x) = 0$$

hence

$$\nabla_\mu \mathcal{L}(x) = \partial_\mu \mathcal{L}(x)$$

ii) consider a field Φ with isospin greater than 1/2 (e.g. I = 2). Then

$$\delta\Phi = i\,\varepsilon^a T^a \Phi$$

T^a being the appropriate matrices describing infinitesimal rotations over the space of the given isospin. T^a obey precisely the same commutation rules as $\tau_a/2$ Then

$$\nabla_\mu \Phi = \partial_\mu \Phi + i g A_\mu^a T^a \Phi$$

iii) Suppose $A(x) = \Psi(x)\Phi(x)$, Ψ and Φ transforming in a given way under (1.6). Then :

$$\delta A = (\delta\Psi)\Phi + \Psi(\delta\Phi)$$

hence

$$\nabla_\mu A = (\nabla_\mu \Psi)\Phi + \Psi(\nabla_\mu \Phi)$$

As this example shows, the covariant derivative shares many properties of the usual derivative. However covariant derivatives do not commute :

$$(\nabla_\mu \nabla_\nu - \nabla_\nu \nabla_\mu)\Phi = i g F_{\mu\nu}^a T^a \Phi$$

T^a being the matrices appropriate to Φ (i.e. $T^a = \tau_a/2$ if Φ has isospin 1/2).

iv) By (2.10), we see that the covariant derivative of any field is determined by the behavior of the field under global transformations. One could therefore try to define a "covariant derivative" of the gauge fields themselves (which transform as I = 1 fields under global transformations) and try to set :

$$F_{\mu\nu} \stackrel{?}{=} \nabla_\mu A_\nu - \nabla_\nu A_\mu$$

It turns out that this is wrong. The right hand side of this equation is not equal to (2.7), and does not transform linearly under (2.1). The "covariant derivative" of A_μ^a has no meaning. We can, of course, define covariant derivatives of $F_{\mu\nu}^a$:

$$(\nabla_\lambda F_{\mu\nu})^a = \partial_\lambda F_{\mu\nu}^a - g\,\varepsilon_{abc} A_\lambda^b F_{\mu\nu}^c$$

The extension of the Yang-Mills formalism to other groups is entirely trivial. For simple groups, i.e. such that we cannot divide the generators into two or more sets of mutually commuting generators, we simply substitute, in the previous formulae, $\tau_a/2$ with matrices (call them $\lambda^\alpha/2$) which obey the commutation rules appropriate to the group :

$$\left[\frac{\lambda^\alpha}{2}, \frac{\lambda^\beta}{2}\right] = i f_{\alpha\beta\gamma} \frac{\lambda^\gamma}{2} \qquad (2.9)$$

and further replace ε_{abc} by $f_{\alpha\beta\gamma}$, the structure constants of the group. Again only one coupling constant appears. If the group is semi-simple (i.e. the generators can be divided in mutually commuting sets, as is the case, for example of chiral $SU(2) \otimes SU(2)$), or it contains abelian factors, the same holds true, but we can have different couplings for each simple factor and for each abelian factor (this is why the Weinberg-Salam model, which is based on the group $SU(2) \otimes U(1)$, has <u>two</u> independent couplings).

3. Properties of the Yang-Mills interactions

We have seen in the last section that it is possible to obtain a well defined gauge invariant interaction of the fields Ψ (which we will call "matter fields") with the gauge fields A_μ^a, by the so-called "minimal prescription". The rule was :
i) to consider the lagrangian $\mathcal{L}(\Psi, \partial_\mu \Psi)$ of the matter fields <u>without</u> Ψ-A interaction;
ii) to make the substitution $\partial_\mu \Psi \to \nabla_\mu \Psi$;
iii) to add the Yang-Mills lagrangian (2.9). In this way, one arrives to the total lagrangian :

$$\mathcal{L}_{tot} = -\frac{1}{4} F_{\mu\nu}^a (F^a)^{\mu\nu} + \mathcal{L}(\Psi, \nabla_\mu \Psi) \qquad (3.1)$$

In the case where Ψ has no other interaction but the Yang-Mills one, $\mathcal{L}(\Psi, \partial_\mu \Psi)$ is the free lagrangian, which is totally determined once we know the kinematic properties of Ψ (spin, isospin, mass). In this case, $\mathcal{L}_{tot}$ is <u>completely determined</u> by kinematics and by the requirement of gauge symmetry. This uniqueness property is a special feature of Yang-Mills theories, and it makes them very attractive for describing the fundamental interactions.

In fact, many think the e.m., weak <u>and</u> strong interactions are to be described by Yang-Mills interactions. If this were the case, knowing which are the fundamental fields (e.g. lepton and quarks) and what is the gauge group, one would determine, from the gauge principle, the form of all interactions, except gravity. At present, this program is far from being completed. To restrict to weak and e.m. interactions, we will see later that one has to introduce new, yet unseen, scalar particles whose couplings to leptons and quarks are largely undetermined. Even in this circumstance, however, the interaction of gauge fields with the matter fields <u>is</u> determined by the gauge symmetry, and it has many peculiar features which we will now illustrate, restricting to a very simple case.

Let us therefore consider the case of a spinor, isodoublet matter field (e.g. electron and neutrino, degenerate in mass) interacting only with the Yang-Mills (isotriplet) gauge fields.

In this very simple case :

$$\mathcal{L}_{tot} = -\frac{1}{4} F^{a}_{\mu\nu} (F^{a})^{\mu\nu} + \bar{\Psi}(i\not{\partial} - m)\Psi$$
$$\Psi = \begin{pmatrix} \nu \\ e \end{pmatrix} \qquad (3.2)$$

$\nabla_\mu \Psi$ is given by (2.3).

Written explicitly, the lagrangian (3.2) gives rise to terms with different degrees of homogeneity in the fields (e.g. terms bilinear, trilinear etc. in the fields) :

$$\mathcal{L} = -\frac{1}{2}\partial_\mu A^a_\nu \left(\partial^\mu A^{a\nu} - \partial^\nu A^{a\mu}\right) + \bar{\Psi}(i\not{\partial} - m)\Psi$$
$$- g A^a_\mu \bar{\Psi}\gamma^\mu \frac{\tau^a}{2}\Psi + g\varepsilon_{abc} A^a_\mu A^b_\nu \partial^\mu A^{c\nu}$$
$$- \frac{g^2}{4}\varepsilon_{abc}\varepsilon_{adf} A^b_\mu A^c_\nu A^{d\mu} A^{f\nu} \equiv$$
$$\equiv "A^2" + "\bar{\Psi}\Psi" + g\,"A\bar{\Psi}\Psi" +$$
$$+ g\,"A^3" + g^2\,"A^4" \qquad (3.3)$$

Note that when $g \to 0$, $\mathcal{L}$ reduces to the quadratic terms, which are therefore indicated as the free part, $\mathcal{L}$ free, of $\mathcal{L}$. According the usual methods in field theory :

i) the bilinear terms, $"A^2"$ and $"\bar{\Psi}\Psi"$, describe the free propagation of the particles associated to the A and Ψ fields; we shall discuss the $"A^2"$ terms in detail, the $"\bar{\Psi}\Psi"$ terms leading to the familiar fermion propagator, as e.g. in standard quantum electrodynamics (QED);

ii) Higher than bilinear terms describe interactions of the fields; we shall discuss the $"A\bar{\Psi}\Psi"$ term and, later on, the $"A^3"$ term;

iii) Unlike QED, the lagrangian (3.2) contains a self interaction of the gauge fields with themselves, represented by the $"A^3"$ and $"A^4"$ terms.

These terms are uniquely determined by the structure of $F^a_{\mu\nu}$, i.e. by the principle of gauge covariance. Their presence is a necessary consequence of the fact that the gauge fields are coupled to all fields carrying a non vanishing isospin, and therefore also to themselves (eq. (2.5) indicates $I = 1$ for A^a_μ).

The self-coupling of gauge fields is a very crucial feature of Y-M theories. It is the main reason why such theories are not a mere transcription of QED, and it is responsible for all the difficulties encountered in getting a consistent treatment to all orders in perturbation theory. In fact, Y-M theories are more similar, in this respect, to quantum gravity than they are to electrodynamics (the graviton is similarly coupled to all forms of energy, including its own). Similarly to gravity, a Y-M theory is not a free theory even in the absence of matter fields.

We restrict now to the $"A^2"$ terms, to derive the equations of motion in the free limit, $g = 0$. Applying eq. (1.4) to $\mathcal{L}_{free} \equiv "A^2"$, and observing that :

$$\frac{\partial \mathcal{L}_{free}}{\partial A^a_\mu} = 0 \quad ; \quad \frac{\partial \mathcal{L}_{free}}{\partial \partial_\mu A^a_\nu} = \partial_\nu A^a_\mu - \partial_\mu A^a_\nu$$

we get ($\Box \equiv \partial^\mu \partial_\mu$) :

$$\left(g^{\beta\lambda}\Box - \partial^\beta\partial^\lambda\right) A^a_\lambda(x) = 0 \qquad (3.4)$$

Taking the Fourier transform of (3.4) ($i\partial_\mu \to k_\mu$), we get

$$G^{\beta\lambda}(k)\, A^a_\lambda(k) \equiv \left(-g^{\beta\lambda}k^2 + k^\beta k^\lambda\right) A^a_\lambda = 0 \qquad (3.5)$$

As is well known, the inverse of the matrix $G^{\beta\lambda}$ is the propagator for the A-field, i.e. the Fourier transform of the amplitude for finding a gauge particle of given type at the space-time point x, if it has been created at $x = 0$. However, the matrix $G^{\beta\lambda}$ has no inverse ! In fact, Lorentz covariance restricts $\left[G^{\beta\lambda}\right]^{-1}$ to be of the form :

$$G^{-1}_{\beta\lambda} = A k^2 g_{\beta\lambda} + B k_\beta k_\lambda$$

A, B being functions of k^2. But :

$$\left(-g_{\beta\lambda}k^2 + k_\beta k_\lambda\right)\left(A k^2 g^{\lambda\sigma} + B k^\lambda k^\sigma\right) =$$
$$= A\left(-\delta^\sigma_\beta k^2 + k_\beta k^\sigma\right)$$

which cannot be equal to δ^σ_β for any function A and B. This is a well-known difficulty, first found in quantizing the photon field. It has to do with the fact that, by gauge invariance, the four components of A^a_μ are not independent dynamical degrees of freedom. For example, by a suitable gauge transformation we may require

$$\partial^\mu A^a_\mu = 0 \qquad (3.6)$$

everywhere. One possible way out is to substitute (3.6) into (3.4). We thus get

$$\Box A^a_\beta(x) = 0$$

or, in Fourier space :

$$g^{\beta\lambda} k^2 A^a_\lambda(k) = 0$$

and we find the so-called Feynman propagator :

$$D_{\mu\nu}(k) = G^{-1}_{\mu\nu}(k) = \frac{g_{\mu\nu}}{k^2} \qquad (3.7)$$

(To reproduce the correct space-time behavior of propagators, here and in the following one should add a positive imaginary part, $+i\varepsilon$, to the denominators; furthermore, the correct propagator has an additional (-i) factor). Alternatively, we can take into account (3.6) by the method of Lagrange multipliers. We add to $\mathcal{L}_{free}$, a term :

$$-\frac{1}{2\alpha}(\partial^\mu A^a_\mu)(\partial^\lambda A^a_\lambda)$$

which vanishes when (3.6) holds, and then take the variation of the lagrangian, with fixed α . We get, in place of (3.4), the equation :

$$\left[-g^{\beta\lambda}\Box + \left(1 - \frac{1}{\alpha}\right)\partial^\beta\partial^\lambda\right] A^a_\lambda(x) = 0$$

which leads to the propagator (again up to a (-i) factor) :

$$D_{\mu\nu} = \frac{1}{k^2}\left[g_{\mu\nu} - (1-\alpha)\frac{k_\mu k_\nu}{k^2}\right] \qquad (3.8)$$

(3.8) gives back (3.7) for $\alpha = 1$, while $\alpha = 0$ leads to the so-called Landau gauge propagator. Physical results will be, of course, independent from α .

Propagators in momentum space have poles at values of k^2 equal to the (mass)^2 of the propagating particle. The previous equations then show that the gauge fields are to be associated to <u>massless particles</u>.

We turn now to the interaction terms, restricting to the A-ψ interaction. The "$A\bar{\psi}\psi$" term in (3.3) can be written as :

$$g\ "A\bar{\psi}\psi" \equiv \mathcal{L}_{A\psi} = -g A^a_\mu (J^a)^\mu \qquad (3.9)$$

where J^a_μ is the Noether current, associated to the global I-spin symmetry of the lagrangian <u>before</u> the introduction of the gauge fields (see eq. (1.14)).

Eq. (3.9) would remain valid also in presence of further matter fields, J^a_μ being in that case the total Noether current associated to I-spin conservation, in absence of the gauge fields. Eq. (3.9) expresses the universality of the coupling of gauge fields to I-spin carrying matter fields.

It is important to observe that J^a_μ is not conserved, in the presence of gauge fields. Indeed, applying Noether's theorem to (3.2), one derives that the total, conserved I-spin current is now :

$$\mathcal{J}^a_\mu = i\,\varepsilon_{abc}\, F^b_{\mu\nu} A^{c\nu} + J^a_\mu \qquad (3.10)$$

The additional term reflects again the fact that the gauge fields themselves carry a non-vanishing I-spin.

Matrix elements of $\mathcal{L}_{A\psi}$ give the amplitude for emission and absorption of a gauge particle by an electron or neutrino.

We can apply the previous considerations to study the scattering of two fermions by the exchange of a gauge field. This is illustrated in Fig. 1, which gives a picture of the process in space-time.

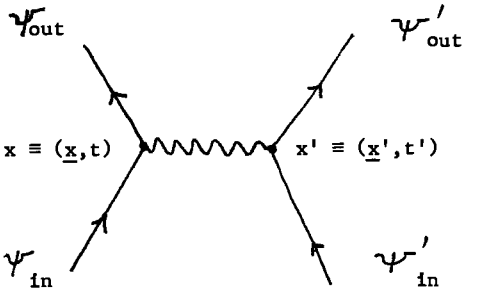

Fig. 1

The amplitude for such a process is the product of three terms :

(production amplitude at x)
(amplitude for propagating from x to x')
(absorption amplitude at x')

to be integrated over all x and x' . In momentum space, this is simply the product :

$$A = g^2 J^a_\mu D^{\mu\nu}(k) J^{a\prime}_\nu \qquad (3.11)$$

where J^a_μ ($J^{a\prime}_\nu$) is the Fourier transform of the matrix element of $J^a_\mu(x)$ ($J^a_\mu(x')$) between ingoing and outgoing fermions and k_μ is the 4-momentum transferred by the vector particle. <u>In this particular case</u>, it is easy to see that the currents $J^a_\mu(x)$ and $J^a_\mu(x')$ are conserved, so that

$$k^\mu J^a_\mu = k^\mu J^{a\prime}_\mu = 0 \qquad (3.12)$$

This is so because we assume the external particles to be real (on the mass-shell) particles. A real, free particle cannot irradiate gauge mesons, so that there will be no loss of isospin from e.g. the ψ- line, except for that which flows into the exchanged gauge field. More formally, the matrix element of the conserved current (3.10) coincides, to the order here considered, with the matrix element of J^a_μ alone. Hence the latter is conserved. Eq. (3.12) makes it

irrelevant the choice between the two propagators (3.7) or (3.8). In either cases we get (we omit from now on the isospin index, which is irrelevant)

$$A = g^2 J_\mu \frac{1}{k^2} J'^\mu =$$

$$= \frac{g^2}{k^2} \left(J_0 J'_0 - J_3 J'_3 - J_1 J'_1 - J_2 J'_2 \right) \quad (3.13)$$

Let us denote by q the space part of k_μ and by ω its 4th component, $(k^2 = \omega^2 - q^2)$, and choose q in the direction of the z-axis. We can use again (3.12) to eliminate J_3 and J'_3 :

$$J_3 = \frac{\omega}{q} J_0 \quad , \quad J'_3 = \frac{\omega}{q} J'_0$$

We find :

$$A = -g^2 \left\{ \frac{1}{q^2} J_0 J'_0 + \frac{1}{k^2} \left(J_1 J'_1 + J_2 J'_2 \right) \right\} \quad (3.14)$$

The two terms in (3.14) have a very simple interpretation. The first one represents an instantaneous, coulombic interaction among the fermions. Indeed, if we Fourier transform back to x space :

$$\frac{1}{q^2} \xrightarrow[F.T.]{} \delta(t-t') \frac{1}{|\underline{x} - \underline{x}'|}$$

which is just the Coulomb interaction; also J_0 and J'_0 give the "charge" densities of the two external particles. The appearance of Coulomb forces confirms that we are exchanging <u>massless</u> particles. The second term in (3.14)has a pole when $q^2 = \omega^2$. At the pole, the amplitude describes the propagation of free waves between x and x' . The bracket in (3.14)indicates that we have only <u>two types</u> of waves, those generated by J_1 (and absorbed by J'_1) and those generated by J_2 . We can transform the square bracket in (3.14) according to :

$$J_1 J'_1 + J_2 J'_2 = \left(\frac{J_1 + i J_2}{\sqrt{2}} \right) \left(\frac{J'_1 - i J'_2}{\sqrt{2}} \right) +$$

$$+ \left(\frac{J_1 - i J_2}{\sqrt{2}} \right) \left(\frac{J'_1 + i J'_2}{\sqrt{2}} \right)$$

Under a space rotation of an angle θ around the z-axis :

$$J_1 \pm i J_2 \rightarrow e^{\pm i \theta} (J_1 \pm i J_2)$$

Such a behavior is typical of the eigenstates of angular momentum in the z-direction. An eigenstate with angular momentum along z equal to J_z picks up, under such a rotation, a factor $\exp(i \theta J_z)$. Hence we see that the two waves have $J_z = \pm 1$.

In conclusion, we have learned that gauge fields describe particles which are :

i) massless ;

ii) exist in only two polarization states (namely $J_z = \pm 1$, if they propagate along the z-axis);

iii) couple to matter fields universally, through the current J^a_μ which is associated by the Noether's theorem to the global symmetry of matter fields.

4. <u>Unbroken Yang-Mills theories and weak interactions</u>

In this section we want to have a first look to the possible applications of the Yang-Mills theory to real weak interactions. Can we describe $\nu_e - e$ scattering or μ -decay or the neutron β -decay by a process similar to that illustrated in Fig. 1? The inspection of the relevant amplitude, (3.13), reveals two features, one very good and one very bad.

The amplitude contains the product of two currents (one for each fermion line), the currents themselves being <u>those</u> currents associated to a global symmetry of the theory without gauge interactions. It is precisely so in weak interactions. The amplitude e.g. for the neutron β -decay is indeed proportional to the product of two currents, (one changing $n \rightarrow p$, the other creating the lepton pair) which are indeed the currents associated to some global symmetry. Discovering the relations between weak currents and particle symmetries (the so-called CVC hypothesis of Feynman and Gell-Mann, the Cabibbo theory, the relation with chiral symmety etc.) has been in fact one of the main lines of progress in weak interactions. An underlying gauge theory would give a solid foundation to this fact. This is the good thing.

The bad feature of (3.13) is the factor $1/k^2$, related to the masslessness of the gauge particles. There is no trace of massless bosons in weak interactions. If weak interactions are to be mediated by vector bosons, they must be on the contrary very heavy. How can we overcome this trouble ? One possibility is to add by brute force a mass term ($+ \frac{1}{2} M^2 A^a_\mu A^{a\mu}$) to the lagrangian (3.1). Such a term is not gauge invariant, so we are contradicting the philosophical bases of Y-M theory.

Let us see, nonetheless, what happens.

If we add a mass term to the free lagrangian in

(3.3), we get the new equation of motion :

$$(g^{\beta\lambda}\,\Box - \partial^{\beta}\partial^{\lambda} + M^2 g^{\beta\lambda})\,A^{a}_{\lambda}(x) = 0$$

i.e., in momentum space :

$$(-g^{\beta\lambda}k^2 + k^{\beta}k^{\lambda} + M^2 g^{\beta\lambda})\,A^{a}_{\lambda}(k) = 0$$

The operator acting on A^{a}_{λ} has now an inverse (we have broken the gauge invariance) and we get the propagator :

$$D_{\mu\nu}(k, M^2) = \frac{1}{k^2 - M^2}\left(-g_{\mu\nu} + \frac{k_\mu k_\nu}{M^2}\right) \qquad (4.1)$$

If we compute again the amplitude for Fig. 1, we get now :

$$A = g^2 \frac{1}{k^2 - M^2}\, J_\mu\, J'^{\mu} \qquad (4.2)$$

(since the currents are still conserved, the $k_\mu k_\nu$ term in (4.1) has no effect). Finally, in the case where $M^2 \gg k^2$, we get :

$$A = -\frac{g^2}{M^2}\, J_\mu\, J'^{\mu} \qquad (4.3)$$

This is precisely the form of the observed weak amplitudes (Fermi interaction) if we identify g^2/M^2 with the Fermi constant. Putting a mass term, we have retained the good feature, and have eliminated the bad one !

The agreement with physics has however been achieved at a very high price. To see this, let us compare the new propagator (4.1), with the old ones, (3.7) or (3.8). For very large k , we see that :

$$(4.1) \sim 1$$
$$(3.7) \text{or} (3.8) \sim \frac{1}{k^2} \to 0$$

The massive theory is much less convergent in the ultraviolet region. This has the very serious consequence that the higher order corrections will be much more divergent now than they were before. Indeed, the structure of divergences of a massive Y-M theory is so bad that the theory cannot be cast in a sensible (technically : renormalizable) form. To elaborate a little more on this, let us consider in detail eq. (4.2). Putting again $k = (\underline{q}, \omega)$ and using the conservation equation for J_μ , we have :

$$A = -g^2\left\{\frac{J_0 J'_0}{\underline{q}^2 + M^2} + \frac{1}{k^2 - M^2}\left(\frac{M^2}{\underline{q}^2 + M^2} J_3 J'_3 + J_1 J'_1 + J_2 J'_2\right)\right\} \qquad (4.4)$$

Comparing (4.4) with (3.14) we see that :

i) the instantaneous interaction (i.e. the first term) is no more coulombic. Fourier transforming to x-space :

$$\frac{1}{\underline{q}^2 + M^2} \xrightarrow{F.T.} \sim \frac{e^{-M|\underline{x} - \underline{x}'|}}{|\underline{x} - \underline{x}'|}$$

and we get a Yukawa type interaction. This had to be expected, since we have given a mass to the exchanged particle.

ii) The second term, at $k^2 = M^2$, represents the propagation of massive waves, but there are now three types of waves! The new wave is generated by J_3 . This is invariant under rotations around the z-axis and so it has $J_z = 0$. Putting a mass term has given to the theory a new degree of freedom, represented by the longitudinally polarized waves. Before, this degree of freedom was eliminated by gauge invariance.

It is precisely the longitudinal wave which is responsible for the incurable ultraviolet pathologies of the massive Yang-Mills theory.

In conclusion, we are faced with a serious dilemma. Either :

i) we stay with the unbroken (massless) theory: this is a consistent theory, which however can have no application in physics;
or :

ii) we introduce a mass term : this gives a theory which is very appealing on phenomenological grounds, but is theoretically impracticable.

We will see a way out to this dilemma in Section 6.

5. Spontaneously broken global symmetries.

Leaving aside Yang-Mills theories for a while, we consider now the problem of symmetry breaking.

Most of the symmetries observed in Nature are not exact. Isospin symmetry is broken, as indicated by the proton-neutron mass difference; SU(3) symmetry is broken, to a larger extent, as indicated by the large proton-Λ mass difference, and so on.

A simple way to describe symmetry breaking would be to add explicit non-invariant terms to the lagrangian. We want to discuss here an alternative way in which a symmetry can be broken, usually referred to as "spontaneous symmetry breaking". The idea is to have a theory where the lagrangian is still exactly symmetric under the group transformations, but it gives rise, for dynamical reasons, to a ground state which is not invariant. The ground state of a field theory represents, in the quantized theory, the vacuum state, i.e. the state with no particles. In

turn, the non invariance of the vacuum state leads to a well definite pattern of symmetry breaking effects. The application of this idea to particle physics, pioneered by the work of Nambu and Jona-Lasinio, has been forbidden for many years by the discovery that, under quite general conditions, the spontaneous breaking of a continuous symmetry leads to the appearance of massless scalar bosons (Goldstone theorem), about the existence of which we have no evidence whatsoever. We will see in the following, how massless Goldstone bosons appear in a particular example.

It is very remarkable that gauge theories do not satisfy the general conditions I have alluded to above, and indeed if we extend the global symmetry into a gauge symmetry, the unwanted massless Goldstone bosons disappear. At the same time a corresponding number of previously massless gauge mesons acquire a mass. This remarkable phenomenon (called the Higgs phenomenon) cures at the same time the bad features of the spontaneously broken symmetry and of the Yang-Mills theory (all related to the presence of massless particles), and opens the way to the construction of realistic models of weak interactions. We will discuss the Higgs phenomenon in the next section.

Let us consider a theory of a self-interacting scalar field φ. The interaction will be isospin invariant, φ being an isodoublet. We will choose the very simple lagrangian:

$$\mathcal{L} = (\partial_\mu \varphi^+)(\partial^\mu \varphi) - \mu^2 \varphi^+\varphi - \lambda (\varphi^+\varphi)^2 \equiv$$
$$\equiv (\partial_\mu \varphi^+)(\partial^\mu \varphi) - V(\varphi^+\varphi) \qquad (5.1)$$

where :

$$\varphi = \begin{pmatrix} K^+ \\ K^0 \end{pmatrix} \equiv \begin{pmatrix} \frac{k_1 + i k_2}{\sqrt{2}} \\ \frac{k_3 + i k_4}{\sqrt{2}} \end{pmatrix} \qquad (5.2)$$

k_i being real fields, and

$$\varphi^+\varphi = (K^+)^* K^+ + (K^0)^* K^0 =$$
$$= \frac{1}{2} \sum_i k_i^2$$

Our aim is to study the mass spectrum of the particles associated to the field φ

The standard procedure, which we followed in Section 3 for the gauge fields is to separate, in the lagrangian, the terms bilinear in φ, from the higher order terms :

$$\mathcal{L} = "\varphi^2" + "\varphi^4"$$
$$"\varphi^2" = (\partial_\mu \varphi^+)(\partial^\mu \varphi) - \mu^2 \varphi^+\varphi \qquad (5.3)$$

and to study the equations of motion of $"\varphi^2"$. In this case, one finds, applying eq. (1.4) the equation of motion :

$$(\Box + \mu^2)\, \varphi(x) = 0$$

which describes the propagation of a spin zero, complex isodoublet, with an I-spin invariant mass :

$$m = \sqrt{\mu^2} \qquad (5.4)$$

Eq. (5.4) evidently requires $\mu^2 > 0$.

In this analysis, however, one is tacitly assuming that the lowest energy state (i.e. the state with no particles, the vacuum) corresponds to the field configuration $\varphi = 0$. Only in this case, in fact, it is meaningful to expand $\mathcal{L}$ in powers of φ, associating the propagation of particles to the small oscillations around $\varphi = 0$.

For scalar fields, on the contrary, it may happen that the lowest energy configuration (the vacuum) corresponds to :

$$\varphi = const = \varphi_0 \neq 0 \qquad (5.5)$$

(the constancy of φ in the ground state is required for the vacuum to be translation invariant).

In that case, particles should be associated to the oscillations of φ around φ_0, rather than around a vanishing value, and the expansion (5.3) would not make sense. Rather, one has to put :

$$\varphi(x) = \varphi_0 + \chi(x) \qquad (5.6)$$

and expand $\mathcal{L}$ <u>in powers of</u> $\chi(x)$:

$$\mathcal{L} = "\chi^2" + "\chi^3" + "\chi^4" \qquad (5.7)$$

The true particle spectrum is then determined by the equation of motion obtained from the $"\chi^2"$ term.

What determines the ground state field configuration ? The answer is that such a configuration must correspond to an <u>absolute minimum</u> of the energy (or hamiltonian) density. The hamiltonian density is given by :

$$\mathcal{H} = \dot{\varphi}^+ \frac{\partial \mathcal{L}}{\partial \dot{\varphi}^+} + \frac{\partial \mathcal{L}}{\partial \dot{\varphi}} \dot{\varphi} - \mathcal{L} =$$
$$= \dot{\varphi}^+\dot{\varphi} + (\vec{\partial}\varphi^+)(\vec{\partial}\varphi) + V \qquad (5.8)$$

($\dot{\varphi} = \frac{\partial \varphi}{\partial t}$, $\vec{\partial}\varphi$ is the space gradient of φ).

To have a sensible theory, $\mathcal{H}$ must be bounded from below, for any field configuration. Since the first two terms in (5.8) are positive definite, this requires the function $V(\varphi^+\varphi)$ to be bounded

from below, and this, in turn, is obeyed provided $\lambda > 0$. Observe that we have not obtained any constraint on the sign of μ^2 . Indeed we will see that $\mu^2 < 0$ is also possible, and leads precisely to the interesting case of spontaneous symmetry breaking.

The form of the hamiltonian, eq. (5.8) is such that an absolute minimum is obtained for a field $\varphi(x)$ such that :

i) $\varphi(x) = \text{const} = \varphi_0$ (so that the derivative terms in $\mathcal{H}$ vanish);

ii) $V(\varphi_0^+ \varphi_0) = \text{minimum}$

Fig 2 shows the shape of V as a function of y $(y^2 = \varphi^+ \varphi)$, for the two cases : $\mu^2 > 0$ (a) and $\mu^2 < 0$ (b). We see that either :

$$\varphi_0 = 0 \qquad \text{(case (a))} \tag{5.9}$$

or

$$\varphi_0^+ \varphi_0 = y_m^2 = \frac{-\mu^2}{2\lambda} \qquad \text{(case (b))} \tag{5.10}$$

The sign of μ^2 , therefore, determines whether the ground state corresponds to a vanishing field or not. The first case, (a), corresponds to the case we have previously discussed, and leads to an I-spin symmetric mass spectrum. Let us consider now the more interesting case (b).

To this aim, we choose our isospin frame, so that the constant isospinor φ_0 is a "down" isospinor :

$$\varphi_0 = \begin{pmatrix} 0 \\ \eta \end{pmatrix} \tag{5.11}$$

whence :

$$\eta = \sqrt{\frac{-\mu^2}{2\lambda}} \tag{5.12}$$

by (5.10). The ground state situation is illustrated in Fig. 3 (a). Here the 4-dimensional Minkowski space is represented as a two dimensional space. To any point $x \equiv (\underline{x}, t)$ there is associated a constant spinor φ_0 , represented by an arrow of constant length and orientation (to be able to draw a picture, I have squeezed also the 3-dimensional isospin space into two dimensions). Fig. 3 (b) illustrates the situation for a perturbation of the ground state. At any point x , the spinor $\varphi(x)$ may differ from φ_0 both in orientation and in length (i.e. $\varphi^+(x)\varphi(x) \neq \varphi_0^+ \varphi_0$) .

To parametrize conveniently the deviations of $\varphi(x)$ from φ_0 , we observe that any spinor $\varphi(x)$ can be considered as a "down" spinor with respect to suitable isospin axes. Let us denote by :

$$U(x) \equiv e^{i \tau_a \theta^a(x)} \tag{5.13}$$

the (2x2) isospin rotation needed to bring the "tilted isospin frame" at the point x (i.e. the frame where $\varphi(x)$ is "down") into the frame where φ_0 is "down" We also denote by :

$$\begin{pmatrix} 0 \\ \eta + \frac{\sigma(x)}{\sqrt{2}} \end{pmatrix} \tag{5.14}$$

the components of $\varphi(x)$ in the tilted frame. Then the components of $\varphi(x)$ in the frame where φ_0 is "down" are given by :

$$\varphi(x) = U(x) \begin{pmatrix} 0 \\ \eta + \frac{\sigma(x)}{\sqrt{2}} \end{pmatrix} \tag{5.15}$$

Following eq. (5.6), we can therefore set :

$$\chi(x) = \varphi(x) - \varphi_0 = U(x) \begin{pmatrix} 0 \\ \eta + \frac{\sigma(x)}{\sqrt{2}} \end{pmatrix} - \begin{pmatrix} 0 \\ \eta \end{pmatrix} \tag{5.16}$$

which, for small perturbations, i.e. for small $\theta^a(x)$ and $\sigma(x)$, reduces to

$$\chi(x) \approx \begin{pmatrix} \eta(\theta^2 + i\theta^1) \\ \frac{\sigma}{\sqrt{2}} - i\eta\theta^3 \end{pmatrix} \tag{5.17}$$

The equations above show that we can parametrize the deviations from the vacuum configuration by 4 real functions (fields) $\theta^a(x)$ (a = 1,2,3) and $\sigma(x)$. Our next task will be to express the lagrangian in eq. (5.1) in terms of these fields, and to examine the structure of the quadratic terms (corresponding to the term "χ^2" in eq. (5.7)). We find :

$$\partial^\mu \varphi^+ \partial_\mu \varphi = \frac{1}{2}(\partial_\mu \sigma)(\partial^\mu \sigma) + \eta^2 (\partial_\mu \theta^a)(\partial^\mu \theta^a)$$

$$+ \text{higher order terms}$$

$$-V(\varphi^+\varphi) = -V\left[\left(\eta + \frac{\sigma}{\sqrt{2}}\right)^2\right] = \text{const} -$$

$$- \frac{1}{2}(4\lambda\eta^2)\sigma^2 + \text{higher order terms}$$

so that :

$$\text{"}\chi^2\text{"} = \frac{1}{2}(\partial_\mu \sigma)(\partial^\mu \sigma) - \frac{1}{2} m^2 \sigma^2 + \frac{1}{2}(\partial_\mu \tilde{\theta}^a)(\partial^\mu \tilde{\theta}^a)$$

$$\tilde{\theta}^a = \sqrt{2}\,\eta\,\theta^a \tag{5.18}$$

$$m^2 = 4\lambda\eta^2 = -2\mu^2 > 0$$

Eq. (5.18) describes 4 types of particles, similarly to the $\mu^2 > 0$ case, but with a different mass spectrum. We have :

i) one massive scalar boson, with mass $m = \sqrt{-2\mu^2}$ associated to the field σ ;

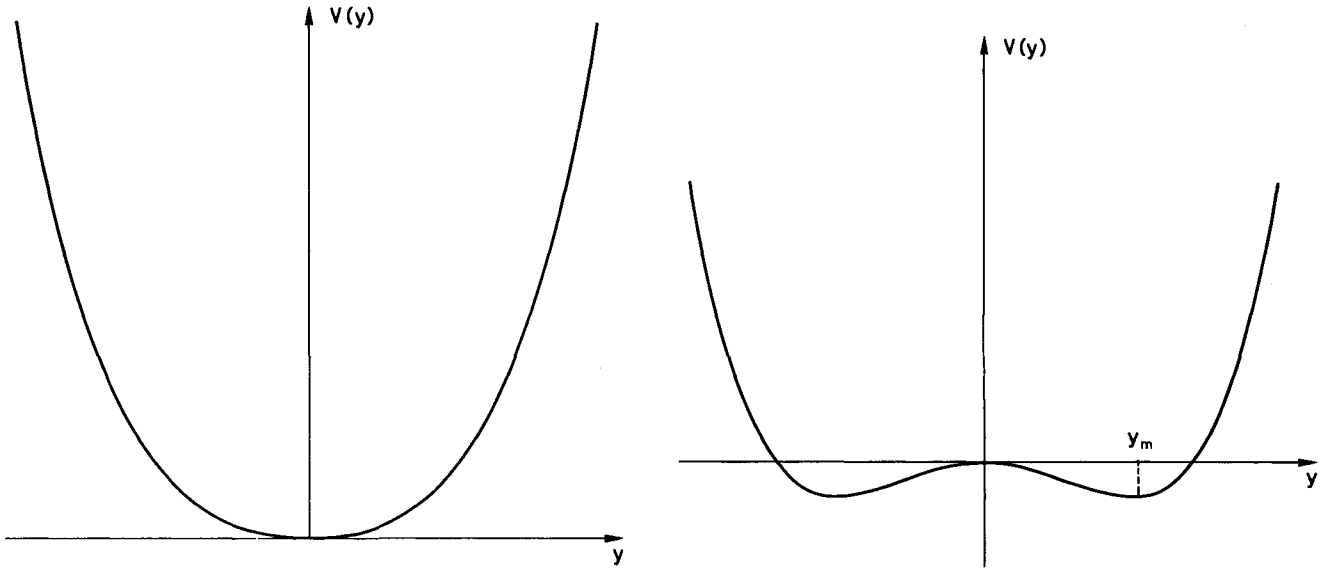

a) $\mu^2 > 0$ b) $\mu^2 < 0$

Fig. 2 Shape of the potential V(y), $y^2 = \varphi^+\varphi$

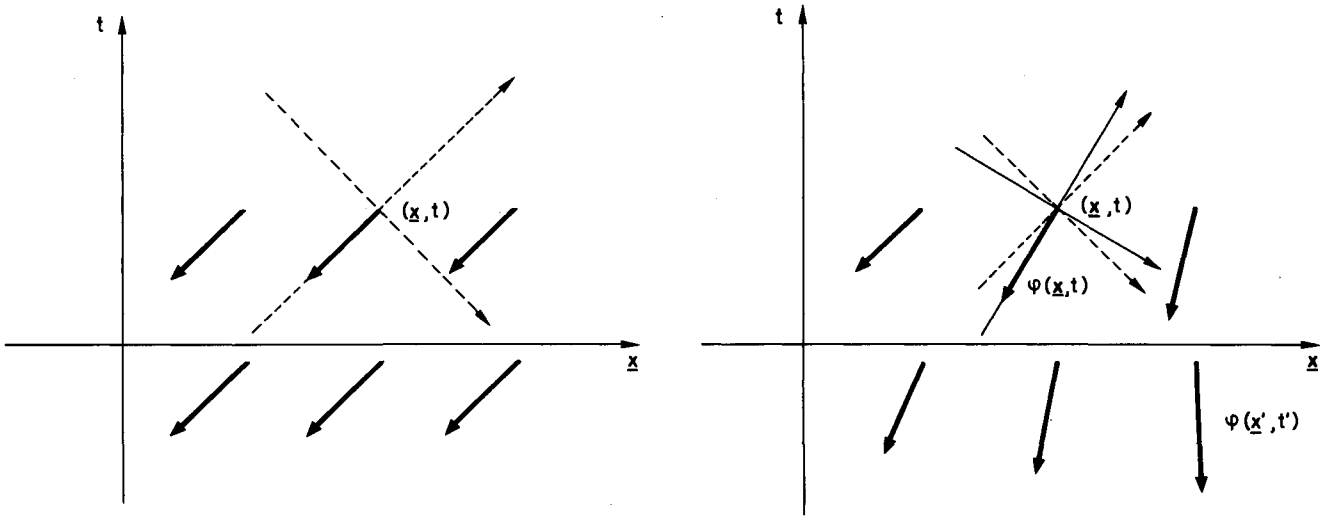

a) Field configuration in the ground state. The heavy arrows represent the value of φ_0, in an isospin frame superimposed to the $(\underline{x},t)$ space. The dotted axes are the axes of the isospin frame where φ_0 is a "down" spinor.

b) Field configuration in a perturbed state. The heavy arrows represent the value of φ at various space-time points. At the point $(\underline{x},t)$, the standard isospin axes, where φ_0 is "down", and the isospin axes defined by $\varphi(\underline{x},t)$ are shown (dotted and undotted axes, respectively).

Fig. 3

ii) three massless (Goldstone) bosons, associated to the fields $\tilde{\theta}^a(x)$.

We may summarize what we have found as follows.

i) we started from an I-spin symmetric lagrangian;

ii) a dynamical condition (i.e. $\mu^2 < 0$) forces the ground state to correspond to a non vanishing, constant field configuration, $\varphi_0 \neq 0$

iii) as a consequence, the mass spectrum is no more I-spin symmetric;

iv) a number of scalar fields (those associated to θ^a or, which is the same, $\tilde{\theta}^a$) correspond to massless (Goldstone) particles.

The fact that the condition $\varphi_0 \neq 0$ removes the mass degeneracy we had in the case $\varphi_0 = 0$, is easy to understand. $\varphi_0 \neq 0$ means that at every point in space-time there is a preferred direction in isospin space (i.e. the one determined by φ_0) which affects differently the propagation of the isospin waves associated to transverse, $\tilde{\theta}^a$, or longitudinal, σ, isospin oscillations.

There is a simple reason why we found precisely three Goldstone bosons. To understand this, we have to go back to the lagrangian (5.1). The invariance group of (5.1) is in fact larger than SU(2), in that it includes also transformations of the form :

$$\delta\varphi = i \frac{\varepsilon}{2} \varphi \qquad (5.19)$$

(ε = infinitesimal parameter, the factor of $\frac{1}{2}$ is purely conventional). The infinitesimal generator of the transformation (5.19) is the 2x2 matrix :

$$\frac{1}{2} \mathbb{1} = \frac{1}{2} \begin{pmatrix} 1 & 0 \\ 0 & 1 \end{pmatrix}$$

which obviously commutes with the generators of SU(2) (i.e. $\frac{\tau_a}{2}$) The full invariance group of (5.1) is therefore the product of SU(2) times an abelian, 1-parameter group generated by (5.19). This is denoted by $SU(2) \otimes U(1)$. What is the symmetry of φ_0 ? That is, what are the transformations of $SU(2) \otimes U(1)$ which leave φ_0 invariant ? This is equivalent to find those generators of $SU(2) \otimes U(1)$ which give zero when applied to φ_0. In fact if T is such a generator :

$$T\varphi_0 = 0 \qquad (5.20)$$

then :

$$e^{i\alpha T} \varphi_0 = \varphi_0$$

for any value of α. It is easy to see that τ_1, τ_2 and $\frac{1-\tau_3}{2}$ do not satisfy (5.20), while $\frac{1+\tau_3}{2}$ does :

$$\left(\frac{1+\tau_3}{2}\right) \varphi_0 = 0$$

In conclusion, out of four generators, only one obeys (5.20) (i.e. annihilates the vacuum), the other three do not, and the symmetry generated by them is broken. Thus there are as many broken generators as many Goldstone particles we found. This is precisely the rule we looked for, and it is absolutely general. If we have a continuous symmetry group, which is spontaneously broken by the non vanishing value, φ_0, that a scalar field takes in the ground state, there will be one Goldstone boson for each group generator T such that

$$T\varphi_0 \neq 0$$

The residual symmetry associated to those generators which obey eq. (5.20) remains unbroken.

6. The Higgs phenomenon

We transform now the lagrangian (5.1) into a gauge invariant lagrangian, using the minimal prescription given in Sects 2 and 3. The new lagrangian is therefore :

$$\mathcal{L} = (\nabla_\mu \varphi)^+ (\nabla^\mu \varphi) - V(\varphi^+\varphi) - \frac{1}{4} F^a_{\mu\nu} F^{a\mu\nu} - \frac{1}{4} G_{\mu\nu} G^{\mu\nu} \qquad (6.1)$$

We have taken into account that the full symmetry of (5.1) is $SU(2) \otimes U(1)$, as discussed in the previous section, and, correspondingly, we have introduced 4 gauge fields : an isotriplet A^a_μ $(a = 1, 2, 3)$ and a singlet B_μ. The corresponding gauge curls are given by (2.7) for $F^a_{\mu\nu}$, while :

$$G_{\mu\nu} = \partial_\mu B_\nu - \partial_\nu B_\mu \qquad (6.2)$$

since B_μ is associated to the abelian group U(1). The covariant derivative of φ is the generalization of (2.3) to $SU(2) \otimes U(1)$ and therefore it contains two coupling constants (see the final comments in Section 2) :

$$\nabla_\mu \varphi = \left(\partial_\mu + ig A^a_\mu \frac{\tau_a}{2} + i g' B_\mu \frac{1}{2} \mathbb{1}\right) \varphi \qquad (6.3)$$

$\mathbb{1}$ denotes the 2x2 unit matrix.

Vacuum state. Again we look for the classical solution of (6.1) which represents the ground (vacuum) state. As before, it is obtained for constant fields φ_0, $(A^a_\mu)_0$, $(B^a_\mu)_0$. However, we must keep into

account the fact that the ground state must be Lorentz invariant. This means that at any space-time point x there must not be any preferred direction in Minkowski space. Non vanishing values for A_μ^a or B_μ would give just that, so we conclude :

$$(A_\mu^a)_0 = (B_\mu)_0 = 0 \qquad (6.4)$$

The hamiltonian density obtained from (6.1), with the conditions (6.4) obviously coincides with (5.8), so we are back to our previous problem, and we find again the two possible solutions (5.9) and (5.10).

Particle spectrum. We put ourselves in the broken symmetry case (5.10). Consider a field configuration $\varphi(x)$ which differs a little bit from the constant distribution, φ_0 . As before, the isospinor $\varphi(x)$ is a "down" spinor in an isospin frame which differs, with respect to the isospin frame defined by φ_0 , by the rotation $U(x)$, given by (5.13). The situation is however different from the one we had before, in that the lagrangian (6.1) is now invariant under space-time dependent (gauge) isospin transformations. As we discussed in Section 2, this means that we can choose at any space time point x any orientation of the isospin axes we please, independently from what we do at any other space-time point x' . In particular, we can choose at x our isospin axes to coincide with those in which $\varphi(x)$ is exactly a down spinor, and at the same time choose the axes at x' as those in which $\varphi(x')$ is also a down spinor. If we do so, then by definition:

$$\varphi(x) = \begin{pmatrix} 0 \\ \eta + \frac{\sigma(x)}{\sqrt{2}} \end{pmatrix} \qquad (6.5)$$

More formally we can get eq. (6.5) by parametrizing $\varphi(x)$ as we did in eq. (5.15), and then absorbing the matrix U(X) into the redefinition of the isospin axes. (A side remark. The possibility of doing so depends upon two facts : gauge invariance and the fact that (5.15) gives an allowed parametrization of $\varphi(x)$. It is possible to show that the second condition is fulfilled in the broken theory, while it is not in the case of the exact symmetry ($\mu^2 > 0$, $\eta = 0$). In the unbroken theory the parametrization (6.5) is illegal and the subsequent analysis does not hold). Eq. (6.5) may seem absurd at first sight. A complex isospin field is described by four real fields (see eqs. (5.2) or (5.17)) while (6.5) contains only one real field, σ . We seem to have lost the transverse degrees of freedom, i.e. those previously associated to the fields θ^a . We will see shortly the solution to this seemingly paradoxical fact. To determine the mass spectrum, we have again to substitute (6.5) into (6.1) and collect all terms which are of 2nd order in the fields σ, A_μ^a and B_μ . The covariant derivative term reduces according to :

$$(\nabla_\mu \varphi^+)(\nabla^\mu \varphi) = \frac{1}{2}(\partial_\mu \sigma)(\partial^\mu \sigma) + \frac{1}{2}\left(\frac{g^2\eta^2}{2}\right)\left[A_\mu^1 A^{1\mu} + A_\mu^2 A^{2\mu}\right] + \frac{1}{4}\eta^2 (g A_\mu^3 - g' B_\mu)(g A^{3\mu} - g' B^\mu) + \text{higher order terms} \qquad (6.6)$$

while $-V(\varphi^+\varphi)$ gives the σ mass term as before :

$$+V(\varphi^+\varphi) = \text{const} + \frac{1}{2}(-2\mu^2)\sigma^2 + \text{h.o.t.} \qquad (6.7)$$

Finally, the 2nd order terms in the gauge field lagrangian give :

$$-\frac{1}{4} A_{\mu\nu}^a A^{a\mu\nu} - \frac{1}{4} G_{\mu\nu} G^{\mu\nu} \qquad (6.8)$$

where we have set $A_{\mu\nu}^a \equiv \partial_\mu A_\nu^a - \partial_\nu A_\mu^a$. Adding up (6.6), (6.7) and (6.8) we get the total free lagrangian. Actually, eq. (6.6) contains mixed products of A_μ^3 and B_μ, and we have to diagonalize it. To this end, we define two orthogonal combinations of A_μ^3 and B_μ :

$$\begin{aligned} Z_\mu &= \cos\theta\, A_\mu^3 - \sin\theta\, B_\mu \\ A_\mu &= \sin\theta\, A_\mu^3 + \cos\theta\, B_\mu \end{aligned} \qquad (6.9)$$

and ask θ to be such as to make the free lagrangian diagonal in Z_μ and A_μ . Evidently, eq. (6.6) implies that :

$$\tan\theta = \frac{g'}{g} \qquad (6.10)$$

whence :

$$\begin{aligned} \mathcal{L}_{free} = {} & \frac{1}{2}(\partial_\mu \sigma)(\partial^\mu \sigma) - \frac{1}{2}(-2\mu^2)\sigma^2 - \\ & - \frac{1}{4} A_{\mu\nu}^1 A^{1\mu\nu} + \frac{1}{2}\left(\frac{g^2\eta^2}{2}\right) A_\mu^1 A^{1\mu} \\ & - \frac{1}{4} A_{\mu\nu}^2 A^{2\mu\nu} + \frac{1}{2}\left(\frac{g^2\eta^2}{2}\right) A_\mu^2 A^{2\mu} \\ & - \frac{1}{4} Z_{\mu\nu} Z^{\mu\nu} + \frac{1}{2}\left(\frac{g^2\eta^2}{2\cos^2\theta}\right) Z_\mu Z^\mu \\ & - \frac{1}{4} A_{\mu\nu} A^{\mu\nu} \end{aligned} \qquad (6.11)$$

Eq. (6.11) shows that in the presence of gauge fields,

a spontaneously broken situation does not lead to massless scalar particles. There is only one, massive scalar field (with $m = \sqrt{-2\mu^2}$ as before). On the other hand, three vector fields have acquired a non vanishing mass. More precisely we have a common mass :

$$M^2 = \frac{g^2\eta^2}{2} \tag{6.12}$$

for A^1_μ and A^2_μ, and a different mass :

$$M_Z^2 = \frac{g^2\eta^2}{2\cos^2\theta} = \frac{M^2}{\cos^2\theta} \tag{6.13}$$

for Z_μ . Recall, from Section 3, that a massive vector field has one more degree of freedom, with respect to the massless case, namely that associated to longitudinal waves. There are, therefore, three more degrees of freedom for vector fields in the broken theory, with respect to the unbroken situation. This exactly compensates for three degrees of freedom we seemed to have lost in discussing eq. (6.5). These degrees of freedom have been simply transferred from the scalar fields to the longitudinal modes of vector fields. As Sidney Coleman puts it, the gauge fields have eaten the Goldstone bosons and grown heavy.

There is still one massless vector field in (6.11), namely A_μ . This is so because the full symmetry of (6.1) has not been completely broken by φ_0 . As we have seen in Section 5, there is still one conserved generator, namely :

$$\frac{1+T_3}{2} = Q \tag{6.14}$$

Indeed, if we go back to (6.3) and express the terms containing A^3_μ and B_μ as functions of A_μ and Z_μ , we get :

$$g A_\mu \frac{\tau_3}{2} + g' \frac{1}{2} B_\mu =$$

$$= \frac{g}{\cos\theta}\left(\frac{\tau_3}{2} - \sin^2\theta Q\right) Z_\mu + g\sin\theta\, Q A_\mu \tag{6.15}$$

Q being the matrix (6.14). We see that Z_μ is coupled to a broken generator (similarly to A^1_μ and A^2_μ which are coupled to $\tau_1/2$ and $\tau_2/2$) while A_μ is coupled precisely to the conserved generator, Q .

What we have seen above is an illustration of the Higgs phenomenon (actually discovered also by Brout and Englert, and by Guralnik, Hagen and Kibble). It enables us to associate massive particles to some of the gauge fields (those corresponding to broken generators) without having to introduce explicitly a mass term in the lagrangian.

The relevance of the Higgs phenomenon is greatly enhanced by the following result (essentially proven by 't Hooft, and which I cannot possibly explain in any detail in these lectures) : a gauge theory spontaneously broken by the Higgs mechanism is renormalizable. In such a theory, similarly to QED and unlikely the massive Y-M theory we sketched in Section 3 , we can compute physical amplitudes to any given order in the coupling constants, in terms of only a finite number of parameters, namely those contained in the lagrangian we started with.

Stated differently, the Higgs phenomenon allows us to have a physically sensible theory (and no unobserved massless particles) which is also theoretically tractable in high orders of perturbation theory.

The example discussed above is the basis of the models of weak and e.m. interactions we shall discuss in the following sections.

Replacing A^1_μ and A^2_μ by the complex fields

$$W_\mu = \frac{1}{\sqrt{2}}\left(A^1_\mu + i A^2_\mu\right) \; ; \; W^*_\mu = \frac{1}{\sqrt{2}}\left(A^1_\mu - i A^2_\mu\right) \tag{6.16}$$

we will identify W_μ and W^*_μ with the fields associated to the charged intermediate boson (the one mediating e.g. the neutron β -decay) and Z_μ with the neutral intermediate boson, responsible for neutral current processes (e.g. $\nu_\mu - e$ scattering). The leftover massless field, A_μ , will of course be identified with the electromagnetic field. The mixing angle θ , defined in eqs. (6.9) and (6.10), is the so-called Weinberg-Salam angle, and, according to eq. (6.15) we will set :

$$g\sin\theta = e \tag{6.17}$$

e = electric charge :

The mixing angle θ has been, actually, first introduced by Glashow[1], who was also the first to consider a unified model based on the gauge group $SU(2) \otimes U(1)$.

7. Weak Interactions of electron-like and muon-like leptons in the Weinberg-Salam model

We are now ready to construct a concrete model for the weak and e.m. interactions of the known leptons (ν, e and ν', μ) based on the gauge group $SU(2) \otimes U(1)$. In doing so, we must keep into account that leptons are coupled in conventional weak interactions (that is in those processes mediated

by W-exchange) through pure V-A currents. To reproduce this feature, we shall associate the action of the charged generators of $SU(2)\otimes U(1)$ on the lepton fields, with the chiral isospin generators we have introduced in Section 1.

Let us, therefore, arrange the four leptons into two independent doublets :

$$E = \begin{pmatrix} \nu \\ e \end{pmatrix} \qquad M = \begin{pmatrix} \nu' \\ \mu \end{pmatrix}$$

We will then define the action of an infinitesimal SU(2) transformation according to :

$$\delta E = i\,\varepsilon^a \frac{\tau_a}{2} \left(\frac{1-\gamma_5}{2}\right)\begin{pmatrix} \nu \\ e \end{pmatrix} = i\,\varepsilon^a L^a \begin{pmatrix} \nu \\ e \end{pmatrix} \tag{7.1}$$

and similarly for δM . As we noticed in Section 1, the transformation (7.1) corresponds, for zero mass particles, to an isospin rotation of the lefthanded states (i.e. states with negative helicity), the righthanded states remaining unaffected. To make this fact more explicit, we define a lefthanded doublet :

$$E_L = \frac{1-\gamma_5}{2}\begin{pmatrix} \nu \\ e \end{pmatrix} \equiv \begin{pmatrix} \nu_L \\ e_L \end{pmatrix} \tag{7.2}$$

and similarly a muonic doublet, M_L . Eq. (7.1) can then be interpreted as saying that the lefthanded fields behave as (weak) isodoublets :

$$\delta E_L = i\,\varepsilon^a \frac{\tau_a}{2} E_L \tag{7.3}$$

(and similarly for M_L) while righthanded fields behave like (weak) isosinglets :

$$\delta e_R = \delta\left(\frac{1+\gamma_5}{2} e\right) = 0 \tag{7.4}$$

and similarly for ν_R , ν'_R , μ_R . To go further, we must specify the action of the U(1) transformations.

This is in fact determined by the requirement that the photon field, defined by (6.9) couples precisely to the electric charge. To see this, let us put all the lepton fields into a single column vector χ :

$$\chi = \begin{pmatrix} \nu_L \\ e_L \\ \vdots \\ \nu'_R \end{pmatrix}$$

and assume :

$$\delta\chi = i\,\frac{\varepsilon}{2}\,Y\chi \tag{7.5}$$

Y being an 8×8 matrix. The coupling of A^3_μ and B_μ to the leptons resulting from (7.3), (7.4) and (7.5) will be :

$$\bar\chi\gamma_\mu\left[g A^3_\mu L^3 + \tfrac{1}{2} g' B_\mu Y\right]\chi =$$

$$= \bar\chi\gamma_\mu\left[A_\mu\left(g\sin\theta\, L^3 + \tfrac{1}{2} g'\cos\theta\, Y\right) + \right.$$

$$\left. + Z_\mu\left(g\cos\theta\, L^3 - \tfrac{1}{2} g'\sin\theta\, Y\right)\right]\chi = \tag{7.6}$$

$$= \bar\chi\gamma_\mu\left\{A^\mu e\left(L^3 + \tfrac{1}{2} Y\right) + \right.$$

$$\left. + Z^\mu \frac{g}{\cos\theta}\left[L^3 - \sin^2\theta\left(L^3 + \tfrac{1}{2} Y\right)\right]\right\}\chi$$

We have therefore to satisfy the condition :

$$Q = L^3 + \tfrac{1}{2} Y \tag{7.7}$$

which determines Y , once Q and L_3 are known. The above condition leads to the weak hypercharge assignment shown in Table 1. Note that, since both Q and L_3 are diagonal, so it is Y , and the U(1) transformations act, in this case, as phase transformations. Note also that Z_μ is coupled to a linear combination of the currents associated to the electric charge and to the 3rd component of weak isospin.

Table 1. Quantum numbers of electron-like leptons. The corresponding table for muon-like leptons, is obtained by replacing $e \to \mu$, $\nu \to \nu'$

	ν_L	e_L	ν_R	e_R
L^3	$+\frac{1}{2}$	$-\frac{1}{2}$	0	0
Y	−1	−1	0	−2

We can now write down the covariant derivatives of the lepton fields :

$$\nabla_\mu E_L = \left(\partial_\mu + i g \frac{\tau_a}{2} A^a_\mu - i \frac{g'}{2} B_\mu\right) E_L$$

$$\nabla_\mu e_R = \left(\partial_\mu - i g' B_\mu\right) e_R$$

$$\nabla_\mu \nu_R = \partial_\mu \nu_R$$

and similarly for muon-like fields. To fully determine the lepton lagrangian, one could make the hypothesis that the leptons have no other interaction than with the gauge fields. In this case one would simply apply the minimal prescription, $\partial_\mu \to \nabla_\mu$, to the free lepton lagrangian. However, to be able to

do so, the free lagrangian itself must be invariant under the global transformations, eqs. (7.3) to (7.5). Since these transformations involve chiral transformations, an invariant free lagrangian can only be achieved in the limit where all leptons have a vanishing mass, as discussed in Section 1.

To obtain a non vanishing mass for electrons and muons, we have to postulate that leptons possess other interactions but the weak and electromagnetic ones. We will see in the next section that a suitable interaction of the leptons with the scalar isodoublet, φ , can indeed give rise to the observed lepton masses.

For the time being, however, we will neglect these additional interactions and, restricting to the limit of zero mass for all leptons, we will construct the lepton lagrangian from the free, massless lagrangian. In this limit, the lepton lagrangian is simply :

$$\mathcal{L}_{lept.} = i\left(\bar{E}_L \not{\partial} E_L + \bar{M}_L \not{\partial} M_L\right) + \tag{7.8}$$
$$+ i\left(\bar{e}_R \not{\partial} e_R + \bar{\mu}_R \not{\partial} \mu_R\right) + i\left(\bar{\nu}_R \not{\partial} \nu_R + \bar{\nu}'_R \not{\partial} \nu'_R\right)$$

while the total lagrangian is the sum of (7.8) and (6.1).

The lagrangian (7.8) describes the weak and e.m. interactions of leptons, which we will now briefly review.

To this aim, we extract from (7.8) the interaction terms, which turn out to be :

$$\mathcal{L}_{int} = -g A^a_\mu \bar{E}_L \gamma^\mu \frac{\tau^a}{2} E_L + \frac{g'}{2}\left(\bar{E}_L \gamma_\mu E_L + \right. \tag{7.9}$$
$$\left. + 2\,\bar{e}_R \gamma^\mu e_R\right) B_\mu + \left(E_L \to M_L\,;\, e_R \to \mu_R\right)$$

It is of course more convenient to express $\mathcal{L}_{int}$ in terms of the physical vector fields W_μ , Z_μ and A_μ . Using eqs. (6.9), (6.10), (6.16) and (6.17), one gets finally :

$$\mathcal{L}_{int} = -\frac{g}{2\sqrt{2}} \bar{\nu} \gamma^\mu (1-\gamma_5) e\, W^*_\mu + h.c.$$
$$- \frac{g}{\cos\theta}\left[\bar{\nu}\gamma^\mu(1-\gamma_5)\nu - \bar{e}\gamma^\mu(1-4\sin^2\theta-\gamma_5)e\right]Z_\mu \tag{7.10}$$
$$+ e\, A_\mu \bar{e}\gamma^\mu e +$$
$$+ \left(e, \nu \to \mu, \nu'\right)$$

The A_μ terms describe the well known e.m. interaction of photons with electrons and muons, which we shall not discuss. The other terms describe the emission and absorption of the heavy intermediate bosons, W and Z. In second order of perturbation theory (as discussed in Sections 3 and 4) they give rise to lepton-lepton scattering, or to crossing related processes, through $W^\pm$ and/or Z exchange.

W-mediated processes (charged currents). W -exchange gives rise e.g. to the process :

$$\nu' + e \to \mu + \nu \tag{7.11}$$

or to the crossing related μ decay. Applying eq. (4.2), and using the weak charged currents given in (7.10), we find the low energy amplitude (valid in the limit of very small momentum transfer with respect to the W mass) :

$$A = \frac{g^2}{8 M_W^2}\left[\bar{\mu}\gamma_\lambda(1-\gamma_5)\nu'\right]\left[\bar{\nu}\gamma^\lambda(1-\gamma_5)e\right] \tag{7.12}$$

The amplitude (7.12) coincides with the V-A current x current amplitude. The coefficient multiplying the four fermion amplitude is conventionally written as $G/\sqrt{2}$, so that one finds the relation:

$$\frac{G}{\sqrt{2}} = \frac{g^2}{8 M_W^2} \tag{7.13}$$

(G = Fermi constant $\sim 10^{-5} M_p^{-2}$; M_p = proton mass).

We may combine eq. (7.13) with eq. (6.17), to obtain a lower bound for the W mass:

$$M_W^2 = \frac{g^2}{4\sqrt{2}G} = \frac{e^2}{4\sqrt{2}G}\frac{1}{\sin^2\theta} =$$
$$= \left(\frac{\pi\alpha}{\sqrt{2}G}\right)\frac{1}{\sin^2\theta} = \frac{(37.5\ GeV)^2}{\sin^2\theta} \tag{7.14}$$

At high energy, the amplitude for the process (7.11) is modified, with respect to (7.12), by the effect of the W-propagator (see eq. (4.2)). Eq. (7.14) indicates that appreciable modifications will appear only for ν' energies above the present FNAL range. Indeed, the experimental lower limit on the W mass that present neutrino experiments have been able to set, is around 10 GeV.

Information coming from semi-leptonic neutral current processes indicates that $\sin^2\theta \sim 0.3$ (with large errors). Correspondingly, one gets $M_W \sim 68\ GeV$.

Leptonic width of the W. Eq. (7.10) gives directly the amplitude for the decay :

$$W^+ \to e^+ \nu$$

which occurs in lowest order. The corresponding width can be computed by standard methods. It is use-

ful to cast the result in a more general form, considering a coupling of the type :

$$W_\mu \left[g_L \bar{e}_L \gamma^\mu e_L + g_R \bar{e}_R \gamma^\mu e_R \right]$$

One finds in this case :

$$\Gamma = \left(\frac{g_L^2 + g_R^2}{4\pi} \right) \frac{M_W}{6} \qquad (7.15)$$

From eq. (7.10), we read : $g_R = 0$, $g_L = g/\sqrt{2}$, whence

$$\Gamma(W \to e\nu) = \frac{1}{12} \left(\frac{g^2}{4\pi} \right) M_W =$$

$$= \frac{\alpha}{12} \frac{37.5\ GeV}{\sin^2\theta} \approx \frac{23\ MeV}{\sin^2\theta}$$

To get the total width, one must add to $\Gamma(W \to e\nu)$ an equal contribution from the $\mu\nu'$ mode, the hadronic width and possible contributions from heavy leptons. In total, this may give about a factor of 10, leading to a value for $\Gamma_{total}(W)$ in the GeV region.

Z-mediated processes (neutral currents). The prototype neutral current process is :

$$\nu' + e \to \nu' + e \qquad (7.16)$$

whose low energy amplitude, derived as before, is :

$$A = \frac{g^2}{16 \cos^2\theta M_Z^2} \left[\bar{\nu}' \gamma_\mu (1-\gamma_5) \nu \right] \left[\bar{e} \gamma^\mu (g_V - g_A \gamma_5) e \right] \qquad (7.17)$$

$$g_V = 1 - 4\cos^2\theta$$

$$g_A = 1 \qquad (7.18)$$

We may observe that :

i) The electron neutral current is not pure V-A .

ii) Using eq. (6.13) we may eliminate the θ dependence of the effective coupling in (7.17) according to :

$$\frac{g^2}{16\cos^2\theta M_Z^2} = \frac{g^2}{16 M_W^2} = \frac{1}{2} \frac{G}{\sqrt{2}} \qquad (7.19)$$

so that the scale of the amplitude (7.17) is determined by the Fermi constants only.

Z exchange contributes also to the process :

$$\nu + e \to \nu + e \qquad (7.20)$$

in addition to W-exchange, see Fig. 4. The low energy amplitude is still a four fermion amplitude, of the form :

$$A(\nu e) = \frac{G}{2\sqrt{2}} \left[\bar{\nu} \gamma_\mu (1-\gamma_5) \nu \right] \left[\bar{e} \gamma^\mu (g'_V - g'_A \gamma_5) e \right] \qquad (7.21)$$

but now :

$$g'_V = -(1 + 4\sin^2\theta)$$

$$g'_A = -1$$

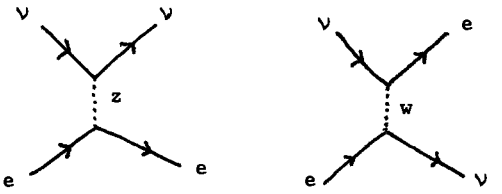

Fig. 4. Feynman diagrams for νe scattering

Summing up, we have seen that the amplitudes of processes (7.16) and (7.20), and of the crossing related processes, are completely determined, in terms of one single parameter, θ . It is obviously of the utmost importance to have experimental checks of these predictions, especially since, in these processes, there are no uncontroled strong interaction effects.

At present, a few events of (7.16) have been observed in Gargamelle and, quite recently, process (7.20) has been unambiguously observed[2]. Within the very limited accuracy presently available, data are in both cases consistent with the Weinber-Salam model, with $\sin^2\theta \sim 0.3$.

Combining eqs. (7.14) and (6.13), we may again obtain a lower bound on the Z mass. We find :

$$M_Z^2 = \frac{(75.0\ GeV)^2}{(\sin 2\theta)^2}$$

Using again $\sin^2\theta \sim 0.3$, we estimate

$$M_Z \sim 82\ GeV .$$

Leptonic width of the Z . From eq. (7.10) we get the couplings of Z to e^+e^- :

$$g_L^2 = \frac{g^2}{4\cos^2\theta} (1 - 2\sin^2\theta)^2$$

$$g_R^2 = g^2 \frac{\sin^4\theta}{\cos^2\theta}$$

and using (7.15), we get :

$$\Gamma(Z \to e^+e^-) = \Gamma(W \to e\nu)\frac{1-4\sin^2\theta+8\sin^4\theta}{2\cos^3\theta}$$

$$\simeq \frac{92\ MeV}{(\sin 2\theta)^3}\left(1-4\sin^2\theta+8\sin^4\theta\right)$$

In the same way, one can find the $\nu\bar{\nu}$ width :

$$\Gamma(Z \to \nu\bar{\nu}) = \frac{g^2}{4\pi}\frac{M_Z^2}{24\cos^2\theta} \simeq \frac{92\ MeV}{(\sin 2\theta)^3}$$

The total Z rate, as in the case of the W , can be about one order of magnitude larger than the previous rates.

Other Z-related processes. Z-exchange gives rise to observable effects also in processes not involving neutrinos. An important example is the production of $\mu^+\mu^-$ pairs in colliding rings :

$$e^+e^- \to \mu^+\mu^- \qquad (7.23)$$

which can take place through one photon and one Z exchange. At low energy the effect of Z-exchange is negligibly small, but it increases linearly with the center of mass energy. Already in the Petra energy range the interference of Z with γ exchange may give rise to detectable effects (e.g. the backward-forward asymmetry of μ^+). When $2E_e = M_Z$, the weak amplitude dominates, as one is producing real Z's.

At still larger energies, γ and Z exchange remain comparable, and gradually weak and e.m. interactions merge together.

Another important effect, is related to Z exchange between electrons and nucleons in atoms. This gives rise to a parity violating potential and therefore to P-violating mixing of the atomic levels. There are, at present, various experimental groups attempting to detect P-violation in heavy atoms. No firm evidence of such effects has been yet achieved.

8. The anomalous magnetic moment of the W

As a side exercise, we consider the coupling of the photon to the W-meson.

This coupling arises from the trilinear self coupling of gauge fields, which we have previously called $"A^3"$. Since the structure of the $"A^3"$ terms is precisely determined by gauge invariance, we will get a well defined γ- W interaction, which, as we shall see, has a very peculiar structure.

In the $SU(2)\otimes U(1)$ model, only the isotriplet fields A^a_μ have a trilinear interaction, of the form already given in eq. (3.3). There are no trilinear terms involving B_μ , since B_μ is associated to an abelian group (see eq. (6.2)) which commutes with SU(2). If we write down explicitly the $g"A^3"$ term in (3.3), we get :

$$\begin{aligned} g"A^3" &= \tfrac{1}{2} g\,\varepsilon_{abc}\,A^a_\mu A^b_\nu A^{c\mu\nu} = \\ &= g\left(A^1_\mu A^2_\nu A^{3\mu\nu} + A^2_\mu A^3_\nu A^{1\mu\nu} + \right. \\ &\left. + A^3_\mu A^1_\nu A^{2\mu\nu}\right) = \\ &= ig\,A^{3\mu\nu} W_\mu W^*_\nu - ig\,A^{3\lambda}\left(W^*_{\mu\lambda} W^\mu - \right. \\ &\left. - W^{*\mu} W_{\mu\lambda}\right) \end{aligned} \qquad (8.1)$$

In eq. (8.1) we have used the shorthand notation $A^a_{\mu\nu} = \partial_\mu A^a_\nu - \partial_\nu A^a_\mu$, and, in the last line, we have used eq. (6.16), to express the interaction in terms of the fields associated to the charged particles $W^\pm$. To get the photon coupling, we have to express A^3_λ in terms of the physical fields A_λ and Z_λ , and keep the terms with A_λ . To this aim, we use eqs. (6.9) and (6.17), to get finally :

$$\mathcal{L}_{\gamma\text{-}W} = ie\left[F^{\mu\nu} W_\mu W^*_\nu + A^\lambda\left(W^*_{\lambda\mu} W^\mu - W^{*\mu} W_{\lambda\mu}\right)\right] \qquad (8.2)$$

($F_{\mu\nu} = \partial_\mu A_\nu - \partial_\nu A_\mu$ = the e.m. field strength tensor). The remarkable feature of eq. (8.2) is the presence of the first term, where the W field is directly coupled to the electric and magnetic fields, contained in $F_{\mu\nu}$.

To see why this is remarkable, let us suppose that, unlike the case we are considering, weak interactions were a completely independent phenomenon from electromagnetic interactions. We could still describe weak interactions as resulting from W-exchange, with a lagrangian of the form :

$$\mathcal{L}_{weak} = \mathcal{L}^W_{free} + \mathcal{L}_{int}(W\text{-lept.}, W\text{-quarks})$$

$$\mathcal{L}^W_{free} = -\tfrac{1}{2} W^*_{\mu\nu} W^{\mu\nu} + M_W^2\, W^*_\mu W^\mu$$

To describe the e.m. interactions of W , we would then perform in $\mathcal{L}^W_{free}$ the "minimal substitution" appropriate to electromagnetism, namely we would

make the replacement

$$\partial_\mu W_\nu \longrightarrow (\partial_\mu - ie A_\mu) W_\nu$$

A_μ being the photon field. If we do so, it is easy to compute what one would call the "minimal" $\gamma - W$ lagrangian, which turns out to be

$$\mathcal{L}^{\text{minimal}}_{\gamma-W} = ie A^\lambda \left(W^*_{\lambda\mu} W^\mu - W^{*\mu} W_{\lambda\mu} \right) \quad (8.3)$$

Eq. (8.3) differs from eq. (8.2) precisely because it does not contain the "non minimal" $F^{\mu\nu} W_\mu W^*_\nu$ term. The way we derived eq. (8.2) should make it clear that the non minimal term is precisely associated to the fact that both weak and e.m. interactions are described by a unified Yang-Mills theory. For this reason, when the W mesons will be experimentally detected, a precise study of the $\gamma - W$ vertex will be a very important thing to do, and could give the first experimental indication that Yang-Mills theories are indeed at work in Nature. The $\gamma - W$ vertex could be determined by a study of the neutrino production of W (Fig.5) or of W pair production in colliding rings

$(e^+e^- \to \gamma \to W^+ W^-)$

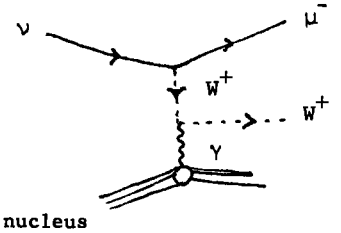

Fig. 5. Neutrino production of W^+ off a target nucleus.

It is possible to see that the non minimal term gives rise to a pointlike anomalous magnetic moment of the W. The "minimal term" (8.3) gives rise to a normal magnetic moment :

$$\vec{\mu}_{\text{normal}} = \frac{e}{2 M_W} \vec{S}$$

$\vec{S}$ being the W spin, while the non minimal term adds to $\vec{\mu}$ an anomalous term : $\vec{\mu}_{an} = \vec{\mu}_{\text{normal}}$ so that eq. (8.2) implies : $\vec{\mu}_{tot} = 2 \vec{\mu}_{\text{normal}}$

9. The lepton masses

Non vanishing masses for the leptons can be generated by suitably coupling leptons to the scalar isodoublet, φ. The general idea goes as follows.

We introduce a Yukawa type interaction (the only one allowed, if we want to keep the theory renormalizable) which we write symbolically as :

$$\mathcal{L}_{\varphi\text{-lept}} = g_s \varphi \bar{\Psi} \Psi \quad (9.1)$$

(we will see later on the the precise lagrangian is actually a sum of terms like (9;1), Ψ running over the various lepton fields; each term has an independent coupling constant). Reexpressing (9.1) in terms of the shifted scalar field σ, eq. (6.5), one obtains :

$$\mathcal{L} = (g_s \eta) \bar{\Psi} \Psi + g_s \frac{\sigma}{\sqrt{2}} \bar{\Psi} \Psi \quad (9.2)$$

The first term, which is bilinear in Ψ, can be added to the free lepton lagrangian, and it corresponds to a lepton mass term. The second term describes a residual, Yukawa type interaction of σ with the leptons, to be added to the weak interactions we described in Section 7. The new interaction is characterized by the coupling constant g_s ; its strenght can be easily compared to the strength of the weak interactions arising from W-exchange. Notice that, from eq. (9.2) :

$$g_s \eta \approx m_\ell \quad (9.3)$$

m_ℓ being a lepton mass (say m_e or m_μ) while, from eq. (6.12) we have :

$$g \eta \approx M_W \quad (9.4)$$

g being the coupling constant of the gauge fields.

One therefore finds :

$$g_s \approx g \left(\frac{m_\ell}{M_W} \right) \ll g \quad (9.5)$$

Furthermore, the lepton-lepton amplitude arising from σ exchange at low energy is of order

$$g_s^2 \frac{1}{M_\sigma^2} \approx \frac{g^2}{M_W^2} \left(\frac{m_\ell^2}{M_\sigma^2} \right) \approx G \frac{m_\ell^2}{M_\sigma^2} \quad (9.6)$$

As a consequence of (9.6), as far as the neutral Higgs boson σ is much heavier than leptons, the addition of the coupling (9.1) does not change appreciably the picture of weak interactions we have outlined previously, and the main effect of the new interaction (9.1) is that of generating lepton masses.

The same line will be followed in the case of quark (hence hadronic) masses, and the above considerations can be repeated for the interaction of quarks with the Higgs fields, replacing g_s with the σ-quark coupling constant and m_ℓ with m_q

(quark mass). It is usually assumed that σ-field is also much heavier than normal hadrons, including charmed particles. We will accept this hypothesis and, in what follows, we will completely neglect σ exchange amplitudes. In this approximation, the only role of the interaction of φ to normal matter is to provide non vanishing leptonic and hadronic mass scales.

We go now to more precise considerations, and determine the most general form of the coupling (9.1).

To this aim, we have to construct all the possible terms of the form (9.1), which are invariant under $SU(2) \otimes U(1)$, and involve the isodoublet φ, the isodoublets E_L and M_L and the isosinglets e_R, ν_R, μ_R, ν'_R.

Consider first E_L and φ. The combination :

$$\bar{E}_L \varphi \equiv \bar{\nu}_L K^+ + \bar{e}_L K^0$$

is obviously an SU(2) singlet. To make it Lorentz invariant we have to multiply it by some right-handed field. Since the weak hypercharge of φ is +1 (compare eqs. (5.19) and (7.5)) and that of $\bar{E}_L$ is also +1, to obtain an U(1) invariant coupling we need a $Y = -2$ field, namely e_R or μ_R. Repeating the same argument also for M_L, we find the invariant coupling :

$$\left(g_1 \bar{E}_L e_R + g_{12} \bar{E}_L \mu_R + g_{21} \bar{M}_L e_R + g_2 \bar{M}_L \mu_R\right)\varphi + \quad (9.7)$$

+ hermitian conjugate

the g's being arbitrary coupling constants, which are a specification of the coupling constant g_S in (9.1).

The term (9.7) is not, however, the only invariant coupling, due to the special property of the group SU(2), that it admits only real representations. This means that we can construct a new isodoublet (to be called $\tilde{\varphi}$) whose components are linear combinations of the components of φ^+, and which transforms precisely like φ. Indeed, if we define :

$$\tilde{\varphi} = -i\left(\varphi^+ \tau_2\right)^{Transp} \equiv \begin{pmatrix} \bar{K}^0 \\ -K^- \end{pmatrix} \quad (9.8)$$

then :

$$\delta\tilde{\varphi} = -i\left(\delta\varphi^+ \tau_2\right)^T = -i\varepsilon^a\left(-i\varphi^+ \tfrac{\tau_a}{2} \tau_2\right)^T =$$

$$= i\varepsilon^a \tfrac{\tau_a}{2}\left(-i\varphi^+ \tau_2\right)^T = i\varepsilon^a \tfrac{\tau_a}{2}\tilde{\varphi} \quad (9.9)$$

due to the identity :

$$\tau_2 \tau_a \tau_2 = -\tau_a^T$$

The transformation rule (9.9) has precisely the same form as (1.6). Note further that $\tilde{\varphi}$ has weak hypercharge -1. Repeating the argument which led to (9.7), one obtains therefore the further coupling :

$$\left(h_1 \bar{E}_L \nu_R + h_{12} \bar{E}_L \nu'_R + h_{21} \bar{M}_L \nu_R + h_2 \bar{M}_L \nu'_R\right)\tilde{\varphi} + \quad (9.10)$$

+ hermitian conjugate

with new, independent, coupling constants. The most general φ-lepton interaction is, finally, the sum of the lagrangians (9.7) and (9.10), which have to be added to (7.8), to obtain the full leptonic weak lagrangian.

The resulting expression can be somehow simplified by the following observation. If we perform orthogonal transformations on corresponding electron-like and muon-like fields, i.e. if we set :

$$E_L = \cos\alpha\, E'_L + \sin\alpha\, M'_L$$

$$M_L = -\sin\alpha\, E'_L + \cos\alpha\, M'_L$$

and similarly for e_R, μ_R and for ν_R and ν'_R (with independent angles β and γ), the lagrangian (7.8) remains unaffected, while (9.7) and (9.10) go into similar expressions, with new constants, g' and h', linearly related to the unprimed constants. By elementary considerations one can show that the parameters α, β and γ can be chosen so that the g' and h' satisfy either the relations :

$$g'_{12} = g'_{21} = 0 \quad ; \quad h'_{12} = h'_{21} \quad (9.11)$$

or, equivalently :

$$g'_{12} = g'_{21} \quad ; \quad h'_{12} = h'_{21} = 0 \quad (9.12)$$

Stated differently, the eight couplings appearing in (9.7) and (9.10) are redundant, and with no loss of generality we may require either (9.11) or (9.12) to hold. In what follows, we shall choose condition (9.11). It can also be shown that, with no loss of generality, the constants g's and h's can be chosen to be real (this corresponds to a CP conserving interaction; the model is therefore intrinsically CP conserving).

According to our previous discussion, we replace now φ by the eq. (6.5) (and similarly for $\tilde{\varphi}$) and keep only the terms linear in η. The sum of (9.7) and (9.10), with the conditions (9.11), reduces then to :

$$\mathcal{L}_{mass} = g_1\eta\ \bar{e}(x)e(x) + g_2\eta\ \bar{\mu}(x)\mu(x) + $$
$$+ h_1\eta\ \bar{\nu}(x)\nu(x) + h_2\eta\ \bar{\nu}'(x)\nu'(x) + $$
$$+ h_{12}\eta\left(\bar{\nu}(x)\nu'(x) + \bar{\nu}'(x)\nu(x)\right) \qquad (9.13)$$

As anticipated, (9.13) corresponds to a mass term for all the lepton fields. In particular we have obtained two independent masses for electrons and muons :

$$m_e = g_1\eta \quad ; \quad m_\mu = g_2\eta \qquad (9.14)$$

In the model there is no way of predicting the μ-e mass ratio : the only thing we can do is to fit the observed masses with g_1 and g_2 .

We consider now the neutrino mass terms. Experimentally, both ν and ν' mass are consistent with zero, the experimental upper bounds being :

$$m_\nu < 60\ eV \quad ; \quad m_{\nu'} < 1.2\ MeV \qquad (9.15)$$

There is, however, no preference for massless neutrinos in (9.13). If like to do so, we can get vanishing neutrino masses, simply by setting : $h_1 = h_2 = h_{12} = 0$. In this case, neutrino fields appear only in (7.8), with the consequence that the right handed neutrinos have no weak interaction at all. In this limit, our model is equivalent to the two component neutrino theory, and we could even drop ν_R and ν'_R from our lagrangian. In any case, even if righthanded neutrinos would exist, we would not see them, as they would interact with the other particles only through the gravitational interaction. In the same limit ($m_\nu = m_{\nu'} = 0$) the lepton lagrangian admits the exact conservation of the electron and of the muon numbers.

It is interesting to study also the case of small, but non vanishing neutrino masses, allowing all h's to be non zero. Since the neutrino mass term is not diagonal, $\nu(x)$ and $\nu'(x)$ do not correspond to freely propagating particles. Rather, we have to consider two orthogonal combinations :

$$\nu_1 = \cos\varphi\ \nu + \sin\varphi\ \nu'$$
$$\nu_2 = -\sin\varphi\ \nu + \cos\varphi\ \nu' \qquad (9.16)$$

such that $\mathcal{L}_{mass}$ is diagonal when expressed in term of ν_1 and ν_2 . This implies :

$$\tan(2\varphi) = \frac{2h_{12}}{h_1 - h_2} \qquad (9.17)$$

At the same time, we have to express also the weak lagrangian (7.8) or (7.10) in terms of ν_1 and ν_2 . This changes the interaction terms involving W emission according to :

$$\mathcal{L}(W\text{-}\nu e,\ W\text{-}\nu'\mu) \rightarrow$$
$$\rightarrow \frac{g}{2\sqrt{2}} W_\mu^* \left[\bar{\nu}_1\gamma^\mu(1-\gamma_5)(\cos\varphi\, e + \sin\varphi\,\mu) + \right. \qquad (9.18)$$
$$\left. + \bar{\nu}_2\gamma^\mu(1-\gamma_5)(-\sin\varphi\, e + \cos\varphi\,\mu)\right]$$

When $\varphi \neq 0$, the interaction (9.18) violates electron and muon number conservation, in that e and μ are coupled at the same time to e.g. ν_1 . A related phenomenon are the so called neutrino oscillations (much similar to $K_0 - \bar{K}_0$ oscillations) which we are now going to discuss[3].

Suppose we have a source of neutrinos, located at the origin of coordinates, x = y = z = 0 , and let us suppose that neutrinos are there produced in association with muons (e.g. from $\pi \rightarrow \mu\nu$ decay). A decay at t = 0 gives rise to a linear superposition of ν_1 and ν_2 , precisely corresponding to ν' . Hence the outgoing neutrino is in the state:

$$|\nu', t=0\rangle = \sin\varphi\ |\nu_1\rangle + \cos\varphi\ |\nu_2\rangle$$

If this state has a momentum p along the z direction, at a later time t (i.e at a distance $z = vt \approx t$, since we are assuming $p \gg m_1, m_2$) we will observe the state :

$$|\nu'(t)\rangle = \sin\varphi\ e^{-i(E_1 t - pz)}|\nu_1\rangle +$$
$$+ \cos\varphi\ e^{-i(E_2 t - pz)}|\nu_2\rangle \approx$$
$$\approx e^{-ip(t-z)}\left\{\sin\varphi\ e^{-i\frac{m_1^2}{2p}z}|\nu_1\rangle + \right.$$
$$\left. + \cos\varphi\ e^{-i\frac{m_2^2}{2p}z}|\nu_2\rangle\right\}$$

where we have used the formula :

$$E = p + \frac{m^2}{2p} + O\left(\frac{m^4}{p^3}\right)$$

The expression in brackets is now not exactly ν' or ν , but rather a z-dependent combination of the two states. If we place at z a piece of iron, a charge exchange interaction of the neutrino with the iron may therefore give rise either to a muon or

to an electron, the probability for the two processes being proportional to :

$$1 - |a_{\nu\nu'}|^2 \quad \text{(for } \mu \text{ production)} \qquad (9.19)$$

$$|a_{\nu\nu'}|^2 \quad \text{(for e production)} \qquad (9.20)$$

where $a_{\nu\nu'}$ is the neutrino-flip amplitude :

$$|a_{\nu\nu'}|^2 = |\langle \nu | \nu'(t) \rangle|^2 = (\sin 2\varphi)^2 \cdot \left(\sin \frac{\pi}{2L_0}\right)^2 \qquad (9.21)$$

and :

$$\frac{1}{L_0} = |E_1 - E_2| = \frac{|m_1^2 - m_2^2|}{2P}$$

In conclusion, if we have a source of μ -neutrinos at $z = 0$, one should see, in a matter target placed a z , a non vanishing number of e-producing (hence muon number violating) events, the ratio of abnormal to normal events being given by the ratio of (9.20) to (9.19). Similar arguments hold in the case of a source of electron neutrinos. In particular, if we consider a source of low-energy neutrinos(such as a nuclear reactor, or the sun) and in the case of maximal mixing $(\varphi = 45°)$, then when $|a_{\nu\nu'}| = 1$ the neutrinos cannot interact by producing a μ , because of energy conservation. At those distances the neutrinos are "sterile". This effect has been invoked to explain, at least partially, the lack of observation of solar neutrinos.

In the experiments performed thus far no evidence has been found for neutrino oscillations. A refinement of the experimental limits is of great importance, especially since, as our previous analysis indicates, in the framework of the Weinberg-Salam model such a phenomenon would be expected to arise quite naturally.

In conclusion, we have seen that the spontaneous breaking of the gauge symmetry can explain quite simply the observed mass spectrum of leptons.

A disappointing feature of the model is, however, that is is not able to shed any light on two fundamental issues : the relation between electron and muon mass, and the smallness or the vanishing of neutrino masses. Perhaps this could be an indication that this simple model is just the phenomenological manifestation of a more fundamental theory.

10. Hadronic interactions with four quarks.

In this and in the following section, we will describe theories of the weak and e.m. interactions of quarks. The reason for doing so is, of course, the quark model, whereby all hadrons are supposed to be bound states of these fundamental fermions.

In this framework, it is indeed quite natural to think that a simple theory can be achieved in terms of the fundamental constituents, rather than directly for the composite objects.

Having said that, however, one has to face the serious problem of obtaining meaningful predictions from the theory, applicable to real experiments where only composite hadrons (π, K , etc.) are produced and observed.

We will not discuss here in any detail how this can be done and shall limit ourselves to the following observations.

i) The very fact that one is dealing with a gauge theory requires (see Section 3) that the weak currents are the Noether currents of some strong interaction symmetry, which is exact, at least prior to spontaneous breaking of the gauge group. This is sufficient in certain instances to derive from the quark theory structure-independent predictions for hadronic processes. In particular this fact will allow us to derive the selection rules obeyed by the transition amplitudes.

ii) According to the parton picture, structure dependent effects become increasingly less important in deep inelastic processes, so that one is able to test there the quark weak couplings directly.

Our framework has to be further specified, and we will assume that :

i) Quarks come in different flavors;

ii) for each flavor, quarks come in three different colors, all observed hadrons being color singlets;

iii) weak and e.m. currents are color singlets and act only on flavor space.(*)

To explain the hadronic spectroscopy, only three flavors were needed, prior to ψ discovery, corresponding to the fractionally charged SU(3) quarks : u , d , s . It is by now well known, however, that it is impossible to construct a gauge theory of weak interactions based on three flavors only, without

(*) This excludes the very important model developed by Pati and Salam. The option of neutral gluons is taken here for simplicity, and we refer the reader to the original papers, for a discussion of the Pati-Salam ideas[4].

predicting first order strangeness changing, neutral current processes, in striking conflict with the observed suppression of, e.g., $K_L \to \mu^+\mu^-$. To avoid this inconsistency, we shall follow the Glashow, Iliopoulos and Maiani (GIM) proposal, and introduce from the outset a fourth flavor, associated to a new (charm carrying) quark c , with electric charge + 2/3.

Now that we have stated our assumptions, we can proceed to assign appropriate $SU(2) \otimes U(1)$ transformation properties to the left and righthanded quark fields.

In doing so, we shall be guided by the lepton-quark symmetry(*). With the addition of the charmed quark, we have in fact, as many quarks as there are leptons, and the charge spectrum is the same, except for an unessential shift of + 2/3 of quark charges with respect to lepton charges.

We can therefore put lepton and quark fields in a one-to-one correspondence, up to one, very essential, arbitrariness.

Suppose we associate $\nu \leftrightarrow u$ and $\nu' \leftrightarrow c$. Then we could associate $e \leftrightarrow d$ (and $\mu \leftrightarrow s$) or $e \leftrightarrow s$ (and $\mu \leftrightarrow d$). Actually, since d and s have the same charges, there is no reason to prefer one choice to the other, or to the more general choice :

$$\begin{aligned} e &\leftrightarrow \cos\theta_c\, d + \sin\theta_c\, s \equiv d_c \\ \mu &\leftrightarrow -\sin\theta_c\, d + \cos\theta_c\, s \equiv s_c \end{aligned} \qquad (10.1)$$

θ_c being any angle.

Up to this arbitrariness, the lepton-quark symmetry enables us to translate the lepton model of Section 7 into a quark model, and leads us to assume that :

$$\begin{pmatrix} u \\ d_c \end{pmatrix}_L \quad \begin{pmatrix} c \\ s_c \end{pmatrix}_L \text{ are weak isodoublets} \qquad (10.2)$$

u_R, d_R, c_R, s_R are weak isosinglets

(Since weak currents are to be color singlets, (10.2) holds for all the three colors, with the same angle θ_c). Furthermore, as in the lepton case, the transformation rule of the quark fields under U(1) (i.e. the weak hypercharge) is uniquely fixed by the above ansatz and by the requirement that the photon field A_μ as defined in eq. (6.9) couples to the electric charge.

In conclusion, the lepton-quark symmetry leads us to a weak and e.m. coupling scheme for quarks uniquely determined, up to the yet unspecified angle θ_c . As it is apparent from (10.2), θ_c is nothing but the Cabibbo angle.

In fact, the coupling of the charged W , to the uncharmed quarks, which we can derive from (10.2), is :

$$-\frac{g}{2\sqrt{2}} W_\mu^* \; \bar{u}\gamma^\mu(1-\gamma_5)(\cos\theta_c\, d + \sin\theta_c\, s) + \text{h.c.}$$

which precisely coincides with the Cabibbo coupling for semileptonic, $\Delta S = 0, 1$, processes. As a consequence, the position (10,2) completely determines the additional weak interactions involving charmed particles (i.e. neutrino production and weak decays) and it enables us to predict intensity and selection rules for these new processes. Before doing this, however, we have still to examine the properties of weak, neutral current processes with $\Delta S \neq 0$, and the arising of quark masses.

Z-quark coupling. As remarked in Section 7, the current coupled to Z_μ is a linear combination of the e.m. current, and of the current associated to the 3rd component of the weak isospin, L^3_μ . From (10.2) it follows that :

$$\begin{aligned} L^3_\mu &= \tfrac{1}{2}\left(\bar{u}_L\gamma_\mu u_L - \bar{d}_{cL}\gamma_\mu d_{cL}\right) + \\ &+ \tfrac{1}{2}\left(\bar{c}_L\gamma_\mu c_L - \bar{s}_{cL}\gamma_\mu s_{cL}\right) = \qquad (10.3) \\ &= \tfrac{1}{2}\left(\bar{u}_L\gamma_\mu u_L + \bar{c}_L\gamma_\mu c_L - \bar{d}_L\gamma_\mu d_L - \bar{s}_L\gamma_\mu s_L\right) \end{aligned}$$

Therefore L^3_μ obeys the selection rule $\Delta S = 0$.

Since also the e.m. current is strangeness conserving, we conclude that $K_L \to \mu^+\mu^-$ cannot occur, to lowest order, through Z exchange.

Actually, the observed ratio :

$$\frac{\Gamma(K_L \to \mu^+\mu^-)}{\Gamma(K^+ \to \mu^+\nu)} = 4.5^{+3}_{-1.5} \cdot 10^{-9}$$

is so small as to put also a strict limit to possible higher order contributions.

A non vanishing $K_L \to \mu^+\mu^-$ amplitude does in fact arise from two W exchange, as illustrated in Fig. 7. A priori, such diagrams should give rise to an amplitude of order :

(*) The introduction of a fourth quark to restore lepton-quark symmetry was considered by Y. Hara in 1963.

$$A(K_L \to \mu^+\mu^-) \propto \frac{\sin\theta_c\, g^4}{M_W^2} \approx G\alpha \sin\theta_c \qquad (10.4)$$

This would still be too large, compared to the experimental result. It turns out, however, that in the model there is still an additional suppression. This is due to the fact that, as indicated in Fig. 6, there are two possible diagrams, one with u exchange and the other with c exchange, and the two diagrams exactly cancel in the limit where u and c have equal masses. The correct estimate must therefore contain a further factor which vanishes when $m_u = m_c$, and indeed one gets :

$$A \propto \frac{\sin\theta_c}{M_W^2}\, g^4\, \frac{m_c^2 - m_u^2}{M_W^2} \approx \qquad (10.5)$$
$$\approx \sin\theta_c\, G^2 (m_c^2 - m_u^2)$$

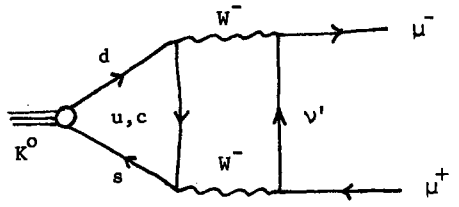

Fig. 6. Feynman diagrams for the $K^0 \to \mu^+\mu^-$ amplitude from two W exchange. In the vertical quark line, both u and c exchange have to be considered.

We can now get agreement with the experiment, provided m_c is not too large. It was in fact estimated, in the GIM paper, that :

$$m_c \approx 1 \div 3 \ GeV \qquad (10.6)$$

Eq. (10.6) can be interpreted as determining the mass scale of the lowest lying charmed particles. It is very satisfactory that all the "new physics" discovered in the last two years (dimuon events, the ψ , the raise in e^+e^- cross section, the narrow $K\pi$ peak etc.) opens up precisely at this range of hadronic masses.

Quark masses. Since the transformation rules implied by (10.2) involve chiral transformations, in the limit where $SU(2) \otimes U(1)$ is exact the quarks have to be massless. Quark masses must arise from the spontaneous breaking, similarly to lepton masses. To see what sort of mass spectrum arises by coupling quarks to the weak isodoublet φ , we have just to repeat, word by word, the analysis given in Section 9, replacing everywhere $\nu \to u$, $\nu' \to c$ and e and μ according to (10.1). Again the most general coupling can be described by eight coupling constants (for which we shall use the same notation even though they differ numerically from the previous ones).

The coupling constants can be chosen to obey either (9.11) or (9.12) and we shall choose (9.12). The mass lagrangian is therefore :

$$\mathcal{L}_{mass} = h_1 \eta\ \bar{u}(x)u(x) + h_2 \eta\ \bar{c}(x)c(x) +$$
$$+ g_1 \eta\ \bar{d}_c d_c + g_2 \eta\ \bar{s}_c s_c + \qquad (10.7)$$
$$+ g_{12} \eta\ (\bar{d}_c s_c + \bar{s}_c d_c)$$

The lagrangian is not diagonal in the charge - 1/3 fields. By definition, we have to require it to be diagonal in the fields d and s , corresponding to the eigenstates of the quantum numbers conserved by strong interactions (i.e. the flavors).

This can be obtained, provided :

$$\tan(2\theta_c) = \frac{2 g_{12}}{g_2 - g_1} \qquad (10.8)$$

which defines θ_c , in terms of the unknown g's.

In all, the five undetermined coupling constants in (10.7) give rise to four independent quark masses m_u , m_c , m_d , m_s and to one mixing angle θ_c . As was the case for leptons, no mass relation is found, and no explanation is given as to why $m_u \simeq m_d$ (which gives rise to isospin symmetry) or why $m_u \lesssim m_s \ll m_c$ (corresponding to the observed broken SU(3) and to the much less respected SU(4) symmetry).

On the other hand, from the above considerations a quite elegant picture on the origin of the Cabibbo angle emerges. A non vanishing value of θ_c arises because the fields which diagonalize the symmetry breaking lagrangian (chosen by the φ -quark interaction) do not agree with those that are matched by the lepton-quark symmetry to e and μ .

It is remarkable that the Cabibbo angle arises precisely through the same mechanism that could give rise to neutrino mixing and to electron and muon number non conservation.

This fact enhances further the interest for a refinement of the experimental limits on the latter phenomenon.

Selection rules for charm-changing weak processes. We close this Section with a brief account of the selection rules one can derive from (10.2) for the weak production and decay of charmed particles. Only W mediated processes are relevant, as we have seen that the Z boson is coupled to a diagonal current. In what follows, we shall assign charm C = +1 to the c quark, and strangeness S = -1 to the s quark.

i) Semi-leptonic processes. They are induced by the elementary processes :

$$c \to s + \ell^+ + \nu_\ell \qquad (10.9)$$

$$c \to d + \ell^+ + \nu_\ell \qquad (10.10)$$

$\ell = e, \mu$. From the definition of s_c we read that the amplitudes (10.9) and (10.10) are in the ratio $\cos\theta_c : \sin\theta_c$. In both cases, if ΔQ represents the net hadronic electric charge variation, we have the selection rule :

$$\Delta C = \Delta Q \qquad (10.11)$$

and since $\cos\theta_c >> \sin\theta_c$, (10.9) is the dominant transition and it obeys

$$\Delta C = \Delta S \qquad (10.12)$$

The selection rule (10.11) is relevant to the interpretation of the dimuon events seen at FNAL as due to the weak neutrino production of a charmed particle and its subsequent semi-leptonic decay. Since the initial and final states of the overall two-step process are both uncharmed, applying twice (10.11) we predict the total dimuon charge must be zero. This rule is indeed obeyed by the bulk of dimuon events, and also by the $e\mu$ events seen at Gargamelle.

There have been seen a few like-charge dimuons $\mu^-\mu^-$ or $\mu^+\mu^+$. It is possible that they arise from the associated production of charmed particles, one of the two undergoing a semi-leptonic decay. In this case, no charge correlation is expected. Eq. (10.12) tells us that non-strange charmed particles (expected to be the easier to produce) should decay into a state with $S \neq 0$. This correlation has been observed in the μe events at Gargamelle and at FNAL (even though in the FNAL events there may be too many K's as one would expect).

ii) Non leptonic processes. They are induced by the elementary processes :

$$c \to W^+ + d \qquad (10.13)$$
$$\hookrightarrow \text{hadrons}$$

$$c \to W^+ + s \qquad (10.14)$$
$$\hookrightarrow \text{hadrons}$$

Since the virtual W goes into hadrons through the Cabibbo coupling, we expect to get from W^+: S = 0 states with amplitude $\cos\theta_c$, S = +1 states with amplitude $\sin\theta_c$. We therefore get, for the overall transition :

$$\begin{aligned} &\text{amplitude for } \Delta S = \Delta C \propto \cos^2\theta_c \\ &\quad " \quad\quad " \quad \Delta S = 0 \propto \sin\theta_c \cos\theta_c \\ &\quad " \quad\quad " \quad \Delta S = -\Delta C \propto \sin^2\theta_c \end{aligned} \qquad (10.15)$$

valid up to phase space corrections.

If we apply these considerations to the rates for non leptonic decays of the charmed non strange pseudoscalar mesons D^0 , D^+ (respectively $c\bar{u}$ and $c\bar{d}$ states), we get the intensity rules :

$$D_0, D^+ \to \begin{cases} K^- + \text{pions}, \ \bar{K}^0 + \text{pions} & \sim \cos^4\theta_c \\ \text{pions} & \sim (\sin\theta_c \cos\theta_c)^2 \\ K^+ + \text{pions}, \ K^0 + \text{pions} & \sim (\sin^2\theta_c)^2 \end{cases}$$

The two narrow states recently discovered at SPEAR at about 1870 Mev nicely fit into this picture. The charge zero state has been seen to decay into $S \neq 0$ states. The charge = +1 state has been seen to decay into K^- + pions but not into K^+ + pions, or into multipions, in agreement with the above rules. An improvement in sensitivity so as to be able to check the $(\sin\theta_c)^2$ modes would be extremely important.

11. More flavors ?

We know of no reason why quarks and leptons should appear in precisely four different flavors. In fact, there exist already arguments in favor of further hadronic and leptonic flavors. Among them :

i) The observation of the process :

$$e^+ e^- \to e^\pm + \mu^\mp + \text{unseen neutrals} \qquad (11.1)$$

has been reported, at SPEAR, at center of mass energies above 4 GeV . The experimental data seem to favor the interpretation of (11.1) as due to the

production of a pair of heavy charged leptons $U^{\pm}$ ($m_U \sim 2$ GeV), each decaying into a charged lepton and two neutrinos. If this interpretation is confirmed, and if we accept the principle of lepton-quark symmetry, then one or more new hadronic flavors are implied.

ii) It may be desirable, for theoretical reasons, to formulate weak interactions in the framework of the so-called vectorlike theories" (see below). This is compatible with the present phenomenology only if there exist more quark flavors.

iii) A four-flavor model is basically CP conserving. It turns out that the observed CP violation can be naturally explained with more than four quark flavors.

iv) To account for the observed violations of scaling in neutrino deep inelastic processes, righthanded couplings of new quarks to the light quarks may be required. These couplings can be introduced only with more than four flavors.

Motivated by these or by other reasons, many models have been proposed and discussed in the recent literature.

The reason for the very large proliferation of models is of course to be found in the fact that our present experimental and theoretical knowledge about weak and e.m. interactions is not precise enough to uniquely determine one model, once one decides to put more flavors into the game. There are, however, a number of constraints that any particular model must satisfy, if it has to prove successfull. These constraints can be stated as follows :

a) No Adler-Bell-Jackiw anomalies. The renormalizability of a theory where fermions are coupled through vector and axial vector currents can be spoiled by the so-called Adler-Bell-Jackiw anomaly. In the case of the gauge group we are considering, namely $SU(2) \otimes U(1)$, and if fermions transform as weak isodoublets or isosinglets, the condition of no ABJ anomaly takes the very simple form :

$$\sum_{\substack{\text{Lefthanded}\\ \text{doublets}}} Q - \sum_{\substack{\text{Righthanded}\\ \text{doublets}}} Q = 0 \qquad (11.2)$$

Q being the electric charge. This statement is sufficient for our discussion. As was first observed by Bouchiat, Iliopoulos and Meyer, eq. (11.2) is satisfied by the four flavor model. In this case we have no righthanded doublets, while :

$$\sum_{\substack{\text{Lefthanded}\\ \text{doublets}}} Q = \underset{\binom{\nu}{e}_L}{-1} \quad \underset{\binom{\nu'}{\mu}_L}{-1} \quad \underset{\binom{u}{d_c}_L}{+3\cdot\frac{1}{3}} \quad \underset{\binom{c}{s_c}_L}{+3\cdot\frac{1}{3}}$$

where we have indicated explicitly the contribution from each weak isodoublet, and the factors 3 for the quark doublets arise because any such doublet comes in three different colors.

b) No $\Delta S \neq 0$ neutral current transitions, to order G and $G\alpha$. Though not universally accepted, it is my opinion that the fulfillment of this selection rule should be independent upon the specific values assigned to the parameters of the model (as it is the case e.g. for the four-flavor model).

c) Agreement with low energy phenomenology. To agree with well established facts, no appreciable right-handed couplings must be present between u quarks and both d and s quarks (as required by the Cabibbo theory). Similarly, no righthanded couplings of e and μ to ν or ν' should be allowed.

d) Charm-strangeness correlation. According to the most recent data about charmed particle decay (see Section 10) the charmed quark must be coupled more strongly to s as to d quarks.

We discuss now a few models. Aiming at an illustration of the main underlying ideas, our discussion will be rather schematic. In particular, no details will be given about the structure of symmetry breaking and the resulting mass-spectrum. Only the couplings to the gauge-fields will be considered.

i) A five flavor model[5]

The following isodoublets are considered :

$$\binom{u}{d_c}_L \quad \binom{c}{s_c}_L \quad \binom{u}{b}_R \qquad \binom{\nu}{e}_L \quad \binom{\nu'}{\mu}_L \quad \binom{\nu''}{\nu^-}_R \qquad (11.3)$$

all other fields being weak isosinglets. Here b stands for the quark field (charge - 1/3) which carries the new conserved flavor (beauty?), and ν'' is a combination of righthanded neutrinos

$$\nu''_R = \cos\alpha\, \nu_R + \sin\alpha\, \nu'_R$$

The model introduces only one additional flavor. It obeys the constraints (a) to (d), but the suppression of $\Delta S \neq 0$ neutral current processes is "unnatural" : a slight mixing of b with d and s quarks :

$$b_R \rightarrow b'_R = \cos\beta\, b_R + \sin\beta\,(\cos\varphi\, d_R + \sin\varphi\, s_R)$$

would give rise to $\Delta S \neq 0$ in the neutral current. This requires $\beta \simeq 0$ to hold within an extraordinary accuracy.

This feature is actually shared by all models where there are more $Q = -1/3$ than $Q = 2/3$ quark fields. To this class belong e.g. the superunified models considered by F. Gursey et al.[6] The mass scale of the "beautiful" (b-containing)particles is not determined. If it is in the presently available energy range, anti neutrino b production off u could help explaining the so-called "y anomaly" in $\bar{\nu}'$ deep inelastic scattering. However, no trace of the $b\bar{b}$ analog of ψ is seen at SPEAR. If m_b is much larger, one gets the same predictions as in the four-flavor model.

ii) A conservative, six flavor model[7]

We introduce lefthanded weak isodoublets only :

$$\begin{pmatrix} u \\ d_c \end{pmatrix}_L \begin{pmatrix} c \\ s_c \end{pmatrix}_L \begin{pmatrix} t \\ b \end{pmatrix}_L$$
$$\begin{pmatrix} \nu \\ e \end{pmatrix}_L \begin{pmatrix} \nu' \\ \mu \end{pmatrix}_L \begin{pmatrix} \nu_\upsilon \\ \upsilon^- \end{pmatrix}_L \qquad (11.4)$$

all righthanded fields being singlets. b is the same as previously, t is another new quark, carrying the sixth flavor (truth ?). All our constraints are satisfied, and (b) holds "naturally", i.e. independent upon the value of the mixing angles. Actually to make both t and b quarks unstable, we have to allow in (11.4) for a small mixing of the new with the old quarks. This can be done, keeping the deviations from the Cabibbo theory within the experimental errors.

In this model, the spontaneous symmetry breaking can lead, in addition to Cabibbo like angles, to the arising of one CP violating phase in the weak currents. What results is a "milliweak" theory, which mimics very well a "superweak" model, including the prediction of a very small electric dipole moment for the neutron.[8]

The t and b mass are usually assumed to be above the SPEAR range. In this case no departure from the four-flavor theory is expected in present experiments. Whether this may cause trouble to explain the y anomaly and other features of neutrino data, is at present unclear.

iii) Vectorlike models.[9]

Vectorlike models confront us with the new idea of a weak interaction theory which is basically parity conserving, the observed parity violation, in e.g. β-decays, arising from the spontaneous breaking of the gauge symmetry. Let us see how this works.

A parity transformation changes a one particle state of given momentum and helicity, into a one particle state with opposite momentum and opposite helicity (see Fig. 7). Applying further a 180° rotation around an axis orthogonal to the momentum, we get a state with the same momentum as the one we started with, but with opposite helicity.

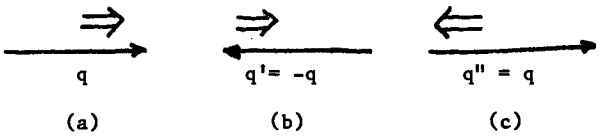

Fig. 7. (a) initial state; (b) parity reflected state; (c) parity reflected and 180° rotated state.

So, if the coupling of quarks to the gauge fields is parity conserving, left and righthanded fields must appear in a symmetrical fashion. To each lefthanded weak isomultiplet there must correspond a righthanded multiplet with the same weak isospin and hypercharge. Suppose we have four flavors (u,d,s,c) and we start with the lefthanded isodoublets :

$$\begin{pmatrix} u \\ d \end{pmatrix}_L \begin{pmatrix} c \\ s \end{pmatrix}_L \qquad (11.5)$$

what are the possible parity conserving assignments for the righthanded fields ? If the fields are massive, there is a natural way in which we can find the righthanded state to be associated to a given lefthanded state : we go from one to the other by slowing down the particle to its rest-frame, reversing the spin, and then boosting it back to the original momentum. If we require this to be a symmetry of the weak interactions, the righthanded isodoublets to be associated with (11.5) are simply :

$$\begin{pmatrix} u \\ d \end{pmatrix}_R \begin{pmatrix} c \\ s \end{pmatrix}_R \qquad (11.6)$$

and the resulting theory is a vector theory, with no parity violation. If we disregard masses, however, and if there are particles with identical charges (like d and s quarks), ambiguities may arise, leading to different, equally acceptable parity definitions. Suppose we decide that, under a parity operation :

$$u_L \xrightarrow[P]{} u_R$$
$$c_L \xrightarrow[P]{} c_R \qquad (11.7)$$

We could then complete (11.7) either by the choice implied by (11.6) or by :

$$d_L \xrightarrow[P]{} s_R$$
$$s_L \xrightarrow[P]{} d_R \qquad (11.8)$$

or by the more general choice :

$$d_L \xrightarrow[P]{} \cos\alpha\, d_R + \sin\alpha\, s_R$$
$$s_L \xrightarrow[P]{} -\sin\alpha\, d_R + \cos\alpha\, s_R \qquad (11.9)$$

All these choices are equally well suitable for the weak interactions and we have a continuous family of possible parity operations. If the one chosen by the weak interactions does not agree with the one defined by the masses (and by the strong interactions) we have a vectorlike theory. In a vectorlike theory, parity is violated by weak amplitudes. For example, choosing the definitions (11.7) and (11.8) one would construct the weak multiplets :

$$\begin{pmatrix} u \\ d \end{pmatrix}_L \quad \begin{pmatrix} c \\ s \end{pmatrix}_L$$
$$\begin{pmatrix} u \\ s \end{pmatrix}_R \quad \begin{pmatrix} c \\ d \end{pmatrix}_R \qquad (11.10)$$

If we restrict e.g. to weak processes involving non strange, uncharmed particles, only the coupling $u_L \to d_L$ is active, and we get out of (11.10) pure V-A (parity violating) amplitudes.

A notable property of any vectorlike theory is that it does never give rise to ABJ anomalies. Eq. (11.2) is always obeyed, since for any weak left isodoublet there is a right isodoublet with the same charge spectrum.

A vectorlike theory with four flavors only, necessarily violates our constraint (c), since the u_R field ends up to be coupled to some linear combination of d_R and s_R .

By introducing two more quark flavors (t and b) we can construct a six flavor model,which is actually uniquely determined by the requirements (c) and (d). The quark lefthanded isodoublets are :

$$\begin{pmatrix} u \\ d \end{pmatrix}_L \quad \begin{pmatrix} c \\ s \end{pmatrix}_L \quad \begin{pmatrix} t \\ b \end{pmatrix}_L$$

(for simplicity of notation, we are neglecting θ_c and other similar angles), while the righthanded doublets are :

$$\begin{pmatrix} u \\ b \end{pmatrix}_R \quad \begin{pmatrix} c \\ s \end{pmatrix}_R \quad \begin{pmatrix} t \\ d \end{pmatrix}_R$$

Leptons are more complicated and we will not discuss them. (We cannot just translate the above formulae, with the substitution $b \to \upsilon^-$, $t \to \nu_\upsilon$, since, in this case, μ_R would turn out to be coupled to some combination of ν_R and ν'_R fields).

If we assume that m_t and m_b are so high that we cannot presently produce them, the six flavor vectorlike model reduces to the conventional, four flavors, one, except for one very remarkable prediction.

Let us compute the current associated to the 3rd component of weak isospin :

$$L^3_\mu = \frac{1}{2}\left(\bar{u}_L \gamma_\mu u_L - \bar{d}_L \gamma_\mu d_L\right) + (u,d \to c,s) + (u,d \to t,b) + \frac{1}{2}\left(\bar{u}_R \gamma_\mu u_R - \bar{b}_R \gamma_\mu b_R\right) + (u,b \to c,s) + (u,b \to t,d)$$

Assembling together terms involving the same fields, it is easy to see that L^3_μ is a pure vector current, with no axial component. This holds true also for those components of L^3_μ associated to the charged leptons. As a consequence :

i) the interaction of the neutral weak boson Z with hadrons, electrons and muons is exactly parity conserving;

ii) inclusive and exclusive neutrino (neutral current) cross-sections are equal to the corresponding anti-neutrino cross-sections.

Statement (i) has to be contrasted with the simple Weinberg-Salam model, where P-violating effects are expected from Z exchange (Sect. 7). It is clear that the experiments sensible to P-violating, Z related effects are very crucial, in particular those attempting to measure P-violation in atoms. No firm data are, unfortunately, still available.

There are,on the other hand, available data about the processes :

$$\nu'(\bar{\nu}') + \text{matter} \to \nu'(\bar{\nu}') + \ldots \qquad (11.11)$$
$$\nu'(\bar{\nu}') + P \to \nu'(\bar{\nu}') + P \qquad (11.12)$$

coming from Gargamelle and FNAL, for (11.11), and from Brookhaven, for (11.12). All present data dis-

agree with the vectorlike model, but, perhaps, they are still not accurate enough to exclude it.

12. Conclusions

Gauge theories are emerging as the most likely candidate to describe weak and e.m. interactions.

On the theoretical side, the present status of gauge theories is comparable to that of the best understood examples of quantum field theory, namely quantum electrodynamics. On the experimental side, they are receiving quite impressive confirmations.

It would be premature, however, to say that a Yang-Mills picture of weak and e.m. phenomena has been established. To accomplish this, quite a number of experimental facts must be ascertained, first of all the existence of weak intermediate bosons (both charged and neutral).

The importance of the experimental observation of the weak bosons and of a study of their interactions with the other particles and with themselves cannot be overemphasized. It stands out, at present, as the most important task for the next generation of accelerators.

Among other things, the mass spectrum of the weak bosons would tell us something useful about the gauge symmetry breaking, about which we have, at present, no experimental information whatsoever.

We have based our discussion on the gauge group $SU(2) \otimes U(1)$, which is a minimal choice, in the sense that it has the minimum number of gauge fields needed to describe the observed phenomena. Even though this model is receiving substantial support from the experiments (as indicated by the agreement of very different experimental results with the same Weinberg-Salam angle), few would concede that this is the final theory of weak interactions. For one thing, the unification of weak and e.m. interactions achieved in this model is not complete : we have still two independent coupling constants and the spectrum of the electric charge is not fixed by the theory, unlikely that of the weak isospin. The natural solution to this problem could be the embedding of $SU(2) \otimes U(1)$ into a larger gauge group, with no abelian factors and only one coupling. No significant progress has however been yet achieved along this line.

There are other unsatisfactory points :

i) the mass scale associatedto quark and lepton flavors are completely undetermined, likewise the Cabibbo angle and all other similar mixing angles; as a consequence we have no explanation whatsoever of the approximate symmetries in strong interactions (e.g. isospin, $SU(3)$) and of the exact or nearly exact vanishing of the neutrino mass;

ii) the number of lepton and quark flavors is undetermined; a theoretically sound model (e.g. with no Adler-Bell-Jackiw anomalies) could be constructed out of only one color triplet of u and d quarks and a lepton doublet ν, e ; so : why the muon, why the strange and charmed particles (let alone new flavors) ?

iii) the V-A structure of weak currents is put into the model by hand; no real explanation of parity violation is given;

iv) the observed CP violation can be introduced in the weak interaction in various ways; with only left-handed weak doublets, CP-violation would arise naturally with six quark flavors and this could give a rationale for the existence of such a large number of different quark types; we are still far, however, from a true comprehension of the problem.

Progress in the determination of a more satisfactory theory is conditioned by the acquisition of a number of very crucial experimental informations. In particular :

i) an extensive search should be done for new quark flavors (e.g. in $e^+e^- \rightarrow$ hadrons, or $\gamma(P) + P \rightarrow l^+l^-$ + anything) and for lepton flavors; in particular a more complete evidence for the proposed heavy lepton U should be achieved;

ii) neutrino and antineutrino processes could give valuable information about the quark weak couplings, as well as about new flavors;

iii) more refined limits on CP-violation other than in the neutral K decays, and in particular further improvements of the limits on the electric dipole of the neutron, are badly needed, to see whether the CP-violation is really a weak interaction phenomenon.

It goes without saying that the intensive study of the weak decays of charmed particles is very important; besides testing weak interaction models, it could give us a general check of our capacity of extracting predictions for physical processes out of a quark-based theory.

Acknowledgements

I would like to acknowledge many very interest-discussions with my colleagues at the Wepion School, in particular with B. de Wit. Support from the

Laboratoire de Physique Théorique, Ecole Normale Supérieure (Paris) and from the Institut des Hautes Etudes Scientifiques (Bures-sur-Yvette) where these lecture notes have been completed, is also gratefully acknowledged.

Appendix I

We consider first an electron with momentum $\underline{p}$. Its wave function is a positive energy spinor, obeying the Dirac equation:

$$(\not{p} - m)\, u(p) = (E\gamma_0 - \underline{p}\cdot\underline{\gamma} - m)\, u(p) = 0 \qquad (I.1)$$

There can be two possible polarization states, corresponding to states with spin component along $\underline{p}$ (i.e. helicity) equals to $\pm 1/2$. The helicity operator is given by

$$h = \frac{1}{2}\,\frac{\underline{\Sigma}\cdot\underline{p}}{|\underline{p}|}$$

In the representation we are using for the Dirac matrices (i.e. the representation used in the Bjorken and Drell book) :

$$\underline{\Sigma} = \begin{pmatrix} \underline{\sigma} & 0 \\ 0 & \underline{\sigma} \end{pmatrix} \qquad (I.2)$$

($\underline{\sigma}$ are the 2×2 Pauli matrices).

Using the explicit matrix form :

$$\gamma_0 = \begin{pmatrix} 1 & 0 \\ 0 & -1 \end{pmatrix} \quad \underline{\gamma} = \begin{pmatrix} 0 & \underline{\sigma} \\ -\underline{\sigma} & 0 \end{pmatrix} \quad \gamma_5 = \begin{pmatrix} 0 & 1 \\ 1 & 0 \end{pmatrix} \qquad (I.3)$$

we see that

$$\gamma_5\gamma_0\underline{\gamma} = \underline{\Sigma} \qquad (I.4)$$

so that, by multiplying eq. (I.1) by $\gamma_5\gamma_0$ from the left, we get :

$$\gamma_5\, u(p) = \left(\frac{\underline{\Sigma}\cdot\underline{p}}{E} + \frac{m}{E}\gamma_5\gamma_0\right) u(p) \qquad (I.5)$$

This shows that, in the limit $m \to 0$ (or equivalently $E \to \infty$)

$$\gamma_5\, u(p) = \frac{\underline{\Sigma}\cdot\underline{p}}{|\underline{p}|}\, u(p) = 2h\, u(p) \qquad (I.6)$$

Therefore the two matrices :

$$a_\pm = \frac{1 \pm \gamma_5}{2} \qquad (I.7)$$

project out righthanded, a_+, or lefthanded, a_-, states. The two negative energy solutions of (I.1) are associated to positron states. If we set :

$$v(E, \underline{p}) = u(-E, -\underline{p})$$
$$E = +\sqrt{p^2 + m^2}$$

then v is the appropriate spinor for a positron traveling with momentum $\underline{p}$. From (I.1) it follows that v obeys the equation:

$$\left[(-E\gamma_0) - (-\underline{p}\cdot\underline{\gamma}) - m\right] u(-E, -\underline{p}) =$$
$$= -(E\gamma_0 - \underline{p}\cdot\underline{\gamma} + m)\, v = 0 \qquad (I.8)$$

If we multiply again eq. (I.8) by $\gamma_5\gamma_0$, we get, in the limit $m = 0$:

$$\gamma_5\, v(p) = \frac{\underline{\Sigma}\cdot\underline{p}}{|\underline{p}|}\, v(p) = -\frac{\underline{\Sigma}\cdot(-\underline{p})}{|\underline{p}|}\, u(+E, -\underline{p}) =$$
$$= -2h\, v(p)$$

so that, applied to a positron wave function, the operators a_+ and a_- given by (I.7) project out the lefthanded and the righthanded parts, respectively.

Finally we consider the quantized field $e(x)$. At $t = 0$, we may expand $e(\underline{x}, 0)$ into creation and annihilation operators, according to :

$$e(\underline{x}, 0) = \frac{1}{(2\pi)^{3/2}} \int \frac{d^3p}{\sqrt{E}} \sum_{h=\pm 1/2} \left(e^{-i\underline{p}\cdot\underline{x}}\, a_h(\underline{p})\, u^h(p) + e^{i\underline{p}\cdot\underline{x}}\, b_h^+\, v^h(p) \right)$$

(we normalize spinors according to : $u^+u = v^+v = 1$, as it is appropriate for massless particles) where h is the helicity, and the operators $a_h(\underline{p})$ ($b_h^+(\underline{p})$) annihilate an electron (create a positron) of momentum $\underline{p}$ and helicity h. We see therefore that $e_L = a_- e$ may annihilate only lefthanded electrons and create only righthanded positrons (and vice versa for $e_R = a_+ e$). These considerations, applied to the neutrino case, show that if in the weak interaction only the field $\nu_L = a_-\nu$ appears, righthanded neutrinos and lefthanded antineutrinos (associated to ν_R) would be never produced or absorbed in a weak process (and would therefore behave as free unobservable particles, except for gravity).

Appendix II

Following the considerations given in Sect. 2, we consider an isodoublet field Ψ, such that :

$$\delta\psi = i\,\varepsilon^a(x)\,\frac{\tau_a}{2}\,\psi(x) \qquad \text{(II.1)}$$

We want to determine the transformation properties of the gauge fields A_μ^a, under the requirement that the covariant derivative

$$\nabla_\mu \psi = \left(\partial_\mu + i g A_\mu^a \frac{\tau_a}{2}\right)\psi \qquad \text{(II.2)}$$

transforms according to :

$$\delta\left(\nabla_\mu \psi\right) = i\,\varepsilon^a(x)\,\frac{\tau_a}{2}\left(\nabla_\mu \psi\right) \qquad \text{(II.3)}$$

To simplify our formulae it is convenient to introduce the notation :

$$\begin{aligned} \varepsilon &\equiv \varepsilon^a \frac{\tau_a}{2} \\ A_\mu &\equiv A_\mu^a \frac{\tau_a}{2} \end{aligned} \qquad \text{(II.4)}$$

ε and A_μ are therefore 2 x 2, space-time dependent, matrices. We now compute the variation of $\nabla_\mu \psi$. Using (II.1) we find :

$$\delta(\nabla_\mu\psi) = \partial_\mu(\delta\psi) + i g A_\mu(\delta\psi) + i g(\delta A_\mu)\psi =$$
$$= i\varepsilon\partial_\mu\psi + i(\partial_\mu\varepsilon)\psi - g A_\mu\varepsilon\psi + i g(\delta A_\mu)\psi$$

and we want to determine δA_μ, so that the r.h.s. coincides with :

$$i\varepsilon\nabla_\mu\psi = i\varepsilon\partial_\mu\psi - g\varepsilon A_\mu\psi$$

Equating the r.h.s. of the last two equations, we find :

$$i g\,\delta A_\mu\psi = -\left[g\left(\varepsilon A_\mu - A_\mu\varepsilon\right) + i\partial_\mu\varepsilon\right]\psi$$

namely :

$$\delta A_\mu \equiv \frac{\tau_a}{2}\delta A_\mu^a = i\left[\varepsilon, A_\mu\right] - \frac{1}{g}\partial_\mu\varepsilon = \qquad \text{(II.5)}$$
$$= \left[-\varepsilon_{abc}\,\varepsilon^b(x) A_\mu^c - \frac{1}{g}\partial_\mu\varepsilon^a(x)\right]\frac{\tau_a}{2}$$

Equating the coefficients of $\tau_a/2$, we get precisely eq. (2.5) of the text. Note that in the expression of δA_μ^a, any reference to the transformation properties of ψ has disappeared. We would have gotten the same result by considering the covariant derivative of any matter field Φ with non trivial transformation properties (i.e. such that $\delta\phi \neq 0$). This is obviously a very important point for the consistency of the whole scheme : the way A_μ^a transforms must be independent from the type of matter fields we are going to couple to it.

Using the representation of A_μ^a as 2 x 2 matrices, it is also easy to work out the transformation properties of $F_{\mu\nu}^a$. Define :

$$F_{\mu\nu} = F_{\mu\nu}^a \frac{\tau_a}{2} = \frac{\tau_a}{2}\left[\partial_\mu A_\nu^a - \partial_\nu A_\mu^a - g\,\varepsilon_{abc} A_\mu^b A_\nu^c\right] =$$
$$= \partial_\mu A_\nu - \partial_\nu A_\mu + i g\left[A_\mu, A_\nu\right]$$

Then :

$$\delta F_{\mu\nu} = \partial_\mu(\delta A_\nu) - \partial_\nu(\delta A_\mu) + i g\left[\delta A_\mu, A_\nu\right] + i g\left[A_\mu, \delta A_\nu\right] =$$
$$= i\left[\varepsilon, \partial_\mu A_\nu - \partial_\nu A_\mu\right] - g\left(\left[\left[\varepsilon, A_\mu\right], A_\nu\right] + \left[\left[A_\nu, \varepsilon\right], A_\mu\right]\right)$$

By using the Jacobi identity, valid for any three matrices A,B,C :

$$\left[\left[A,B\right],C\right] + \left[\left[B,C\right],A\right] + \left[\left[C,A\right],B\right] = 0$$

the double commutators can be simplified to give :

$$\delta F_{\mu\nu} = i\left[\varepsilon, \partial_\mu A_\nu - \partial_\nu A_\mu\right] - g\left[\varepsilon, \left[A_\mu, A_\nu\right]\right] =$$
$$= i\left[\varepsilon, F_{\mu\nu}\right] = i\left[\frac{\tau^b}{2}, \frac{\tau^c}{2}\right]\varepsilon^b F_{\mu\nu}^c =$$
$$= \frac{\tau_a}{2}\left(-\varepsilon_{abc}\,\varepsilon^b F_{\mu\nu}^c\right) = \frac{\tau_a}{2}\,\delta F_{\mu\nu}^a$$

Equating the coefficients of $\tau^a/2$, we get eq. (2.8) of the text.

Finally we prove the invariance of the Yang-Mills lagrangian, given in eq. (2.9) of the text. To this aim we observe that we can write

$$\mathcal{L}_{YM} = -\frac{1}{4} F_{\mu\nu}^a F^{a\mu\nu} =$$
$$= -\frac{1}{2}\,\mathrm{Tr}\left(F_{\mu\nu} F^{\mu\nu}\right)$$

where, as before :

$$F_{\mu\nu} = \frac{\tau_a}{2} F_{\mu\nu}^a$$

and :

$$\mathrm{Tr}\left(\tau_a \tau_b\right) = 2\,\delta_{ab}$$

The variation of $\mathcal{L}_{YM}$ under gauge transformation is therefore :

$$\delta\mathcal{L}_{YM} = -\frac{1}{2}\,\mathrm{Tr}\left[\delta F_{\mu\nu}F^{\mu\nu} + F^{\mu\nu}\delta F_{\mu\nu}\right] =$$

$$= -\frac{i}{2}\,\mathrm{Tr}\left(\left[\varepsilon, F_{\mu\nu}\right]F^{\mu\nu} + F^{\mu\nu}\left[\varepsilon, F_{\mu\nu}\right]\right) =$$

$$= -\frac{i}{2}\,\mathrm{Tr}\left(\left[\varepsilon, F_{\mu\nu}F^{\mu\nu}\right]\right) = 0$$

Q.E.D.

The last step follows because the trace of the commutator of any two matrices is always zero.

References

1. S.L. Glashow, Nucl. Phys. 22 (1961) 579.
2. F. Reines, H.S. Gurr, H.W. Sobel, Phys. Rev. Letters 37 (1976) 315.
3. For a recent discussion, see e.g. S.M. Bilenky , B. Pontecorvo, Phys. Letters 61B (1976) 248.
4. J.C. Pati, A. Salam, Phys. Rev. D8 (1973) 1240; Phys. Rev. Letters 31 (1973) 661; Phys. Rev. D10 (1974) 275; Trieste ICTP preprint IC 76/76, presented at the "Neutrino Conference 1976", Aachen (FRG).
5. R.M. Barnett,Phys. Rev. D13 (1976) 671 and references therein. Righthanded couplings of light to new, heavy quarks had been considered earlier by A. De Rujula, H. Georgi, S.L. Glashow, H.R. Quinn, Rev. Mod. Phys. 46, (1974) 391.
6. F. Gursey, P. Sikivie, Phys. Rev. Letters 36, (1976) 775 and references therein.
7. H. Harari, Proc. of the SLAC conference, 1975.
8. M. Kobayashi, T. Maskawa, Progr. Theor. Physics 49 (1973) 652; L. Maiani, Phys. Letters 62B (1976) 186; S. Pakvasa, H. Sugawara, Phys. Rev. D14 (1976) 305.
9. A. De Rujula, H. Georgi, S. Glashow, Phys. Rev. D12 (1975) 3589; F.A. Wilczek, A. Zee, R.L. Kingsley, S.B. Treiman, ibidem D12 (1975) 2768; S. Pakvasa, W.A. Simmons, S.F. Tuan, Phys. Rev. Letters 35 (1975) 702; H. Fritzsch, M. Gell-Mann, P. Minkowski, Phys. Letters 59B (1975) 256.

General references

1) Field theory
   - J.D. Bjorken, S. Drell, Relativistic Quantum Fields. Mc Graw-Hill Co.
2) Historical development of gauge theories
   - M. Veltman, Proc. of the "Interantional Symposium on Electron and Photon Interactions at High Energies", Bonn 27-31 August 1973, and CERN preprint, TH-1742, 1 Sept. 1973.
3) Gauge theories
   - C.N. Yang, R.L. Mills, Phys Rev. 96 (1954) 191
   - R. Feynman, Acta Physica Polonica 24 (1963) 697
   - E.S. Abers, B.W. Lee, Physics Reports 9C, n. 1 (1973)
4) Spontaneous symmetry breaking and the Higgs Phenomenon
   - S. Coleman, Proc. of the Eltore Majorana Summer School, Erice, 1973.
5) Weak interactions,charmed particles etc.
   - C.H. Llewellyn Smith, talk delivered at the Bonn Symposium quoted in (2).
   - B. Zumino, Proc. of the GIFT School, Madrid, 1972 and CERN preprint, 1972.
   - M.K. Gaillard, B.W. Lee, J. Rosner, Rev. Mod. Phys. 47 (1975) 277.
   - J. Iliopoulos, Proc. of the London Conference, 1974.
   - N. Cabibbo, Proc. of the Palermo Conference, 1975.
   - Proc. of the Gif-sur-Yvette Summer Schools held in 1974, 1975, 1976.
   - Proc. of the E. Majorana Summer School, Erice, 1975.
   - Proc. of the Neutrino Conference 1976, Aachen.

HIGH-ENERGY NEUTRINO EXPERIMENTS

J. Steinberger
CERN, Geneva, Switzerland

1. Introduction

It is the aim of these lectures to review high-energy neutrino experiments, both from the point of view of techniques and of results.

It may not be amiss to begin by pointing out that experiments that use neutrino projectiles have given very important results in recent years and may be expected to do so in the near future. Among the most incisive results the following may be recalled:

i) Discovery of the separate identity of muon and electron neutrinos in the first high-energy neutrino experiment[1].

ii) The measurement of neutrinos from the sun by Davis[2]. The most recent (unpublished) result of this remarkably difficult experiment is one interaction ($\nu + {}^{37}Cl \rightarrow {}^{37}Ar + e$) observed in 3 ± 0.7 days, in a detector of 600 tons of C_2Cl_4. This is not too different from expectations based on models of the sun's thermonuclear processes and the ^{37}Ar lifetime.

iii) The discovery of neutral weak currents in the big heavy-liquid bubble chamber at CERN in 1973 [3].

iv) The discovery of particles with new (charm) quantum numbers in very recent experiments at FNAL, Brookhaven and at CERN. These experiments will be discussed in Section 8.

At present, some of the more interesting questions being studied in neutrino experiments are the following:

a) Neutrino-electron scattering. This purely leptonic process can give an important insight into the structure of the weak neutral current.

b) Isotopic and Lorentz structure of neutral currents in hadronic processes.

c) The quark structure of the nucleons.

d) The properties of charmed particles, which seem to be readily produced in neutrino reactions.

This review is intended for physicists who have already an understanding of the weak interaction as manifested in β decay and in elementary particle decay. The level is simple and directed at experimentalists.

For an up-to-date review of the more classic aspects of the weak interaction, I can recommend the book of Commins[4]. In preparing the present lectures I followed very closely the recent lectures of Seghal[5].

2. Neutrino beams

2.1 Sources of neutrinos

The two main sources of neutrinos for high-energy neutrino beams are the decays $\pi^{\pm} \rightarrow \mu^{\pm} + \nu(\bar{\nu})$ and $K^{\pm} \rightarrow \mu^{\pm} + \nu(\bar{\nu})$. It is important that both are sources of muon neutrinos, and both are two-body decays. They therefore produce flat neutrino spectra with energies

$$0 < E_\nu/E_{\pi,K} < 1 - m_\mu^2/m_{\pi,K}^2$$

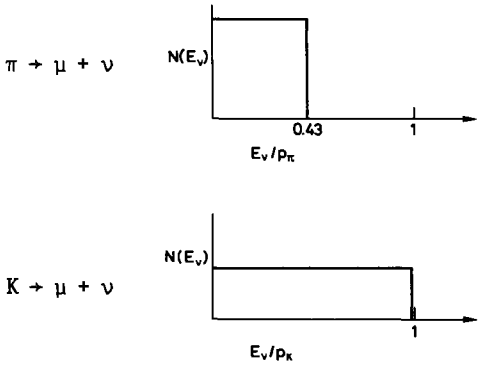

The main background to the spectrum is due to the three-body decay $K \rightarrow \pi + \mu + \nu$, and is a few percent. The main background of electron neutrinos is due to the decay $K \rightarrow e + \pi + \nu$ and is also a few percent.

2.2 Elements of a high-energy neutrino beam

Present-day neutrino beams consist in general of the following elements:

a) Protons from an accelerator hit a target and produce secondary hadrons.

b) These are sign-selected and momentum-selected by some sort of focusing device.

c) They pass through a decay region.

d) They enter a massive shield which absorbs the remaining hadrons, and the muons which have been produced. The shielding length necessary is roughly E_μ(GeV)/2 metres of iron, or the equivalent.

e) Monitoring devices to permit an evaluation of the spectrum and absolute flux of the neutrinos.

The layout of these main elements for the CERN Super Proton Synchrotron (SPS) neutrino facility is shown in Fig. 1.

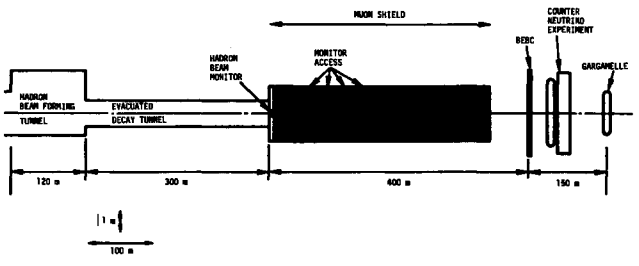

Fig. 1

2.3 Wide-band neutrino beams

The focusing element in these beams is an achromatic device such as the Van der Meer magnetic horn (Fig. 2).

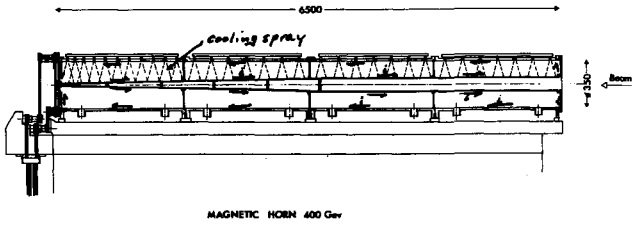

Fig. 2

A strong, pulsed current, travelling down the narrow inner conductor and returning on the larger diameter outer conductor, produces a toroidal magnetic field which has a focusing effect on the hadrons of one charge, and a defocusing effect on the other. The hadron-producing target is immediately in front of the horn.

Typical wide-band neutrino and antineutrino spectra are shown in Fig. 3.

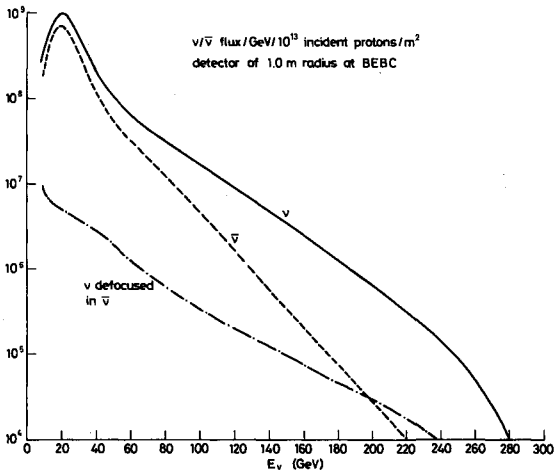

Fig. 3

The spectra have the following features:

a) They are broad-band, falling off roughly exponentially with energy. The high-energy tail is due to kaon neutrinos. The average neutrino energy is only about one-tenth of the proton energy.

b) Since positive hadron production at high energy is more intense than that of negative hadrons, the neutrino beams are more intense than antineutrino beams. For the high-energy tail this is a factor of the order of 10.

c) For the same reason, ν background in $\bar{\nu}$ beams is larger than in the reverse case.

d) Because of the rapid fall-off of the flux with energy, precise monitoring poses difficulties.

2.3.1 Monitoring. As mentioned above, this is a somewhat delicate problem. At the SPS it will be achieved, following the technique already employed successfully in the Gargamelle experiments at the CERN Proton Synchrotron (PS), by measuring the absolute number of muons as function of penetration and transverse position in the shield. In each of eight gaps in the shield an array of solid-state detectors will measure muon flux as function of transverse position. These are intercalibrated by a single similar detector, and this in turn is calibrated by counting tracks in nuclear emulsions.

The muon distributions permit a reconstruction of the kaon and pion spectra, and from these the neutrino fluxes are calculated.

2.4 Narrow-band beams

2.4.1 General. In this type of beam a momentum-selected hadron beam is first formed. It is similar to normal secondary beams, but particular effort is necessary to limit the neutrinos produced in hadron decays before the beam is fully selected, because these neutrinos do not have the correct energy or even sign. This is accomplished in the beam design by requiring that the initial proton beam, as well as the hadron beam before momentum selection, point sufficiently away from the neutrino detectors; the hadron beam is steered in the direction of the detectors only after the momentum is selected.

2.4.2 Neutrino energy. About 99.9% of pion neutrinos and 90% of kaon neutrinos are associated with two-body decays. For these the neutrino energy can be inferred from the hadron energy and the decay angle, subject of course to the uncertainties in these, and to a K-π ambiguity. The kinematics of E_ν versus decay angle is shown in Fig. 4.

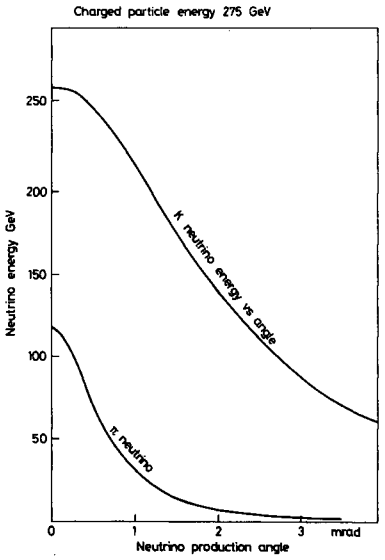

Fig. 4

The decay angle is inferred on the basis of the impact radius of the neutrino event in the detector (see Fig. 5).

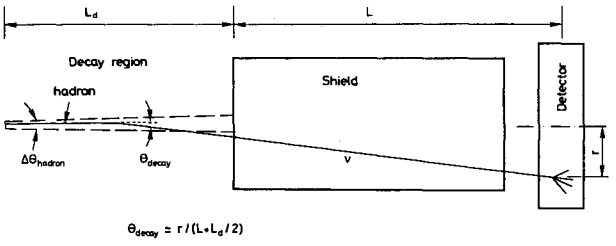

Fig. 5

The uncertainties in the neutrino energy are chiefly due to: a) hadron beam momentum spread, typically ±5%; b) hadron beam angular spread, $\sim \pm 2 \times 10^{-4}$ radians for the SPS narrow-band beam, and c) the relative length of the decay tunnel. The expected uncertainties in ΔE_ν for kaon neutrinos and the SPS beam are shown in Fig. 6. They vary between 5% and 20%, depending on neutrino energy or impact radius.

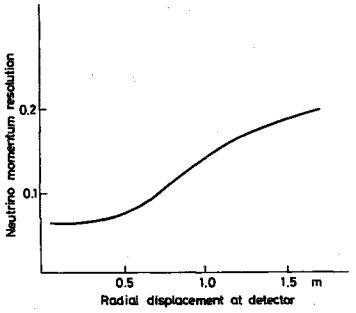

Fig. 6

2.4.3 CERN SPS narrow-band beam. Two neutrino beam facilities, a narrow-band and a wide-band, are being prepared at the CERN SPS. The hadron-focusing elements are side by side in a common hall, and they use common decay tunnels and shields (Fig. 7).

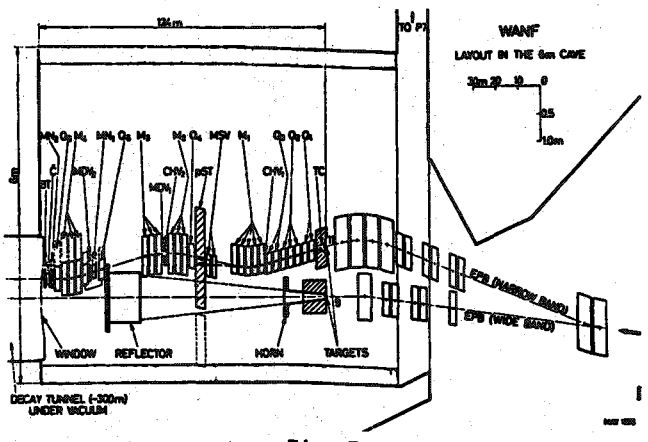

Fig. 7

The changeover from one beam to the other can be accomplished in a few days. The length of the hall is $\sim$ 120 m, the decay region $\sim$ 300 m, and the shielding region $\sim$ 400 m. The shield material is chiefly iron.

Schematically, bending and focusing in both horizontal and vertical planes are shown in Fig. 8.

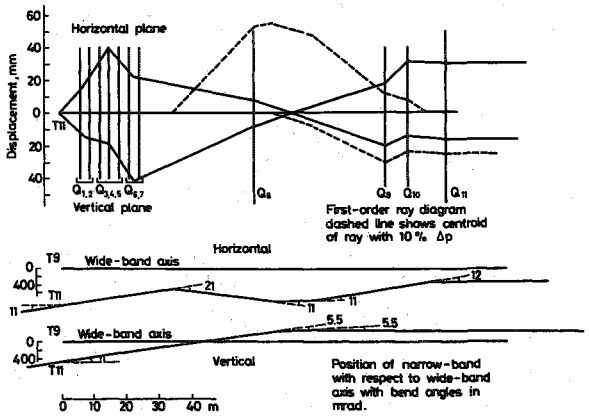

Fig. 8

The angle of the proton beam, as it hits the target, with respect to the detector is $\sim$ 15 mrad. The secondary hadron beam in a momentum interval $\Delta p/p \simeq$ $\simeq$ 0.05 is accepted into an aperture of $\sim$ ±2 mrad in both planes, and doubly focused on a momentum slit. After that it is made parallel to ±0.2 mrad and directed towards the detector.

2.4.4 Neutrino spectrum. It is necessary to distinguish between the observed neutrino spectrum and the uncertainty in the energy of the neutrino, which was discussed in Section 2.4.2. If both the detector and the hadron momentum are sufficiently large, the entire neutrino spectrum from E_ν near zero to $E_\nu = 0.95\ E_{hadron}$ are observed at the same time. This is a tremendous experimental advantage, since the spectrum is given immediately in terms of the K/π ratio alone, which can be measured easily. (To measure absolute cross-sections, a measurement of the absolute hadron flux is of course also required.) The spectra of kaon and pion neutrinos, separately, are of course flat. Figure 9 shows the expected neutrino spectrum for a 275 GeV positive hadron beam as seen in the 3.75 m diameter electronic detector at the SPS, and Fig. 10 shows the same for the antineutrinos produced by negative hadrons.

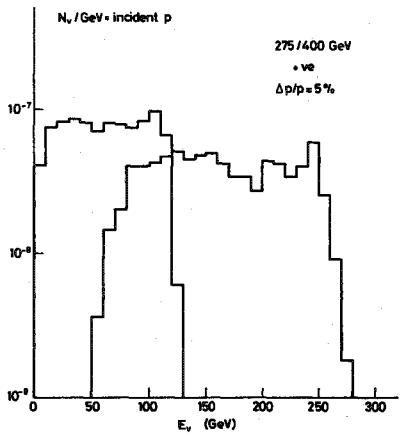

Fig. 9

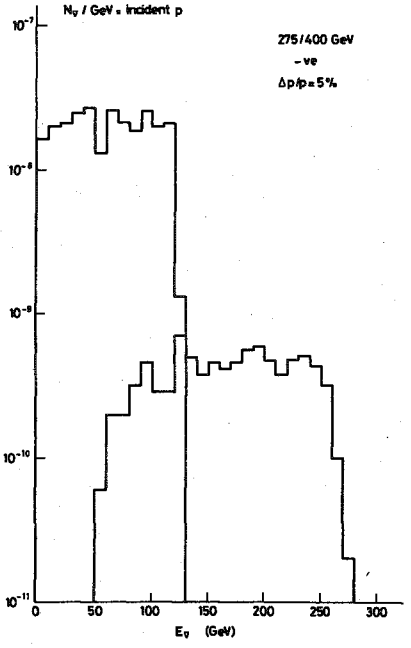

Fig. 10

2.4.5 Monitoring of the narrow-band beam. The neutrino properties must be inferred from those of the hadrons. The hadron spectrum is narrow and known from the beam design, and will not be measured. It is necessary only to measure the total hadron flux and the hadron composition. At the SPS the total flux will be measured in two ways. The first is by means of a so-called "beam transformer" which measures, by magnetic induction, the total hadron beam current, pulse for pulse. The second device is a calorimeter, a block of iron placed just before the shield at the end of the decay path, sufficiently large to contain $\sim$ 99% of the ionization produced by the hadrons. In this calorimeter the heat deposited by the hadron beam is measured.

The beam composition needs to be measured only once for any particular beam. It is measured at the SPS by a very simple differential Čerenkov counter which measures, not the number of particles of particular types traversing, which is difficult, but only the light produced by a whole burst of particles (typically $\sim 10^{10}$) as a function of gas pressure, which is easier to do.

2.4.6 Intensity. The integrated intensities of narrow-band beams are roughly 100 times less than those of wide-band beams. They are therefore better matched to the heavier electronic detectors than to the bubble chambers.

2.4.7 Contamination

a) *Neutrinos of the same type but wrong energy.* The biggest source is the decay $K \to \pi + \mu + \nu$. At the higher energies the relative fluxes of these are of the order of 2-3%.

b) *Neutrinos of the opposite type.* These are expected from decays very near the target, before sign selection is effective. They are expected to be very few ($< 10^{-3}$) for typical neutrino energies because of the substantial angle between the beam in this region and the detector ($\sim$ 15 mrad). At very small energies this background becomes more important.

3. Neutrino detectors

3.1 General comments

The characteristic detection problem of neutrino physics is that the detector and the target are necessarily one unit, since the target mass, necessitated by the small cross-sections and diffuseness of the beam, is so large that the detecting elements must be contained within it. For this reason, large bubble chambers make ideal detectors. A large part of what we have learned about neutrino interactions has been by means of bubble chambers filled with freon or propane for bubble chambers working above room temperature, and hydrogen, deuterium and neon for cryogenic bubble chambers. For high energies these are usually augmented by an electronic muon identifier.

For electronic detectors the large amount of matter required imposes severe limitations. The earliest electronic detectors consisted chiefly of aluminium plates arranged as spark chambers, but these are not a match for the present-day large heavy-liquid bubble chambers. More recent electronic detectors consist of a target section in which the total hadron energy, its position, and perhaps its direction can be measured by means of scintillators embedded in the target material, usually iron. A second section of the detector identifies and measures the momenta of muons by means of wire chambers and magnetized iron deflectors. These detectors cannot recognize details of the hadron shower, nor can they identify electrons, both important elements in the understanding of neutrino events. On the other hand, they can be made in a much larger size than the bubble chamber, and yield more accurate measurement of the hadronic energy, so that they are well suited to the measurement of some of the systematic aspects of the inclusive features of both charged and neutral current interactions.

3.2 Bubble chamber detectors

As examples of bubble chamber detectors for neutrino interactions, we will discuss the two installations at the SPS.

3.2.1 Gargamelle. This is a bubble chamber which can be filled with liquids operating near room temperature, typically freon and propane. The liquid volume is a cylinder, 4.9 m long, 1.9 m diameter, with a visible volume of $\sim$ 8 m^3, and a fiducial volume $\sim$ 3 m^3 corresponding to $\sim$ 5 tons of freon.

It is embedded in a magnet which produces a field of 20 kG.

Figure 11 shows a photograph of the ensemble, and Fig. 12 shows a cross-section of magnet and chamber.

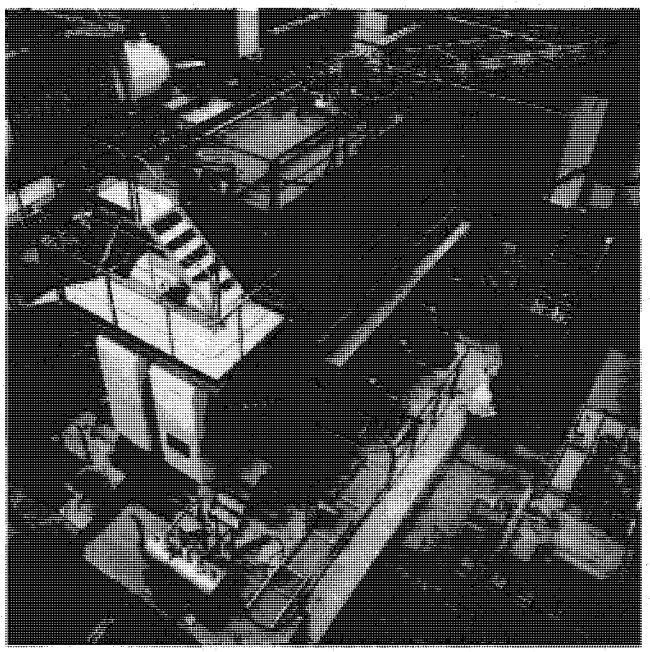

Fig. 11

Gargamelle has been installed in a neutrino beam at the PS since 1971, and has been the instrument of the one great discovery at CERN (if we discount the split A_2): the discovery of neutral currents. It has also played a good part in the discovery of the new particles, probably charmed. It is now being transferred to the SPS to continue its noble career. At the new installation it will be equipped with an EMI (external muon identifier). This is just an iron absorber downstream of the chamber, followed by planes of wire chambers covering an area of 30 m^2 and which measure the positions of particles traversing the plane. Since the iron is thick enough to absorb hadrons, comparison of EMI hits with chamber tracks permits the identification of muons.

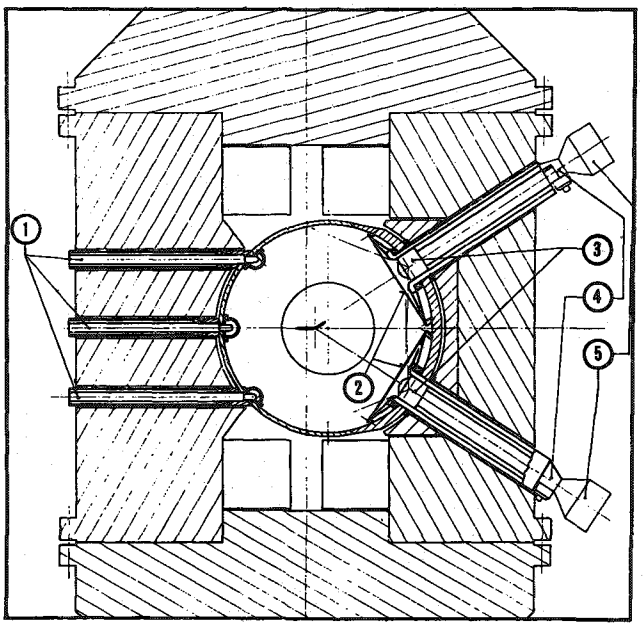

Fig. 12

3.2.2 Big European Bubble Chamber (BEBC). BEBC is a cryogenic bubble chamber. The liquid volume, $\sim$ 32 m^3, is basically a cylinder 3.5 m in diameter and 4 m high. The visible volume is $\sim$ 20 m^3 and a reasonable fiducial volume is $\sim$ 10 m^3. It is surrounded by a superconducting magnet which produces 30 kG. The magnetic return path is an iron cylinder 12 m in diameter. Downstream of this an EMI of 150 m^2 area of proportional wire chambers is being constructed. The whole is shown in Fig. 13.

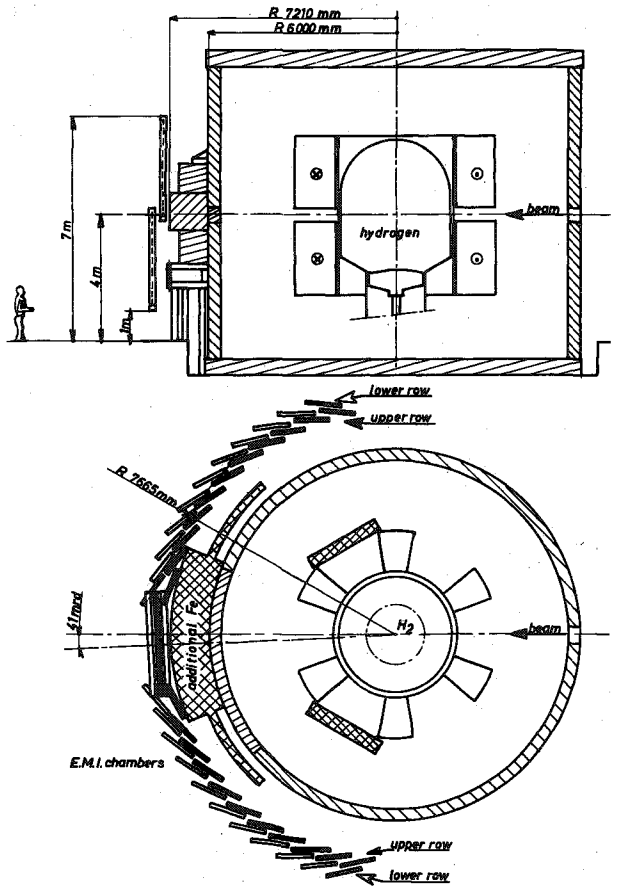

Fig. 13

Three types of filling are foreseen for BEBC: i) H_2 or D_2; ii) neon; iii) A H_2 or D_2 central section, so-called TST (track-sensitive target) in a transparent plastic box, surrounded by neon.

The H_2/D_2 filling offers the advantages of a target with nucleons in their simplest state, and precise measurement conditions in the bubble chamber with a minimum of obscuration by multiple scattering and secondary interactions; but with the disadvantages of poor particle identification, the loss of the neutral parts of the hadron shower, and rather small target weight, effectively $\sim$ ¾ ton H_2 or 1½ tons D_2.

The neon filling offers the advantages of

a) larger target mass ($\sim$ 10 tons);

b) neutral particle detection, especially γ-rays through shower production; this makes it possible to measure the energy also of the neutral component of the hadronic shower; and

c) better particle identification, especially for electrons and positrons,

in return for replacing the simple by a complex nucleus.

The track-sensitive target now in preparation is a box of plexiglas $\sim$ 1 m × 0.8 m × 2.4 m long, or about 2 m^3. It makes it possible to investigate ν-nucleon processes and at the same time have good track identification. The price is the reduction of target mass to ⅛ ton in the case of H_2 and ¼ ton in the case of D_2.

3.3 Electronic detectors

We will discuss here the most common type of electronic detector at present available, consisting of a target-hadron calorimeter and a muon magnet. Since it is a relatively new technique, we discuss at some length the experimental aspects of hadron calorimetry and, very briefly, those of iron core magnets, and give as an example the counter neutrino experiment now being prepared for the SPS.

3.3.1 Sampling hadron calorimeters. This technique is finding a big market at the two 400 GeV machines and in particular in neutrino experiments, and perhaps a discussion is in place, especially of the physical effects that are responsible for the energy uncertainty.

The standard device is illustrated in Fig. 14. It consists of plates of absorber with detecting material in between (scintillator or liquid argon) and is characterized by the sampling thickness and its transverse and longitudinal dimensions.

In these devices the hadronic energy is degraded in successive nuclear collisions and finally appears as ionization which is sampled in the sensitive material. The required length and lateral

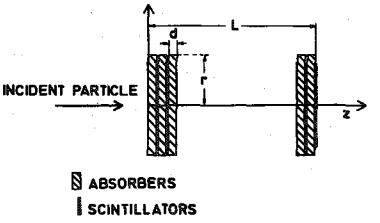

Fig. 14

dimensions depend only logarithmically on the energy. To give an idea, for 95% containment in solid iron, a radius of $\sim$ 30 cm and length of $\sim$ 120 cm is necessary for a 100 GeV particle. If the average density is reduced by a certain factor, for instance by the insertion of the detecting material, of course these dimensions are correspondingly increased.

The resolution is dominated by three effects, as follows:

i) Sampling fluctuations, that is the fluctuations in the number of traversals for a fixed track length. This will of course be proportional to $\sqrt{d}$.

ii) The fluctuations in the "missing energy". The "missing energy" is the energy "lost" either to nuclear excitation and neutrino emission, or to saturation effects in the detector, since the light output in scintillator is appreciably less, per unit energy loss, for slow, densely ionizing particles than for fast, minimum ionizing particles. Saturation effects are particularly large for nuclear evaporation prongs, so the "missing energy" is associated with nuclear stars.

iii) The fluctuations in the fractional energy carried off by γ-rays, particularly from π^0 decay. These γ-rays are dissipated in a soft shower of minimum ionizing particles and therefore there is no missing energy for these. Fluctuations in the fractional energy of the shower in γ radiation contribute therefore to the resolution.

The sampling fluctuations can be very crudely estimated if we assume that the energy E of the shower results in $N = E/\alpha d$ traversals of the sampling elements, where α is the energy loss per unit track length. The fluctuations are then:

$$\Delta E/E \simeq \frac{1}{\sqrt{N}} = \sqrt{\frac{\alpha d}{E}} .$$

With d = 5 cm, α = 0.02 GeV/cm, the sampling fluctuations are approximately:

$$\Delta E/E \simeq 0.3/\sqrt{E(\mathrm{GeV})} .$$

For a Monte Carlo calculation of the effects of sampling thickness, we can refer to the work of Baroncelli[6].

The missing energy, as well as its effect on the resolution, can be seen in Fig. 15, where measured pulse-height distributions for 21 GeV hadrons and positrons are shown[7].

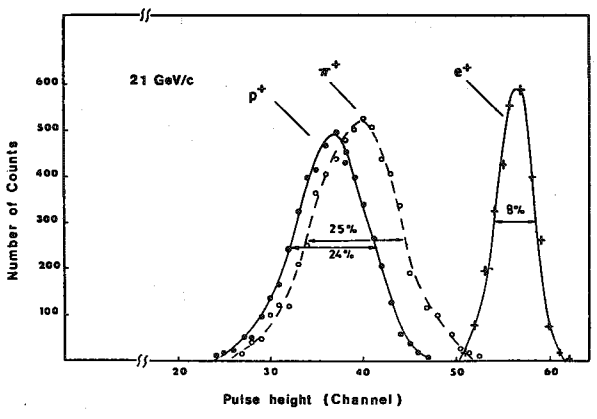

Fig. 15

The average missing energy is a function of the hadron energy, because at higher energy a larger fraction of the energy is converted to π^0. It seems to vary from $\sim$ 20% at 10-15 GeV to $\sim$ 15% at 100 GeV. If there is roughly one nuclear star per GeV of primary energy, and if the missing energy per star is 0.2 $\pm$ 0.2 GeV, the expected fluctuations on this account are of the order of $\sim 0.2/[0.8\sqrt{E(\mathrm{GeV})}]$. It can be seen that this missing-energy effect dominates the sampling effect for sampling thicknesses of a few centimetres or less.

The fluctuations due to the fraction of π^0's are of the order of

$$\frac{\Delta E}{E} \sim \pm \frac{0.2}{0.8} \Delta f ,$$

where Δf is the fluctuation in the π^0 component of the shower, which may be estimated to be of the order of ± 0.15, so that $(\Delta E/E)_{\pi^0} \simeq 0.04$.

The contribution of this effect to the total uncertainty can, however, be reduced to a small fraction of it if the π^0 contribution is measured differentially. This is possible at least for the initial π^0 contribution, which contributes also the dominant effect to the fluctuation, because the electromagnetic shower development is several times more rapid, even in iron, than the hadronic one, as illustrated in Fig. 16.

The resolution which can be expected in such a sampling calorimeter, if the sampling thickness is small enough and if the π^0 component is measured differentially, is shown in Fig. 17 as function of

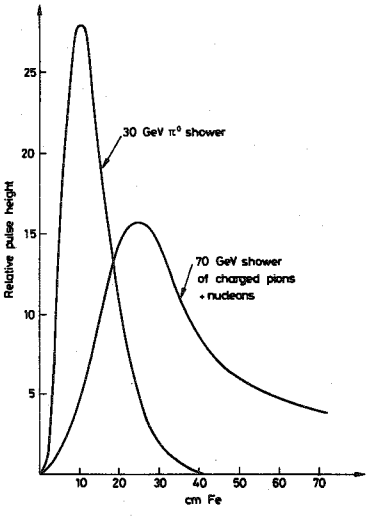

Fig. 16

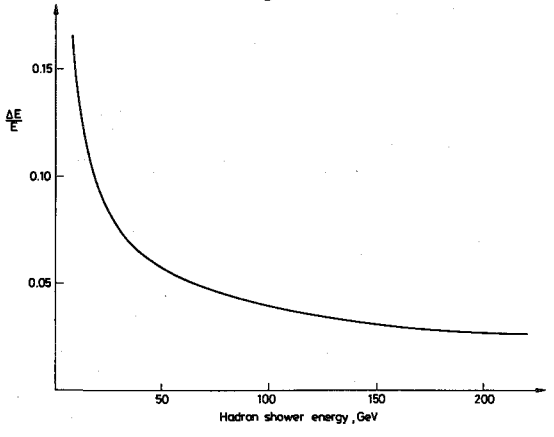

Fig. 17

energy. The resolutions at the lower energy ($\sim$ 20 GeV) have actually been measured. The resolutions, of the order of 3% at 200 GeV, are estimates based on the foregoing discussion and have yet to be attained.

3.3.2 Iron core magnets. Because of its permeability, iron is cheaper to magnetize than vacuum or air. It has the disadvantage that particles are deflected not only by the field, but also by multiple scattering. Of course such a magnet can only be used for penetrating particles, that is muons. In a typical magnet of this type, the iron is saturated with 17-18 kG, and the best resolution which can be achieved in a magnet of length L is given by the competition between multiple scattering deflection,

$$\sim \frac{0.1}{p(\mathrm{GeV/c})} \sqrt{L(\mathrm{m})} \ ,$$

and the magnetic deflection

$$\frac{0.5}{p} \cdot L(\mathrm{m}) \ ,$$

so that

$$\frac{\Delta p}{p} = \pm 0.2/\sqrt{L(\mathrm{m})} \ .$$

To get 10% resolution, the muon must go through 4 m of iron. To get 1% resolution it must go through 400 m! Most such magnets content themselves with 5-15% resolution.

3.3.3 Electronic detector for the SPS. (CERN-Dortmund-Heidelberg-Saclay Collaboration). This detector is of the sampling calorimeter - iron core magnet type, and can therefore measure, in neutrino interactions, the vector momentum of the muon and the hadron energy. However, the magnet and calorimeter are telescoped into one, by magnetizing the calorimeter plates. This has substantial advantages in muon acceptance and in cost.

The over-all layout is shown in Fig. 18. Note that the beam is sloping upwards at 2½ degrees, a consequence of the fact that the SPS is 35 m underground. There are 19 magnetic iron toroids, each 3.75 m in diameter, containing 75 cm of iron plate, and weighing 65 tons. Between units there are three sets of drift wires at 60° to each other, to measure the muon tracks. The first seven magnet units consist of fifteen iron plates, each 5 cm thick, the remaining twelve, of five 15 cm thick plates. All are magnetized by means of two vertical coils, with a total of $\sim$ 40,000 ampere-turns, to have an average toroidal field of 16.5 kG. The variations of this field in radius and azimuth are shown in Fig. 19.

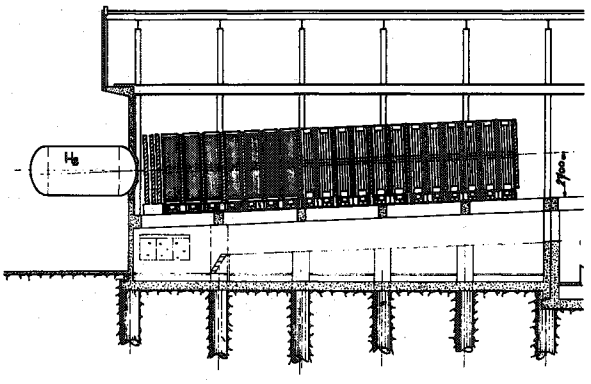

Fig. 18

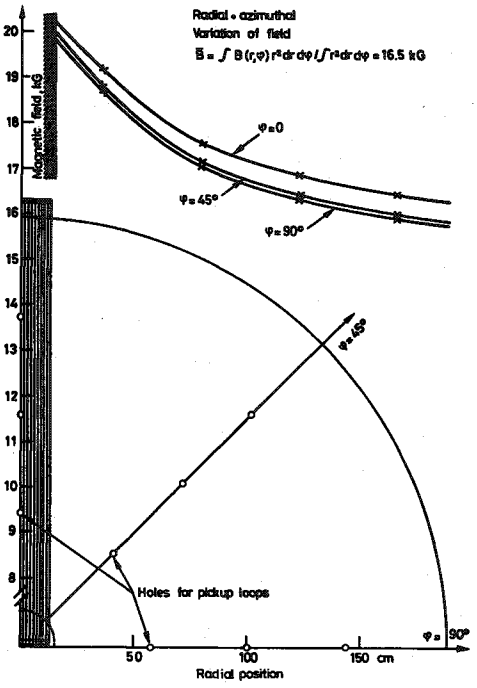

Fig. 19

The hadron shower energy is sampled in the scintillators, arranged in planes in the gaps between the iron plates. Each plane consists of eight horizontal scintillators, 6-8 mm thick, viewed from both sides. The ratio between the right and left pulse heights is used to determine the position along the length of the scintillator. The response of a typical scintillator is shown in Fig. 20 as seen from the left, from the right, and for the sum. The step in the centre is due to the discontinuity produced by unequal thicknesses and the glue joint between the two separate pieces. Some details of the construction and instrumentation are shown in Fig. 21.

The detector will be used chiefly in the narrow-band beam, where, with a good resolution target of $\sim$ 400 tons and an additional poorer resolution target of 800 tons, it will be used to study the systematics of charged, neutral current and multimuon neutrino interactions in iron.

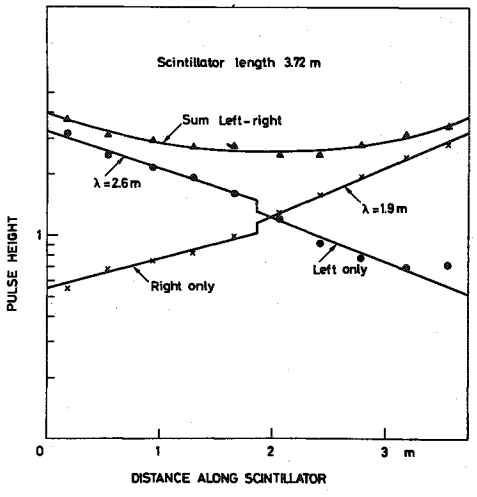

Fig. 20

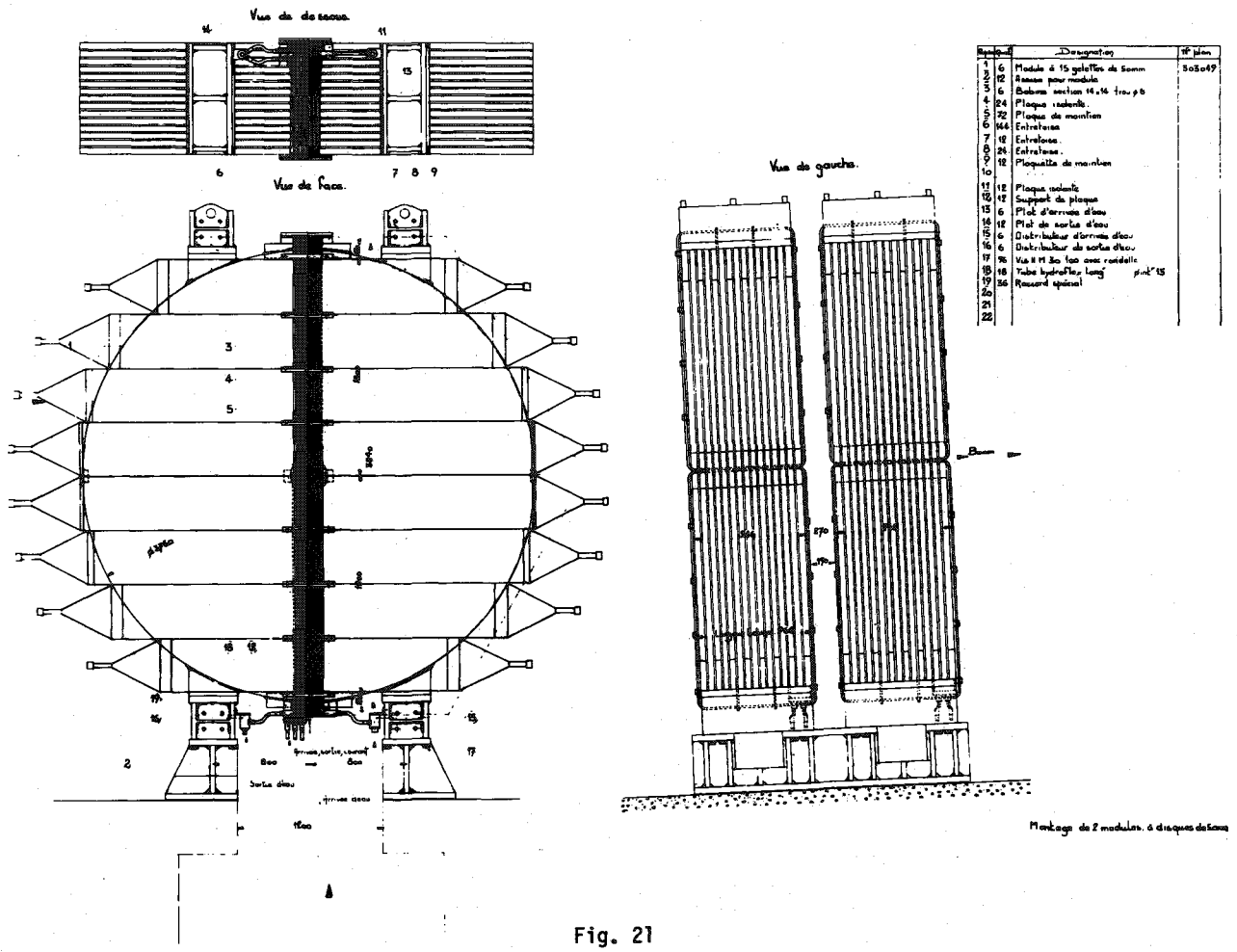

Fig. 21

In front of the magnetic detector is a tank of $\sim$ 35 m^3 which can be filled with hydrogen or deuterium (whichever is not used in BEBC), and a set of multiwire proportional chambers, which are used to reconstruct the charged tracks to check the origin (tank or tank wall) of the events. This set-up will be used, together with the calorimeter-magnet, to measure inclusive distributions in H_2 and D_2 in the wide-band beam.

3.3.4 CERN-Hamburg-Moscow-Rome detector. The present generation of electronic detectors does not offer the possibility of measuring the direction of the hadron shower. Such a directional measurement is particularly desirable for neutral current interactions, because a measurement of the hadron energy, together with the incident neutrino energy, defines only two of the three inclusive variables E_ν, $x = |q^2|/|q^2_{max}(y)|$, and $y = E_h/E_\nu$, but if the hadron direction is known, all three parameters are in principle defined.

Measurement of the hadron shower direction requires "fine grain" measurement of the hadronic energy deposited, and therefore many thin scintillators or proportional wires, and perhaps also a low-Z, low-density matrix in which electromagnetic and hadronic showers will develop comparably and over larger distances.

Such an apparatus, with marble as the matrix material and both thin scintillators and proportional chambers to measure the shower development, is being developed and will occupy the neutrino counter hall behind the experiment described in the foregoing section.

The 80 marble sheets, each $\sim$ 8 cm thick and 3 × 3 m square, are surrounded by a dual-purpose picture frame magnet. By putting the energizing coils in series, this magnet can be used in the magnetic measurement of muons. By putting the energizing coils in opposition, a small ($\sim$ 50 gauss), uniform magnetic field is created in the marble plates, where it can be used to precess muons generated in the CDHS experiment (see 3.3.3 above) to measure their polarization.

4. Introduction to the standard model of neutrino interactions

4.1 Lepton conservation

The known leptons can be classified into two groups, electron and muon, each with 2 × 2 = 4 members: particle-antiparticle, charged and neutral, as follows:

$$L_e = +1 \quad L_e = -1 \quad L_\mu = +1 \quad L_\mu = -1$$

$$\begin{pmatrix} e^- \\ \nu_e \end{pmatrix} \quad \begin{pmatrix} e^+ \\ \bar{\nu}_e \end{pmatrix} \quad \begin{pmatrix} \mu^- \\ \nu_\mu \end{pmatrix} \quad \begin{pmatrix} \mu^+ \\ \bar{\nu}_\mu \end{pmatrix}$$

To the best of our knowledge, the "lepton numbers" L_e and L_μ are separately conserved. That is, for any reaction,

$$\sum_{\text{right}} L_e = \sum_{\text{left}} L_e \quad \text{and} \quad \sum_{\text{right}} L_\mu = \sum_{\text{left}} L_\mu .$$

Examples

Allowed: $\mu^+ \to \bar{\nu}_\mu + e^+ + \nu_e$

$K^- \to \mu^- + \bar{\nu}_\mu$

Forbidden: $\mu^\pm \to e^\pm + \gamma$

$\bar{\nu}_\mu + p \to e^+ + n$

4.2 Current-current Lagrangian

It is supposed that the Lagrangian can be written as the product of two charged currents:

$$\mathcal{L} = \frac{G}{\sqrt{2}} \mathcal{J}_\alpha^+ \mathcal{J}_\alpha^- , \qquad (4.1)$$

where $G \simeq 10^{-5}/M_p^2$ from the muon lifetime and

$$\mathcal{J}_\alpha = j_\alpha + J_\alpha ,$$

where j_α = lepton current and J_α = hadron current.

This implies that all combinations of weak interactions exist (lepton-lepton, lepton-hadron, and hadron-hadron), always with the same coupling constant and always the product of two currents of vector - axial vector type.

It is known now that the Lagrangian (4.1) must be extended to include also neutral currents. We come back to this later.

4.3 Lepton current

Consistent with a large body of experimental evidence, the charged lepton current can be written:

$$\begin{aligned} j_\alpha^- &= \bar{e}^- \gamma_\alpha (1-\gamma_5) \nu_e + \bar{\mu}^- \gamma_\alpha (1-\gamma_5) \nu_\mu \\ j_\alpha^+ &= \bar{\nu}_e \gamma_\alpha (1-\gamma_5) e^- + \bar{\nu}_\mu \gamma_\alpha (1-\gamma_5) \mu^- \end{aligned} \qquad (4.2)$$

where, for example, $\bar{e}^- \gamma_\alpha (1-\gamma_5) \nu_e$ means: annihilate a left-handed neutrino or create a right-handed antineutrino, and create a left-handed*) electron or annihilate a right-handed*) positron.

This form of the lepton current contains the two-component neutrino hypothesis, as well as electron-muon universality.

4.4 Hadron current

The weak hadron current is coupled to the complications of the strong interactions; it is therefore not as clearly understood as the lepton current. In the standard model it is supposed to have the following general properties:

i) Strangeness. Only $\Delta S = 0$ and $\Delta S = \Delta Q = \pm 1$ terms are present.

ii) Conserved vector current (CVC). The vector terms of the $\Delta S = 0$ current are the charged components of an isovector triplet, of which the electromagnetic isovector current is the neutral component. Therefore all aspects of the vector current, form factors, etc., are known if the corresponding electromagnetic terms are known. Moreover, because the current is conserved, the vector coupling constant is not renormalized and is just equal to the one for lepton currents. On the other hand, the axial vector coupling constant suffers renormalization.

iii) Charge symmetry of $\Delta S = 0$ part. For example,

$$\langle p|J_\alpha^+|n\rangle = \langle n|J_\alpha^-|p\rangle$$

$$\langle \Sigma^+|J_\alpha^+|\Lambda\rangle = \langle \Sigma^-|J_\alpha^-|\Lambda\rangle ,$$

iv) Cabibbo current. J_α is assumed to be a rotation in hyperspace of the current $p \to n$. This is most easily seen in the quark model. If u is the up (proton) quark, d the down (neutron) quark, and s the strange (Λ) quark, then it is supposed that

$$J_\alpha^- = \cos\theta_c [\bar{d}\gamma_\alpha(1-\gamma_5)u] + \sin\theta_c [\bar{s}\gamma_\alpha(1-\gamma_5)u] .$$

From a comparison of K and π decay,

$$\tan\theta_c \simeq 0.22 - 0.27 .$$

v) Modifications indicated or demanded by recent experiments

a) *Heavy leptons*

There are indications ($e\mu$ events at SPEAR) that there is at least one more lepton.

b) *Charm*[8]

The Cabibbo current probably has to be extended to include charmed (c) quarks. In the Glashow, Iliopoulos, Maiani (GIM) model[9] the quark scheme looks like this:

	I	I_3	Q	s	c
u	$\frac{1}{2}$	$\frac{1}{2}$	$\frac{2}{3}$	0	0
c	0	0	$\frac{2}{3}$	0	1
d	$\frac{1}{2}$	$-\frac{1}{2}$	$-\frac{1}{3}$	0	0
s	0	0	$-\frac{1}{3}$	-1	0

and the hyperspace nature of the weak currents can be written in terms of the matrices:

$J_\alpha^{(C)-}$

	u	c	d	s
$\bar{u}$	0	0	$\cos\theta_c$	$\sin\theta_c$
$\bar{c}$	0	0	$-\sin\theta_c$	$\cos\theta_c$
$\bar{d}$	0	0	0	0
$\bar{s}$	0	0	0	0

$J_\alpha^{(C)+}$

	$\bar{u}$	$\bar{c}$	$\bar{d}$	$\bar{s}$
u	0	0	0	0
c	0	0	0	0
d	$\cos\theta_c$	$-\sin\theta_c$	0	0
s	$\sin\theta_c$	$\cos\theta_c$	0	0

*) In the limit of zero electron mass.

$J_\alpha^{(N)}$ =

	u	c	d	s
$\bar{u}$	1	0	0	0
$\bar{c}$	0	1	0	0
$\bar{d}$	0	0	1	0
$\bar{s}$	0	0	0	1

The charged hadronic current

$$J_\alpha^- = \cos\theta_c[\bar{d}\gamma_\alpha(1-\gamma_5)u] + \sin\theta_c[\bar{s}\gamma_\alpha(1-\gamma_5)u] -$$

$$- \sin\theta_c[\bar{d}\gamma_\alpha(1-\gamma_5)c] + \cos\theta_c[\bar{s}\gamma_\alpha(1-\gamma_5)c]$$

has large ($\cos\theta_c$) terms with $\Delta s = \Delta c = 0$ and $\Delta s = -\Delta c = 1$, and small ($\sin\theta_c$) terms with $\Delta s = 1$, $\Delta c = 0$ and $\Delta s = 0$, $\Delta c = -1$.

The neutral current in this model is diagonal in all the quarks and therefore strangeness and charm conserving. The space time character of the neutral current is among the interesting topical questions in neutrino physics, and will be discussed later.

4.5 Warning

In the following presentation this "standard" model will be used as the basis of the discussion. It will not be necessary to caution experimenters that the facts may very well be otherwise, and it is our business to find this out.

5. ν-e scattering

5.1 Reactions and diagrams

a) $\nu_e + e^- \to \nu_e + e^-$

$\bar{a}$) $\bar{\nu}_e + e^- \to \bar{\nu}_e + e^-$

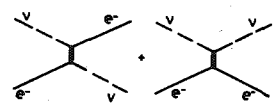

b) $\nu_\mu + e^- \to \nu_\mu + e^-$

$\bar{b}$) $\bar{\nu}_\mu + e^- \to \bar{\nu}_\mu + e^-$

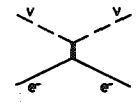

The ν_e scattering can proceed via both neutral and charged current terms, and would be a delightful way to study their interference. Unfortunately, high-energy neutrino beams are dominantly ν_μ, so this reaction can be studied at present only with reactor neutrinos[10].

The ν_μ scattering can proceed only through the neutral current, and can therefore also provide a test of the existence of neutral currents.

In addition, at higher energies ($E_\nu \geq m_\mu^2/2m_e$ = = 11 GeV) the reactions

c) $\nu_\mu + e^- \to \mu^- + \nu_e$

and

$\bar{c}$) $\bar{\nu}_e + e^- \to \bar{\nu}_\mu + \mu^-$

can be studied. These reactions are different forms of the inverse muon decay, and involve the charged lepton current only.

5.2 The weak neutral current and the Lagrangian

We assume that also the neutral weak current has the vector - axial vector form, but without *a priori* assumption about the magnitudes of the V and A parts. The neutral lepton current can then be written

$$j_\alpha^{(N)} = \bar{\nu}_e\gamma_\alpha(1-\gamma_5)\nu_e + \bar{\nu}_\mu\gamma_\alpha(1-\gamma_5)\nu_\mu +$$

$$+ C_V\left[\bar{e}\gamma_\alpha e + \bar{\mu}\gamma_\alpha\mu\right] + C_A\left[\bar{e}\gamma_\alpha\gamma_5 e + \bar{\mu}\gamma_\alpha\gamma_5\mu\right] . \qquad (5.1)$$

With the charged current (4.2) the Lagrangian is

$$\mathcal{L} = \frac{G}{\sqrt{2}}\left[j_\alpha^{(C)^+} j_\alpha^{(C)^-} + j_\alpha^{(N)} J_\alpha^{(N)}\right] . \qquad (5.2)$$

5.3 Kinematics

Since $E_\nu \gg m_e$, the kinematics are dominated by the fact that the centre-of-mass energy is very small, and consequently also the momentum transfer and the laboratory scattering angle. This is particularly important because the small scattering angle is the chief experimental tool for isolating the reaction.

a) *Laboratory-c.m. transformation:* $\gamma = \sqrt{E_\nu/2m_e}$.

b) *Centre-of-mass energy:*

$$E_{cm} \simeq \sqrt{2m_e E_\nu} \quad \text{for } E_\nu \gg m_e .$$

c) *Electron energy in laboratory:* With θ^* the c.m. scattering angle of the neutrino,

$$E_e \simeq \frac{E_\nu}{2}(1 - \cos\theta^*) , \quad E_\nu \gg m_e .$$

It should be noticed that the electron energy goes from zero to E_ν, with a uniform spectrum if the c.m. angular distribution is isotropic.

d) *Electron angle in the laboratory:*

$$\theta_e \simeq \frac{1}{\gamma}\sin\theta^*/(1 - \cos\theta^*) , \quad E_\nu \gg m_e .$$

The relationship θ_e versus θ^* is shown in Fig. 22.

e) *Energy and momentum transfer:*

$$y \equiv E_e/E_\nu \simeq (1 - \cos\theta^*)/2$$

$$Q^2 \equiv -q^2 \equiv -(p_\nu - p'_\nu)^2 \cong$$

$$\cong s(1 - \cos\theta^*)/2 = sy = 2m_e E_e .$$

f) *Magnitude of cross-section.* For a four-fermion point interaction, the cross-section is proportional to the square of the centre-of-mass energy. Because at high energies this is proportional to the target mass, ν-e cross-sections are three orders of magnitude smaller than nucleon cross-sections.

5.4 Charged current ν-e scattering

$$\nu_e(\bar{\nu}_e) + e^- \to \nu_e(\bar{\nu}_e) + e^- .$$

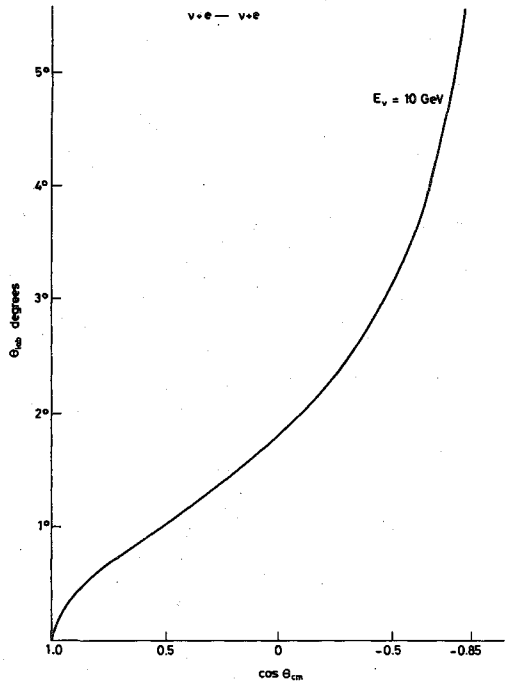

Fig. 22

If neutral currents were not to exist, and only the charged currents (4.2) were operative, the cross-sections would be:

$$d\sigma_\nu/dy = \frac{2G^2 m_e E_\nu}{\pi} ; \qquad \frac{d\sigma_{\bar\nu}}{dy} = \frac{2G^2 m_e E_\nu (1-y)^2}{\pi} ;$$

$$\sigma_\nu = \frac{2G^2 m_e E_\nu}{\pi} ; \qquad \sigma_{\bar\nu} = \frac{2}{3\pi} G^2 m_e E_\nu .$$

The $(1-y)^2$ factor, which is present in the anti-neutrino case but not in the neutrino case, is the angular factor $[(1 + \cos\theta^*)/2]^2$, and is due to the fact that a right-handed antineutrino cannot scatter backwards and push a left-handed electron forward.

It is instructive to consider the cross-sections as the sum of V, A, and interference terms.

	V	A	Interference
$\frac{d\sigma_\nu}{dy} \propto$	$1 + (1-y)^2$	$1 + (1-y)^2$	$4y-2y^2$
$\frac{d\sigma_{\bar\nu}}{dy} \propto$	$1 + (1-y)^2$	$1 + (1-y)^2$	$-(4y-2y^2)$

The V and A terms separately are parity conserving and are the same for neutrino and antineutrino. The interference term changes sign in going from neutrino to antineutrino.

5.5 Neutral current ν-e scattering

If only the neutral current (5.1) is operative, as in the case of $\nu_\mu(\bar\nu_\mu)$-e^- scattering, the cross-sections are

$$\frac{d\sigma_\nu}{dy} = \frac{2G^2 m_e E_\nu}{\pi}\left[\left(\frac{C_V+C_A}{2}\right)^2 + \left(\frac{C_V-C_A}{2}\right)^2 (1-y)^2\right] , \tag{5.3}$$

$$\frac{d\sigma_{\bar\nu}}{dy} = \frac{2G^2 m_e E_\nu}{\pi}\left[\left(\frac{C_V+C_A}{2}\right)^2 (1-y)^2 + \left(\frac{C_V-C_A}{2}\right)^2\right] .$$

It is the most interesting case from the experimental point of view, since high-energy neutrino beams contain ∿ 99% muon neutrinos.

5.6 Both charged and neutral current ν-e scattering

To get the cross-section in this case, which is relevant to ν_e-e^- scattering, just replace $C_V \to 1 + C_V$ and $C_A \to 1 + C_A$ in (5.3).

5.7 Weinberg-Salam model prediction for ν_μ-e scattering

In the Weinberg-Salam model[11], the neutral weak current is a combination of the electromagnetic current and the neutral component of the isovector current of which the charged weak currents form the charged components:

$$j_\alpha^{WS} = j_\alpha^3 - 2\sin^2\theta_w\, j_\alpha^{em} ,$$

$$j_\alpha^3 = \tfrac{1}{2}\left[\bar e\gamma_\alpha(1-\gamma_5)e + \bar\mu\gamma_\alpha(1-\gamma_5)\mu\right] ,$$

$$j_\alpha^{em} = \bar e\gamma_\alpha e + \bar\mu\gamma_\alpha\mu ,$$

so that, in the notation of (5.1):

$$C_V = \tfrac{1}{2} - 2\sin^2\theta_w ; \quad C_A = -\tfrac{1}{2} .$$

The neutral current, in this theory, is known except for the single parameter $\sin^2\theta_w$. The expected cross-sections are shown in Fig. 23 as function of the Weinberg angle.

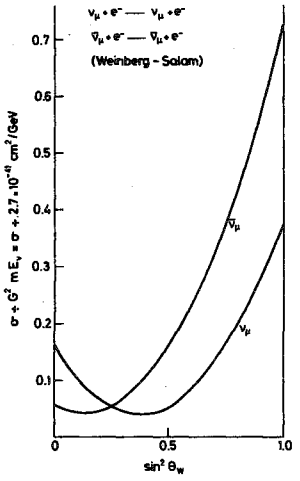

Fig. 23

5.8 Experimental results on ν-e scattering

5.8.1 Gargamelle Collaboration[12]. Gargamelle, filled with 6.3 m³ CF_3Br, density 1.5 g/cm², radiation length 11 cm, was exposed to the wide-band $\bar\nu$ beam at the CERN PS, and 1.4×10^6 pictures were taken. The $\bar\nu$ spectrum and various contaminations are shown in Fig. 24. The experimental problem is to isolate the electron scattering events, which are characterized by an electron track going near the forward direction, and nothing else. Electrons are rather easily identified in Gargamelle. The problem is to isolate these events, which are rare (∿ 10^{-3} of all events), from background, such as neutral current events in which only a π^0 is emitted, and

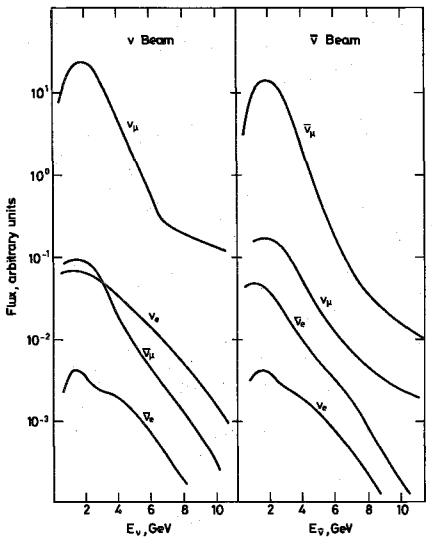

Fig. 24

somehow only one electron is seen, or $\nu_e + n \to e^- +$ + p, p not seen. To exclude this background as much as possible, but still retain a reasonable fraction of $\bar{\nu}$-e events, the following cuts were made:

$$0.3 < E_e < 2 \text{ GeV (see Fig. 25)}$$

$$\theta_e < 5^\circ .$$

Three events were found. The background can be rather reliably estimated, on the basis of observed γ-rays and electrons at larger angles, to be 0.4 events. The observed cross-section, uncorrected for cuts, is $\sigma_{obs} \simeq 0.05 \times 10^{-41} E_{\bar{\nu}}$ cm^2/GeV. The losses due to cuts are model-dependent. In the

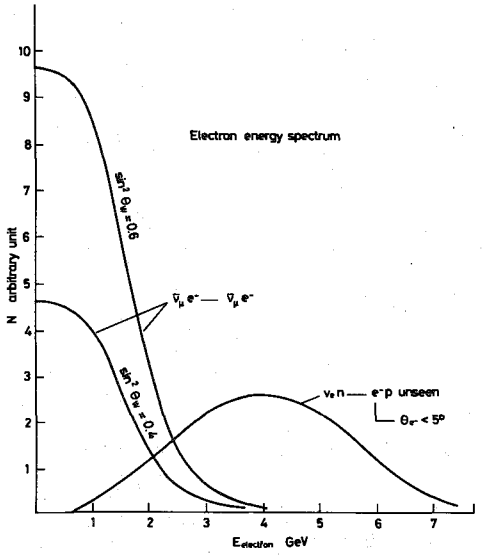

Fig. 25

Weinberg-Salam model they are $\sim$ 50%. The cross-section of $\sim 0.1 \times 10^{-41} E_{\bar{\nu}}$ is compatible with the Weinberg model for any $\sin^2 \theta$ less than ~ 0.4 (see Fig. 23).

In an exposure to a neutrino beam only one event was found, compatible with background.

5.8.2 Aachen-Padua Collaboration (as reported at the 1976 International Neutrino Conference at Aachen). A 50-ton aluminium plate spark chamber assembly was exposed behind Gargamelle and to the same beam. The electrons are identified by the spark pattern, and the energy estimated by spark counting. With cuts similar to those of Gargamelle, the following results were given (Table 1).

These cross-sections are preliminary, and $\sim$ 5-10 times higher than those found in Gargamelle. It is important to resolve this question.

6. Neutrino hadron reactions

6.1 Kinematics

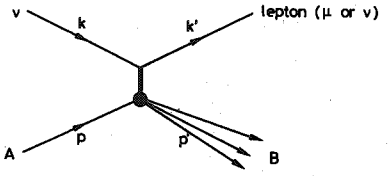

We consider the high-energy region only, $E_\nu \gg M$, where M is the nucleon mass. The lepton mass is neglected. The incident hadron can be taken to be a nucleon for the typical processes for which the momentum transfer is much greater than a few hundred MeV/c. The outgoing hadron system B is characterized by the momentum p'. The following is the usual notation and will be used here:

$\theta \equiv$ lepton scattering angle in the laboratory;

$$s \equiv (k+p)^2 \simeq 2E_\nu M ;$$

$$Q^2 \equiv -q^2 \equiv -(k-k')^2 \simeq 4E_\nu E_\ell \sin^2 \theta/2 ;$$

$$\nu \equiv p \cdot q = M(E_\nu - E_\ell) = M(E_h - M) \simeq ME_h$$

where E_h is the laboratory hadron energy;

$$W = M_h = M_B = \sqrt{p'^2} \simeq \sqrt{2\nu - Q^2} ;$$

$$x \equiv \frac{Q^2}{2\nu} = \frac{2E_\nu E_\ell \sin^2 \theta/2}{M(E_h - M)} \simeq \frac{2E_\nu E_\ell \sin^2 \theta/2}{ME_h}$$

$$y \equiv \frac{\nu}{k \cdot p} = \frac{E_h - M}{E_\nu} \simeq E_h/E_\nu .$$

The "inclusive" process, where only the momenta of the leptons are observed, independent of lepton polarization or configuration of B, can be described in terms of three variables only. These are usually taken to be either

$$E_\nu, Q^2, \nu \text{ or } E_\nu, x, y .$$

Table 1

	Events observed	Estimated background	Events net	No. of protons on target	σ_{obs}
$\nu_\mu e$	25	12 ± 2	13 ± 5	3.4×10^{18}	$(0.18 \pm 0.08) \times 10^{-41}$ cm^2/GeV
$\bar{\nu}_\mu e$	19	3 ± 1	16 ± 5	3.4×10^{18}	$(0.45 \pm 0.13) \times 10^{-41}$ cm^2/GeV

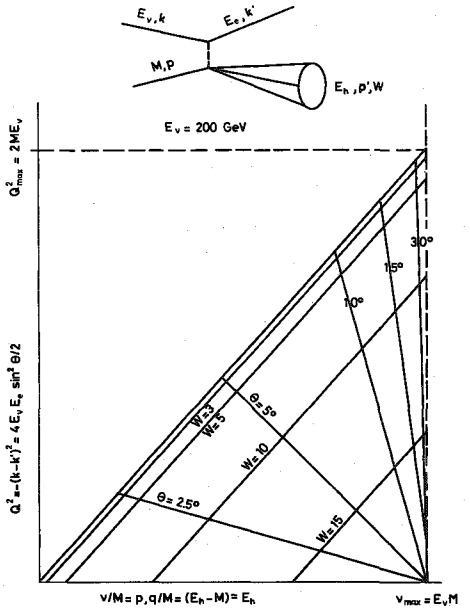

Fig. 26

Figure 26 illustrates the physical domain in the Q^2-ν plot. Events are constrained to the triangular region:

$$Q^2 \leq Q^2_{max} = 2ME_\nu$$

$$\nu \leq \nu_{max} = ME_\nu$$

and $2\nu \geq Q^2$.

The line $2\nu = Q^2$ corresponds to elastic scattering; lines parallel to this correspond to hadron states of given mass. The straight lines which radiate from the point $Q^2 = 0$, $\nu = \nu_{max}$ correspond to a given scattering angle.

A similar situation exists in the x-y plot, but the triangular region of the Q^2-ν plot corresponds here to the square $0 \leq x \leq 1$, $0 \leq y \leq 1$.

6.2 Form of interaction and structure functions

The Lagrangian can be written

$$\mathcal{L}^{(C)} = \frac{G}{\sqrt{2}} \left[j^+_\alpha J^-_\alpha + j^-_\alpha J^+_\alpha \right]$$

for charged current reactions, where the emitted lepton is a muon, and j^+_α and J^+_α are the lepton and hadron currents, respectively, which increase charge by one unit, and j^-_α and J^-_α those which reduce the charge by one unit. For neutral current interactions it can be written:

$$\mathcal{L}^{(N)} = \frac{G}{\sqrt{2}} j^{(N)}_\alpha J^{(N)}_\alpha \ .$$

Some of the properties of these currents were discussed in Sections 4 and 5.

For the process

$$\nu + A \to \ell + B \ ,$$

$$\sigma \propto m_{\alpha\beta} M_{\alpha\beta} \ ,$$

where

$$m_{\alpha\beta} = \langle k | j^\pm_\alpha | k' \rangle \langle k' | j^\mp_\beta | k \rangle$$

$$\left[\text{or } \langle k | j^{(N)}_\alpha | k' \rangle \langle k' | j^{(N)}_\beta | k \rangle \right] ,$$

and

$$M_{\alpha\beta} = \langle A | J^\mp_\alpha | B \rangle \langle B | J^\pm_\beta | A \rangle$$

$$\left[\text{or } \langle A | J^{(N)}_\alpha | B \rangle \langle B | J^{(N)}_\beta | A \rangle \right] .$$

In the following, since we ignore polarization effects, $m_{\alpha\beta}$ and $M_{\alpha\beta}$ should be considered summed over final and averaged over initial polarization states; $m_{\alpha\beta}$ can be immediately evaluated for the form of the currents already given. In the charged case, for example,

$$m^{(C)}_{\alpha\beta} = 8 \left[k'_\alpha k_\beta + k_\alpha k'_\beta - g_{\alpha\beta} k \cdot k' - i\varepsilon_{\alpha\beta\gamma\delta} k'_\gamma k_\delta \right] ,$$

where $g_{\alpha\beta}$ is the metric tensor and $\varepsilon_{\alpha\beta\gamma\delta}$ is the totally antisymmetric tensor.

On the basis of the form of the Lagrangian, and after summing over all polarizations, the hadron part can be written in terms of three structure functions[13]):

$W_1(Q^2,\nu)$, $W_2(Q^2,\nu)$, and $W_3(Q^2,\nu)$:

$$M_{\alpha\beta} = -g_{\alpha\beta} W_1 + \frac{p_\alpha p'_\beta}{M^2} W_2 - i\varepsilon_{\alpha\beta\gamma\delta} \frac{p_\gamma p'_\delta}{2M^2} W_3 \ .$$

This expression, in the absence of a theory of strong interactions, serves as definition of W_1, W_2, and W_3.

6.3 Pseudoelastic neutrino scattering

$$\nu_\mu + n \to p + \mu^-$$

$$\bar{\nu}_\mu + p \to n + \mu^+$$

6.3.1 Phenomenology

a) One degree of freedom is lost. With $W^2 = M^2 = (p+q)^2$, $x = Q^2/2p\cdot q = 1$ and $Q^2 = 2ME_\nu y$.

b) Definition of form factors:
Write $\langle p | J^+_\alpha | n \rangle = \cos\theta_C \langle \bar{u}(p') | \Gamma_\alpha(q^2) | u(p) \rangle$, where $\bar{u}$ and u are Dirac spinors, and $\Gamma_\alpha(q^2)$ is the most general vector - axial vector matrix:

$$\Gamma_\alpha(q^2) = \gamma_\alpha F_V + i\sigma_{\alpha\beta} q_\beta F_M/2M + q_\alpha F_S +$$

$$+ \left[\gamma_\alpha F_A + i\sigma_{\alpha\beta} q_\beta F_T/2M + q_\alpha F_P \right] \gamma_5 \ .$$

In principle, the six form factors $F_i = F_i(q^2)$ can be determined from experiment. At present the experiments are insufficient for this task, and it is the practice to make certain assumptions:

i) The vector form factors, in line with CVC, are those found from electron scattering experiments:

$$F_V = F_1^p - F_1^n \simeq \frac{1}{(1-q^2/M_V^2)^2} \quad (M_V = 0.84 \text{ GeV}) ;$$

$$F_M = \mu_p F_2^p - \mu_n F_2^n \simeq (\mu_p - \mu_n) F_V ,$$

where μ_p and μ_n are proton and neutron magnetic moments, respectively, in units of the nuclear magneton;

$$F_S = 0.$$

ii) $F_T = 0$; this would be a consequence of T invariance or the absence of second-class currents.

iii) $F_P \simeq 0$; we know from muon capture experiments that F_P is small.

iv) This leaves F_A as the only unknown form factor. It is supposed that the q^2 dependence of F_A is the same as F_V, except for the magnitude of the mass:

$$F_A = \frac{1.23}{1+q^2/M_A^2} ;$$

the factor 1.23 comes from nuclear β-decay ($Q^2 \simeq 0$). This leaves only the number M_A to be determined from experiment.

c) The cross-sections can then be written

$$\frac{d\sigma_{\nu(\bar{\nu})}}{dQ^2} = \frac{G^2}{\pi}\left(\frac{F_V \mp F_A}{2}\right)^2 + (1-y)^2\left(\frac{F_V \mp F_A}{2}\right)^2 - \frac{1}{4}(F_V^2 - F_A^2)\frac{Q^2}{2E_\nu^2} +$$

$$+ \frac{F_M y}{2}\left[F_M(1-y)\frac{E_\nu}{2M} + y(F_M + F_V \mp F_A) \pm 2F_A\right] \qquad (6.1)$$

with $y = Q^2/2ME_\nu$.

For $E_\nu \gg M$, only terms with $y \ll 1$ contribute. The cross-section then becomes independent of E_ν and equal for neutrinos and antineutrinos:

$$\left.\frac{d\sigma_\nu}{dQ^2}\right|_{E_\nu \to \infty} = \left.\frac{d\sigma_{\bar{\nu}}}{dQ^2}\right|_{E_\nu \to \infty} = \frac{G^2}{2M}\left[F_V^2 + F_A^2 + F_M^2\frac{Q^2}{4M^2}\right] .$$

6.3.2 Experimental results for charged pseudo-elastic neutrino scattering.

a) *Gargamelle Collaboration*[14]: The exposure and beam are described in Section 5.8.1. Events $\nu + N \to \mu^- + X$ are assumed pseudoelastic if there is no more than one fast proton; events $\nu + N \to \mu^+ + X$ are assumed pseudo-elastic if there is at most one fast neutron candidate. Two independent analyses are performed to find M_A: a fit to σ_{tot} versus E_ν (Fig. 27) and a fit to the momentum transfer dependence of the cross-section (Fig. 28).

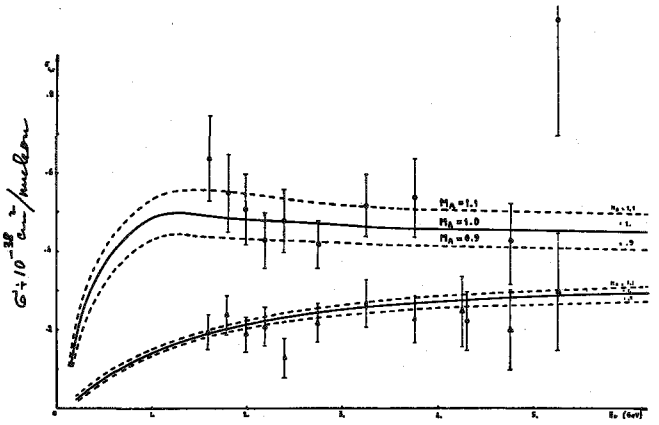

Fig. 27

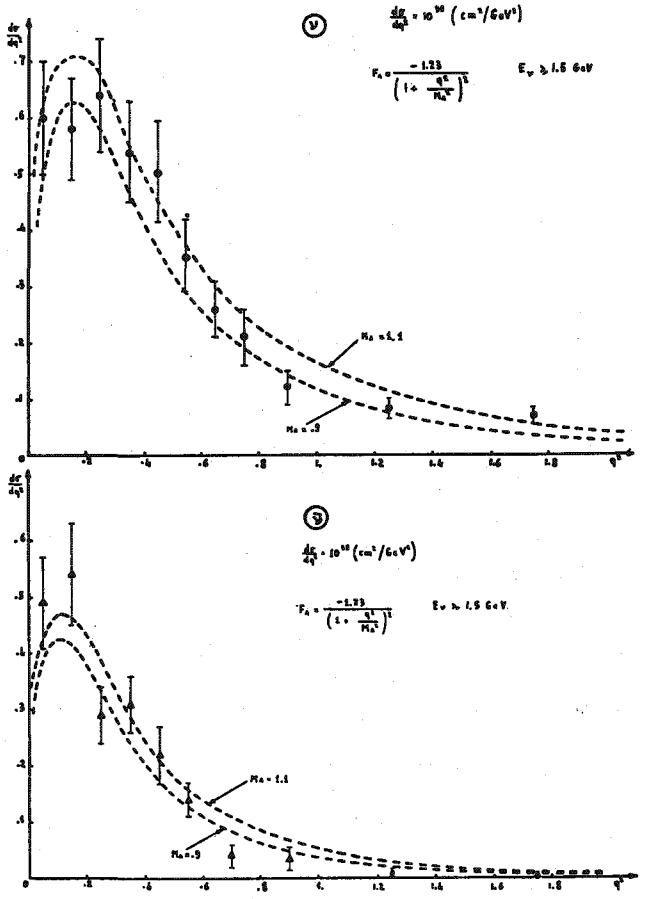

Fig. 28

From the Q^2 distribution:

$M_A^\nu = 1.0 \pm 0.1$ GeV , $M_A^{\bar{\nu}} = 0.91 \pm 0.12$ GeV .

From the energy distribution:

$M_A^\nu = 0.96 \pm 0.1$ GeV , $M_A^{\bar{\nu}} = 0.7 \pm 0.2$.

All results are consistent with

$$M_A = 0.94 \pm 0.06 \text{ GeV} .$$

b) *Argonne National Lab. 12' D_2 Bubble Chamber Group*[15]. The chamber was exposed to a wide-band neutrino beam with a spectrum similar to that of Fig. 24, but with somewhat lower energy.

Approximately 400 events ascribable to the reaction $\nu + d \to \mu^- + p + p_{spect}$ were found. The data are shown in Figs. 29 and 30. With similar analysis, from the Q^2 distribution:

$$M_A^\nu = 0.84 \begin{matrix}+0.12\\-0.10\end{matrix} \text{ GeV}$$

and from the energy dependence:

$$M_A^\nu = 0.98 \begin{matrix}+0.13\\-0.14\end{matrix} \text{ GeV} .$$

Both results are consistent with the average:

$$M_A = 0.89 \pm 0.08 \text{ GeV} .$$

c) *Experiments on the production of pions by electrons.* On the basis of the "Partially Conserved Axial Vector Current" theory and CVC, such experiments can be analysed to yield a value of M_A, for comparison. The most recent experiments[16]) give the value

$$M_A = 0.96 \pm 0.03 \text{ GeV} .$$

All experiments seem to give very similar results, and the Q^2 dependence of the axial form factor seem to be quite similar to the vector form factor.

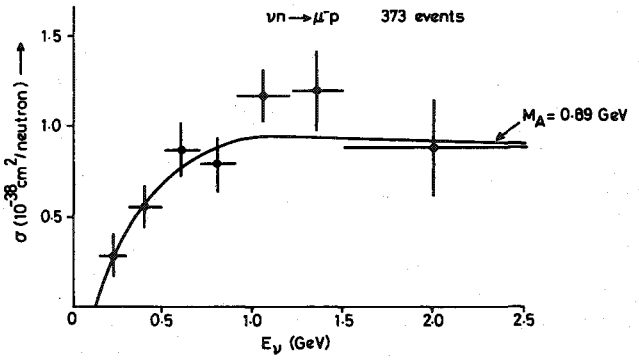

Fig. 29

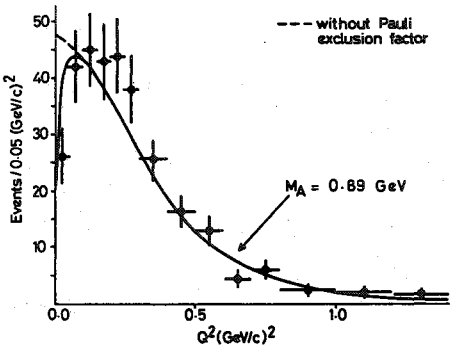

Fig. 30

6.4 Neutral current elastic interactions

There are four reactions:

i) $\nu + p \to \nu + p$

ii) $\bar\nu + p \to \bar\nu + p$

iii) $\nu + n \to \nu + n$ and

iv) $\bar\nu + n \to \bar\nu + n$.

The last two are hard to see. The phenomenology is the same as for the charged current case, with the addition that F_S and F_P are zero if both neutrinos are massless, and F_T is zero on hermiticity grounds if the initial and final neutrino are the same. We are again left with $F_V^{(N)}$, $F_M^{(N)}$, and $F_A^{(N)}$, but know much less about these than in the charged current case. In the Weinberg-Salam model (see Section 5.7), $J_\alpha^{(N)} = J_\alpha^{(3)} - 2 \sin^2\theta_W J_\alpha^{em}$, and here again, as in neutrino-electron scattering, the form factors are known if the charged current and e.m. form factors are known:

$$F_V^{(N)} = \frac{1}{2} F_V^{(C)} - 2 \sin^2\theta\, F^{em}$$

$$F_A^{(N)} = \frac{1}{2} F_A^{(C)} , \text{ etc.}$$

So again there is only the single free parameter, $\sin^2\theta_W$, in principle already known from the e-ν_μ scattering experiments.

Experiments in progress at BNL [Lee et al.[17]) and Cline et al.[18])] have reported preliminary results for process (i).

7. The inclusive scattering process

As we saw in Section 6.2, the inclusive process can be written in terms of three functions of the variables Q^2 and ν, the only invariants defined at the hadron vertex. The cross-section for the reaction

$$\nu(\bar\nu) + A \to \mu^-(\mu^+) + B$$

is then:

$$\frac{d^2\sigma_{\nu(\bar\nu)}}{dQ^2 d\nu} = \frac{G^2}{2\pi M}\frac{E_\ell}{E_\nu}\left[\cos^2\frac{\theta}{2} W_2(Q^2,\nu) + 2\sin^2\frac{\theta}{2} W_1(Q^2,\nu) \mp \right.$$
$$\left. \mp \frac{E_\nu + E_\ell}{M} \sin^2\frac{\theta}{2} W_3(Q^2,\nu)\right] . \qquad (7.1)$$

7.1 Scaling

It was first suggested by Bjorken[19]) that in the limit $Q^2, \nu \to \infty$ while $x = Q^2/2\nu$ remains fixed, the structure functions should be independent of neutrino energy, but functions of x only. The scaling argument can be made on dimensional grounds as follows:

a) The basic assumption is that there are no intrinsic masses in the system above some fixed mass (perhaps the nucleon mass), and at neutrino energies very much higher, $E_\nu \gg M$, the cross-section should become independent of this mass M. If it turns out that higher mass particles are involved, such as perhaps charmed particles or intermediate bosons, then scaling should set in at correspondingly higher energies.

b) It is now useful to write Eq. (7.1) in terms of the invariants in the following form:

$$\frac{d^2\sigma_{\nu(\bar\nu)}}{dxdy} = \frac{G^2 s}{2\pi}\left[\left(1 - y - xy\frac{M^2}{s}\right)\nu W_2 + xy^2 W_1 \mp \right.$$
$$\left. \mp x(y - y^2/2)\,\nu W_3\right] . \qquad (7.2)$$

The term in M^2/s can be dropped because it is small if $E_\nu \gg M$.

In the scaling limit, $d^2\sigma/dxdy$ must be independent of M. Therefore, for dimensional reasons, in terms of the variables s, x, and y, it must have the form:

$$\frac{d^2\sigma}{dxdy} = G^2 s\, \mathcal{F}(x,y) \ , \qquad (7.3)$$

where in particular, the function $\mathcal{F}$ cannot depend on s.

c) The structure functions are functions of ν and Q^2 only, since these are the only variables entering at the hadronic vertex. In the scaling limit, since they are dimensionless they can be functions only of $Q^2/2\nu = x$. Comparing Eq. (7.2) with Eq. (7.3), we see that we can take the following as structure functions in the scaling limit:

$$F_1(x) = W_1(Q^2,\nu)$$

$$F_2(x) = \nu\, W_2(Q^2,\nu)$$

$$\text{and } F_3(x) = \nu\, W_3(Q^2,\nu) \ .$$

d) We then end up, in the scaling limit, with the expression:

$$\frac{d^2\sigma_{\nu(\bar\nu)}}{dxdy} = \frac{G^2 M E_\nu}{\pi}\left[(1-y)F_2(x) + xy^2F_1(x) \mp (y-\frac{y^2}{2})xF_3(x)\right]$$

$$G^2 M E_\nu = 1.56 \times 10^{-38}\ \text{cm}^2/\text{GeV} \ .$$

Note: $d^2\sigma/dxdy$ is a quadratic function of y.

Since the y dependence is explicit, it is possible to integrate over y:

$$\frac{d\sigma}{dx} = \frac{G^2 M E_\nu}{\pi}\left[F_2/2 + xF_1/3 \mp xF_3/3\right] . \qquad (7.5)$$

e) The chief results of this hypothesis are:

i) The cross-sections are proportional to neutrino energy; and

ii) The x-y dependence is independent of neutrino energy.

7.2 Parton model

It is assumed that hadrons are made up of constituents of different types j, each with its distribution function $f_j(\xi)$, representing the probability that the j^{th} constituent carries the fraction ξ of the momentum of the fast moving hadron.

It follows that

$$\int d\xi\, f_j(\xi) = N_j \ ,$$

the number of constituents of type j in the hadron, and

$$\sum_j \int d\xi\, \xi f_j(\xi) = 1 \ .$$

It is further assumed that the partons interact freely and independently, without interference, with point-like interactions. After the scattering, the partons rearrange themselves to form the observed hadrons. It is assumed that the inclusive cross-section, after all the final states are summed over, is just the sum of the elementary parton cross-sections.

It is now important to notice that if a parton of momentum ξp is scattered, it will result in a momentum transfer $Q^2 = \xi \cdot 2\nu$. Since x is defined to be $Q^2/2\nu$, $\xi = x$. This can be seen if one looks at the reaction in the frame in which the recoil momentum of the parton is equal and opposite to the incident momentum:

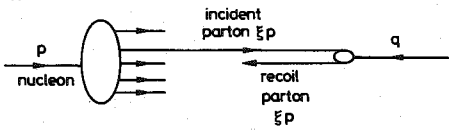

$$p = (P,0,0,P); \quad q = (0,0,0,q); \quad q = -2\xi P$$

$$Q^2 = 4\xi^2P^2; \quad \nu = p\cdot q = 2\xi P^2 \ ,$$

so that

$$x = Q^2/2\nu = \xi \ .$$

In this model, the neutrino-nucleon cross-section can be immediately written in terms of the parton cross-sections and distribution functions:

$$\frac{d^2\sigma}{dxdy} = \sum_j f_j(x)\, d\sigma_j/dy \qquad (7.6)$$

7.3 Quark parton model (QPM)

It is assumed that the partons responsible for electromagnetic and weak interactions are the spin $\frac{1}{2}$ quarks of Section 4.4. These may be bound by so-called gluons, but the gluons are assumed not to have electromagnetic or weak interactions, so that we ignore them here. The nucleons are supposed to be made of three "valence" quarks and a "sea" of quark-antiquark pairs. The valence quarks of the proton are two u and one d quarks. There are eight quark distributions for the proton: u(x), d(x), s(x), c(x), $\bar u$(x), $\bar d$(x), $\bar s$(x) and $\bar c$(x). In line with SU(4) it will be supposed that the sea antiquark distributions are the same: $\bar u(x) = \bar d(x) = \bar s(x) = \bar c(x)$. Since s(x) and c(x) occur only in the sea, $s(x) = \bar s(x)$ and $c(x) = \bar c(x)$. In line with charge symmetry, the neutron distributions are obtained from the proton distributions by the exchange of u and d. From the fact that the charge of the proton is 1, the baryon number is one, and the strangeness and charm are zero:

$$\int[u(x) - \bar u(x)]\, dx = 2; \quad \int[s(x) - \bar s(x)]\, dx = 0$$

$$\int[d(x) - \bar d(x)]\, dx = 1; \quad \int[c(x) - \bar c(x)]\, dx = 0 \ .$$

The charged current will be supposed to be the Cabibbo current, as extended by GIM to include charm, and already seen in Section 4.4. The neutral current in the GIM scheme is diagonal in the four quarks and has the Weinberg-Salam V-A structure already seen in the case of electrons:

$$J_\alpha^{(N)} = \bar u(x)\, \gamma_\alpha\left(\frac{1}{2} - 2\sin^2\theta_W - \frac{1}{2}\gamma_5\right) u(x), \text{ etc.}$$

More generally,

$$J_\alpha^{(N)} = \bar u(x)\, \gamma_\alpha(C_V + C_A\gamma_5)\, u(x), \text{ etc.}$$

7.4 Some elementary cross-sections in the quark parton model

Process	$\frac{d\sigma/dy}{G^2 M E_\nu/\pi}$
a) $\nu + d \to \mu^- + u$	$\cos^2\theta_c\ 2x$
$\bar\nu_\mu + u \to \mu^+ + d$	$\cos^2\theta_c\ 2x\ (1-y)^2$

b) $\bar{\nu}_\mu + \bar{d} \to \mu^+ + \bar{u}$ $\quad \cos^2\theta_c \; 2x$

$\nu_\mu + \bar{u} \to \mu^- + \bar{d}$ $\quad \cos^2\theta_c \; 2x \; (1-y)^2$

c) $\nu_\mu + u \to \nu_\mu + u$ $\quad \cos^2\theta_c \; 2x \left[\left(\frac{C_V^u - C_A^u}{2}\right)^2 + \left(\frac{C_V^u + C_A^u}{2}\right)^2 (1-y)^2\right]$

$\nu_\mu + d \to \nu_\mu + d$ $\quad \cos^2\theta_c \; 2x \left[\left(\frac{C_V^d - C_A^d}{2}\right)^2 + \left(\frac{C_V^d + C_A^d}{2}\right)^2 (1-y)^2\right]$

d) $\bar{\nu}_\mu + u \to \bar{\nu}_\mu + u$ $\quad \cos^2\theta_c \; 2x \left[\left(\frac{C_V^u + C_A^u}{2}\right)^2 + \left(\frac{C_V^u - C_A^u}{2}\right)^2 (1-y)^2\right]$

$\bar{\nu}_\mu + d \to \bar{\nu}_\mu + d$ $\quad \cos^2\theta_c \; 2x \left[\left(\frac{C_V^d + C_A^d}{2}\right)^2 + \left(\frac{C_V^d - C_A^d}{2}\right)^2 (1-y)^2\right]$

e) Electromagnetic current:

$\left.\begin{matrix} e + u \to e + u \\ e + \bar{u} \to e + \bar{u} \end{matrix}\right\} \; \frac{4}{9}\frac{4\pi\alpha^2 ME x}{Q^4}\left[1 + (1-y)^2\right]$

$\left.\begin{matrix} e + d \to e + d \\ e + \bar{d} \to e + \bar{d} \end{matrix}\right\} \; \frac{1}{9}\frac{4\pi\alpha^2 ME x}{Q^4}\left[1 + (1-y)^2\right]$.

7.5 Cross-sections for nuclei with equal numbers of protons and neutrons in QPM

We ignore here possible contributions from strange or charmed quarks. Then the cross-sections, on the basis of the elementary cross-sections of the last section, are:

(C)
$$\frac{d^2\sigma^-}{dxdy} = \frac{G^2 ME_\nu}{\pi}\left[q + (1-y)^2\,\bar{q}\right] \text{ (per nucleon)}$$
$$\frac{d^2\sigma^+}{dxdy} = \frac{G^2 ME_\nu}{\pi}\left[q(1-y)^2 + \bar{q}\right] \quad "$$

(N)
$$\frac{d^2\sigma^0}{dxdy} = \frac{G^2 ME_\nu}{\pi}\left[A_L + A_R(1-y)^2\right] \quad "$$
$$\frac{d^2\bar{\sigma}^0}{dxdy} = \frac{G^2 ME_\nu}{\pi}\left[A_L(1-y)^2 + A_R\right] \quad "$$

where $q(x) = x[u(x) + d(x)]$; $\bar{q}(x) = x[\bar{u}(x) + \bar{d}(x)]$

$$A_L = A^- q + A^+ \bar{q} \; ; \quad A_R = A^+ q + A^- \bar{q}$$

and

$$A^- = \left(\frac{C_V^u - C_A^u}{2}\right)^2 + \left(\frac{C_V^d - C_A^d}{2}\right)^2 \; ; \quad A^+ = \left(\frac{C_V^u + C_A^u}{2}\right)^2 + \left(\frac{C_V^d + C_A^d}{2}\right)^2$$

$$\text{(e.m.)} \; \frac{d^2\sigma^{ed}}{dxdy} = \frac{4\pi\alpha^2 ME}{Q^4}\left[1 + (1-y)^2\right]\left[\frac{5}{18}(q+\bar{q})\right]$$

7.6 Some consequences of the quark parton model

On the basis of the cross-sections of Section 7.5 and the scaling expression for neutrino cross-sections, we can make the following correspondences, for charge-symmetric nuclei, between parton distributions and structure functions, and the following sum rules:

a) $2x\,F_1 = F_2 = q + \bar{q}$ (Callan-Gross relation);

b) $F_2^{\nu,N} = \frac{18}{5} F_2^{e,d}$ (correspondence between electromagnetic and weak structure functions);

c) $-xF_3 = q - \bar{q}$;

d) $$\frac{1}{A}\left(\sigma_{\nu N} + \sigma_{\bar{\nu}N}\right) = \frac{4}{3}\frac{G^2 ME_\nu}{\pi}\int (q+\bar{q})\,dx = \frac{4}{3}\frac{G^2 ME_\nu}{\pi}\int F_2\,dx \; ;$$

e) $$\frac{1}{A}\left(\sigma_{\nu N} - \sigma_{\bar{\nu}N}\right) = \frac{2}{3}\frac{G^2 ME_\nu}{\pi}\int (q-\bar{q})\,dx = -\frac{2}{3}\frac{G^2 ME_\nu}{\pi}\int xF_3\,dx \; ;$$

f) $$\frac{1}{A}\left(3\sigma_{\bar{\nu}N} - \sigma_{\nu N}\right) = \frac{8}{3}\frac{G^2 ME_\nu}{\pi}\int \bar{q}\,dx = \frac{4}{3}\frac{G^2 ME_\nu}{\pi}\int (F_2 + xF_3)\,dx \; ;$$

g) if $R = \sigma_{\bar{\nu}N}/\sigma_{\nu N}$ and $B = \frac{\int -xF_3\,dx}{\int F_2\,dx}$, then
$$B = \frac{2\left(\sigma_{\nu N} - \sigma_{\bar{\nu}N}\right)}{\sigma_{\nu N} + \sigma_{\bar{\nu}N}} = \frac{2(1-R)}{1+R} \; ;$$

h) if $\kappa \equiv \frac{\int \bar{q}\,dx}{\int q\,dx}$, $\kappa = \frac{R - 1/3}{1 - R/3}$.

8. Inclusive neutrino scattering: Experimental results

8.1 Total charged cross-sections

8.1.1 Neutron-to-proton ratio. In the simple quark parton model (QPM),

$$\sigma_{\nu n}/\sigma_{\nu p} = \frac{\int x\,u(x)\,dx + \frac{1}{3}\int x\,\bar{d}(x)\,dx}{\int x\,d(x)\,dx + \frac{1}{3}\int x\,\bar{u}(x)\,dx} \; .$$

This is of the order of 2, if the antiquark contribution is much smaller than the quark distribution, as expected. Unfortunately, at low energies, say below ∿ 1 GeV, the model must be wrong, since the neutrino-proton reaction cannot go without emitting at least one pion.

There are three results, all using bubble chambers. The results of an experiment in the Argonne deuterium-filled chamber are shown in Fig. 31 [20]. More recently[21] the average for $E_\nu > 1.5$ GeV was reported to be 2.08 ± 0.23.

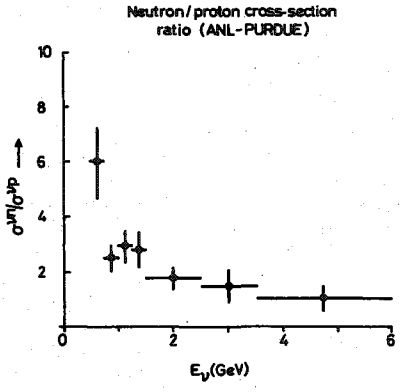

Fig. 31

From a similar experiment, performed at slightly higher energies at BNL, Samios reported[22] 1.62 ± 0.15 for E_ν ∿ 2 GeV.

The Gargamelle Collaboration has made an effort to distinguish neutron and proton reactions in freon, and has obtained the ratio 2.1 ± 0.03 [23].

All the results are in quite good agreement with QPM, but at energies where the model can hardly be expected to be valid, and in part under conditions where the identification of neutron and proton reactions is not clean. It would be most interesting to have some results from deuterium at higher energies.

8.1.2 σ_{tot} versus E_ν, $E_\nu < 10$ GeV. The total cross-section, which might seem to be easy to measure correctly, is in fact not so easy. There are the problems of absolute calibration of the neutrino flux, efficiency of the detector, the neutrino spectrum, the effect of poor energy resolution of the event coupled with a rapidly varying neutrino spectrum (as is the case for wide-band beams), and the contributions of all sorts of backgrounds.

Probably the most careful work is due to the Gargamelle Collaboration[24]. The beam and the filling are those discussed in Section 5.8.1. The results are shown in Fig. 32. In addition to the statistical errors shown, systematic uncertainties are estimated at ∿ 10-15%. Also shown in the figure are the results of ANL [20] averaged over neutrons and protons. The cross-sections are startlingly compatible with linear energy dependence, as expected if scaling is good, although it is mysterious why scaling should be good at such low energies.

The linear slopes are:

$$\sigma_{\nu N} = 0.74 \times 10^{-38} E_\nu \text{ cm}^2/\text{GeV}$$

$$\sigma_{\bar\nu N} = 0.28 \times 10^{-38} E_\nu \text{ cm}^2/\text{GeV} ,$$

and $R = \sigma_{\bar\nu}/\sigma_\nu = 0.37 \pm 0.02$; $2 < E_\nu < 14$ GeV.

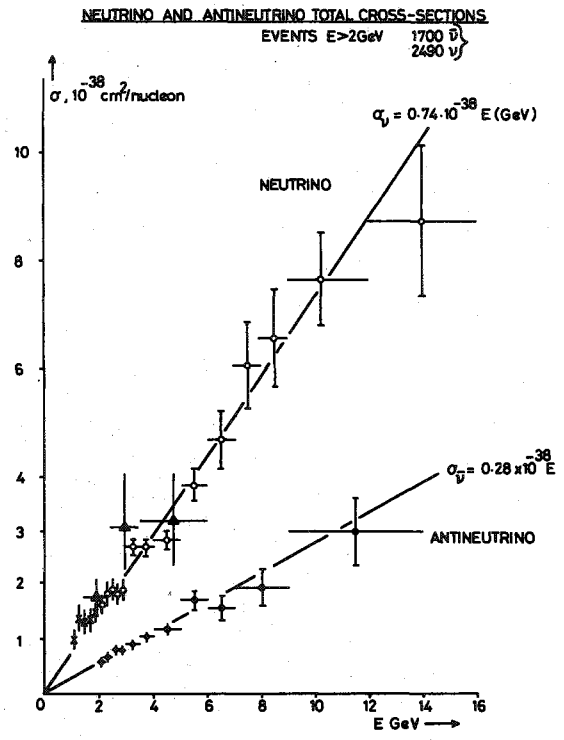

Fig. 32

Both the relative slopes R and the absolute value of the slopes of the energy dependence are of great interest. Let $A = \int 2xF_1\,dx/\int F_2\,dx$ and $B = -\int xF_3\,dx/\int F_2\,dx$.

Positivity of the cross-sections requires $B \le A \le 1$. Assuming scaling, and integrating Eq. (7.5),

$$\sigma_{\nu(\bar\nu)} = \frac{G^2 M E_\nu}{\pi} \int F_2\,dx \left[\frac{1}{2} + \frac{A}{6} \pm \frac{B}{3}\right]$$

and

$$R = (3 + A - 2B)/(3 + A + 2B) .$$

It can then be seen, from the experimental value of R and using the positivity condition, that A and B must be within the limits $0.9 \pm 0.05 \le A \le 1$; $0.9 \pm 0.05 \le B \le 0.92 \pm 0.04$. Both A and B are very close to 1, as a consequence of the fact that R is close to ⅓. The value A = 1 corresponds to the Callan-Gross relation and the QPM prediction that $F_2 = 2xF_1$. This is a huge boost to the QPM, and from here on we assume this result.

The difference between R and ⅓ then gives the relative antiquark contribution to the momentum of the nucleon. According to Section 7.6, result (h):

$$\frac{\int \bar q\,dx}{\int q\,dx} = \frac{R - 1/3}{1 - R/3} = 0.04 \pm 0.02 .$$

From the absolute values of the cross-sections, and relations (d) and (e) of Section 7.6, the absolute contribution of quarks to the nucleon momentum can also be found:

$$\int (q + \bar q)\,dx = 0.51 \pm 0.06$$

$$\int \bar q\,dx = 0.02 \pm 0.01 .$$

In other words, only about one-half of the nucleon is accounted for by the quarks. In this

model, the other half must be due to the gluons. I suppose we should not worry too much about these invisible gluons, that make up half of all matter! After all, we have not seen the quarks either. It is in any case remarkable how much one can learn on the basis of these Gargamelle total cross-sections.

8.1.3 σ_{tot} versus E_ν; $20 < E_\nu < 150$ GeV. Both of the counter experiments at FNAL have published results on σ_{tot} versus E_ν. The description of the detectors is deferred to the next sections; here the total cross-section results are briefly reported.

In the experiment of CalTech-FNAL[25] the detector is exposed to a narrow-band beam (called dichromatic). The neutrino spectrum consists of two broad peaks, as shown in Fig. 33. The beam of Fig. 33 corresponds to a hadron energy $\sim$ 25% higher than that used for the total cross-section measurements, but the spectra roughly scale. The beam was monitored in an absolute way with an uncertainty of about 10%. The total cross-section measurements suffer mainly from two problems: a) The detection efficiency for the muon is low and must be corrected by computation. This correction is large, and depends on muon angular distribution and is therefore model-dependent. b) The statistics, especially for high-energy antineutrinos, are poor.

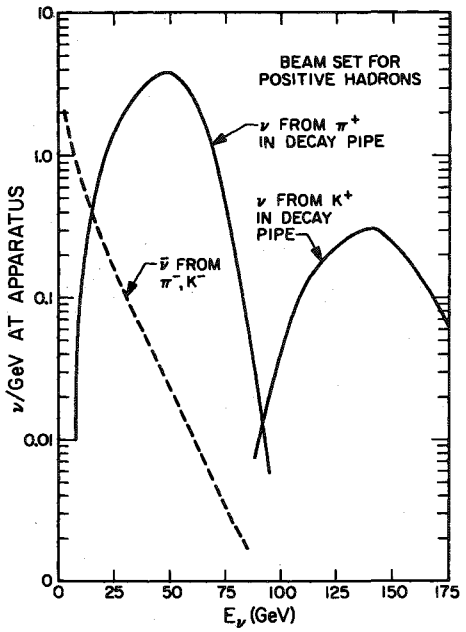

Fig. 33

The results are given in Table 2 and shown in Fig. 34, together with the low-energy Gargamelle results.

Table 2

Parent particle	Energy (GeV)	Efficiency (model-dependent)	Number of events	$\sigma \div 10^{-38}$ cm^2
π^+	38 ± 14	0.33	234	30 ± 5
K^+	107 ± 21	0.45	103	99 ± 20
π^-	38 ± 14	0.53	98	12 ± 3
K^-	102 ± 21	0.65	11	23 ± 9

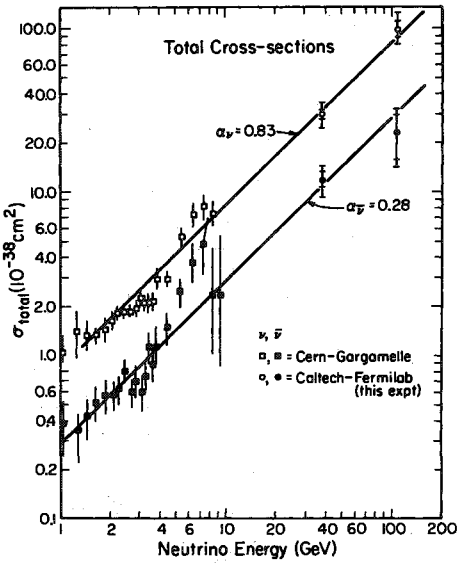

Fig. 34

The cross-sections follow very nicely the linear slopes found at the lower energies and therefore support scaling. From this experiment:

$$\sigma_\nu = 0.83 \pm 0.11 \times 10^{-38} \text{ cm}^2/\text{GeV}$$

$$\sigma_{\bar\nu} = 0.28 \pm 0.06 \times 10^{-38} \text{ cm}^2/\text{GeV}$$

$$R = \sigma_{\bar\nu}/\sigma_\nu = 0.34 \pm 0.08 \ .$$

In the HPWF (Harvard-Princeton-Wisconsin-Fermilab) experiment[26] no absolute monitor exists, and therefore only cross-section ratios are reported. Both a wide-band beam, and a quadrupole-focused beam were used at different times. In the case of the latter, positive and negative hadrons are focused with equal acceptance, and the relative production of the different particles, as well as their energy dependence, was measured in an auxiliary experiment. Neutrino and antineutrino events are distinguished by the sign of the muon charge. The energy dependence of the ratio $\sigma_{\bar\nu}/\sigma_\nu$ obtained on the basis of the observed rates and the relative production cross-section measurements are shown in Fig. 35.

A complementary evaluation of the data, which does not use the relative flux normalizations but instead assumes that the quasi-elastic and low W cross-sections are equal for neutrinos and antineutrinos, gives the results of Fig. 36. The two methods give results which are in fair agreement with each other, and, at low energy, also with Gargamelle. They indicate however a very large energy dependence of the ratio $\sigma_{\bar\nu}/\sigma_\nu$ in the energy region 40-100 GeV, which was not found by the CalTech group, and which is in clear violation of scaling. Moreover, in this energy region one might really expect scaling to be good.

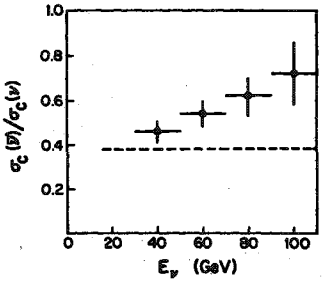

Fig. 35

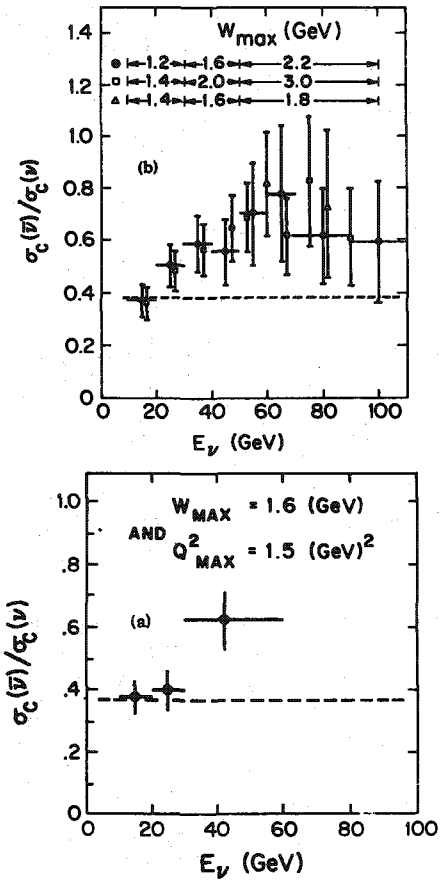

Fig. 36

8.1.4 Conclusion, σ_{tot} versus E_ν. At low energy there is beautiful confirmation of scaling from Gargamelle, which is confirmed by CalTech at higher energy, but sharply challenged by the HPWF result. Because of the importance of possible large scaling violations, it would seem essential that the high-energy experiments be repeated, especially with absolutely monitored narrow-band beams and with detectors of high efficiency.

8.2 Q^2-ν (x-y) distributions for charged currents

This is the study of the three structure functions $W_1(Q^2,\nu)$, $W_2(Q^2,\nu)$, and $W_3(Q^2,\nu)$. The results can give insight into the connection between the electromagnetic and weak hadron currents, into the question of scaling and possible scaling violations, on the validity of parton models and the distributions of partons in nucleons.

8.2.1 Gargamelle results. The main results[27] are with the chamber filled with freon, and neutrino spectra as in Fig. 24, covering the energy region $1 < E_\nu < 10$ GeV. The analysis is based on 2700 events $\nu + N \to \mu^- + X$ and 1000 events $\bar{\nu} + N \to \mu^+ + X$, with energy resolution, after corrections, of the order of ±10-15%. There are some ambiguities in the identification of muons and classification of events, but they do not seem to be serious. In the analysis, scaling [$W_1(Q^2,\nu) = F_1(x)$, etc.] and the Callan-Gross relation ($2xF_1 = F_2$) are assumed. The data are analysed separately in x and y; that is, after integration over the other variable. When the analysis is restricted to the "scaling region" used at SLAC, $Q^2 > 1$ GeV^2 and $W > 2$ GeV, only 200 ν and 29 $\bar{\nu}$ events remain.

a) x distributions. Figure 37 shows the distributions for $F_2(x) \leftrightarrow \sigma_\nu + \sigma_{\bar{\nu}}$ and $-xF_3(x) \leftrightarrow \leftrightarrow \sigma_\nu - \sigma_{\bar{\nu}}$. The data, unfortunately very sparse, are in quite good agreement with the curves (note that also the absolute normalization is given) of the quark distributions as obtained from electron deuterium scattering. In Fig. 38 all data, without scaling cuts, are plotted, but as function of $x' = x/(1 + xM^2/Q^2)$. (x' reduces to x in the scaling limit, but may be a better variable to use at very low energy.) The quark distribution $q = \frac{1}{2}(F_2 - xF_1)$ is peaked near $x = 0.15$, with an average of $x \simeq 0.3$; the antiquark distribution $\bar{q} = \frac{1}{2}(F_2 + xF_3)$ is much smaller, peaked at $x = 0$ with an average $x \sim 0.1$. The agreement with electron scattering is good, despite the fact that one is very far from the scaling limit.

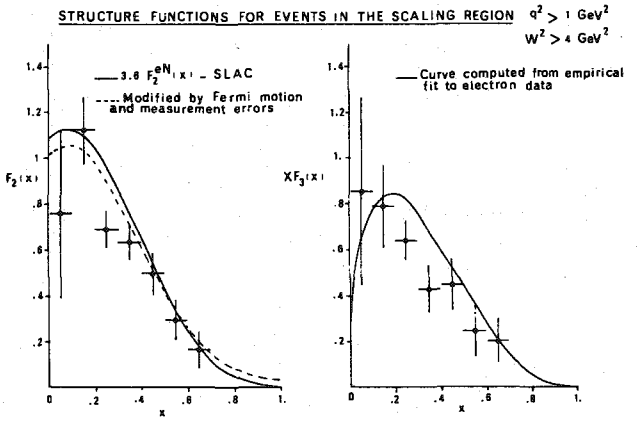

Fig. 37

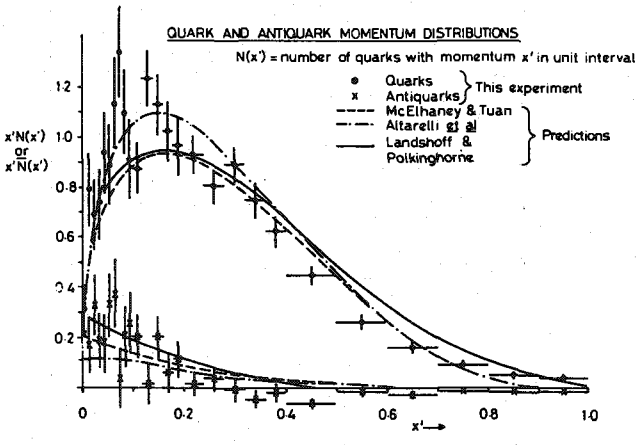

Fig. 38

b) y distributions. The y distributions with "scaling cuts" are shown in Fig. 39. The distributions without these cuts, for various energy bins, are shown in Figs. 40 and 41. For these latter the low-y region is disfigured by elastic events, but otherwise the flat y distribution dominates for neutrinos, and the $(1-y)^2$ distribution dominates for antineutrinos, just as expected in the QPM.

c) Number of valence quarks. In the QPM we expect $-\int F_3(x)\,dx = \int (u+d-\bar{u}-\bar{d})\,dx = 3$. Using the distribution functions found above, $\int F_3\,dx = 3 \pm 0.6$, for $E_\nu > 2$ GeV, in agreement with the QPM. These Gargamelle results would seem to constitute an impressive confirmation of the QPM. But, especially because of the low energies and momentum transfers typically involved, it is most important to see how they hold up at higher energy.

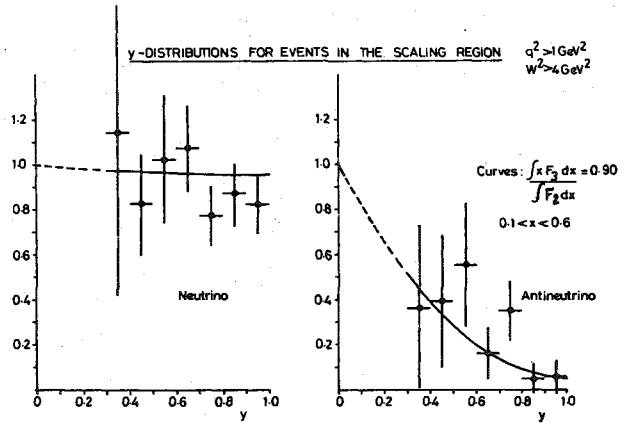

Fig. 39

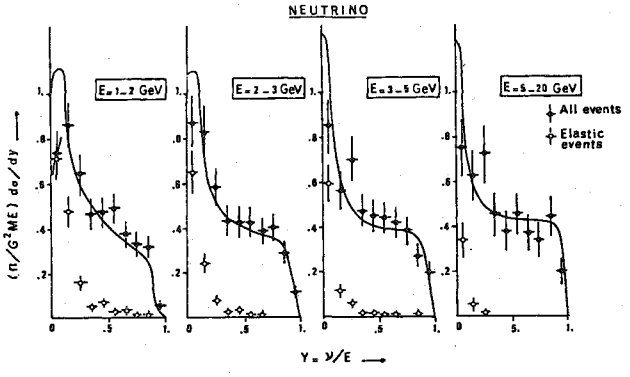

Fig. 40

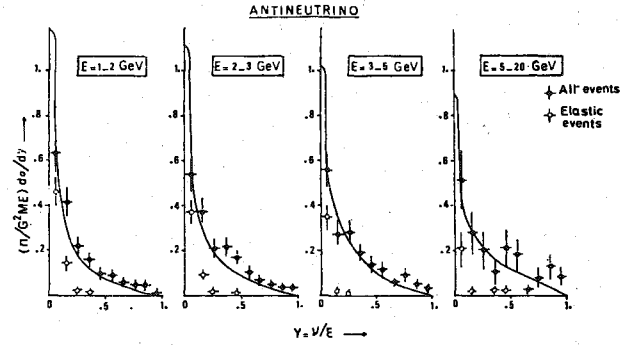

Fig. 41

8.2.2 CalTech experiment

a) Apparatus. The apparatus consists of a target-calorimeter followed by a magnet (see Fig. 42). The target consists of 70 plates of iron, each 10 cm thick, 1.5 m × 1.5 m on each side, and separated by liquid scintillators to sample the hadron shower energy. For every second plate there is also a wire spark chamber with magnetic read-out to measure the muon position (see detail, Fig. 42). The magnet is a magnetized iron toroid, outer diameter 1.5 m and 2.5 m long, with wire chambers before and after to measure the muon momentum. The total target weight is ∿ 125 tons, and the weight of a reasonable fiducial volume is ∿ 50 tons. The energy resolution for the hadron shower is $\sim 1/\sqrt{E_h(GeV)}$. The momentum resolution for muons is ∿ 20%. The neutrino beam spectrum, shown in Fig. 33, consists of two broad peaks at ∿ 50 and ∿ 140 GeV.

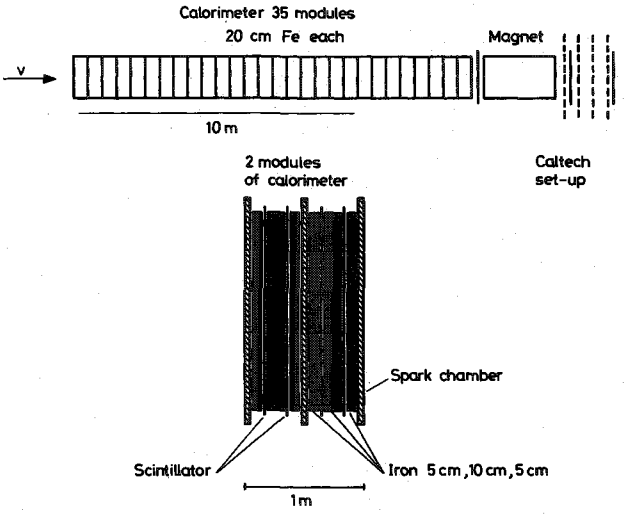

Fig. 42

The results on x-y distributions were given at the 1974 London Conference[28]). Figure 43 shows the measured energy distribution for some neutrino events, and shows the pion and kaon peaks. The chief limitation of the apparatus is the small muon acceptance at larger muon production angles (Fig. 44). This reduces the acceptance at large y to very low levels.

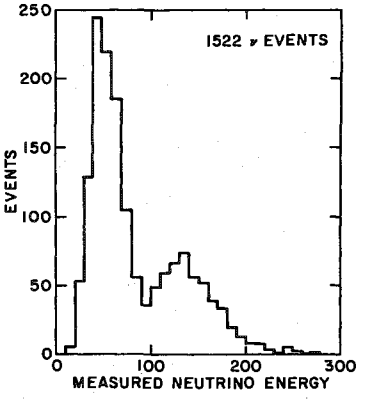

Fig. 43

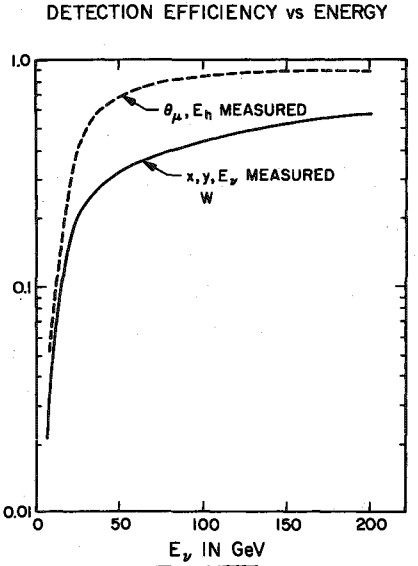

Fig. 44

The x and y distributions of ∿ 1000 ν events are shown in Figs. 45 and 46, and y distributions for various categories of ∿ 200 $\bar{\nu}$ events in Fig. 47. The rather severe distortions caused by the limited muon acceptance are everywhere apparent. But, when the acceptance is taken into account, the data are consistent with the structure functions as found in e-d scattering and at lower energies in Gargamelle, with flat y distribution for neutrinos, and $(1-y)^2$ distribution for antineutrinos. They are in agreement with scaling to these higher energies and the expectations of the QPM.

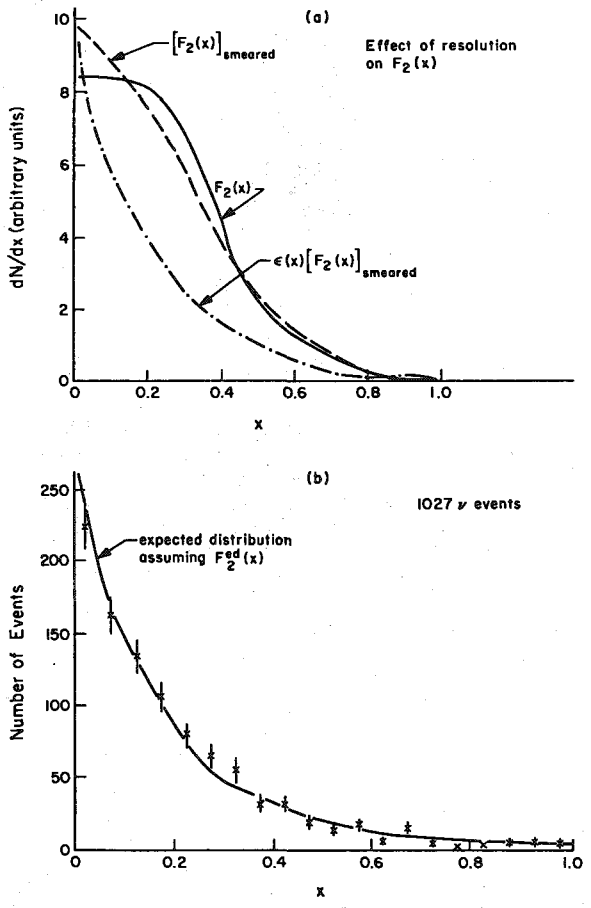

Fig. 45

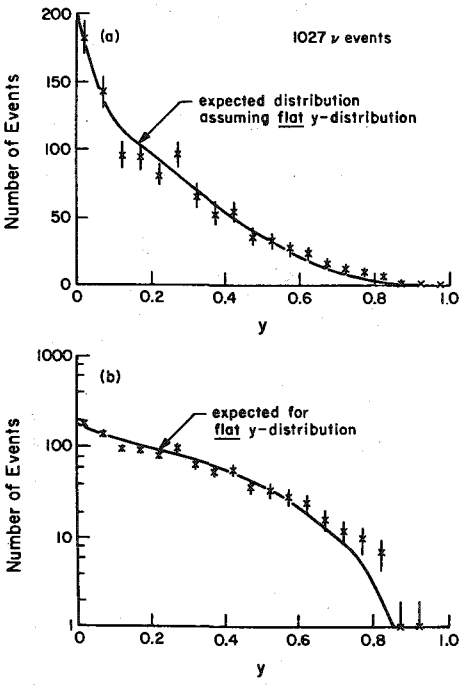

Fig. 46

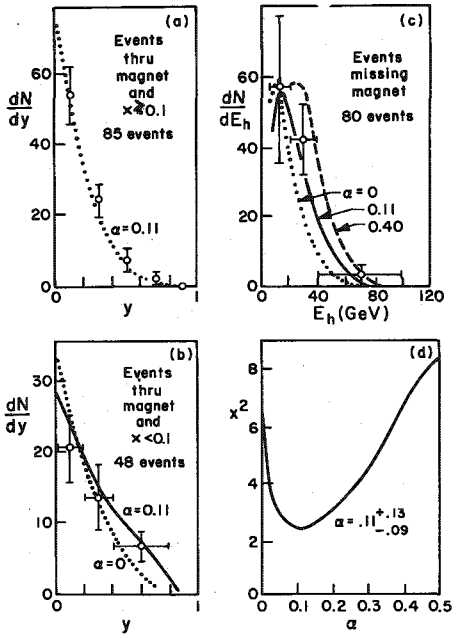

Fig. 47

8.2.3 HPWF results on x-y distributions of charged current reactions. The apparatus consists of a target-hadron calorimeter followed by a muon spectrometer, as in the previous experiment. (Fig. 48. Note that the vertical and horizontal scales are not the same.) The hadron calorimeter consists of 15 tanks of scintillating liquid (density ∿ 0.8), each 3 m × 3 m × 0.5 m. After the last tank there is a slab of iron 0.5 m thick to absorb remaining hadrons. The light output of these tanks is measured in arrays of phototubes on both sides. Between groups of tanks, wide-gap spark chambers are inserted, and give information on the positions and angles of traversing tracks. The total target weight is ∿ 60 tons and a useful fiducial weight may be ∿ 15 tons. The measured energy resolution and energy fraction detected (see Section 3.3.1) versus incident hadron energy is shown in Fig. 49.

The muon spectrometer consists of four magnetized iron toroids, each 3.6 m in diameter and 1.2 m thick, with 3 m × 3 m wide-gap spark chambers to measure the trajectories. The muon momentum resolution is ∿ 10%.

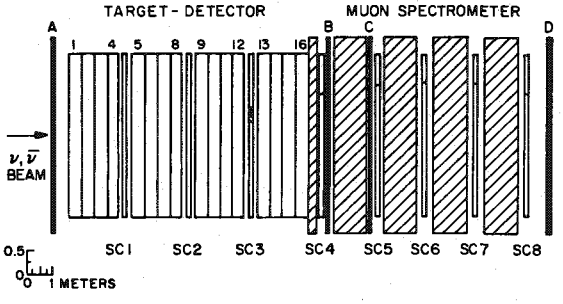

Fig. 48

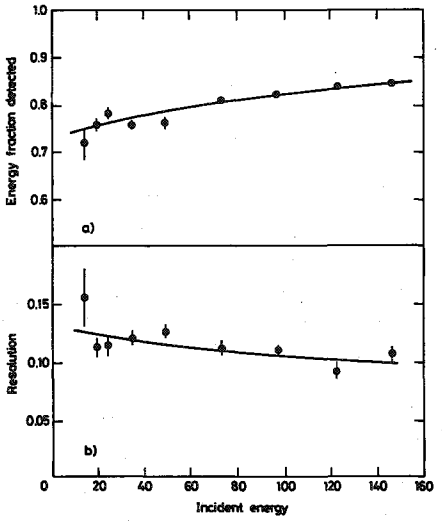

Fig. 49

The recent data are obtained chiefly with a quadrupole focused wide-band beam which contains both neutrinos and antineutrinos. Events are classified according to the sign of the muon.

Earlier results[29] on the x and y distributions are shown in Figs. 50 and 51, as they were summarized by D. Perkins at the 1975 SLAC Conference[30]. At that time all neutrino distributions, and the lower energy antineutrino distributions, were in agreement with the Gargamelle results and scaling.

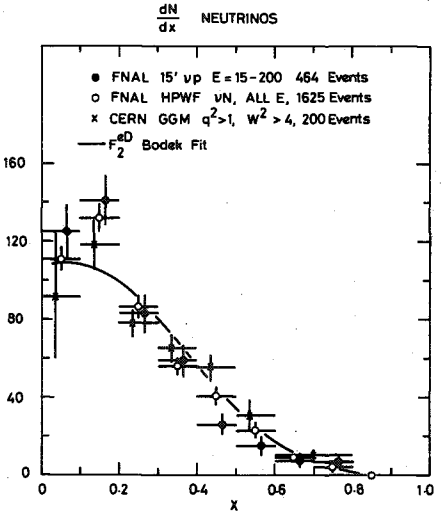

Fig. 50

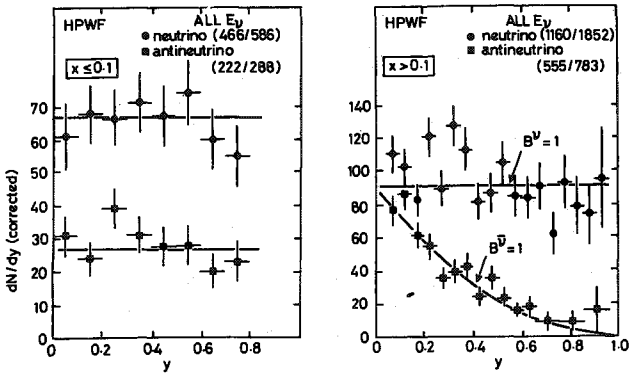

Fig. 51

However, at high-energy and small x, the antineutrino y distributions are flat, a striking deviation from scaling.

The most recent results[31] on the y distributions are shown in Figs. 52 and 53. For energies below 30 GeV, the results scale very well from the Gargamelle results, and the B parameter ($B = -\int xF_3\,dx/\int F_2\,dx$) is near to one. At high energies the antineutrino distribution becomes noticeably flatter, and corresponds to $B = 0.41 \pm 0.13$. In Figs. 54 and 55 (Ref. 31) both x and y distributions for the higher energy (E > 30 GeV) data are shown. The flattening of the y distribution is seen to be most pronounced at small x.

These results, together with the total cross-section data from the same group (Section 8.1.3), show very large deviations from scaling for antineutrinos above 30 GeV. This indicates the onset of new phenomena on a massive scale. The magnitude of these deviations seems to be too large to be attributable to charmed particle production, since the effects of charm are expected to be of the order of 5-10%.

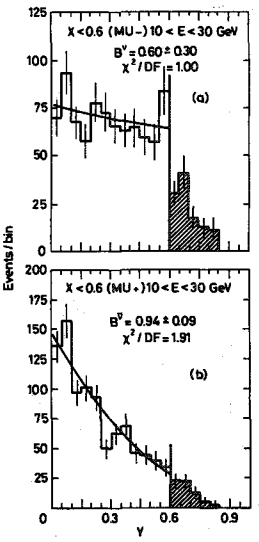

Fig. 52

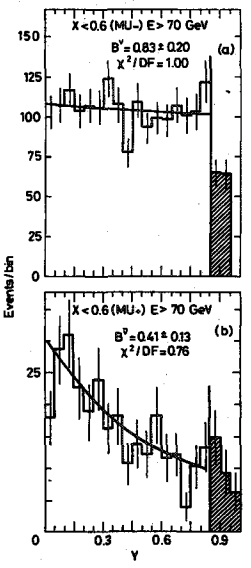

Fig. 53

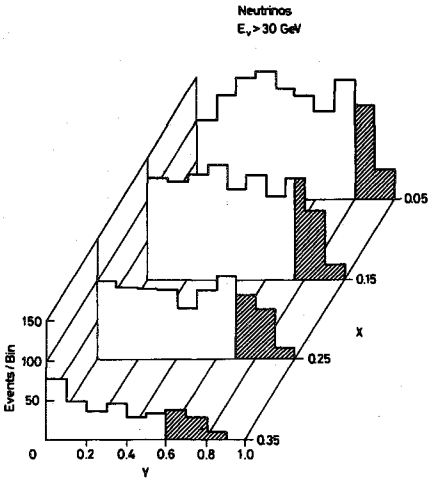

Fig. 54

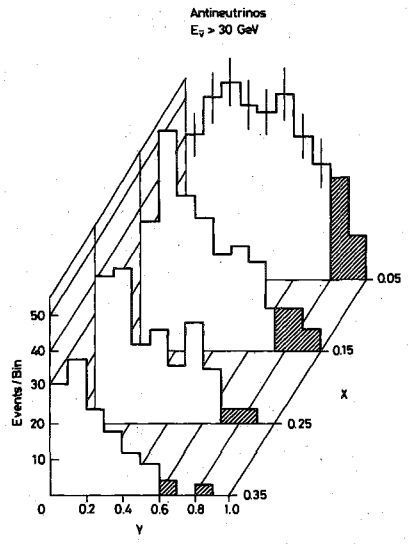

Fig. 55

8.2.4 Other experiments on the x-y distributions at higher energy. In the first studies[32,33] of ν-p and $\bar{\nu}$-p interactions in the FNAL bubble chamber, no deviation from scaling has been observed. However, the numbers of reported events are still small, and the average energies somewhat lower than those of the HPWF Collaboration. It is therefore not yet possible to speak of confirmation or disagreement.

8.3 Experimental results on neutral currents

The experimental problem is much more difficult than for charged currents:

i) Since the outgoing lepton cannot be detected, there is a much bigger problem of background from neutrons. This is the reason why neutral currents were found only recently, and only after prodding by the theorists.

ii) Since the outgoing lepton is not measured: a) in general the incident neutrino energy E_ν will not be known, unless the hadron beam is monochromatic, and then with bigger errors. In the latter case, if E_h is also known, one can at least measure the y distributions. b) Determination of x requires in addition a measurement of the direction of the hadron shower. This is not possible with present counter experiments, and only with large errors in bubble chambers. For these reasons, there are at present very few data relevant to the y distributions, and none relevant to the x distributions.

The phenomenology has recently been reviewed by Sakurai[34]. Since very little is known experimentally, there are many open questions. For instance: Are the outgoing neutrinos the same as the incoming ones? Is the neutral interaction also of the current-current type? And are the currents V,A mixtures or something else? What is the isospin character of the neutral interaction?

For the following discussion it is assumed that the neutral current is a mixture of V and A. A simple test of whether or not both are present, which is also a test of parity violation, is to compare ν and $\bar{\nu}$ cross-sections. If only V or A terms are present, these must be equal. A difference between the two shows V-A interference and parity violation.

If the neutral current forms an isotriplet with the charged current, then for a nucleus with Z = N,

$$\sigma^- = \sigma(\nu+N \to \mu^-+x) = V+A+I$$

$$\sigma^+ = \sigma(\bar{\nu}+N \to \mu^++x) = V+A-I$$

$$\sigma^0 = \sigma(\nu+N \to \nu+x) = \tfrac{1}{2}(V+A+I) = \tfrac{1}{2}\sigma^-$$

$$\bar{\sigma}^0 = \sigma(\bar{\nu}+N \to \bar{\nu}+x) = \tfrac{1}{2}(V+A-I) = \tfrac{1}{2}\sigma^+ .$$

If the neutral current is an isoscalar, $\sigma^0 = \bar{\sigma}^0$. If the neutral current is a mixture, then the isoscalar and isovector cross-sections add; there is no interference [Pais and Treiman[35]].

Two specific models may be considered: in the vector model [Sakurai[36]]

$$C_V^u = C_V^d = C_V; \quad C_A = 0; \quad \text{(see Section 7.4)} .$$

Then

$$A^- = A^+ = \tfrac{1}{2} C_V^2 \quad \text{(see Section 7.5)} ,$$

$$d\sigma/dy \propto 1 + (1-y)^2$$

and

$$\sigma_0 = \bar{\sigma}_0$$

In the Weinberg-Salam model,

$$j_\alpha^{(N)} = J_\alpha^3 - 2 \sin^2 \theta_w J_\alpha^{em} . \qquad (8.1)$$

Then

$$C_V^u = \frac{1}{2} - \frac{4}{3} \sin^2 \theta_w ; \quad C_A^u = -\frac{1}{2}$$

$$C_V^d = -\frac{1}{2} + \frac{2}{3} \sin^2 \theta_w ; \quad C_A^d = +\frac{1}{2} .$$

With the notation of Section 7.5,

$$A^- = \frac{1}{2} - \sin^2 \theta_w + \frac{5}{9} \sin^4 \theta_w$$

$$\text{and} \quad A^+ = \frac{5}{9} \sin^4 \theta_w . \qquad (8.2)$$

Here $\sigma_0 \neq \bar{\sigma}_0$. Ignoring antiquark contribution to total cross-sections,

$$R = \frac{\sigma_0}{\sigma^-} = \frac{1}{2} - \sin^2 \theta_w + \frac{20}{27} \sin^4 \theta_w ,$$

$$\bar{R} = \frac{\bar{\sigma}_0}{\sigma^+} = \frac{1}{2} - \sin^2 \theta_w + \frac{20}{9} \sin^4 \theta_w .$$

At present, quantitative results which permit an insight into the neutral current structure are virtually restricted to two quantities: σ_0 and $\bar{\sigma}_0$, or, which is better from an experimental point of view,

$$R = \frac{\sigma_0}{\sigma^-} \quad \text{and} \quad \bar{R} = \frac{\bar{\sigma}_0}{\sigma^+} .$$

In the future, we can hope soon to have reliable data on y distributions, but it will certainly be longer before also decent x distributions become available.

8.3.1 Results from Gargamelle. The most important result is, of course, the discovery of neutral currents[3]. This initial experiment also provided the result:

$$R = 0.21 \pm 0.03 \quad \text{and} \quad \bar{R} = 0.45 \pm 0.09 \ .$$

The analysis has continued and was recently reviewed by Brisson[12]. Events are selected in a fiducial volume of 3 m^3. A neutral current event (N) is defined as an event with no muon candidate. A charged current event (C) is defined as an event with one and only one muon candidate. In both cases it is required that the visible hadron energy is more than 1 GeV. The event numbers are given in Table 3.

$$\sigma^0/\sigma^- = R^{obs} = 0.27 \pm 0.04$$

$$\bar{\sigma}^0/\sigma^+ = \bar{R}^{obs} = 0.50 \pm 0.08 \ .$$

In three years the two numbers (and the two errors) have not changed a great deal, but probably the systematic problems are much better understood.

These ratios are averages over a wide neutrino spectrum, and uncorrected for the cut $E_h > 1$. This correction is model-dependent, and larger for $\bar{\nu}$ than ν. If $\phi(E_\nu)$ is the spectrum, and $d\sigma(E_\nu,y)/dy$ the theoretical cross-section, then

$$R^{obs} = \frac{\int \phi(E_\nu)\left\{\int_{y_{min}}^{1} \left[d\sigma^{(N)}(E_\nu,y)/dy\right] dy\right\} dE_\nu}{\int \phi(E_\nu)\left\{\int_{y_{min}}^{1} \left[d\sigma^{(C)}(E_\nu,y)/dy\right] dy\right\} dE_\nu}$$

$$y_{min} = E_{h,\text{cut-off}}/E_\nu = 1 \text{ GeV}/E_\nu \ .$$

The analysis is performed using (see Section 7.6)

$$d\sigma^{(C)}/dy = \frac{G^2 M E_\nu}{\pi}\left[q + \bar{q}\,(1-y)^2\right] ,$$

$$d\sigma_\nu^{(C)}/dy = \frac{G^2 M E_\nu}{\pi}\left[q\,(1-y)^2 + \bar{q}\right] ,$$

where we know, from charged current experiments (see Section 8.2.1) that $\int q\,dx = 0.49 \pm 0.06$, $\int \bar{q}\,dx = 0.02 \pm 0.01$. For the neutral currents write:

$$d\sigma_\nu^{(N)}/dy = \frac{G^2 M E_\nu}{\pi}\left[A_L + A_R(1-y)^2\right] ,$$

$$d\sigma_{\bar{\nu}}^{(N)}/dy = \frac{G^2 M E_\nu}{\pi}\left[A_L(1-y)^2 + A_R\right] ,$$

where A_L is the quark contribution from V-A terms and antiquark contribution from V+A terms, and A_R the converse (see Section 7.5). The data then give $A_L = 0.03 \pm 0.01$ and $A_R = 0.13 \pm 0.02$. Parity-conserving theories have $A_L = A_R$, so the data do not support such theories. Furthermore, on the basis of the definitions of Section 7.5 and the experimental ratio of $\bar{q}/q \sim 0.04$, it can be seen that both V-A and V+A terms must be present. This is in fact a feature of the Weinberg-Salam theory.

Table 3

No. of pictures	Type of event	Observed event numbers	Estimated neutron background	Estimated false C	Estimated neutrino contamination	Corrected event number
ν 150,000	N	183	20			163
	C	783		27		756
$\bar{\nu}$ 325,000	N	172	14		10	148
	C	242		11		251

In terms of this theory, using Eqs. (8.2),

$$A_L = a\left(\frac{1}{2} - \sin^2\theta_w + \frac{5}{9}\sin^4\theta_w\right) + \bar{a}\,\frac{5}{9}\sin^4\theta_w$$

and

$$A_R = a\,\frac{5}{9}\sin^4\theta_w + \bar{a}\left(\frac{1}{2} - \sin^2\theta_w + \frac{5}{9}\sin^4\theta_w\right) ,$$

where $a = \int q\,dx$ and $\bar{a} = \int \bar{q}\,dx$. It is important to note that both A_L and A_R are predicted in terms of one parameter only, $\sin^2\theta_w$. There is good agreement if $\sin^2\theta_w$ is taken to be 0.28 ± 0.05, as can be seen in Fig. 56. This can be considered as a test of the Weinberg-Salam model.

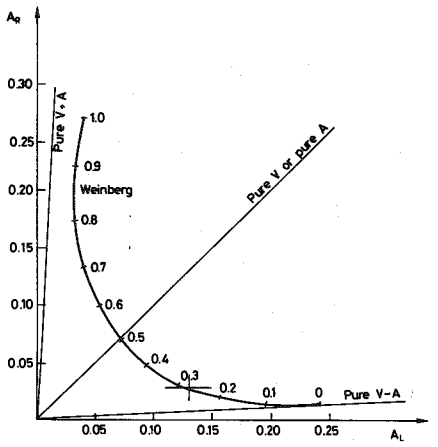

Fig. 56

8.3.2 Results of the CalTech Collaboration[37]. In this apparatus (see Section 8.2.2), neutral current events are events with no penetrating particles. For the study of neutral currents, the chief selection of events is therefore on the basis of non-penetration. In Fig. 57 the distribution depths for the most penetrating particles are shown for neutrinos and antineutrinos. The ordinate is in units of 10 cm Fe. The peaks at small penetration depth cannot be attributed to charged current events, and are presumably neutral. This constitutes an important confirmation of the Gargamelle results.

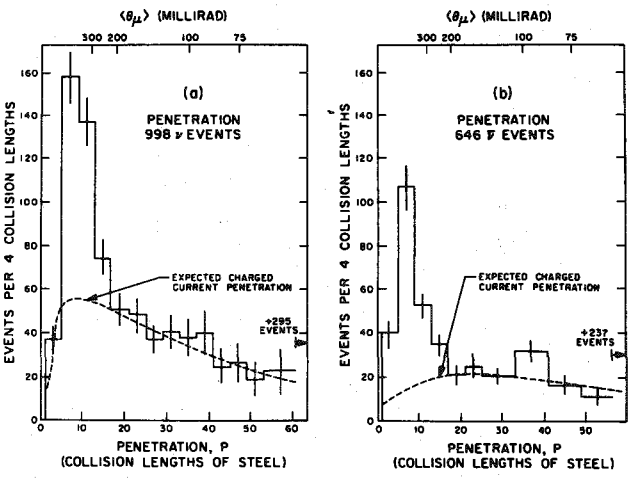

Fig. 57

The most recent analysis of the magnitude of the effect [Buchholtz[38]] gives:

$$R^{obs} = 0.24 \pm 0.02$$

$$\bar{R}^{obs} = 0.34 \pm 0.09 ,$$

and $A_R/A_L \simeq 0.5$, in reasonable agreement with the results of Gargamelle and leading to similar conclusions about V-A and V+A currents as well as parity violation.

The results may also be analysed to learn about the y dependence of the cross-sections. The basis for the analysis is the hadron energy spectrum of Fig. 58. The long penetration distributions (a) are presumably the charged current E_h distributions, the short penetration distributions (b) contain the neutral current events as well as charged background, and (c) is the short penetration distribution after some charged current subtraction. Comparison of (a) and (c) permits the conclusion that the neutral current is not dominated by a y^2 dependence, as would be expected for S or P neutral currents. The data are consistent with the y dependence expected in the Weinberg model, but the comparison is not as yet incisive.

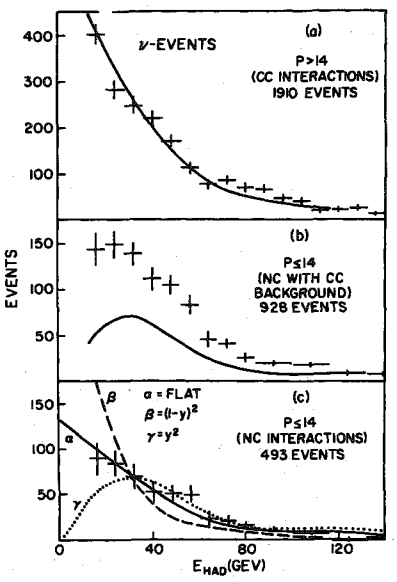

Fig. 58

8.3.3 HPWF Collaboration. This group, using the detector described in Section 8.2.3, and the wide-band beams, has confirmed the existence of neutral currents[39]. The most recent values of the cross-section ratios, reported at the Aachen Conference[40] were given as:

$$R_\nu = 0.29 \pm 0.04$$

$$E_\nu \sim 70 \text{ GeV} ,$$

$$R_{\bar{\nu}} = 0.39 \pm 0.10$$

in agreement with the lower energy results of Gargamelle.

8.3.4 Summary of the status of neutral currents.

a) They exist, and have been observed in neutrino-electron scattering, in elastic scattering on protons, and in inelastic nuclear scattering.

b) Parity is violated.

c) V-A and V+A currents exist.

d) The observations constitute a test of the Weinberg model, although the errors are still large. If the model is correct, $\sin^2 \theta_W \simeq \simeq 0.3 \pm 0.1$.

9. New particles

9.1 Intermediate bosons

The striking parallel (except for parity violation) of the vector structure of weak and electromagnetic interactions makes it natural to postulate that also the weak interactions are mediated by vector particles:

$$\mathcal{L}_C = g\bar{u}\gamma_\alpha(1-\gamma_5)\nu W^-_\alpha + g\bar{d}\gamma_\alpha(1-\gamma_5)uW^-_\alpha + \ldots + \text{h.c.} .$$

The typical reaction involves the exchange of the $W^\pm$ just as the photon is exchanged in the electromagnetic interaction, for example:

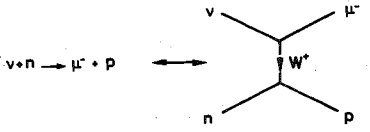

If $g^2/M_W^2 = G$, then the predicted cross-sections are the same as in the Fermi theory, except for the propagator factor $[1/(1 + Q^2/M_W^2)]^2$. The cross-sections at low energy are unaffected by this factor; at high energies they are diminished rather abruptly for $Q^2 \gtrsim M_W^2$. Experimentally this would manifest itself as a deviation from scaling at high energy in the Q^2-ν plot.

Possible propagator effects have been searched for both in the CalTech and the HPWF experiments, but have not been found. This makes it possible to give a lower bound of $\sim$ 10-15 GeV to the intermediate boson mass.

In the gauge theories of weak interactions, intermediate vector bosons are predicted, both neutral and charged. In particular, in the Weinberg-Salam model the masses of these particles are related to the electromagnetic and weak coupling constants through the "Weinberg angle" θ_W as follows:

$$M^2_{W^\pm} = \frac{e^2}{\sqrt{32}\, G \sin^2 \theta_W} = (37 \text{ GeV})^2/\sin^2 \theta_W ,$$

$$M^2_{Z^0} = \frac{4e^2}{\sqrt{32}\, G \sin^2 2\theta_W} = (73 \text{ MeV})^2/\sin^2 2\theta_W .$$

With $\sin^2 \theta_W = 0.3 \pm 0.1$ the expected masses would be:

$$M_{W^\pm} \simeq (68 \pm 40) \text{ GeV}$$

and

$$M_{Z^0} \simeq (80 \pm 25) \text{ GeV} .$$

These masses are much larger than could be observed at present accelerators, so the theorists may be safe for a while.

9.2 Dimuons and charm

Production of muon pairs in high-energy neutrino collisions was first observed by the HPWF group[41]) and confirmed by the CalTech group[42]). More recently, 61 events were reported by the HPWF group[43]) from an exposure to the quadrupole focused beam, with a neutrino-antineutrino composition of ∿ 6:1. After correction for relative detection efficiencies, the dimuon to single muon rate is 0.008 ± 0.003, roughly 1%.

Of the 61 events, 51 (the large majority) are $\mu^+\mu^-$, 7 are $\mu^-\mu^-$, and 3 are $\mu^+\mu^+$. The like-charge events are extremely interesting, but more troubled by background from π-μ decay because of their smaller number.

We concentrate then on the $\mu^+\mu^-$ events. In Fig. 59 the muon energies for each event are shown, as well as the dimuon invariant mass distribution. The hadron energy, for the 17 events, for which it is known, is written next to the triangle which represents the event.

It can be seen from Fig. 59 that:

a) the negative muons are more energetic than the positive; for the 51 events $\langle p_- \rangle / \langle p_+ \rangle = 3.7$;

b) the $\mu^+\mu^-$ mass distribution is continuous from 0 to 7 GeV.

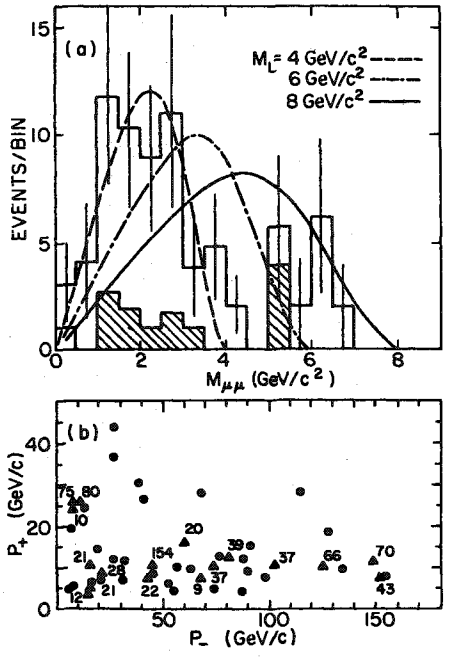

Fig. 59

The distribution in the visible energy (Fig. 60) of the 17 events for which the hadron energy is known, is not so different from normal neutrino events, and shows that if there is a threshold for this type of event, it is not very high.

Figure 61 illustrates three possible sources for dimuon production: (a) an intermediate boson, (b) an intermediate heavy neutral lepton, and (c) an intermediate new type (charmed) particle which decays weakly with emission of muon and neutrino.

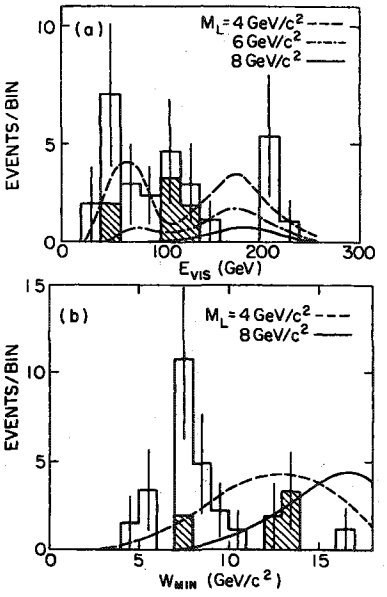

Fig. 60

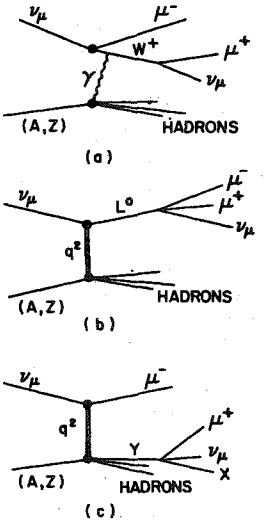

Fig. 61

The data do not fit very well with the intermediate boson hypothesis, because in this hypothesis, i) the positive muon should carry the bulk of the momentum, ii) the hadron energies would be expected to be considerably less than observed, and iii) the data on possible propagator effects indicate a lower limit of 10-15 GeV for its mass (see Section 9.1). This is inconsistent with the low observed thresholds for dimuon production.

The data are also difficult to reconcile with neutral heavy lepton production (b), because the observed momentum asymmetry is larger than can be imagined, even if the lepton were produced in a highly polarized state.

The data seem to be quite consistent with what might be expected in the GIM scheme of charm[9]), where charmed particles of masses of ∿ 2-3 GeV are

expected to be produced, some of which would be expected to decay semileptonically. The production is expected to be of the order of $\sin^2 \theta_C \simeq 0.05$ (see Section 4.2) for production on down quarks:

$$\nu + d \rightarrow C + \mu^- \quad (C \rightarrow \mu^+ + \nu + \ldots)$$

In addition, production on the sea of strange quarks proceeds with $\cos^2 \theta_C \simeq 1$, but is also expected to be of the order of 5% if the Gargamelle results on $\bar{q}/q \simeq 0.04$ are steering us straight. The sea production mechanism would have to account for the antineutrino production of dimuons. The observed production ratio for dimuon/single muon events of $\sim$ 1% is consistent with this picture if the semileptonic branching ratios for these charmed particles are of the order of 10-20%, which some theorists consider reasonable.

9.3 Charm in the bubble chamber

9.3.1 BNL event. In the 7-foot bubble chamber of BNL, filled with H_2 and exposed to a wide-band neutrino beam, a most interesting event was found[44]). The event corresponds to the reaction $\nu + p \rightarrow \mu^- + \Lambda^0 + \pi^+ + \pi^+ + \pi^+ + \pi^-$, $E_{vis} = 13.5$ GeV. The resultant momentum of the outgoing particles is in the direction of the incident neutrino, and the invariant mass is zero within experimental error, so that it can safely be assumed that there are no missing particles. It can be shown that none of the tracks of the outgoing particles are compatible with being kaons. The event would then be a case of ΔS-ΔQ violation, and would be very unexpected without charm because this rule in other instances is very good. The event is, however, quite normal if charmed baryons are produced. The invariant mass of the Λ and four pions is 2.426 ± 0.012 GeV, quite reasonable in the charm scheme. The decay into a particle of positive strangeness is also to be expected on the basis of the charmed weak current of Section 4.4. Recently, charmed baryons of mass 2.26 GeV, decaying in the mode $\bar{\Lambda} + \pi^+ + \pi^- + \pi^-$, have been clearly seen in photoproduction experiments[45]).

9.3.2 Three Gargamelle events. Three events, closely related to the dimuon events of HPWF and also to the Brookhaven event, have been observed in Gargamelle. Two of these are published[46]). These events are of the form $\nu + N \rightarrow \mu^- + e^+ + V + x$. The pictures were scanned for events of the type $\mu^- + e^+ + x$, and 19 events found, with an estimated background of 5 events, with faked e^+. Three of these events also have a V^0, with negligible corresponding background (Table 4).

Table 4

Topology	Event number	Estimated background
μ^-e^+	16	5 ± 3
$\mu^-e^+V^0$	3	0.09
μ^-e^-	23	26 ± 8 a)
$\mu^-e^-V^0$	5	2.5 ± 1
e^+	6	5 ± 2

a) This background is due to the reaction $\nu_e + N \rightarrow e^- + \pi^- + x$.

In normal neutrino events, the probability of finding a V^0 associated is 1/90. The fact that for μ^-e^+ events the association is 3/11 is strong evidence for the special nature of the events. In one case the V^0 is identified as Λ^0, for the other two cases it may be either Λ^0 or K^0. Some of the properties of the three events are given in Table 5.

Table 5

E_{vis} (GeV)	p_{μ^-}	p_{e^+}	$p_{\Lambda \text{ or } K}$	$M_{\Lambda e}$	M_{Ke}	x	y	W_{min} assoc. to muon
3.6	0.2	0.25	2.1/1.8	1.2	0.6	0.04	0.94	2.1
3.9	1.1	0.9	1.1/1.4	1.9	1.6	0.3	0.7	1.9
6.1	0.9	0.8	3.7/ -	2.0	-	0.3	0.8	2.7

The events are most simply understood as production of charmed particles, with subsequent semileptonic decay to positron, neutrino, and a strangeness +1 hadron state, consistent with the HPWF results and the BNL event.

9.3.3 μ-e strange particle events in the 15-foot H_2/Ne filled bubble chamber at FNAL[47]). In the 15-foot FNAL bubble chamber, filled with a 20% Ne/H_2 mixture, and exposed to a wide-band neutrino beam (spectrum similar to Fig. 3), 13 events had been found, up to March 1976, in a sample of $\sim$ 3000 charged current neutrino events. Some of the properties of these events are given in Table 6.

Table 6

Summary FNAL 15' Ne/H_2 + $\nu \rightarrow \mu^- + e^+ + x$ 13 ev. (as of 18/3/76)													Average
E_{vis}(GeV)	11	21	25	26	28	29	32	34	95	100	31 $\sim$ 30?	8.4	36.2
μ^- ident.		EMI	EMI	EMI		EMI	•	EMI	EMI	EMI	?	?	
E_{μ^-}	3.4	14.1	15	21.9	9.3	5	11.8	14.3	57	9.3	26.2	3.3	15.9
E_{e^+}	1.1	1.2	0.4	2.2	5.3	0.6	17.7	2	2.1	5.3	1.27	3.7	3.6
Strange particles	$K^0 \rightarrow \pi^+\pi^-$	$K^0 \rightarrow \pi^+\pi^-$	$K^0 \rightarrow \pi^+\pi^-$ Λ/K $I \rightarrow \Lambda$?	$K^0 \rightarrow \pi^+\pi^-$	$K^0 \rightarrow \pi^+\pi^-$	-	$K^0 \rightarrow \pi^+\pi^-$	$K^0 \rightarrow \pi^+\pi^-$	$K^0 \rightarrow \pi^+\pi^-$ $K^0 \rightarrow \pi^0\pi^0$	K^0 int.	K^0/Λ Λ	-	0.8 K^0_S 0.15 Λ
m_{Ke^+}	0.9	1.04		1.1	0.7		2.1	1.3		2.1	1.4		
x	0.09	0.02	0.3	0.9	0.2	0.24	0.23	0.003	0.003	0.06	0.14	0.12	0.19
y	0.7	0.33	0.4	0.2	0.6	0.8	0.63	0.6	0.4	0.9	0.15	0.6	0.56

The distribution in visible energy for the 13 events is compared to simple charged current events in Fig. 62.

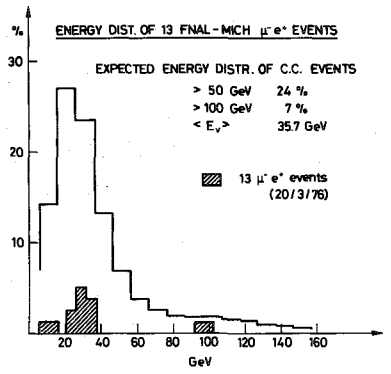

Fig. 62

The relative rate of $\mu^- e^+$ to charged current events is estimated to be 1.7%.

We can try to summarize the properties of these $\nu + N \to \mu^- + e^+ + x$ events as follows:

i) The energy dependence of the cross-sections is similar to ordinary charged current events.

ii) There is nothing striking about the x or y dependence.

iii) The invariant mass m_{Ke^+}, where it can be determined, is never more than 2.1 GeV, quite in line with the decay of particles of mass 2-3 GeV into a lepton pair and a kaon.

iv) All but two of the events have V's. Nine K^0 and one Λ^0 are definitely identified. If one corrects for undetected decay modes, the average number of K^0 and Λ^0 is $\sim$ 1.8 and 0.2, respectively. If one imagines an equal number of charged kaons, the average number of kaons per event is 3.6 -- a rather large number!

Except for the V^0 multiplicity (ten V^0 in 13 events, compared to Gargamelle's three V^0 in 11 events), the properties of these events are comparable to those of Gargamelle. There is therefore good reason, at least provisionally, to assume that this difference is due to a statistical fluctuation in small numbers, and that the true strange-particle multiplicity is somewhere in between. It would still be very high, and in the charm picture would indicate that a considerable part of the charm production is on the strange quark sea,

$$\nu + s\bar{s} \to c + \bar{s} + \mu^- \quad (c \to s + \mu^+ + e^+ + \nu),$$

because there are then typically two strange particles per event, one from the production process and one from the decay of the charmed particle.

9.4 Summary on "charm" production in neutrino reactions at high energy

Dimuon production has been observed in counter experiments, and muon-positron production in association with a large strange-particle rate has been observed in bubble chambers, with rates of the order of 1-2% relative to normal charged current interactions. Neither of these two types of events can be understood in terms of previously known processes, but both would seem to follow very naturally from the GIM model in which charmed bosons and baryons, of masses 2-3 GeV, would be produced, often in association with a strange particle, and with relative probability of 5-10%. If these decay semileptonically with branching ratios of the order of 10-20%, and usually with the emission of another strange particle, as is expected in the model, all observations can be understood. These neutrino experiments constitute the first evidence for charmed particles, and are now beautifully supplemented by the observation of narrow, strange resonances in the region 1.8-2.5 GeV at SLAC[48] and FNAL[45].

References

1) G. Danby et al., Phys. Rev. Letters 9, 36 (1962).

2) R. Davis, Jr., D.S. Harmer and K.C. Hoffman, Phys. Rev. Letters 20, 1205 (1968).

3) F.J. Hasert et al., Phys. Letters 46B, 138 (1973).

4) E.D. Commins, Weak interactions (McGraw Hill, New York, 1973).

5) L.M. Seghal, Phenomenology of neutrino reactions, Lectures given at Argonne National Laboratory, ANL Report HEP-PR-75-45 (1975).

6) A. Baroncelli, Nuclear Instrum. Methods 118, 445 (1947).

7) J. Engler et al., Nuclear Instrum. Methods 106, 189 (1973).

8) For a simple introduction, see J. Iliopoulos, CERN 76-11 (1976).

9) S.L. Glashow, J. Iliopoulos and L. Maiani, Phys. Rev. D 2, 1285 (1970).

10) F. Reines, H.S. Gurr and H.W. Sobel, Phys. Rev. Letters 37, 315 (1976).

11) S. Weinberg, Phys. Rev. D 5, 1412 (1972).
A. Salam, *in* Elementary particle theory, Proc. 8th Nobel Symposium, Aspenäsgården, 1968 (ed. N. Svartholm) (Almqvist and Wiksell, Stockholm, 1968), p. 367.

12) Gargamelle Collaboration, as reported by V. Brisson at the XIth Rencontre de Moriond, Flaine, 1976 (to be published).

13) For a very good review, see, for example, C.H. Llewellyn Smith, Phys. Reports 3C, No. 5, 261 (1972).

14) Gargamelle Neutrino Collaboration (Aachen-Brussels-CERN-Ec. Polytechnique-Orsay-UC London), Proc. Internat. Symposium on La physique du neutrino à haute énergie, Paris, 1975 (CNRS, Paris, 1975), p. 349.

15) S.J. Barish et al., Report ANL-HEP-CP-75-40 (1975).

16) A. Del Guerra et al., Daresbury preprint DL P256, February 1976.

17) W. Lee et al., Phys. Rev. Letters 37, 186 (1976).

18) D. Cline et al., Phys. Rev. Letters 37, 252 (1976).

19) J.D. Bjorken, Phys. Rev. 179, 1547 (1969).

20) S.J. Barish et al., Proc. 1975 Internat. Symposium on Lepton and Photon Interactions at High Energies, Stanford, 1975 (Univ. California, Stanford, 1975), p. 511.

21) M. Derrick, Proc. Internat. Neutrino Conf., Aachen, 1976 (to be published).

22) E.G. Cazzoli et al., Proc. Internat. Symposium on La physique du neutrino à haute énergie, Paris, 1975 (CNRS, Paris, 1975), p. 317.

23) Gargamelle Neutrino Propane Collaboration (Aachen-Brussels-CERN-Ec. Polytechnique-Orsay-Padua), Proc. Internat. Symposium on La physique du neutrino à haute énergie, Paris, 1975 (CNRS, Paris, 1975), p. 327.

24) Gargamelle Collaboration, Phys. Letters 46B, 274 (1973).
D. Perkins, Proc. 1975 Internat. Symposium on Lepton and Photon Interactions at High Energies, Stanford, 1975 (Univ. California, Stanford, 1975), p. 571.
The results quoted are from the latter.

25) B.C. Barish et al., Phys. Rev. Letters 35, 1316 (1975).

26) A. Benvenuti et al., Phys. Rev. Letters 37, 186 (1976).

27) H. Deden et al., Nuclear Phys. B85, 269 (1975).

28) F.J. Sciully, Proc. 17th Internat. Conf. on High-Energy Physics, London, 1974 (Science Research Council, Rutherford Lab., Didcot, UK, 1974), p. IV-105.

29) A. Benvenuti et al., Phys. Rev. Letters 33, 984 (1974); 34, 575 (1975); and 36, 1478 (1976).

30) D.H. Perkins, Proc. 1975 Internat. Symposium on Lepton and Photon Interactions at High Energies, Stanford, 1975 (Univ. California, Stanford, 1975), p. 571.

31) C. Rubbia, XIth Rencontre de Moriond, Flaine, 1976 (to be published).

32) J.P. Berge et al., Phys. Rev. Letters 36, 639 (1976).

33) M. Derrick et al., Phys. Rev. Letters 36, 936 (1976).

34) J.J. Sakurai, Neutral currents without gauge theory prejudice, Lectures given at DESY, 1975 (CERN TH 2099, 1975).

35) A. Pais and S.B. Treiman, Phys. Rev. D 9, 1459 (1974).

36) J.J. Sakurai, Phys. Rev. D 9, 250 (1974).

37) B.C. Barish et al., Phys. Rev. Letters 34, 538 (1975).
B.C. Barish, A review of neutrino physics at Fermilab, CALT 68-535, December 1975.

38) D. Buchholtz, Proc. Internat. Neutrino Conf., Aachen, 1976 (to be published).

39) A. Benvenuti et al., Phys. Rev. Letters 32, 800 (1974).

40) T. Ling, Proc. Internat. Neutrino Conf., Aachen, 1976 (to be published).

41) A. Benvenuti et al., Phys. Rev. Letters 34, 419 (1975).

42) B.C. Barish et al., Proc. Internat. Symposium on La physique du neutrino à haute énergie, Paris, 1975 (CNRS, Paris, 1975), p. 131.

43) A. Benvenuti et al., Phys. Rev. Letters 35, 1199 (1975) and 35, 1203 (1975).

44) E.G. Cazzoli et al., Phys. Rev. Letters 34, 1125 (1975).

45) B. Knapp et al., Observation of a narrow anti-baryon state at 2.26 GeV/c^2, submitted to Phys. Rev. Letters, Aug. 1976.

46) H. Deden et al., Phys. Letters 58B, 361 (1975).
J. Blietschau et al., Phys. Letters 60B, 207 (1976).

47) J. von Krogh et al., Phys. Rev. Letters 36, 710 (1976).

48) G. Goldhaber et al., Phys. Rev. Letters 37, 255 (1976).
I. Peruzzi et al., Phys. Rev. Letters 37, 569 (1976).

THE NEW PARTICLES

B.H.Wiik
Deutsches Elektronen Synchrotron DESY, Hamburg, Germany

The first of the new particles was discovered twice[1]. The MIT group[2] working at BNL measured the effective mass of e^+e^- pairs produced by 28 GeV/c protons incident on Be. The spectrum showed a sharp peak around 3.1 GeV/c^2 resulting from the decay of a new particle with a width less than the experimental resolution. They named this new state J. The SLAC-LBL group[3] produced the same resonance, which they named ψ, in e^+e^--annihilation and observed its decay into e^+e^-, $\mu^+\mu^-$ and hadrons. The observed width of about 2 MeV (FWHM) was consistent with the experimental resolution. The long lifetime of the J/ψ clearly demonstrated that this was not a hadron of the garden variety. Therefore a large experimental and theoretical effort was launched to search for further resonances and to understand their properties. Within a few days the J/ψ was seen both at Adone and DORIS while SPEAR observed a second long lived state[4]. This state, called ψ', was shortly afterwards confirmed at DORIS. Measurements of the total cross section[5] at SPEAR revealed a threshold region between 4 GeV and 5 GeV with a complex structure containing further new states presumably related to the J/ψ and the ψ'.

Many theories were advanced to explain the data. One particular attractive theory and so far the only one which explains all the data rather naturally, introduces a new heavy quark Q with a new quantum number respected by the strong and the electromagnetic interactions. In this picture the J/ψ , the ψ' and the other new vector mesons are bound $Q\bar{Q}$ states[6,7] and the step in the total cross section is interpreted as a threshold for the production of a new class of hadrons obtained by combining an old and a new quark. The most natural choice for Q is to identify it with the charmed[8] quark, originally proposed to achieve symmetry between leptons and quarks and later to explain the absence of strangeness changing neutral currents[9].

In the main part of these lectures I'll discuss the experimental information now available on the new particles and compare them to predictions based on the charm model. However, since most of you are presumably more familiar with hadron beam experiments I'll start out by discussing the characteristic features of e^+e^- colliding rings in some detail and then remind you of the general properties of hadrons produced in electron-positron collisions. Some examples of detectors used at electron-positron colliding rings will also be given. The subjects to be discussed are listed below:

I Electron-Positron colliding rings
II Hadron production in e^+e^- collisions
III Detectors
IV Quantum numbers of J/ψ and ψ'
V Charmonium
  1) New 1^{--} states
  2) Narrow C = +1 states
VI Anomalous lepton events
  1) Evidence for a new heavy lepton

I) Electron-positron colliding rings[10]

I.1 Why storage rings?

Why bother with an e^+e^- storage ring - why not just collide the positrons from an accelerator with the electrons bound in an atom ?

Fig. 1

Table 1 - Storage Ring versus Stationary Target

Energy (cms) GeV	Beam Energy accelerator (GeV)	storage ring (GeV)
1	10^3	0.5
10	10^5	5
100	10^7	50

Fig. 1 and Table 1 make the conclusion clear; e^+e^- collision at large cms energies can only be studied using a storage ring.

I. 2 Layout

A schematic layout of a simple e^+e^- storage ring is shown in Fig. 2

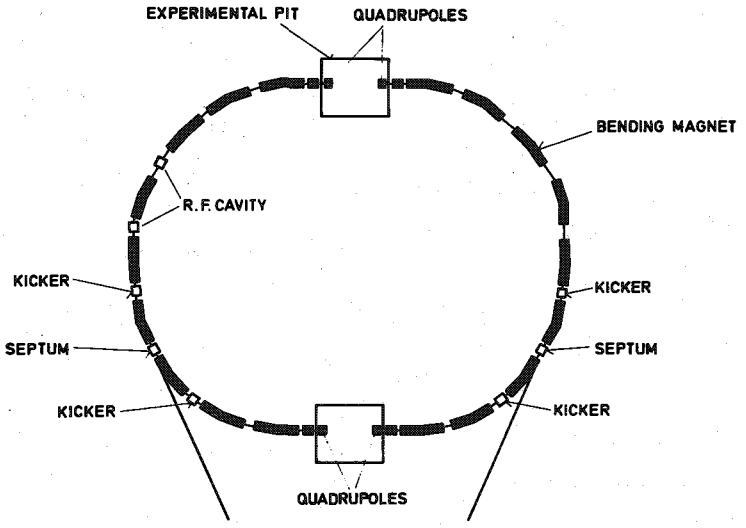

Fig. 2 - Schematic layout of the SLAC e^+e^- storage ring SPEAR

Electrons and positrons from an accelerator are injected in two bunches travelling in opposite directions in a single magnetic guide field. These bunches will cross twice during each revolution - i.e. there are two interaction regions. Strong focussing devices (in general quadrupole doublets) are mounted on each side of the interaction region. The smallest beam spot and thereby the highest luminosity is obtained when the quadrupoles are close together. Typically they are 5 m apart to leave room for the detectors.

An electron deflected in a magnetic field will emit photons. The energy loss due to this synchrotron radiation depends on the energy E of the electron L and the bending radius ρ. The energy loss per turn for a single electron U is given by;

$$U = \left(88 \frac{\text{keV}}{c^2}\right) \frac{E^4(\text{GeV})}{\rho\ (\text{m})} \qquad (1)$$

This is a substantial loss which must be replaced by passing the electrons through large r.f. cavities. As a consequence the electrons and the positrons are not spread continously along the circumference, but collected into tight bunches with a length depending mainly on the properties of the r.f. system - a typical bunch length varies between a few cm in DORIS and SPEAR to about 50 cm in ADONE.

I. 3 Luminosity and beam dimensions[10)]

The event rate N for a reaction with a cross section σ can be written as $N = L \cdot \sigma$. The luminosity L obtained by colliding two bunches containing respectively N^- electrons and N^+ positrons can be estimated from Fig. 3.

Fig. 3

A = cross section of the bunch at the interaction point

$= 4\pi\, \sigma_x^* \sigma_y^*$ assuming a Gaussian particle density with rms radii σ_x^*, σ_y^*

f = revolution frequency

B = number of bunches traveling in the same direction

$$N = \left(\frac{\text{Target particles}}{\text{cm}^2}\right) \cdot \left(\frac{\text{number of incident particles}}{\text{sec}}\right) \sigma$$

$$N = \frac{N^+}{4\pi\,\sigma_x^*\sigma_y^*} \cdot N^- \cdot B \cdot f \cdot \sigma \quad , \text{ or}$$

$$L = N^+ \cdot N^- \cdot B \cdot f \,/\, 4\pi\,\sigma_x^*\sigma_y^*$$

Expressing the luminosity L in terms of the beam currents $I^{\pm} = N^{\pm} \cdot e \cdot f \cdot B$ one obtains;

$$L = \frac{1}{4\pi e^2}\left(\frac{I^+ I^-}{\sigma_x^*\sigma_y^* \cdot f \cdot B}\right) \qquad (2)$$

It is clear that in order to maximize the luminosity and thereby the event rate one would like to store as much current as possible in a few bunches and to focus the beam to small transverse dimensions ($\sigma_x^*\sigma_y^*$ small) at the interaction point. Typical beam dimensions in the crossing point are $\sigma_x^* = 0.1$ cm (bend plane) and $\sigma_y^* = 0.01$ cm (normal to the bend plane). The stored current at low energies and a few bunches is in general limited by the beam - beam interaction. The particles in each bunch make betatron oscillations around the ideal orbit in vertical and horizontal directions as indicated in Fig. 4.

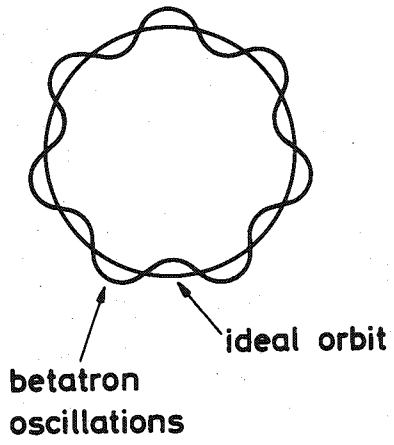

Fig. 4 - Betatron oscillations

If the betatron frequency is a integral multiple (or submultiple) of the revolution frequency then the particle always traverses the magnets in the same orbit. In this case the same small imperfection in the magnetic field will be encountered on each revolution and its effect on the beam will be amplified. In practice this will lead to a very rapid loss of the beam and one therefore selects a working point far away from such resonances. However, when the bunches cross, each bunch act as a electromagnetic lens on the other - i.e. the crossing leads to a "smearing" of the working point by an amount

$$\Delta Q_x^- = \frac{r_e\, N^+\, \beta_x^*}{\gamma \cdot 2\pi\sigma_x^*(\sigma_x^* + \sigma_y^*)} \text{ (equivalent for } \Delta Q_y) \qquad (3)$$

Here: r_e = the classical electron radius
$= 2.82 \times 10^{-13}$

$\gamma = E/m_e$

$\beta_{x,y}^*$ = the amplitude functions at the interaction point ($\sim$ 10 cm - 100 cm).

If this smearing is so large that any part of the bunch will have a betatron frequency close to an integer (or a submultiple) of the revolution frequency the bunch will be lost. In practice stable operation can be achieved for $\Delta Q_{x,y} \lesssim 0.06$.

The maximum number of electrons which can be stored per bunch is therefore given by:

$$N_{max}^+ = \frac{\gamma \cdot 2\pi\,\sigma_x^*(\sigma_x^* + \sigma_y^*) \cdot 0.06}{r_e \cdot \beta_x^*} \qquad (4)$$

Using the parameters from DORIS and SPEAR ($f \sim 10^6$/sec, $\beta^* \simeq 10$ cm, $\sigma_x \simeq .1$ cm, $\sigma_y \simeq 0.01$ cm) one finds that roughly 10 mA/bunch can be stored at 2 GeV. This corresponds to maximum luminosity on the order of a few times 10^{30}. How does the luminosity scale with energy ? Apart from constants

$$L \sim \frac{N^+ N^-}{\sigma_x^*\sigma_y^*}$$

With increasing energy $\sigma_x^*(\sigma_y^*) \sim E$ and $N^{\pm} \sim \sigma_x^*(\sigma_y^* + \sigma_y^*) \cdot \gamma \sim E^3$.

The luminosity will therefore increase with E^4 until all the available r.f. power is used to sustain the beam. The r.f. needed to compensate for losses due to the synchrotron radiation is given by $P_{r.f.} = U_{syn} \cdot (I^+ + I^-)$ neglecting cavity and other losses. The r.f. power will therefore grow proportional to E^7 until the maximum r.f. power available has been reached.

Beyond this limit the energy can only be increased by decreasing the current proportional to E^{-4} leading to a luminosity decreasing with energy as E^{-10}.

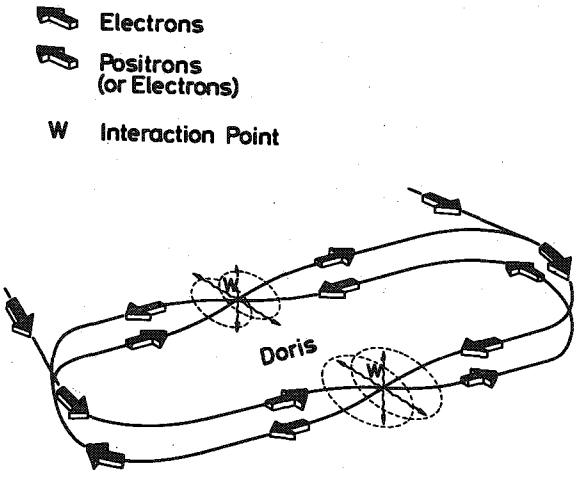

Fig. 5 - Schematic layout of the DESY storage ring DORIS

The luminosity at energies below the r.f. limit can be increased by increasing the number of bunches until the r.f. limit is reached again. A many bunch operation, however, requires a double ring structure to avoid beam crossings outside the interaction regions. DORIS, shown in Fig. 5, is made of two nearly independent rings one stacked on top of the other. The beams cross at a small angle and as many as 480 bunches can be stored in each ring. However, as can be seen from equation (2) to reach the same luminosity one needs to store higher currents, since less particles partake in each collision and also because of the finite crossing-angle which reduces the particle density. This increases the background from beam-gas interactions. (Beam-gas interactions $\sim$ current $\cdot$ residual pressure $\sim I^2$). A unique advantage of a double ring structure is the possibility to study e^-e^- and ep interactions as well as e^+e^- collisions.

A summary over past, present and future storage rings is listed in Table 2.

Table 2 - ee Storage Rings

Ring		Start of operation		Beam energy (GeV)
Princeton-Stanford	Stanford	1962	e^-e^-	0.55
ACO	Orsay	1966	e^+e^-	0.2 - 0.55
VEPP-2	Novo-sibirsk	1966	e^+e^-	0.2 - 0.55
ADONE	Frascati	1969	e^+e^-	0.7 - 1.55
BYPASS	Cambridge (USA)	1971	e^+e^-	1.5 - 3.5
SPEAR	Stanford	1972	e^+e^-	1.2 - 4.2
DORIS	Hamburg	1974	e^+e^- e^-e^-,ep	1 - 4.5
VEPP-2M	Novo-sibirsk	1975	e^+e^-	0.2 - 0.67
DCI	Orsay	1976	e^+e^-	0.5 - 1.7
PETRA	Hamburg	1979	e^+e^-	7 - 19
PEP	Stanford	1980	e^+e^-	7 - 15
Cornell	Ithaca	1980	e^+e^-	5 - 8

I. 3 Energy spread

The electrons and the positrons stored in a single bunch have an energy spread increasing quadratically with energy. The spread within the bunch is given by

$$\sigma_E(\text{MeV}) = 0.86 \frac{E^2(\text{GeV})}{\rho(\text{m})} \qquad (5)$$

The rms width of the cms energy is given by

$$\sigma_W = 1.22 \text{ MeV } (\frac{E^2(\text{GeV})}{\rho(\text{m})} \qquad (6)$$

or $\sigma_W = .1 \text{ MeV } (E/\text{GeV})^2$ at DORIS and SPEAR.

I. 4 Beam polarization

Synchrotron radiation will lead to a polarization of the electrons (positrons) with the spin parallel (antiparallel) to the magnetic guide field. The polarization P(t) builds up according to

$P(t) = 0.92(1-e^{-t/\tau})$

$$\tau^{-1} = \frac{5\sqrt{3}}{8} \cdot c \cdot (\frac{r_e^2}{\alpha}) (\frac{\gamma^5}{\rho^2 \cdot R}) \qquad (7)$$

ρ is the bending radius and R the average radius of the accelerator. Using the parameters for DORIS and SPEAR one obtains;

$$\tau(\text{hr}) = \frac{165}{E^5(\text{GeV})} \qquad (8)$$

i.e. τ = 1.5 hr at E = 3 GeV/beam. Since the average lifetime of the beam (defined as the time the luminosity drops by a factor e) is on the order of 3 to 5 hrs, studies with polarized beams at DORIS and SPEAR became practical for energies above 3 GeV/beam.

II) Hadron production in e^+e^- collisions

II. 1 Orders of magnitude[11)]

At present energies there is no evidence for a strong interaction in electron-positron collisions and furthermore the weak interaction can safely be neglected. The production of hadrons at present energies is therefore to a good approximation a purely electromagnetic process and the relevant Feynmann graphs are listed below in increasing order of α

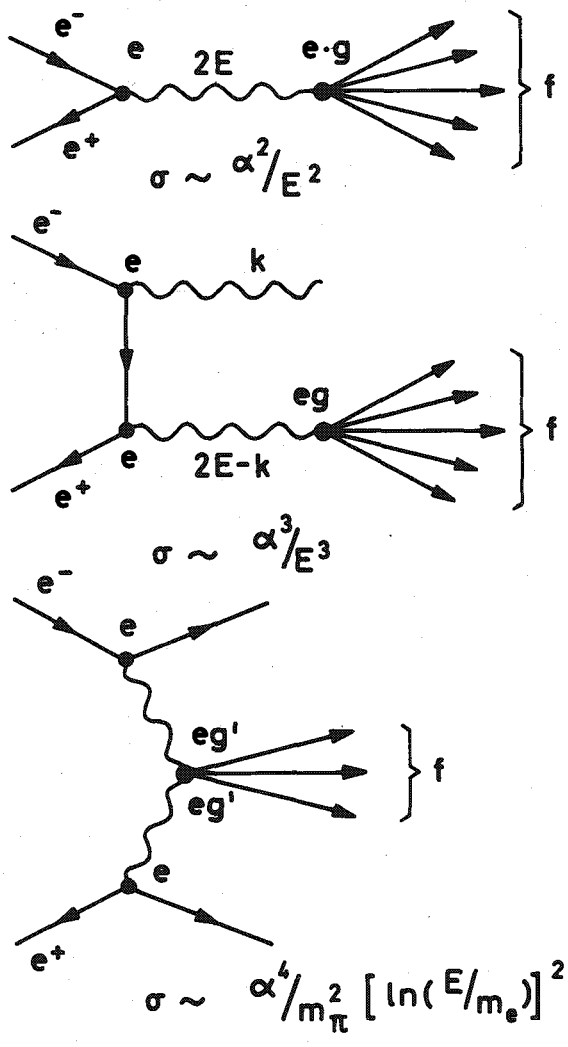

Fig. 6 - Hadron production to different order of α in e^+e^- collisions. The two first graphs involve the decay of a timelike photon into hadrons and the third graph the collision of two spacelike photons.

To lowest order in α the electron-positron pair annihilate into a timelike virtual photon of mass 2E which propagates and decays into hadrons. The cross section for this process can be estimated as $\sigma \sim \alpha^2 \cdot R^2$ in analogy to the cross section for a hadron-hadron collision ($\sigma \sim \pi^2 R^2$). The interaction radius R is inferred from the angular momentum L of the incident electron-positron system; $L = R \cdot E$. The value of L is limited to 0 or 2, since the intermediate state must have the quantum numbers of a photon $J^{PC} = 1^{--}$. The interaction radius therefore decreases with increasing energy as 1/E, leading to a total cross section for hadron production decreasing with energy as α^2/E^2. This is also the energy dependence predicted for a pointlike coupling between the virtual photon and the final state system.

Since the intermediate state has $J^P = 1^-$ the angular distribution for a single hadron with respect to the beam axis is given by:

$$\frac{d\sigma}{d\Omega} = a + b \cos^2\theta. \qquad (9)$$

The next graph which is of order α^3 does not add any new physics. Its contribution is in general included as a radiative correction to the one photon annihilation graph 6a.

However, a new class of processes is encountered in Fig. 6c. Associated with a moving electron is a cloud of nearly real photons. A real photon behaves very much like a hadron with an effective interaction strength of α. The cross section can therefore be written as

$$\sigma \sim \alpha^2 \cdot R^2 \cdot N_\gamma^2$$

R = range of the strong interaction $\sim 1/m_\pi$

N_γ = number of quasi real photons/electron $\sim \alpha \cdot \ln(E/m_e)$

This leads to $\sigma \sim \frac{\alpha^4}{m_\pi^2} \cdot \left[\ln(E/m_e)\right]^2$ for hadron production via the two photon graphs. Unlike the one photon process the two photon process has a cross section increasing with energy and it produces final state hadrons strongly peaked at small angles.

Detailed computations and measurements show that the two photon contribution can be neglected because of the low energies presently available and also because the detectors do not cover angles close to the beam axis. We will therefore only consider hadron production via the one photon graph in Fig. 6a.

II. 2 One photon annihilation

In the one photon annihilation graph everything is known except the coupling of a timelike photon to hadrons. This coupling is estimated below using two different models.

In the first model indicated in Fig. 7 the photon

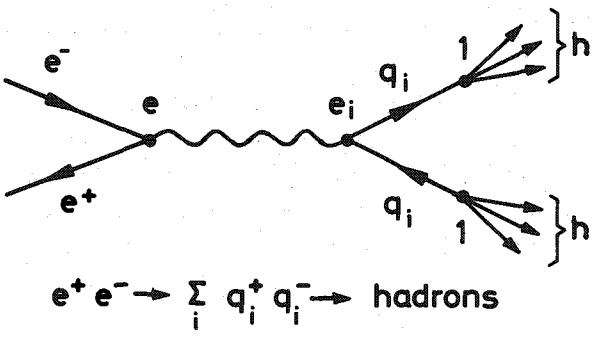

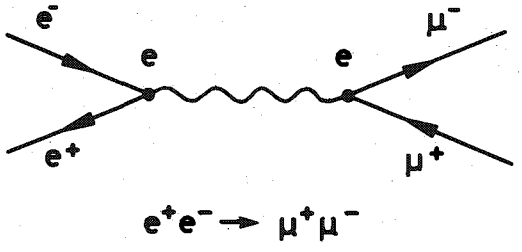

Fig. 7 - Pairproduction and decay of pointlike particles (partons) compared to muon pairproduction

couples directly to a pair of pointlike partons with charge q_i. The partons transform by some unspecified mechanism into hadrons with limited transverse momenta around the direction of the parton. They will therefore show up in the laboratory as jets of hadrons produced back to back. This graph is completely anagolous to the graph describing muon pair production. That is:

$$\sigma(e^+e^- \to \text{hadrons}) = R \cdot \sigma(e^+e^- \to \mu^+\mu^-) = R \cdot \frac{4\pi\alpha^2}{3} \cdot 1/s \quad (10)$$

The angular distribution of the jet axis is $1 + \cos^2\theta$. R can be estimated by summing over the charges of all the partons participating

$$R = \frac{1}{e^2} \left(\sum_i e_i^2 + \frac{1}{4} \sum e_i^2 \right) \quad (11)$$

The first term is the sum over all partons with spin 1/2, the second term is the sum over all partons with spin 0.

To evaluate R one needs to make assumptions about the charge and the number of the fundamental constituents participating. Identifying the partons with the u, d and s quarks we obtain

$$R = \left((2/3)^2 + (1/3)^2 + (1/3)^2 \right) = 2/3$$

Since one believes that all quarks come in 3 colors:

$$R = 3 \cdot 2/3 = 2$$

A new quark with a charge 2/3e will lead to a step in the cross section $\Delta R = 3(2/3)^2 = 4/3$. This step will begin at the threshold for the production of a new class of hadrons which is made by combining old and new quarks.

The photon can also couple directly to a vector meson ($J^{PC} = 1^{--}$) which propagates and decays into hadrons. This process is depicted in Fig. 8.

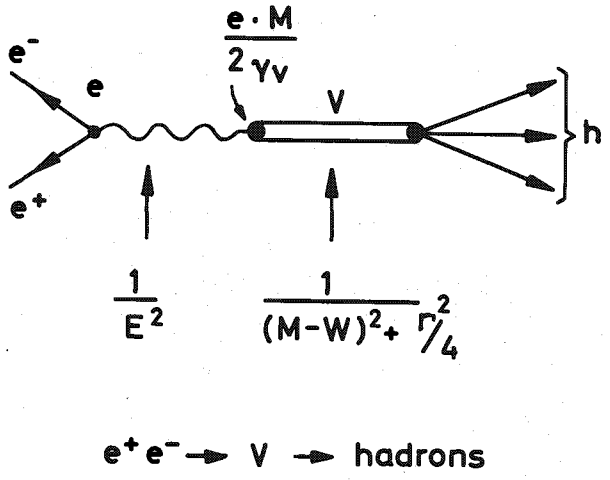

Fig. 8 - Production and decay of a vectormeson V of mass M

It leads to a cross section

$$\sigma = \frac{3}{W^2} \left(\frac{\Gamma_e \cdot \Gamma_h}{(M-W)^2 + \Gamma^2/4} \right) \quad (12)$$

Here W is the total energy in cms, M the mass of the vector meson, Γ the total width and Γ_e the width for the decay into e^+e^-. Defining the direct coup-

ling between the photon and the vector meson by $\frac{eM^2}{2\gamma_v}$ one finds

$$\Gamma_e = \frac{\pi \alpha^2}{3} \cdot \frac{M}{\gamma_v^2} \qquad (13)$$

This process will lead to a typical Breit-Wigner resonance centered at the mass of the vector meson.

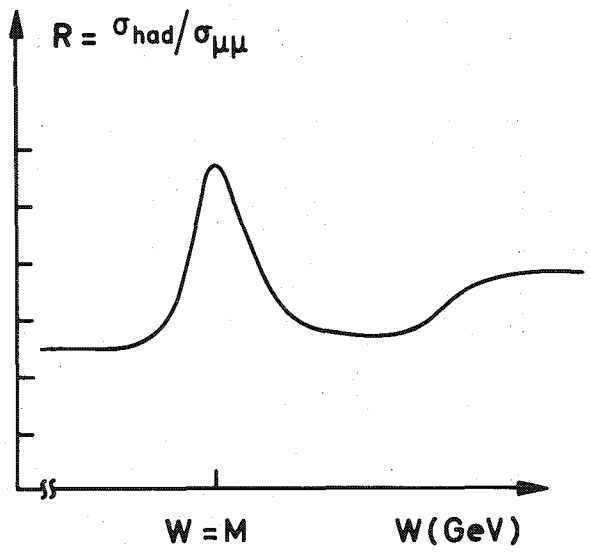

Fig. 9 - Schematic sketch of the total cross section in units of the point cross section, as a function of energy

We therefore expect to observe resonances, corresponding to the direct production of vector mesons, superimposed on a smoothly decreasing cross section from the process discussed above.

III. Detectors

The layouts of present e^+e^- experiments are strongly influenced by the low event rates and the slow variation with angle. A typical cross section is the point cross section $\sigma(e^+e^- \to \mu^+\mu^-) = 88$ nb / s (GeV^2). At s = 4 (GeV^2) and a luminosity of 10^{30} cm^{-2}sec^{-1}, this corresponds to one event per 3 minutes. Hadrons are produced with a rate a few times larger.

Such a low event rate makes it desirable to cover a large solid angle and to use loose enough trigger requirements that all genuine e^+e^- events are accepted. The trigger requirements must, however, be tight enough to avoid flooding the data acquisition system with events from beam-gas and cosmic ray interactions. The slow variation of the cross section with production angle makes it unnecessary to cover angles close to the beam line where the background and the contribution from two photon interaction will peak. So far, the detectors used can be grouped into three classes.

III. 1 Nonmagnetic detectors

These detectors in general subtend a large solid angle, and measure the direction and in some cases the energy of charged and neutral particles. They can separate the observed particles into electrons, photons, muons and hadrons and are well suited for measurements of the total cross section and for investigations of final states with low multiplicities. Reactions producing less than four particles in the final state can be reconstructed from a measurement of the particle directions and the known cms energy. For this reason such detectors are most useful at low energies; indeed the first e^+e^- rings were all equipped with detectors of this type. As an example we will discuss the set up used by the DESY-Heidelberg group at DORIS.

III. 2 The DESY-Heidelberg detector

The DESY-Heidelberg detector is shown in Fig. 10.

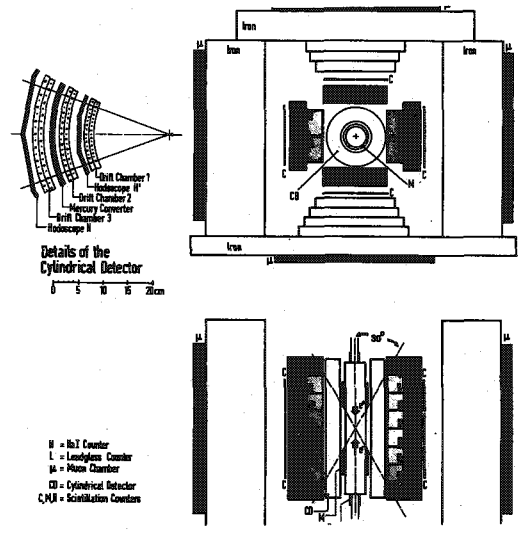

Fig. 10 - The layout of the DESY-Heidelberg detector viewed along the beam direction (top) and from above (bottom)

It consists of a cylindrical inner part made of drift chambers, two rings of scintillation counter hodoscopes and a removable photon converter. This part covers 86% of 4π and measures the direction of charged particles and the conversion points of photons. Very forward and backward angles ($15^\circ < \theta < 30^\circ$, $150^\circ < \theta < 165^\circ$) are covered by scintillation counters - i.e. charged particles are detected in 95% of 4π. Surrounding the cylindrical detector is an arrangement of NaI and lead glass counters covering 60% of 4π. These counters are used to measure the energy of electrons and photons. The energy resolution (FWHM) is 11% at 1 GeV for the NaI and lead glass combination and 30% for the lead glass alone.

The hadron absorber consists of 60 cm thick iron plates. Muons with momenta above 1.0 GeV/c penetrate the iron shield and are registered in drift chambers mounted in the rear which cover 45% of 4π. The detector is triggered on charged and neutral tracks.

III. 3 Magnetic solenoids

These detectors cover a large solid angle with a rather homogenous magnetic field. The field is oriented either parallel (MARK I at SPEAR, PLUTO at DORIS) or normal (MEA at ADONE) to the beam direction. The first generation of such detectors were mainly instrumented to measure the momenta and directions of charged particles. However, they can also identify photons, electrons, muons and hadrons. In some cases pions, kaons and protons can be identified at low momenta by time of flight. Further detectors of this type will incorporate Cerenkov counters to extend the hadron identification to higher energies and segmented shower counters to measure the direction and energy of the photons. As an example we will discuss the MARK I detector at SPEAR.

III. 4 MARK I

An exploded view of the MARK I detector is shown in Fig. 11. The coil is 3.56 m long with a diameter of 3.2 m producing a magnetic field of 4 kgauss parallel to the beam axis. A particle emerging from the interaction point first traverses a thin beam tube, one of two scintillation counters surrounding the beam pipe, a pair of cylindrical proportional wire chambers, a set of four cylindrical multiwire spark chambers one of 48 scintillation counters, the aluminium coil (about 7.5 cm thick) and one

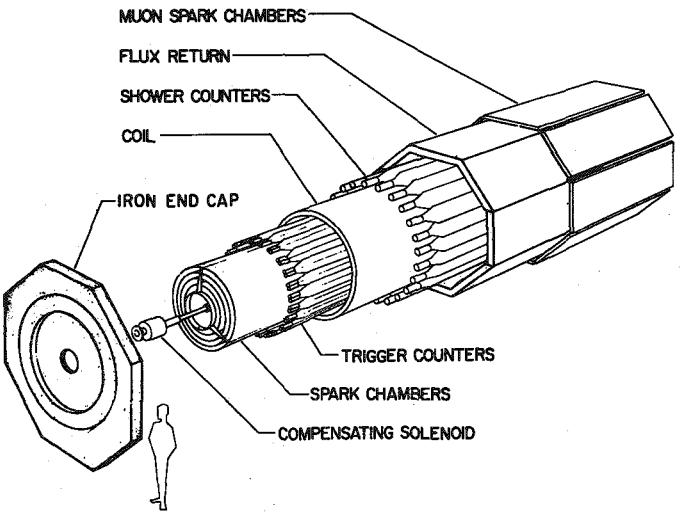

Fig. 11 - Exploded view of SLAC-LBL detector at SPEAR. The scintillation counters mounted adjacent to the beam pipe and the cylindrical drift chambers are not shown

of 24 shower counters, mounted between the iron yoke for the return flux and the coil. The detector subtends 65% of 4π. The momentum resolution (rms) for charged tracks is $\Delta p/p = 0.015$. The iron yoke (20 cm thick) serves as a hadron filter and is followed by a set of spark chambers for muon identification. The muon identification is improved over a small fraction of the solid angle by mounting slabs of concrete interleaved with spark chambers above the detector. Muons with momenta above 900 MeV/c can be identified using this system.

Electrons are identified by the pulseheight in the shower counters. Pions, kaons and protons are separated by a measurement of the time of flight between the two first layers of scintillation counters. A separation can be made for momenta less than 0.7 GeV/c (πK) and 1.2 GeV/c (Kp).

The apparatus is triggered by two or more charged particles with transverse momenta greater than 200 MeV/c.

III. 5 Magnetic spectrometers

This type of detector consists in general of one or two magnetic spectrometer arms covering a limited

solid angle in conjunction with a non magnetic detector surrounding the interaction point and covering a large solid angle. The spectrometer arms measure the particle momenta with high precision and identify the particles using the information from Cerenkov counters, shower counters, and range counters in addition to a measurement of the time of flight. The vertex detector can either be a single set of tracking chambers or a rather complex non magnetic detector as discussed above. We will discuss the DASP detector as a prototype of such a device.

III. 6 DASP

A layout of the DASP detector is shown in Fig. 12. Two large H-magnets are positioned symmetric with respect to the interaction point and spaced 2.1 m apart. The geometric acceptance of each magnet is from 48° to 132° in production angle and $\pm 9^{\circ}$ in azimuth resulting in a solid angle of 2 x 0.45 sterad for both magnets. The acceptance for a charged particle is smaller than this and depends on the momentum, the field strength and last detector plane required. The maximum field strength is 1.1 Tesla, the integrated field length 1.8 Tm.

A charged particle emerging from the interaction point traverses the following detectors before reaching the magnet gap: a scintillation counter adjacent to the beam pipe, a second scintillation counter which starts the time of flight measurement, two proportional chambers, a threshold gas Cerenkov counter, a third scintillation counter and a wire spark chamber with magnetostrictive readout. The momentum of a charged particle is determined from the measurement of one space point on the trajectory in front of the magnet and the knowledge of the trajectory of the particle behind the magnet. The trajectory behind the magnet is measured by 6 wire spark chambers. At the present a resolution of $\pm$ 0.8% is reached for a particle with 1.0 GeV/c momentum.

Particles are identified by the information from the time of flight system, the threshold Cerenkov counter, the shower counter and the range counter. It is feasible to separate pions and kaons for momenta less than 3 GeV/c, by time of flight alone. Using the present Cerenkov counter, pions can be separated from kaons for momenta above 2.4 GeV/c.

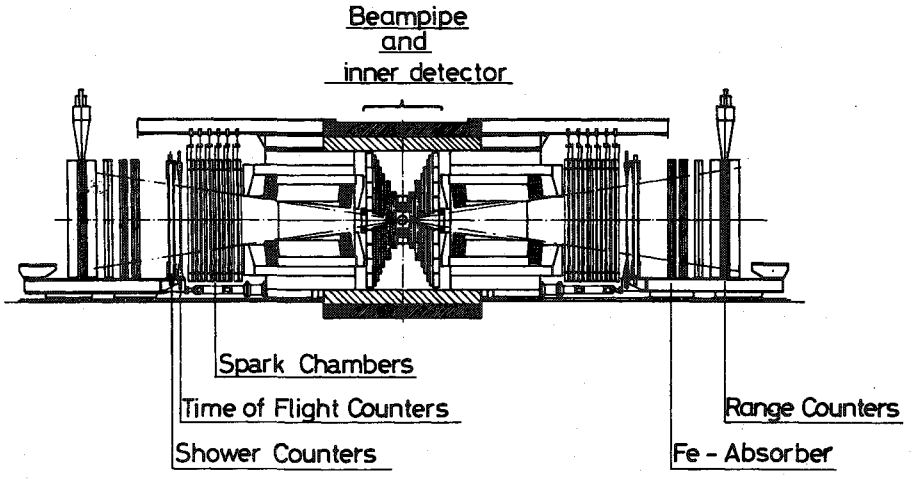

Fig. 12 - The DASP detector viewed along the beam direction

Hadrons and muons are separated from electrons by the pulseheight in the shower counter and the information from the gas Cerenkov counter. The muons are positively identified by their range. The absorbers in the range telescope are made of iron a total of 90 cm thick, subdivided into plates of different thickness in order to allow for an optimal pion/muon separation at a chosen momentum. After each plate sufficient space for either a scintillation counter hodoscope or a spark chamber is provided.

The inner detector shown in Fig. 13 covers 70% of 4π and is located in the free space between the magnets.

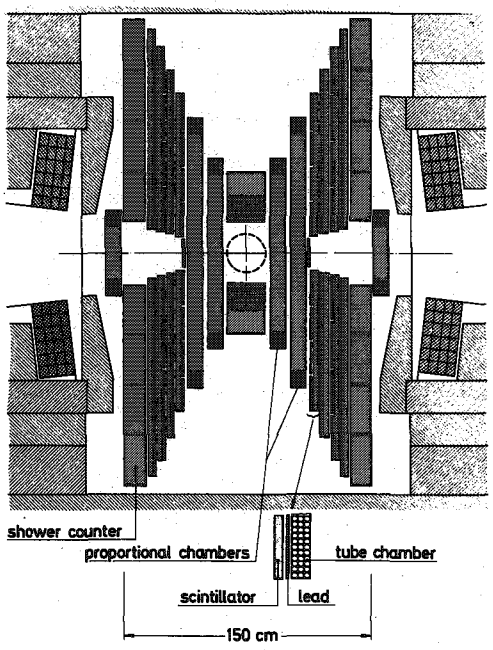

Fig. 13 - The DASP innerdetector viewed along the beam direction

The basic unit is a scintillation counter hodoscope, a sheet of lead 5 mm thick and a proportional tube chamber. The tube chambers consist of three (two) signal planes and measure the position to $\pm$ 5 mm ($\pm$ 7.5 mm). A particle emitted in the direction of the inner detector first traverses one of the 22 scintillation counters surrounding the beam pipe, the proportional chambers (in a part of the azimuthal acceptance), then four of the units just described, and finally a lead-scintillator shower counter. The energy resolution (rms) for photons is around 13% for an incident photon of 1 GeV. The detector has a 50% efficiency for detecting a 50 MeV photon travveling towards the detector. This efficiency increases to close to 100% for photons above 200 MeV. The detector can either be triggered by a single charged particle traversing one of the magnetic arms of the spectrometer, or by a combination of charged and neutral tracks in the inner detector.

IV Quantum numbers of J/ψ and ψ'

The total cross section for $e^+e^- \to$ hadrons normalized to the point cross section is plotted in Fig. 14 as a function of energy. Data at high energies are from SPEAR, at low energies from ADONE, ACO and VEPP2. The cross section at low energies is dominated by the production of the known vector mesons ρ, ω and ϕ. No firm conclusion can be drawn from the data at medium energies. However, R is clearly consistent with a constant value of 2.5 for cms energies between 2 and 3.5 GeV. Remember that the standard 3 quark-model with color predicts R = 2. Superimposed on the smooth cross section there are two peaks, the J/ψ and the ψ'. R shows a comlex structure between 4 and 5 GeV, apparently setting down to a value around 5 at higher energies.

The J/ψ and the ψ' resonances can be explained as a bound $Q\bar{Q}$ state of a new quark Q. The complex structure is caused by pair production of new hadrons consisting of an old and a new quark. However, a new quark with charge 2/3 e would lead to a step of 4/3 in R. Neglecting the estimated systematic errors of 15% in the SLAC experiment, this leaves about 1 unit of R unacounted for. A possible explantion might be the production of a pair of new heavy leptons to be discussed later. If the $Q\bar{Q}$ interpretation is correct then the J/ψ and the ψ' must be vector mesons - i.e. $J^{PC} = 1^{--}$ and the width for the decay into lepton pairs must be on the order of a few keV. The resonances must also have isospin 0, i.e. odd G-parity and be an SU(3) scalar. The determination of the widths and the quantum numbers of the J/ψ and the ψ' will be discussed next.

IV. 1 Leptonic and hadronic widths

Data from SPEAR on the production[12] and the decay of the J/ψ and the ψ' into e^+e^-, $\mu^+\mu^-$ and hadrons are shown in Fig. 15 and 16.

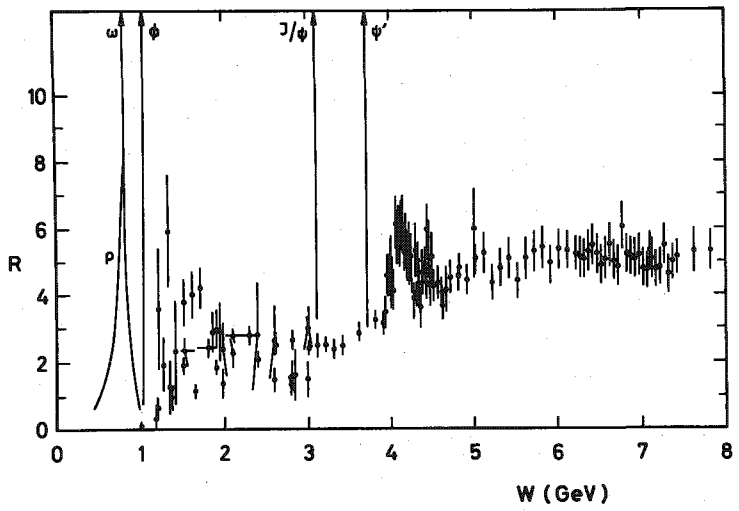

Fig. 14 - The total cross section for e^+e^- → hadrons as of June 1975

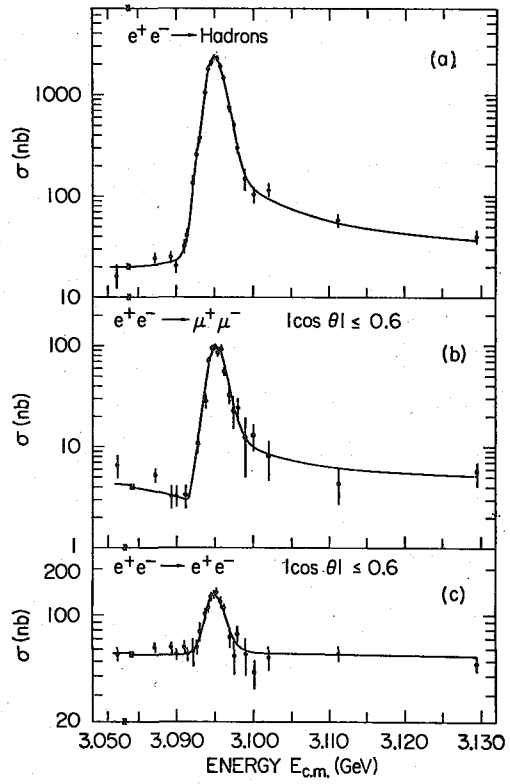

Fig. 15 - The cross section for a) e^+e^- → hadrons, b) e^+e^- → $\mu^+\mu^-$, c) e^+e^- → e^+e^- measured by the SLAC-LBL collaboration for cms energies between 3.05 GeV and 3.13 GeV

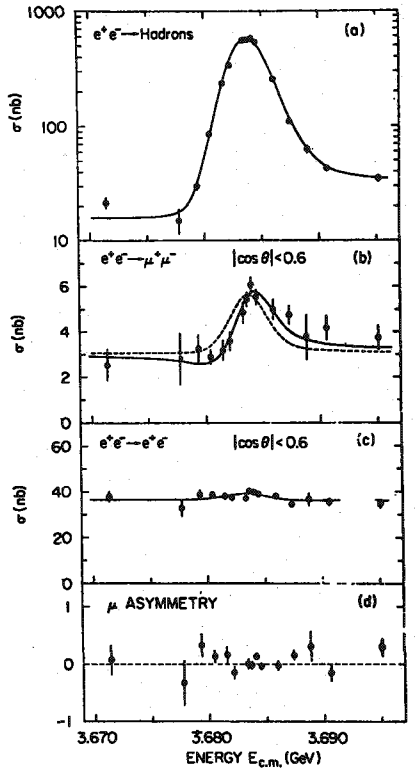

Fig. 16 - The cross section for a) e^+e^- → hadrons, b) e^+e^- → $\mu^+\mu^-$, c) e^+e^- → e^+e^- measured by the SLAC-LBL collaboration for cms energies between 3.67 and 3.695 GeV

Note that the peaks are not symmetric but exhibit a sharp rise and a long tail extending to higher energies. The long high energy tail results from beam particles which lose exactly enough energy via bremsstrahlung to come down to the resonance energy. Radiative effects[13] are also very important at the resonance proper. If the initial electron or positron radiates a photon of energy large compared to the width of the resonance, then the e^+e^- pair will not contribute to resonance production but will be counted in the luminosity. The effective luminosity is therefore smaller than the measured. This leads to a correction on the order of 40% for the J/ψ resonance.

The width of the peaks does not reflect the total width of the resonance, but rather the energy-spread of the beams (Eq. 6). However, the area under the peak is unaffected, i.e. the experiment can measure the integrated cross section $\int\sigma(W)dW$. The value of the integral, assuming J = 1 and that the resonance has a Breit-Wigner shape, is given by

$$\int\sigma(W)dW = \frac{6\pi^2}{W^2}\,\frac{\Gamma_e\cdot\Gamma_f}{\Gamma^2} \qquad (14)$$

where Γ_f represents the decay width into the observed final state.
The values for Γ_e, Γ_μ and Γ can therefore be determined from a measurement of the cross sections for

$$e^+e^- \to J/\psi \to e^+e^-,\ \mu^+\mu^- \text{ and hadrons.}$$

Such measurements have been made at ADONE, DORIS and SPEAR. They are all in reasonable agreement. The values[12] obtained by the SLAC-LBL group are listed in Table 3.

Table 3 - Width of the J/ψ and ψ'

	J/ψ	ψ'
Γ	69±15 keV	228±56keV
$\Gamma_e=\Gamma_\mu$	(4.8±0.6)keV	(2.1±0.3)keV
$\Gamma_{\overline{\gamma h}}$	12.0±2 keV	6.6±0.9 keV

Are these values consistent with the assumption that the new resonances are made of two heavy quarks $c\bar{c}$? Adding a fourth quark enlarges SU(3) to SU(4). The e.m. current in a unbroken SU(4) symmetry can be written as:

$$J_{em} = 2/3(u\bar{u}) - 1/3(d\bar{d}) - 1/3(s\bar{s}) + 2/3(c\bar{c}). \qquad (15)$$

This current can be rewritten in terms of the known vector mesons:

$\rho = 1/\sqrt{2}\ (u\bar{u} - d\bar{d})$, $\omega = 1/\sqrt{2}\ (u\bar{u} + d\bar{d})$,
$\phi = s\bar{s}$ and the conjectured $J/\psi = c\bar{c}$ as

$$J_{em} = \frac{1}{\sqrt{2}}\rho + \frac{1}{3\sqrt{2}}\omega - \frac{1}{3}\phi + \frac{2}{3}J/\psi \qquad (16)$$

The electromagnetic widths of these resonances should therefore be in the ratio:

$$\Gamma_e^\rho : \Gamma_e^\omega : \Gamma_e^\phi : \Gamma_e^{J/\psi} = 9 : 1 : 2 : 8$$

This can be compared to the experimental values in keV

$$\Gamma_e^\rho : \Gamma_e^\omega : \Gamma_e^\phi : \Gamma_e^{J/\psi} =$$

$$(6.5\pm1.2):(0.77\pm0.2):(1.35\pm0.15):(4.8\pm0.6)$$

$$9 \quad : \quad 1.07 \quad : \quad 1.87 \quad : \quad 6.65$$

In this picture the ψ' is the first recurrence of the J/ψ. Since Γ_e is proportional to the value of the wave function at the origin squared it might indeed be resonable to expect $\Gamma_e^{J/\psi}$ to be larger than $\Gamma_e^{\psi'}$. It therefore seems that the coupoing between a photon and the J/ψ(ψ') is consistent with expectations based on a bound state of two heavy quarks with charge 2/3 e. However, note that attempts to include the symmetry breaking leads to either $M\cdot\Gamma_e$ or Γ_e/M as the relevant quantities. In both cases the agreement with the SU(4) predictions becomes worse.

What about the hadronic widths ? The wave function of the old hadrons does not contain new quarks. Therefore the decay of the J/ψ and the ψ' into normal hadrons should be suppressed by the Okubo-Zweig-Iizuka[14] rule in analogy to the decay $\phi \to 3\pi$.

Note that the rate for $\phi \to 3\pi$ is suppressed by about a factor of 50 as compared to a suppression factor of 1000-10000 needed to understand the width for J/ψ and ψ' to decay into hadrons. However, theoretical argaments indicate that the OZI suppression should indeed be much more effective for the J/ψ and the ψ' than for the φ.

IV.2 Determination of spin, parity and charge conjugation

The value of Γ_e makes it reasonable to assume that the J/ψ (ψ') is produced via the one photon annihilation diagram in Fig. 8. In this case the resonance must have the quantum numbers of a photon $J^{PC} = 1^{--}$.
These quantum numbers can also be determined from a measurement of the cross section for $e^+e^- \to \mu^+\mu^-$ at energies at and adjacent to the resonance. At

these energies the reaction proceeds either via the production and the decay of the J/ψ into muons or directly via QED. The relevant diagrams and the cross sections are listed in Fig. 17.

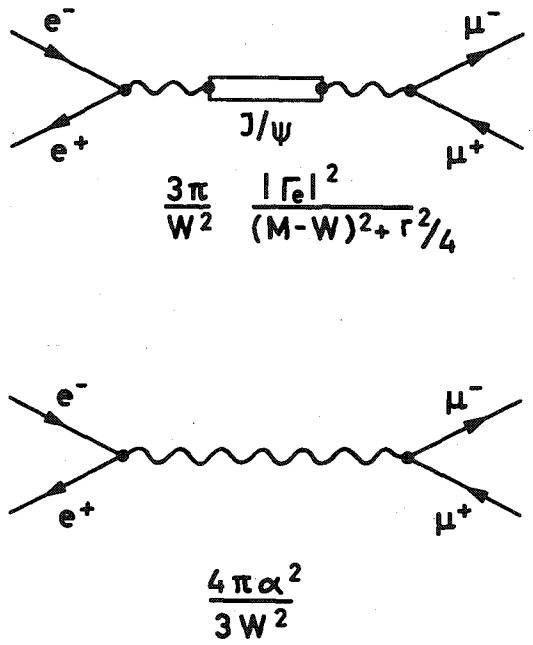

Fig. 17 - Muon pairproduction
a) via the resonance
b) via QED

The two diagrams in Fig. 17 can interfere if the resonance has $J^P = 1^-, 2^-, 3^-$. The cross section for (M-W) >> Γ can be written, assuming $J^P = 1^-$ as

$$\sigma(e^+e^- \to \mu^+\mu^-) = |A^\gamma + A^R|^2 \approx \frac{3\pi}{W^2}\left|\frac{\Gamma_e}{M-W} - \frac{2}{3}\alpha\right|^2 . \qquad (17)$$

This leads to a clear interference pattern, constructive above and destructive below the peak with a dip at $W = M - 3/2\alpha\ \Gamma_e$. Using the values of Γ_e listed in Table 3 we find that the dip occurs 1.0 MeV below the J/ψ peak and .43 MeV below the ψ' peak. This interference pattern will be somewhat washed out since $(3\alpha\Gamma_e)/2$ is comparable to the natural spread in beam energies (Eq. 6). However, a clear interference pattern is still visible as seen in Fig. 18 where the ratio $\sigma_{\mu\mu}/\sigma_{ee}$ is plotted as a function of energy. The data were obtained by the SLAC-LBL group. The dashed curve shows the predicted energy dependence assuming no interference; the solid curve represents the energy dependence assuming amximum interference. The data are clearly consistent with the maximum interference excluding no interference by 2.7σ (J/ψ) and 4.9σ (ψ') respectively. The observation of negative interference below the peak strongly favors $J^P = 1^-$. This is reinforced by a measurement of the muon angular distribution which finds $d\sigma/d\Omega \sim 1 + \cos^2\theta$ as expected for $J^P = 1^-$.

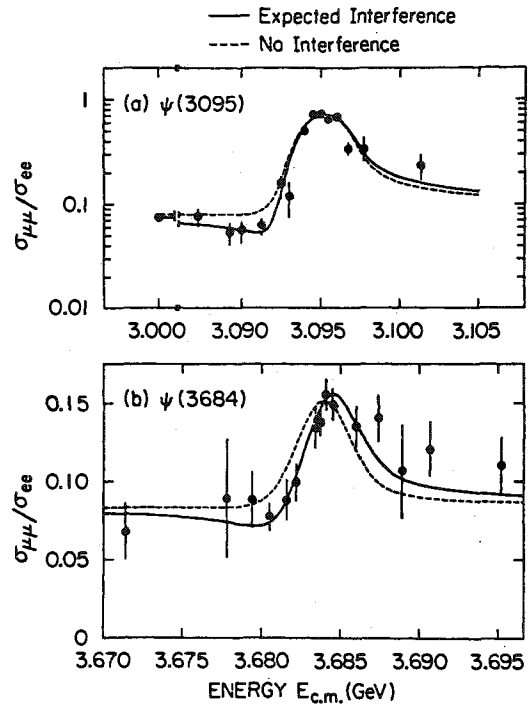

Fig. 18 -

It follows from P = -1 that the resonance must have negative charge conjugation:

$$(\mu^+\mu^-) = CP(\mu^+\mu^-) = -C(\mu^+\mu^-).$$

This assignment is also consistent with the absence of the decay J/ψ(ψ') → γγ. Such a decay is forbidden for a spin 1 particle but allowed for all

other values of J provided the charge conjugation is even. There are three independent vectors in the decay, the two polarization vector of the photon $\vec{\varepsilon}_1$, $\vec{\varepsilon}_2$ and the relative momentum $\vec{k}$. There are three independent combinations of these vectors which are linear in $\vec{\varepsilon}$ and transform like a vector under rotations:

$$\vec{\varepsilon}_1 \times \vec{\varepsilon}_2 \quad , \quad (\vec{\varepsilon}_1 \cdot \vec{\varepsilon}_2) \cdot \vec{k}$$

$$\vec{k} \times (\vec{\varepsilon}_1 \times \vec{\varepsilon}_2) = \vec{\varepsilon}_1 (k\vec{\varepsilon}_2) \cdot \vec{\varepsilon}_2 (k\vec{\varepsilon}_1)$$

The two first combinations are forbidden because the wave function of two bosons must be symmetric under the interchange $1 \rightleftarrows 2$. The third invariant is forbidden because of gauge invariance ($\vec{\varepsilon}\vec{k} \equiv 0$).

The cross section for the reaction $e^+e^- \to \gamma\gamma$, measured by the DASP group, is plotted in Fig. 19 as a function of energy. The data runs smoothly

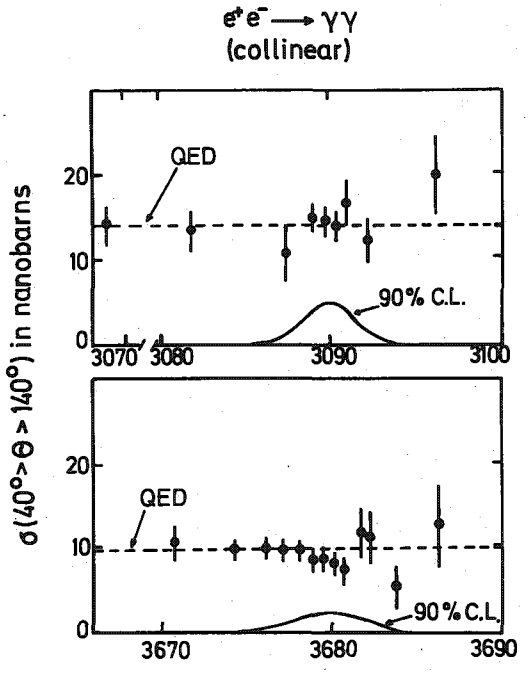

Fig. 19 - Energy dependence of $\sigma(e^+e^- \to \gamma\gamma)$ for energies at and adjacent to J/ψ and ψ'. The dotted line represents the rate expected from QED. The Breit-Wigner curves represent the 90% upper confidence limit to a resonance contribution.

through both resonance regions with no evidence for peak at the position of the J/ψ or the ψ'. The limits obtained are listed in Table 4.

Table 4 - Limit on J/ψ, ψ' into γγ

Decay	Fraction %	Reference
$J/\psi \to \gamma\gamma$	< 0.3	15 DASP
$\psi' \to \gamma\gamma$	< 0.5	16 STANFORD
	< 0.8	15 DASP

IV. 3 G-parity and isospin

The G-parity of a neutral, non strange meson is given by $G = C\,(-1)^I = -(-1)^I$. Therefore in principle the G-parity and hence the isospin can be determined by counting the number of final state pions produced in the direct decay of the resonance. However, because of the narrow width of the J/ψ, second order radiative decays as shown in Fig. 20 are important.

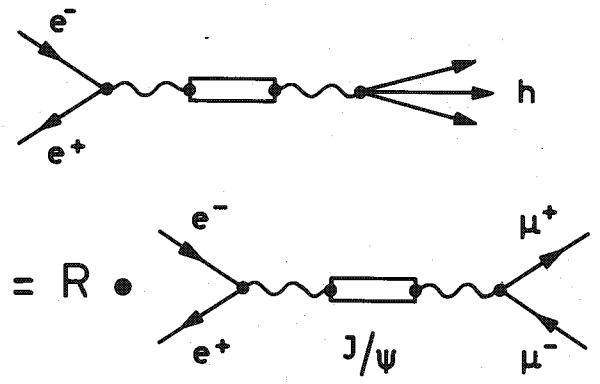

Fig. 20 - Second orter radiative decay via the resonance. The strength of this decay $\Gamma_{\gamma h}$ is given by $\Gamma_{\gamma h} = R \cdot \Gamma_\mu$ with $R = \sigma_{tot}/\sigma_{\mu\mu}$ evaluated at adjacent energies.

Such decays will lead to final states which are characteristic of the photon and not of the resonance. The width for the radiative decay can be estimated from $\Gamma_{\gamma h} = R\Gamma_\mu$, where R is measured at adjacent energies. This estimate follows from the assumption that the decay $J/\psi \to \mu^+\mu^-$ always proceeds via an intermediate photon. Using this relation we find (Table 3) that about 20% of all J/ψ decays proceed via a second order radiative decay.

Since we expect the isovector part of the photon to dominate this will lead to a final state with a predominantly even number of pions. However, the remaining decays of the J/ψ will indeed reflect its G-parity.

The branching ratios for the J/ψ to decay into various final states with pions only are listed in Table 5.

Table 5 - J/ψ to pions only

Decay mode	Fraction %	References
$\pi^+\pi^-$	0.01	17 DASP
$\pi^+\pi^-\pi^o$	1.6 ± 0.6	18 SLAC-LBL
$2\pi^+2\pi^-$	0.4 ± 0.1	18 SLAC-LBL
$2\pi^+2\pi^-\pi^o$	4.0 ± 1.0	19 PLUTO
$3\pi^+3\pi^-$	0.4 ± 0.2	18 SLAC-LBL
$3\pi^+3\pi^-\pi^o$	2.9 ± 0.7	18 SLAC-LBL
$4\pi^+4\pi^-\pi^o$	0.9 ± 0.3	18 SLAC-LBL

It is clear that the decay into final states with an odd number of pions is favoured. The decay rate into even number of pions is consistent with the rate expected from a second order radiative decay. If this is so then the ratio

$$\alpha = \frac{\sigma^H_{on}/\sigma^{\mu\mu}_{on}}{\sigma^H_{off}/\sigma^{\mu\mu}_{off}} \quad \text{should be one.}$$

$\sigma^H_{on}/\sigma^{\mu\mu}_{on}$ is the cross section for a particular pion multiplicity on the resonance normalized to the cross section for muon pairs and $\sigma^H_{off}/\sigma^{\mu\mu}_{off}$ the same quantity measured off the resonance. This ratio, plotted in Fig. 21, is indeed consistent with one for final states with even number of pions and well above one for states with odd number of pions. The J/ψ has therefore odd G-parity and even isospin. Since J/ψ decays into $\pi^+\pi^-\pi^o$ the value of the isospin must be either 0 or 2. I = 2 can be excluded since the direct decay of J/ψ into $p\bar{p}$ and $\Lambda\bar{\Lambda}$ has been observed.

The G-parity of the ψ' cannot be determined by counting the number of pions in the final state. This is because only a small fraction (∿ 15%) of the ψ' decays are direct ones, the rest are decays via the J/ψ or intermediate states with even charge conjugation.

Evidence for the decay ψ' → J/ψ + X is shown in Fig. 22. Here the yield of muon pairs, produced at

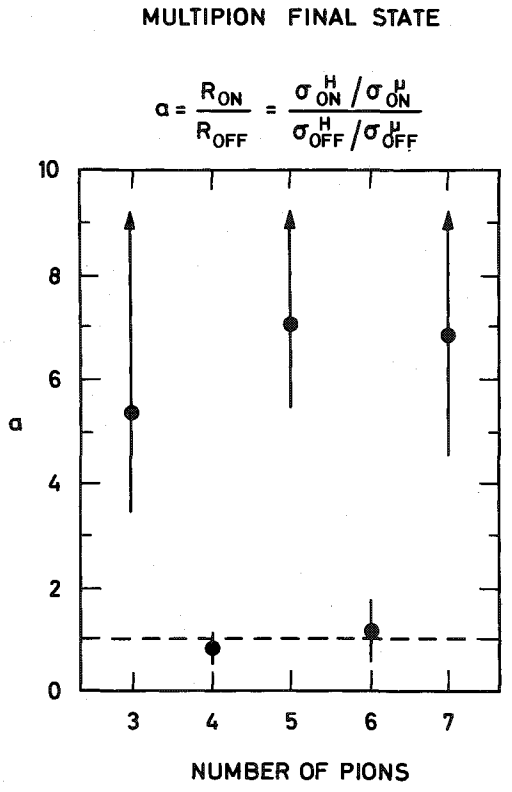

Fig. 21 - Plot of α versus pion multiplicity for the decay of the J/ψ. The data were obtained by the SLAC-LBL group

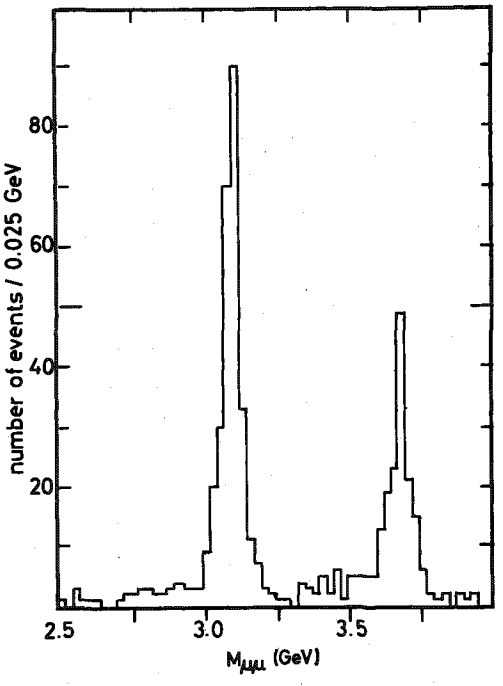

Fig. 22 - The yield of muon pairs produced at the ψ' as a function of invariant mass. The data are from DASP

the ψ' resonance, are plotted as a function of effective mass. The spectrum, obtained by the DASP group[15], has two peaks. The first peak is centered at the mass of the ψ' and are the sum of the decays of the ψ' into a pair of muons and muons directly produced by QED.

The second peak, at a mass of 3.09 GeV, is from the characteristic decay of the J/ψ resonance into a pair of muons and is direct evidence for the decay $\psi' \to J/\psi + X$. Branching ratios for various decay modes are listed in Table 6.

Table 6 - Cascade Decay $\psi' \to J/\psi + X$

Decay Mode	Fraction %	Reference
$\pi^+\pi^- J/\psi$	32 ± 4	20 SLAC-LBL
	36 ± 6	15 DASP
$\pi^o\pi^o J/\psi$	17 ± 2.9	20 SLAC-LBL
	18 ± 6.0	15 DASP
$\eta J/\psi$	4.3 ± 0.8	21 SLAC-LBL
	3.7 ± 1.5	15 DASP
$\gamma J/\psi$ $\pi^o J/\psi$	< 0.15	21 SLAC-LBL

The ratio $\frac{\psi' \to \pi^o\pi^o J/\psi}{J/\psi \to \pi^o\pi^o J/\psi}$ is consistent with 0.5, the value predicted for a $\Delta I = 0$ transition. For $\Delta I = 1$ or 2 this ratio should be 0 or 2, which is incompatible with the data. That J/ψ and ψ' have the same isospin is reinforced by the existence of the decay $\psi' \to \eta\, J/\psi$ observed both by the DASP and the SLAC-LBL group.

SU(3)

The decays of the new resonances into ordinary hadrons can be used to determine their SU(3) classification, provided the decay mechanism conserves SU(3)[22].

The direct decay of the J/ψ into $\pi^+\pi^-, \rho^+\rho^-, \pi^+A_2^-$ is forbidden by isospin and G-parity. If the J/ψ is a SU(3) singlet as expected for a bound state of a pair of heavy quarks then it decays with a single SU(3) amplitude. Therefore the decay rates should be equal for any states which are related to one another by a rotation around the axis normal to the I_3 Y plane. Fig. 23 shows an example. Decays into K^+K^-, $K_L^oK_s^o$, K(890) $\overline{K(890)}$ and K $\overline{K(1420)}$ should thus be forbidden.

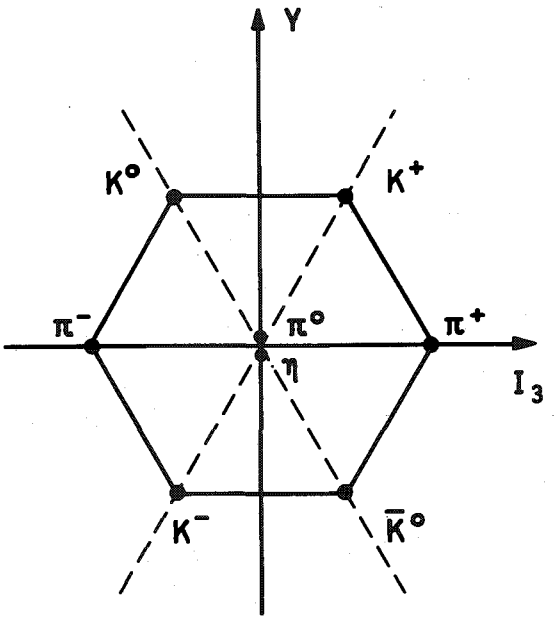

Fig. 23 - SU(3) - Multiplet

Branching ratios for these decays are listed in Table 7.

Table 7 - Branching ratios for J/ψ

Decay Mode	Branching Ratios %	References
K^+K^-	0.014 ± 0.014	17 DASP
K_sK_L	0.008	23 SLAC-LBL
$K^o(890)$ $\overline{K^o(890)}$	< 0.05	24 SLAC-LBL
$K^{o+}(1420)$ $K^o(1420)$	< 0.29	24 SLAC-LBL
$K^oK^o(1420)$	< 0.20	24 SLAC-LBL

This rotation principle also holds when the decay particles are members of two different octets. For example

$$\Gamma(J/\psi \to \pi^+\rho^-) = \Gamma(J/\psi \to K^+K^-(890))$$

This last equality has been investigated at DASP by measuring the missing mass of states recoiling against charged pions and kaons. The pions and kaons were identified and their momenta measured using the magnetic arms of the spectrometer. The data[17] plotted in Fig. 24 show clear peaks at the masses of the ρ and the $K^-(890)$.

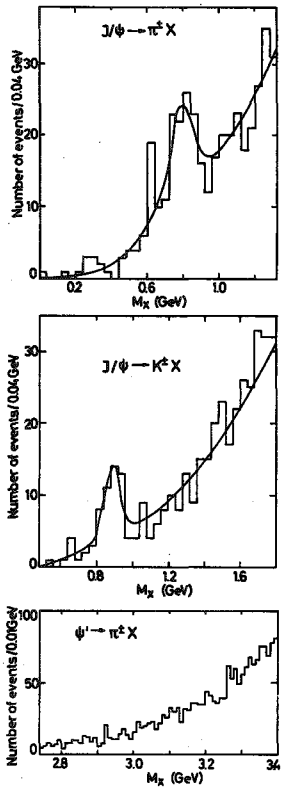

Fig. 24 - Missing mass spectrum observed in the decay a) $J/\psi \to \pi^{\pm}X$
b) $J/\psi \to K^{\pm}X$
c) $\psi' \to \pi^{\pm}X$

The experimental result is $\frac{\Gamma(\pi^-\rho^+)}{\Gamma(K^-K^+(890)} =$ 1.9 ± 0.7 or 1.6 ± 0.6 after a small phase space correction.

If the J/ψ has both singlet (A_1) and octet (A_8) components then the decay amplitude will be of the form:

$$A(\pi^+\rho^-) = A_1 - 2A_8$$

$$A(K^+K^-(890)) = A_1 + A_8$$

With the above branching ratio one obtains $\frac{|A_8|}{|A_1|}\cos\delta = -0.07 \pm 0.06$, where δ is the phase between A_1 and A_8.

The SLAC-LBL group finds $\frac{\Gamma(\pi^-\rho^+)}{\Gamma(K^+K^+(890)} = 2.7 \pm 0.8$.

This corresponds to $\left|\frac{A_8}{A_1}\right| \cos\delta = -0.18 \pm 0.06$ after phase space correction.

These results, and also data available on the decay into baryons, favour an SU(3) singlet assignment for the J/ψ.

All the properties of the J/ψ and the ψ' discussed so far are indeed consistent with these being the bound states of a new heavy quark Q. If this is the correct interpretation then more states both with and without the quantum numbers of a photon must exist. These states are isoscalar and SU(3) singlets. The discovery of such states shows rather conclusively that this interpretation is the correct one. The most natural choice for Q would be to identify it with the charmed quark c (charge 2/3 e, spin 1/2, charm = 1, I = Y = 0). However, any new quark with spin 1/2 will lead to similar predictions for the $Q\bar{Q}$ states. The properties of the new quark can only be studied by finding a new class of hadrons which result from combining an old with a new quark.

Such hadrons, carrying a new quantum number, can decay only weakly into normal hadrons. The signature for new hadrons would therefore be to find their semileptonic decays or to observe very narrow resonances. The charm hypothesis, however, can be identified by the preferred decay of the charmed quark into a strange quark. $c \to -d \cdot \sin\theta_c + s \cdot \cos\theta_c$. This leads to properties specific to the charm hypothesis like eK correlations and apparently exotic decays.

In the following the predictions based on the charmonium model - the name generally adopted for the bound $Q\bar{Q}$ system - will be given. These predictions will then be compared to the data.

V) Charmonium

The forces acting between the $c\bar{c}$ quarks are in nonrelativistic computations approximated by a steeply rising attractive potential. At short distances this force might be represented by the exchange of massless, colored vector particles; the gluons. This will give rise to a term $\frac{\alpha_s}{r}$ in the potential where α_s is the strong interaction coupling constant. To prevent the quarks from appearing in the final state one in general adds a confining term increasing as $a \cdot r$ with the separation between the quarks, i.e.

$$V(r) = \frac{\alpha_s}{r} + V_o + a \cdot r. \qquad (18)$$

A potential of this type will lead to the level scheme shown below in Fig. 25.

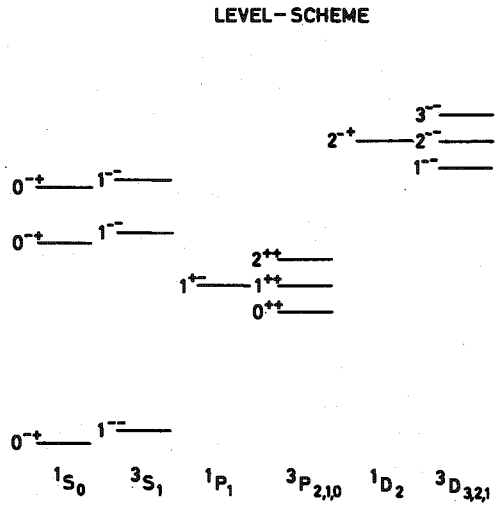

Fig. 25 - Levels predicted for two fermions bound in a strongly atractive potential

The levels are labeled by J^{PC} with $P = -(-1)^L$ and $C = (-1)^{L+S}$. Each value of L gives two bands of radial excitations with opposite charge conjugation depending on S = 1 (spin parallel) or S = 0 (spin antiparallel). The spectroscopic notation $^{2S+1}L_J$ is written below each set of radial excitations.

In this picture the J/ψ and the ψ' are identified as the 1^3S_1, and the 2^3S_1 respectively. The potential above will lead to a small spin-spin force and hence to a small mass splitting between the $^3S_1$ and the $^1S_0$ states.

The P-levels will split into one state with odd and three states with even charge conjugation. In a pure Coulomb potential the first set of P levels would be nearly degenerate in mass with the 2^3S_1 level. The addition of any confining potential will push the mass of the 2P-levels below the mass of the 2^3S_1 level.

The D-level split into one level with even and three levels with odd charge conjugation. These levels should also be close in mass to the 2^3S_1 state. Note that the $^3D_1$ level has the quanum numbers of a photon and hence in principle can be produced in an e^+e^- collision. The coupling of a photon to a vector meson is proportional to the value of the wave function at the origin. For a D-state the wave function disappears at the origin. But since the $^3D_1$ and the $^3S_1$ states should be nearly mass-degenerate they will mix. Through the mixing the $^3D_1$ state will acquire a finite value of the wave function at the origin. The $^3D_1$ states will presumably show up in the e^+e^- collision satellite vector mesons with a rather small value for Γ_e.

The existence and the number of such levels are firm predictions of the charm model, independent of the details of the potential.

In the level scheme shown in Fig. 25 there are four levels with even charge conjugation between the ψ' and the J/ψ and one below the J/ψ. These levels can be reached by radiative decays from the ψ' or the J/ψ respectively. The rates for these decays are model dependent.

Only a M1 transition is allowed for the decay $n^3S_1 \to n^1S_o + \gamma$. The only unknown in evaluating this rate is μ, the magnetic moment of the new quark. With $\mu = \frac{2/3\ e}{2m_Q}$ one obtains:

$$\Gamma(2^3S_1 \to n^1S_o + \gamma) = \frac{16}{27}\ \alpha\ \frac{k^3}{m_Q^2} \qquad (19)$$

These decays are strongly suppressed if the two states have different values of n, because the wave functions overlap poorly.

The decay into the P-levels can proceed to lowest order by an electric dipole transition. The rate for the E1 transitions can be written as:

$$\Gamma(2^3S_1 \to \gamma 2^3P) = (\tfrac{16}{243})\alpha(2J+1)\ k^3 |\langle 2P|J|2S\rangle|^2. \qquad (20)$$

Note that in this case the wave functions for the P states and the S states must be known. Only the transition $(2^3S_1 \to 2^3P_o + \gamma)$ is uniquely a E1 transition. This E1 transition gives an angular distribution of the photon with respect to the beam axis of $1 + \cos^2\theta$. The $2^3S_1 \to 2^3P_1 + \gamma$ and $2^3S_1 \to 2^3P_2 + \gamma$ transition can proceed by

E1, M2 and E1, M2, E3 transitions respectively. For these states, no firm prediction can be made for the angular distribution.

The most model dependent predictions are those trying to understand the absolute width of the $c\bar{c}$ states. The decay is a short range effect; the relevant distances are on the order of 1/M. The $c\bar{c}$ state annihilates into massless glouns which in turn materialize into normal hadrons. These can largely be obtained by analogy to similar formulas derived for positronium decays with α suitably replaced. Some of the relevant formulas are listed below:

a) decay of the ^1S_o proceeds via two photons or two gluons

$$\Gamma(^1S_o \to \gamma\gamma) = \frac{256\pi}{27}\alpha^2 \frac{|^1S_o(0)|^2}{M^2} \qquad (21)$$

$$\Gamma(^1S_o \to \gamma\gamma \to \text{hadrons}) = \frac{32\pi}{3}\alpha_s^2 \frac{|^1S_o(0)|^2}{M^2} \qquad (22)$$

b) The $^3S_1$ state decays to lowest order into hadrons via a 3 gluon intermediate state (one gluon forbidden by color, two gluons by charge conjucation and higher order neglected since $\alpha_s < 1$).

$$\Gamma(^3S_1 \to e^+e^-) = \frac{64\pi\alpha^2}{9} \frac{|^3S_1(0)|^2}{M^2} \qquad (23)$$

$$\Gamma(^3S_1 \to ggg \to \text{hadrons}) = \frac{160}{81}(\pi^2-9)\alpha_s^3 \frac{|^3S_1(0)|^2}{M^2} \qquad (24)$$

c) The widths of the intermediate P states have been estimated by Barbieri, Gatto and Kögerler. They find: $\Gamma(0^{++}) > \Gamma(2^{++}) > \Gamma(1^{++})$. The total widths of the P states are also proportional to the wave function at the origin- i.e. the states are expected to be quite narrow. One therefore naively expects the unsuppressed radiative decays $P_{2,1,0} \to \gamma\, ^3S_1$ to be rather important, at least for the $^3P_1$ level.

This picture[25] can be tested by comparing the widths of the J/ψ and the ψ'. First a value for α_s can be extracted from the measured values of Γ_e and Γ_h at the J/ψ resonance.

$$\frac{\Gamma(1^{--} \to ggg \to \text{hadrons})}{\Gamma(1^{--} \to e^+e^-)} = \frac{5(\pi^2-9)}{18\pi} \cdot \frac{\alpha_s^3}{\alpha^2} \qquad (25)$$

Using the values for $\Gamma_e = (4.8 \pm 0.6)$ keV and $\Gamma_h(1^{--} \to \text{hadrons}) = 48$ keV one obtains $\alpha_s = 0.2$.

This justifies neglecting the emission of five and more gluons. Since α_s changes only slowly with q^2 we can use this value to predict $\Gamma(2^3S_1 \to \text{hadrons})$. Using $\Gamma(2^3S_1 \to ee) = 2.1$ keV we find $\Gamma(2^3S_1 \to ggg \to \text{hadrons}) = 22$ keV as compared to the experimental value of roughly 36 keV. This is satisfactory agreement considering the large uncertainties in the experimental value.

This is consistent with the short range picture, however, note that any model which explains the Zweig rule will tend to give the same answer. A prediction unique to this short range picture is the relative widths of the $^3S_1$ states and the ^1S_o states. The wave functions of the $^3S_1$ and the ^1S_o state are supposed to be similar in the $c\bar{c}$ model.
We therefore obtain:

$$\frac{\Gamma(^1S_o \to gg \to \text{hadrons})}{\Gamma(^3S_1 \to ggg \to \text{hadrons})} = \frac{27\pi}{5(\pi^2-9)\cdot\alpha_s} \sim 100.$$

The ^1S_o widths should therefore be on the order of a few MeV.

V. 1 New 1^{--} states

The cross section for observing a vector meson in e^+e^- annihilation is given by the Breit-Wigner formula

$$\int\sigma(e^+e^- \to \text{hadrons}) = \frac{3}{W^2}\frac{\Gamma_e \cdot \Gamma_h}{(M-W)^2+\Gamma^2/4}$$

If the width of the resonance is narrow compared to energy spread in the accelerator, then the quantity measured is the area under the resonance.

$$\int\sigma\, dW = \frac{6\pi^2}{m^2} \cdot \Gamma_e \cdot \Gamma_{h/\Gamma}$$

The experiment is then sensitive to Γ_e since in general $\Gamma_h/\Gamma \sim 1$. If the resonance has a width much larger than the beam resolution then the peak cross section is given by

$$\frac{12}{M^2} \cdot \frac{\Gamma_e \cdot \Gamma_h}{\Gamma^2}$$

Therefore such a measurement is essentially sensitive to $B_e = \Gamma_e/\Gamma$ since $\Gamma_h/\Gamma \sim 1$.

Groups at Adone[26] have searched the mass region from 1.9 GeV to 3.1 GeV in narrow energy steps. No narrow resonances were found. The 90% upper confidence limit on the width Γ_e of the resonance to decay into electrons is roughly $\Gamma_e < .5$ keV $(M/3.1\ \text{GeV})^2$.

The SLAC-LBL group[5,27] has searched for narrow resonances in the mass range 3.2 GeV to 7.4 GeV. None were found; the limits are listed in Table 8.

Table 8 - SPEAR results on narrow 1^{--} states

Mass Range (GeV)	Percentage of $\sigma_{J/t}\, dW$
3.2 - 5.9	< 9%
5.9 - 7.6	< 4%
5.7 - 6.4	≤ 2%
7.0 - 7.4	≤ 1%

The total cross section[5,27] in the mass region from 3.8 to 4.5 GeV normalized to the point cross section is plotted in Fig. 26. The data are from the SLAC-LBL group and show a rather complex structure with several bumps. The peak at 3.85 GeV has only a 2σ significance. The 90% upper confidence limit B_e is 3×10^{-5}. For comparison, the branching ratios for the known vector mesons ρ, ω and φ to decay into electrons are $B_e^{\rho} = 4.3 \times 10^{-5}$, $B_e^{\omega} = 7.6 \times 10^{-5}$ and $B_e^{\phi} = 3.2 \times 10^{-4}$ respectively. There is also evidence for a resonance at 3.95 GeV. The interpretation of this structure as a bump depends on the low points at 3.99 GeV. Between 4.0 GeV and 4.2 GeV there are possibly several new resonances. The sharp rise seen between 3.99 GeV and 4.03 GeV indicates that the first one might be quite narrow. At 4.414 GeV there is clear evidence for a new state. These states are presumably related to the J/ψ and the ψ' resonances, although so far there is little direct evidence for this. Three 1^{--} states are naively expected in this energy region according to the level scheme in Fig. 25. These levels have a larger width than the J/ψ and the ψ' since they are above the threshold for decay into pairs of charmed hadrons. Such decays are not suppressed by the OZI-rule. It is therefore somewhat surprising that the lifetime of the 4.414 GeV resonance is comparable to the lifetime of the states closer to threshold. Data for these resonances are listed in Table 9.

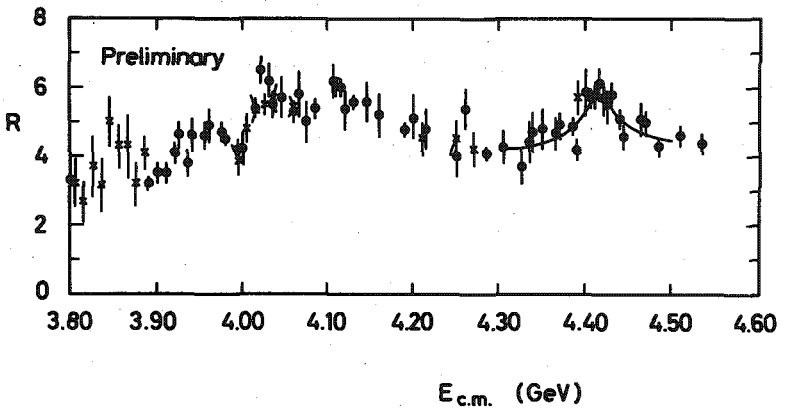

Fig. 26 - Preliminary data on the total cross-section obtained by the SLAC-LBL collaboration in the 4 GeV region

Table 9 - Summary of the 1^{--} states

Mass	Γ_{tot} (MeV)	$\Gamma_{e^+e^-}$ keV	B_e
3.095	0.069	4.8	6.9×10^{-2}
3.684	0.228	2.1	9.3×10^{-3}
3.95 [1]	60	.2	3.3×10^{-6}
4.1 [2]	250	1.8	7.2×10^{-6}
4.414	33	.44	1.3×10^{-5}

1) not yet fully established

2) presumably several resonances

V. 2 Narrow C = +1 states

The new states[28,29] with even charge conjugation located below the ψ' are produced via photon emission from the ψ' and the J/ψ. Possible detection schemes are indicated in Fig. 27.

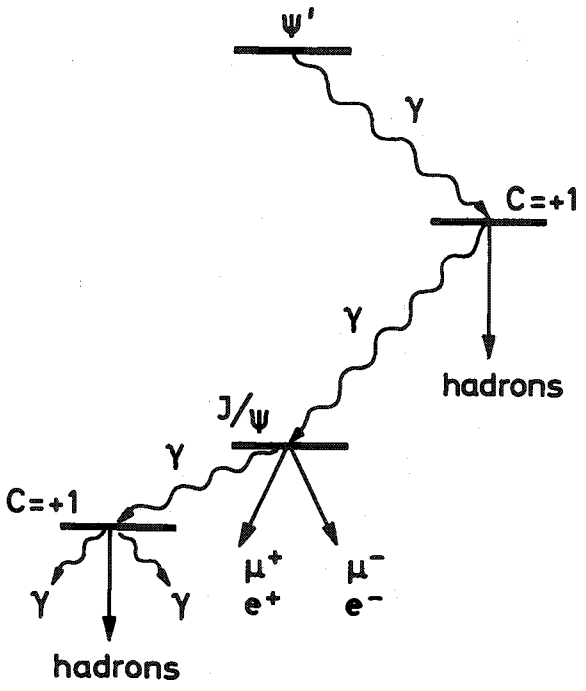

Page 27 - Various decay modes used to search for C = +1 states below the ψ'

We will start by discussing the evidence for the pseudoscalar 1^1S_0 state. One technique for finding this state is to search for the decays $1^3S_1 \to \gamma\, 1^1S_0 \to \gamma\gamma\gamma$ and $2^3S_1 \to \gamma\, 1^1S_0 \to \gamma\gamma\gamma$. Some evidence for the first decay have been given earlier[15,30]. The experiments will be discussed in more detail since the data are to large extent unpublished.

V. 2. 1 The three photon final state

At the mass of the J/ψ and the ψ' a three photon final state might arise from:

a) the radiative decay of these resonances into a state with even charge conjugation and spin different from one which subsequently decays into two photons.

b) The direct decay of the J/ψ or the ψ' into three photons[31]. The branching ratio for this decay has been estimated and found to be small.

c) Hard photon correction to the e^+e^- annihilation into two photons, leading to a final state with three photons. The cross section for this QED reaction is large, however, it can be computed[32] and unlike the decay via a resonance, it will not lead to a peak in effective mass between any pair of photons.

New experimental results on these decays have been reported by the DESY-Heidelberg group and by the DASP collaboration. Both groups used non-magnetic detectors to select the three photon final state and to measure the directions of the photons. Demanding a three photon final state removes the background from beam-gas interactions, multihadron events or cosmic ray events. This is shown in Fig. 28, where the number of three photon candidates observed by the DASP group at the J/ψ resonance is plotted as a function of χ^2. The χ^2 is calculated from 1C fit to the hypothesis that the three conversion points and the interaction point lie in a plane. Events with missing tracks will in general

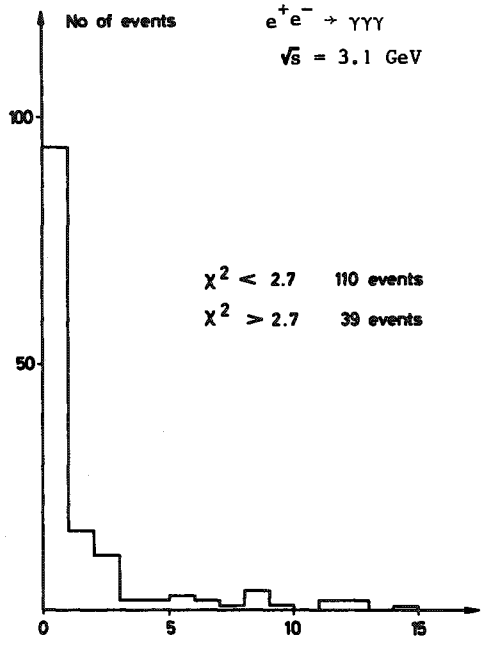

Fig. 28 - Number of apparent three photon events observed by the DASP group at the J/ψ resonance. The events are plotted as a function of χ^2 calculated from a fit to the hypothesis that the conversion points and the interaction point lie in a plane.

not be coplanar. The photon energies for the 110 events with a χ^2 less than 2.7 were computed from the measured directions of the three photons and the known cms energy. A Dalitz plot of the events is shown in Fig. 29a,b for events from the J/ψ and the ψ' respectively. Note the low mass boundary in the Dalitz plot which results from demanding an opening angle greater than 30° between any pair of photons. This cut effectively excludes $J/\psi \to \pi^0\gamma$. The data obtained at the J/ψ show a

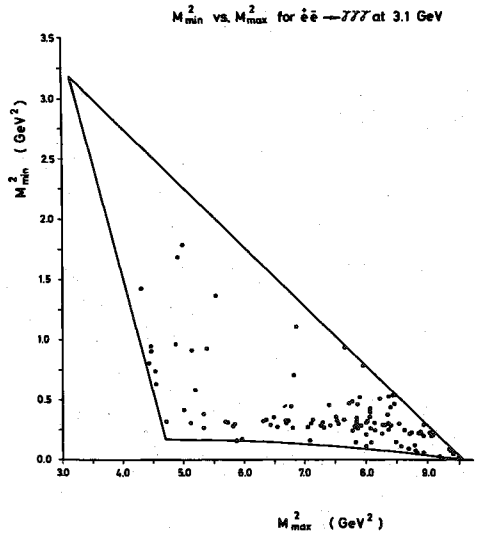

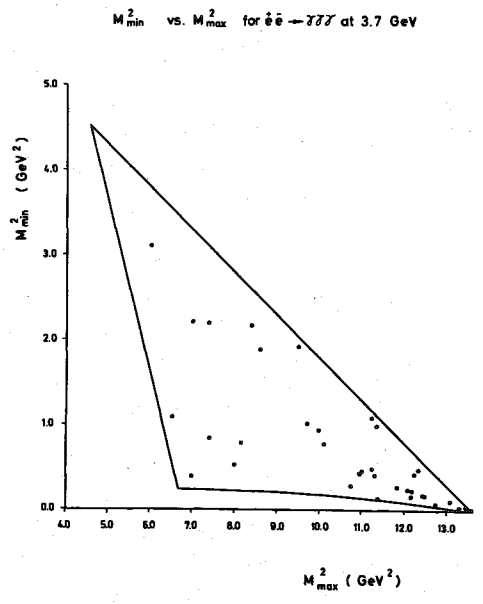

Fig. 29a,b - Dalitz plot of the three photon events observed by the DASP group at the J/ψ(a) and the ψ'(b) resonance.

clear cluster at the mass of the η, a few events consistent with the η' and some events with a mass between 2.8 GeV and 2.9 GeV, which might result from the 2γ decay of a new heavy resonance. No clear clustering of events along any fixed mass line is observed at the ψ'. In Fig. 30a, the events

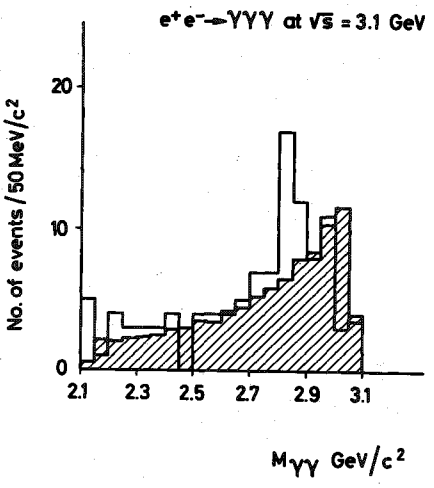

Fig. 30a - The three photon events from the Dalitz plot in Fig. 29a (J/ψ region) projected on to the high mass axis. The hatched area shows the background from QED and reflexions.

at the J/ψ resonance are projected onto the high mass axis. A clear peak, superimposed on a smooth background, is observed between 2.8 GeV and 2.9 GeV. The width is consistent with the experimental resolution. The sum of the contributions from the QED. process and reflexions from ηγ and η'γ are indicated by the hatched area. It is clear that the events outside the resonance region can be accounted for by these sources alone. Between 2.8 GeV and 2.9 GeV the DASP group observes 29 events compared to an expected background of 14 events. Assuming the observed enhancement to result from the decay of a narrow resonance they obtain M = (2.83 ± 0.05) GeV and $BR(J/\psi \to X\gamma) \cdot BR(X \to \gamma\gamma) = (1.5 \pm 0.4) \times 10^{-4}$.

The DESY-Heidelberg group[37], using the same method, finds an enhancement of 8 events above a background of 10 ± 4 events around a mass of 2.7 GeV. If this excess is attributed to a resonance they find:

$BR(J/\psi \to \gamma X)\ BR(X \to \gamma\gamma) = (1.4 \pm 0.8) \times 10^{-4}$.

These branching ratios agree well with earlier results reported by both groups based on less than half the present luminosity.

In Fig. 30b the three photon events observed by the DASP group at the ψ' resonance are plotted as a function of the highest mass found in the event. The events observed above a mass of 2.9 GeV are consistent with the rate expected from QED alone, shown as the hatched area. Between 2.7 GeV and 2.9 GeV 5 events are found compared to a predicted QED background of 1.3 events. From these data a 90% confidence upper limit of 3.7×10^{-3} can be derived for the decay $\psi' \to \gamma X(2.8) \to \gamma\gamma\gamma$.

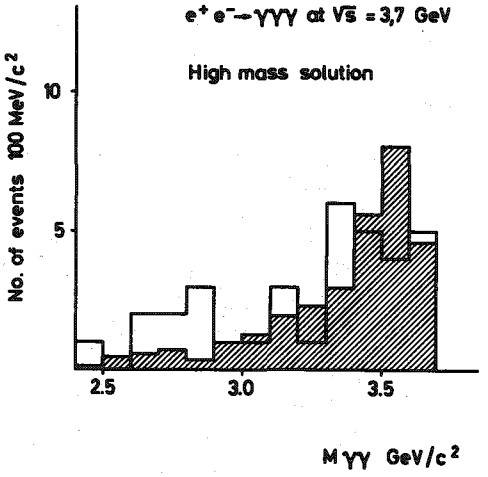

Fig. 30b - The three photon events from the Dalitz plot in Fig. 29b (ψ' region) projected on to the high mass axis. The hatched area shows the background from QED and reflexions.

The X(2.8) must have even C-parity since it decays into two photons. It can therefore in principle be associated with the pseudoscalar 1^1S_0 state. We will now discuss whether this assignment is consistent with the experimental information available.

In the simple charmonium picture the difference in mass between the $^3S_1$ and the $^1S_0$ should be on the order of 30 to 60 MeV. The experimental value from the DASP group is (260 ± 50) MeV. This seems to be inconsistent, however, one should bear in mind that the potential used (Eq. 18) is by no means unique. For example Schnitzer[33] has shown that a large $^1S_0 - {}^3S_1$ splitting can be obtained by adding a long range spin dependence to the potential.

In experiments to be discussed later the Maryland, Pavia, Princeton, UC San Diego, SLAC and Stanford Collaboration[34] has set an upper limit on the decay $1^3S_1 \to \gamma 1^1S_0$ by looking for monochromatic photons in the debris from the decay of the J/ψ. They find with 90% confidence that $BR(1^3S_1 \to \gamma\, 1^1S_0) < 5 \times 10^{-2}$ or 3.5 keV. The SLAC-LBL group[35] finds $BR(2^3S_1 \to \gamma\, 1^1S_0) < 1.1 \times 10^{-2}$ or 2.5 keV. The transitions above are all M1 transitions and the rate can be estimated using equation 19. With k = 250 MeV and M_Q = 1.55 GeV we find $\Gamma(1^3S_1 \to \gamma\, 1^1S_0) = 28$ keV. Moving the mass of the resonance within the errors from 2.83 to 2.88 GeV reduces the predicted rate by a factor of 2. The large mass splitting between the $^3S_1$ and the $^1S_0$ indicate that the radial wave functions for these states are not identical, which leads to another reduction in rate. Despite these excuses the lower limit on the M1 transition is clearly an embarassment. The limit on the decay $2^3S_1 \to \gamma\, 1^1S_0$ is not serious since in this case a large reduction in rate is expected from the bad overlap between the 2^3S_1 and the 1^1S_0 wave functions.
The short range picture predicts (Eq. 22) the total width of the $^1S_0$ to be in the order of 5 MeV and that the $BR(^1S_0 \to \gamma\gamma)$ (Eq. 21) should be on the order of 10^{-3}. Using $BR(^3S_1 \to \gamma\, {}^1S_0) < 5\%$, the observed rate for $J/\psi \to \gamma X \to \gamma\gamma\gamma$ gives $BR(^1S_0 \to \gamma\gamma) > 3 \times 10^{-3}$, consistent with the value above.

Since the predicted width of the $^1S_0$ is rather large one might expect to observe its decay into hadron final states. At the Stanford meeting the DASP group[15] reported two candidates for the cascade decay $J/\psi \to \gamma X \to \gamma p\bar{p}$. Increasing the data by more than a factor of two failed to produce any new events and therefore only an upper limit $BR(J/\psi \to \gamma X)\ BR(X \to p\bar{p}) < 2 \cdot 10^{-4}$ can be given. The SLAC-LBL group[36] has also searched for events of this type. They find no signal; the 90% confidence upper limit is $BR(J/\psi \to \gamma X) \cdot BR(X \to p\bar{p}) < 4 \times 10^{-5}$.

Conclusion: more data on the X(2.83) are needed.

Radiative decay to π^0, η, η'

In Fig. 31 the three photon events observed by the DASP group at the J/ψ resonance are plotted as a function of the lowest mass observed in the event. A clear peak at the mass of the η is observed, whose width of 30 MeV is consistent with the experimental resolution. The background from QED events and events from the kinematic reflexion of the X(2.8) is shown as the hatched area. From this data a $BR(J/\psi \to \eta\gamma) = (1.0 \pm 0.2) \times 10^{-3}$ was found, in good agreement with $(0.9 \pm 0.4) \times 10^{-3}$

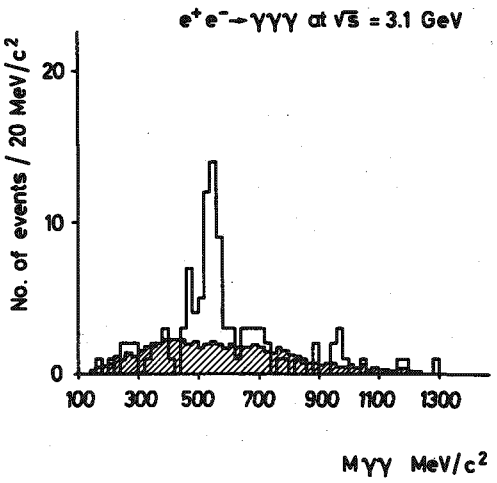

Fig. 31 - The three photon events from the Dalitz plot in Fig. 29a (J/ψ region) projected on to the low mass axis.

obtained by the DESY Heidelberg group using a similar analysis. The few events consistent with $J/\psi \to \eta'\gamma$ correspond to $BR(J/\psi \to \eta'\gamma) = (1.5 \pm 0.9) \times 10^{-3}$. This is in agreement with a measurement of this decay mode identifying η' by its decay $\eta' \to \rho\gamma$ as discussed below.

A preliminary analysis by the DASP group of the three photon final states with no cut on the minimum opening angle yield at present only an upper limit of $BR(J/\psi \to \pi^0\gamma) < 1.6 \times 10^{-4}$.

The DESY-Heidelberg group has measured[37] the decay $J/\psi \to \eta'\gamma \to \rho\gamma\gamma \to \pi^+\pi^-\gamma\gamma$. The momenta of the final state particles are computed using the measured directions as an input to the energy and momentum equations assuming that the charged particles are pions. Events with negative energy solution, in general corresponding to events with unseen particles, were rejected. The decay $J/\psi \to \rho\pi$, feeding the same topology, has in all charge states a π^0 in the final state. This decay was therefore excluded by requiring the $\gamma\gamma$ effective mass to be greater than 0.35 GeV. In addition the $\pi^+\pi^-$ were required to have a mass between .55 GeV and 1.0 GeV, consistent with the mass of the ρ-meson. The resulting invariant mass spectrum for $\pi^+\pi^-\gamma$ is plotted in Fig. 32. A clear η' peak with a total of 57 ± 13 events is observed superimposed on a smooth background from kinematic reflexions. The branching ratio is $BR(J/\psi \to \eta'\gamma) = (2.4 \pm 0.7) \times 10^{-3}$. This is also in agreement with preliminary data from the DASP group using the $\eta' \to \rho\gamma$ decay to identify the η'.

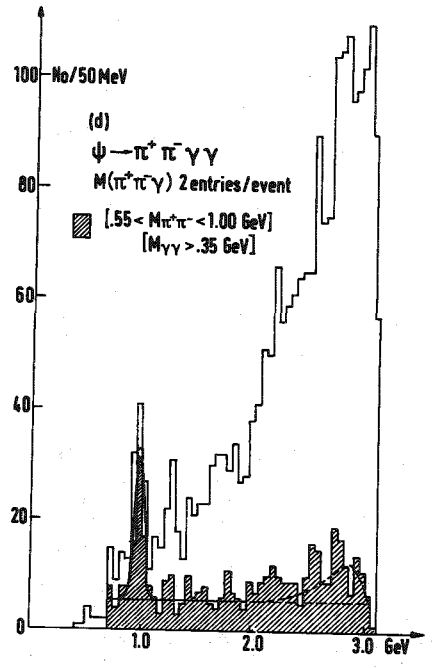

Fig. 32 - Invariant mass spectrum for $\pi^+\pi^-\gamma$ observed by the DESY-Heidelberg group in the decay $J/\psi \to \pi^+\pi^-\gamma\gamma$.

If the η and the η' consist of old quarks only then the radiative decay must proceed via the two graphs shown[38] in Fig. 33a,b.

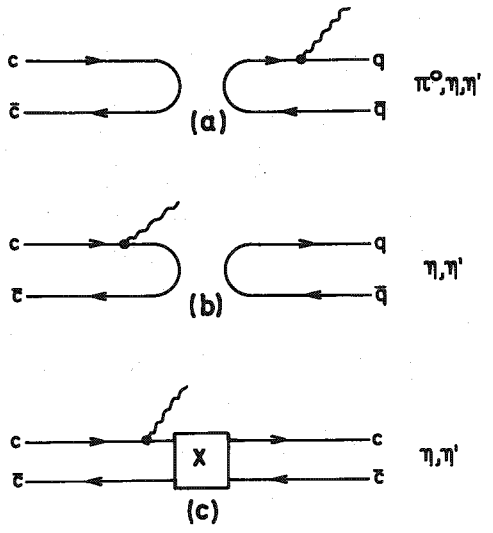

Fig. 33 - Feynmann graphs for the radiative decays of the J/ψ (ψ') into a meson.

In the diagramm 33a the photon couples only to the octet part of the $q\bar{q}$ pair and furthermore the strength of the γ-q coupling is proportional to the quark charge.

Assume that the η and the η' are in the usual mixture of singlet and octet.

$$\eta = \eta_8 \cdot \cos\theta + \eta_1 \sin\theta$$
$$\eta' = -\eta_8 \cdot \sin\theta + \eta_1 \cos\theta$$

with

$$\eta_8 = \sqrt{2/3}\, s\bar{s} - \sqrt{1/6}\,(u\bar{u} + d\bar{d})$$
$$\eta_1 = \sqrt{1/3}\,(s\bar{s} + u\bar{u} + d\bar{d})$$

and $\theta = 11^\circ$.

Isospin conservation requires that π° contains only u and d quarks;

$$\pi^\circ = \frac{1}{\sqrt{2}}(u\bar{u} - d\bar{d}).$$

The relative rate of radiative decays into the pseudoscalars can now be estimated neglecting phase space corrections.

$$\Gamma(^3S_1 \to \gamma\pi^\circ) \sim \left|\frac{1}{\sqrt{2}}\left(\frac{2}{3} + \frac{1}{3}\right)\right|^2 = \frac{1}{2}$$

$$\Gamma(^3S_1 \to \gamma\eta) \sim \cos^2\theta \left|\frac{1}{\sqrt{6}}(2(-1/3)-(2/3-1/3))\right|^2 = \cos^2\theta/6$$

$$\Gamma(^3S_1 \to \gamma\eta') = \Gamma(^3S_1 \to \gamma\eta) \cdot \frac{\sin^2\theta}{\cos^2\theta}$$

Therefore according to 33a

$$\Gamma(^3S_1 \to \gamma\pi^\circ) : \Gamma(^3S_1 \to \gamma\eta) : \Gamma(^3S_1 \to \gamma\eta')$$
$$3 : \cos^2\theta : \sin^2\theta$$

This prediction is clearly at variance with the data.

The photon in 33b is emitted from the $c\bar{c}$ system - i.e. the photon must be SU(3) singlet and an isoscalar. By the reasoning above:

$$\Gamma(^3S_1 \to \gamma\pi^\circ) : \Gamma(^3S_1 \to \gamma\eta) : \Gamma(^3S_1 \to \gamma\eta')$$
$$0 : \sin^2\theta : \cos^2 0$$

This diagram is consistent with the observed smallness of $\Gamma(^3S_1 \to \gamma\pi^\circ)$ but it predicts the ratio

$$\frac{\Gamma(^3S_1 \to \gamma\eta')}{\Gamma(^3S_1 \to \gamma\eta)}$$ to be

on the order of 25. Experimentally the ratio is (2.4 ± 0.7). If 33b is indeed the relevant graph then this would imply a large SU(3) breaking not seen in other decay modes. Also note that the absolute rates of these decays are comparable to the rate for strong decays like $J/\psi \to \rho^\circ\pi^\circ$ ($\Gamma(J/\psi\, \pi^\circ\rho^\circ) = (0.4 \pm .1) \times 10^{-2}$) despite the factor of α present in the amplitude for the radiative decay.

It has been suggested[38,39] as a possible solution to this problem that the η, η' and the charm pseudoscalar states mix. Then the η and the η' would acquire a small $c\bar{c}$ component and the radiative decay could proceed as indicated in Fig. 33c without suppression from the OZI rule[14]. The π° cannot acquire a $c\bar{c}$ component because of isospin.

The assumption of a non negligible $c\bar{c}$ component in the η is also suggested by the large rate for $\psi' \to \eta\, J/\psi$. This mode accounts for about 4% of the total ψ' width despite the small phase space and the fact that η is mainly SU(3) octet.

However, note that this mixing would also lead to $u\bar{u}$, $d\bar{d}$ and $s\bar{s}$ components in the ^1S_o wave functions and make its predicted width of 5 MeV even larger.

Intermediate States with C = +1

For any reasonable potential there should be several C = +1 states below the ψ'. These states might be observed by searching the ψ' decay debris for:

1) Monochromatic photons
2) The J/ψ together with one monochromatic and one nearly monochromatic photon
3) A monochromatic photon together with hadrons.

1) Monochromatic photons

The SLAC-LBL group measures[35] the single photon spectrum produced in the decay of the J/ψ and the ψ' resonance by using the magnetic solenoid as a pair spectrometer. A photon converted in the material ($\sim$ 0.05 of an radiation length) mounted in front of the chambers is identified by demanding a pair of oppositely charged particles to have an invariant mass less than 0.0275 GeV. The photon energy is the sum of the measured electron and positron energies; the resulting resolution (rms) is 4%. The photon spectra so obtained are plotted in Fig. 34a,b for the J/ψ and the ψ' respectively. At the ψ' resonance the spectrum shows a clear peak centered at (261 ± 10) MeV corresponding to a mass for the intermediate state of (3413 ± 10) MeV. The observed width is consistent with the experimental resolution. The branching ratio is $(6.5 \pm 2.2) \times 10^{-2}$ assuming the photon to have a $(1+\cos^2\theta)$ angular distribution with respect to the beam axis, or $(5.5 \pm 1.9) \times 10^{-2}$ for an isotropic distribution.

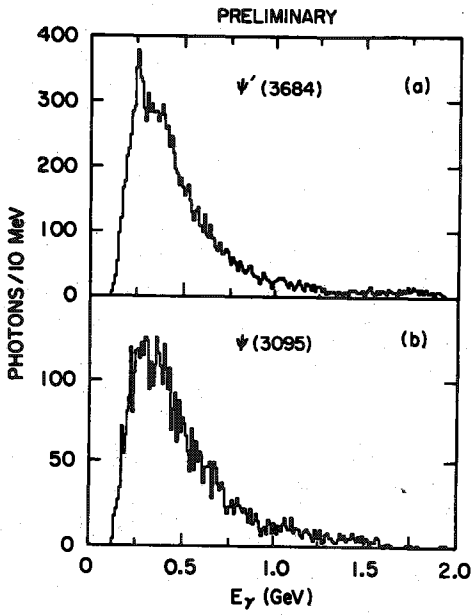

Fig. 34 a,b - The raw photon spectrum observed in the decay of the J/ψ and the ψ' resonances by the SLAC-LBL group.

The other P_c or χ states give photons with energies below 250 MeV and are masked by the rapid variation of the photon detection efficiency at low energy. Photon lines from the decay of the intermediate states into the J/ψ plus a photon are not observed, presumably because of Doppler broadening.

The decay of the ψ' into X(2.8) would lead to a monochromatic photon line at around 750 MeV. No such line is observed. The 90% confidence upper limit is 1.1%. No peak resulting from the decay $J/\psi \to \gamma X$ is found in the spectrum measured at the J/ψ resonance. However, note that the sensitivity for observing this decay depends strongly on the mass of X since the detection efficiency for low energy photons depends strongly on the photon energy.

The Maryland, Pavia, Princeton, UC San Diego, SLAC and Stanford Collaboration determines[35] the photon energy spectrum by measuring the energy deposited in two sets of segmented NaI(Tl) crystals mounted above and below the beam pipe. The energy resolution varied between 2.5% at 1500 MeV and 5% at 200 MeV. An event was recorded when two or more charged particles were registered in the tube chambers surrounding the interaction region and more than 110 MeV was deposited in any of the three NaI(Tl) arrays. Electronic threshold effects were eliminated by demanding that the measured photon should not be a part of the trigger. The resulting photon spectrum obtained at the J/ψ and the ψ' resonance is plotted in Fig. 35. The spectrum ob-

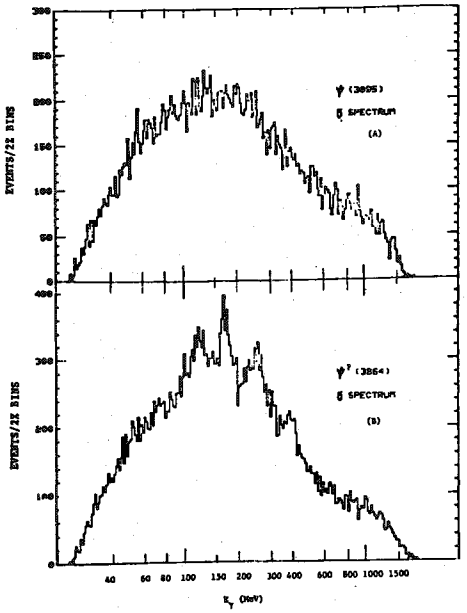

Fig. 35a,b - The raw photon spectrum observed in the decay of the J/ψ and the ψ' resonances by the Maryland, Pavia, Princeton, UC San Diego, SLAC and Stanford Collaboration.

tained at the ψ' resonance shows several bumps superimposed on a smoothly varying background in contrast to the structureless spectrum observed at the J/ψ resonance.

Photon lines centered at 121 MeV, 168 MeV, 256 MeV and 383 MeV are observed in the debris of the ψ'. The three first transitions correspond to intermediate states with masses of 3561 MeV, 3512 MeV and 3418 MeV. This proves that the P_c states first observed at DESY in the γγ cascade are the same as the χ states observed at SPEAR. The peak at 383 MeV can be identified with the decay $P_c(3.51) \to \gamma\ J/\psi$.

There are two major problems in extracting a branching ratio for these transitions. Firstly, the observed widths of the three peaks corresponding to monochromatic photon lines are not the same. Whereas the 168 MeV peak has a width corresponding to the expected resolution, both the 121 MeV line and the 256 MeV line are wider than expected. Since these resonances should be narrow, this might indicate the presence of additional, as yet unresolved, photon lines or unknown experimental problems. The fit was made assuming a width (rms) of 7%, the maximum allowed for the 121 MeV and the 256 MeV transition. A second problem is the proper shape of the non-resonant photon spectrum at the ψ' resonance. As a temporary solution the authors assumed this to be similar to the spectrum observed at the J/ψ resonance. This can clearly only be an approximation since photons from the cascade decay $\psi' \to \pi^o\pi^o$ J/ψ will make a large contribution to the ψ' spectrum. The result of the fit is shown in Fig. 36 and the branching ratios listed in Table 10.

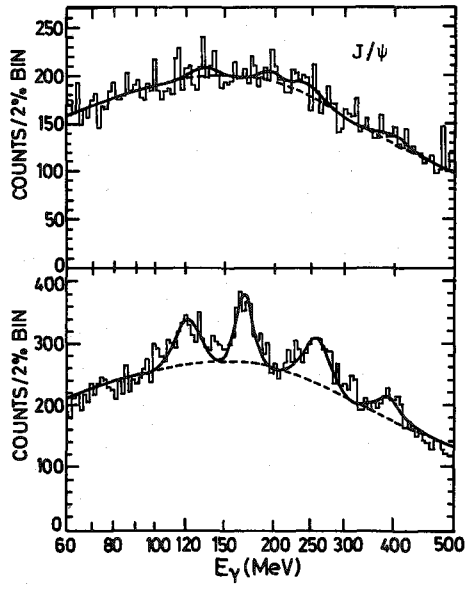

Fig. 36 a,b - The results of a fit to the photon spectrum shown in Fig. 35a,b.

Table 10 - Radiative decays into P_c/χ and X

Decay	BR[1] %	Reference
$\psi' \to \gamma\ \chi(3.41)$	10 ± 4	34
	6.5 ± 2.2	35
$\gamma\ \chi(3.45)$	< 5	34
$\gamma\ P_c(3.51)$	9 ± 3	34
$\gamma\ \chi(3.55)$	8 ± 3	34
γ X(2.83)	< 5	34
$J/\psi \to \gamma$ X(2.83)	< 1.1	35
γ X(2.83)	< 5.0	34

1) A $(1+\cos^2\theta)$ distribution assumed for $\psi' \to \gamma\chi(3.41)$, otherwise isotropic.

The systematic uncertainties dominate the error. Note that the branching ratio observed for the decay $\psi' \to \gamma\chi(3.41)$ is substantially larger than the value observed by the SPEAR group. However, the value $P_c(3.51) \to \gamma J/\psi$ / $\psi' \to$ all of $(4\pm3) \times 10^{-2}$ is consistent with earlier measurements at DESY and SPEAR.

No significant structure in the photon spectrum is observed at the J/ψ resonance. A 90% confidence upper limit of 5% is found for the decay $J/\psi \to \gamma$X(2.8).

2) The $\gamma\gamma$ cascade

The cascade decay $\psi' \to \gamma P_c \to \gamma\gamma$ J/ψ was first observed by the DASP group[28] at DESY and later by the SLAC-LBL group[40] at SPEAR.

The DASP group searched for events of the type $\psi' \to \gamma\gamma\mu\mu$ with the two muons detected in the magnetic arms of the spectrometer and the two photons observed with the inner detector. A 3C fit was made to the 34 events satisfying the selection criteria assuming they all resulted from a $\gamma\gamma$ cascade via an intermediate state. Of the 11 events with an acceptable χ^2 of 8 or less, 3 events had a $\gamma\gamma$ effective mass greater than 0.27 $(\mathrm{GeV}/c^2)^2$ and were attributed to the decay $\psi' \to$ J/ψ η. The remaining events are plotted in Fig. 37 as a function of the low mass solution versus the high mass solution. A clear cluster of events with a mass around 3.5 GeV is seen with three single events. A background of 0.6 events is expected in the sample. The location of

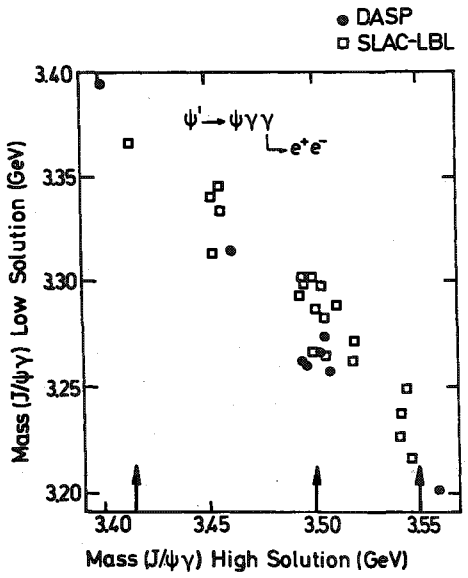

Fig. 37 - The decay $\psi' \to \gamma P_c/\chi \to \gamma\gamma\ J/\psi$. The events obtained by the DASP group and the SLAC-LBL collaboration are plotted as a function of the low mass solution versus the high mass solution. The position of the resonances as determined by other methods are indicated.

resonances observed by other decay modes is shown by the arrows.

The SLAC-LBL group[40] selected events of the type $\psi' \to \gamma\ J/\psi + X$ with the photon converted in front of the chambers and the J/ψ identified by its characteristic decay into a pair of leptons. Demanding an opening angle between the electron and the positron of less than 177.5° and a collinearity angle between the photon and either of the electron greater than 10° led to a sample of 54 events. Of these, 27 events had a missing mass squared recoiling against the $J/\psi\ \gamma$ system between $-0.03\ (\mathrm{GeV}/c^2)^2$ and $+0.03\ (\mathrm{GeV}/c^2)^2$ as expected for a $\gamma\gamma$ cascade. The $\psi' \to J/\psi\ \eta$ were excluded by a cut in the $\gamma\gamma$ effective mass leading to a final sample of 21 events with an estimated background of 1 event. These events are also plotted in Fig.37. Besides a clear cluster of events around 3.500 GeV there are 4 events clustered around 3.455 GeV and 3.545 GeV and a single event at 3.41 GeV. Note that the single events from the DASP experiment more or less agree with these latter SPEAR events.

The branching ratios

$$\frac{P_c\ /\ \chi \to \gamma\ J/\psi}{P_c\ /\ \chi \to \mathrm{all}}$$

are listed in table 11. Note that the decay of the 3.41 GeV state is based on only one event from each experiment.

The resonance at 3.455 GeV (or at 3.331 GeV) is not observed in any other decay mode. Although the existence of this state needs to be confirmed, note that the background in these experiments is rather low and hence the observation of five events might well be significant. The upper limit of 5% set on the decay $\psi' \to \gamma\ \chi(3.45)$ can be used to obtain a lower limit of 24% on the decay $\chi(3.45) \to \gamma\ J/\psi$.

The DESY-Heidelberg group[37] has used the non-magnetic detector described earlier to measure the angular distribution with respect to the beam axis of the photons emitted in the cascade decay

$$\psi' \to \gamma\ P_c(3.51) \to \gamma\gamma\ J/\psi$$

The J/ψ is identified by its decay into a pair of electrons or muons. The kinematics of the event are fully determined by the directions of the four final state particles. A total of 77 events with an estimated bakcground of 8 events satisfied the selection criteria. The resolution is not sufficient to separate the transitions from the closely spaced intermediate states. However, the DASP and the SLAC-LBL data show that the cascade transition via the $P_c(3.51)$ state is the most prominent one. This transition is further enhanced by demanding the higher energy photon to have an energy between 350 MeV and 450 MeV. A total of 60 events with an estimated background of 3 events satisfied this condition. The angular distribution with respect to the beam axis of the higher and lower energy photons is plotted in Fig. 38. A fit to the angular distribution of the lower energy photons of the form $1 + \alpha\cos^2\theta$ gives $\alpha = -(1.1 \pm 0.3)$, whereas $\alpha = +1$ for a spin 0 state. This measurement therefore excludes spin 0 for the $P_c(3.51)$ state.

Table 11 - Properties of the Intermediate States

Mass(P_c/χ) (GeV)	α ($1+\cos^2\theta$)	Decay	BR($\psi' \to \gamma P_c/\chi$) BR($P_c/\chi$ decay) $\cdot 10^{-3}$	Fraction $\rho\pi^+\pi^-/2\pi^+2\pi^-$ $K^{*}K^{\pm}\pi^{\mp}/\pi^+\pi^-K^+K^-$	BR(P_c/χ decay)[a] $\cdot 10^{-2}$	Ref.
3.414 ± 4	1.4 ± 0.4	$\pi^+\pi^-$	0.7 ± 0.2		1.0 ± 0.3	
		K^+K^-	0.7 ± 0.2		1.0 ± 0.3	
		$2\pi^+2\pi^-$	3.2 ± 0.6	0.39 ± 0.12	4.4 ± 0.8	
		$\pi^+\pi^-K^+K^-$	2.7 ± 0.7	0.41 ± 0.10	3.7 ± 1.0	
		$3\pi^+3\pi^-$	1.4 ± 0.5		1.9 ± 0.7	
		γ J/ψ	(3)		(4)	
			(10)		(14)	
3.454 ± 7		$\pi^+\pi^-$	< 0.3			
		K^+K^-	< 0.3			
		$\pi^+\pi^-K^+K^-$	< 0.5			
		$2\pi^+2\pi^-$	< 0.4			
		$3\pi^+3\pi^-$	< 0.7			
		γ J/ψ	12 ± 6		> 24	
			(10)			
3.508 ± 4		$\pi^+\pi^-$ + K^+K^-	< 0.15		< 0.17	
	0.26 ± 0.5	$2\pi^+2\pi^-$	1.1 ± 0.3	0.24 ± 0.20	1.2 ± 0.4	
		$\pi^+\pi^-K^+K^-$	0.6 ± 0.3	0.35 ± 0.18	0.67 ± 0.33	
	-1.1 ± 0.3	$3\pi^+3\pi^-$	1.25± 0.4		∿ 1.4	
		γ J/ψ	37 ± 11		42 ± 12	
			40 ± 20			
			40 ± 30			
		$\gamma\gamma$	< 0.013		< 0.014	
3.552 ± 6		$\pi^+\pi^-$ + K^+K^-	0.23 ± 12		0.29 ± 0.15	
		$2\pi^+2\pi^-$	1.6 ± 0.4	0.31 ± 0.17	2.0 ± 0.5	
		$\pi^+\pi^-K^+K^-$	1.4 ± 0.4	0.25 ± 0.13	1.8 ± 0.5	
	0.22 ± 0.4	$3\pi^+3\pi^-$	1.25 ± 0.4		∿ 1.6	
		γ J/ψ	12 ± 6		15 ± 8	
			(10)			

a) The values listed in table 2 for the decay $\psi' \to \gamma P_c/\chi$ were used to extract the branching ratios for the various P_c/χ decays. An average value of 7.3% was used for the BR($\psi' \to \gamma\chi(3.41)$

b) The numbers in bracket correspond to only 1 event

c) Only the sum $\chi(3.55) + P_c(3.51) \to 3\pi^+3\pi^-$ is measured. In the table the observed $3\pi^+3\pi^-$ yield is divided evenly on the two states.

d) Forbidden for a state with spin 1

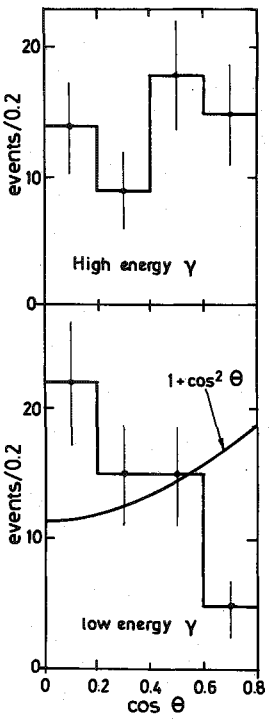

Fig. 38 - The angular distribution with respect to the beam axis of photons from the decay $\psi' \to \gamma P_c \to \gamma\gamma J/\psi$. The data were obtained by the DESY-Heidelberg group.

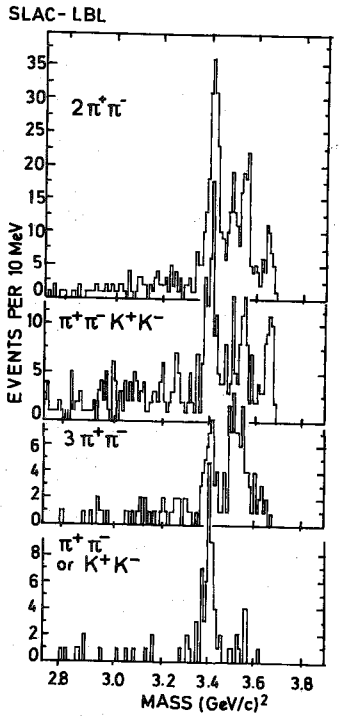

Fig. 39 - Effective mass spectra observed by the SLAC-LBL group in the decay of the ψ' into a single photon and charged hadrons

3) Hadronic decays of the intermediate states

New exciting data[41] on the decay $\psi' \to \gamma\chi \to \gamma$ + charged hadrons have been reported by the SLAC-LBL collaboration. The criteria used to select these events and early evidence for the decay modes

$$\chi \to \pi^+\pi^-\pi^+\pi^-$$
$$\to \pi^+\pi^- K^+K^-$$
$$\to \pi^+\pi^-\pi^+\pi^-\pi^+\pi^-$$
$$\to \pi^+\pi^-, K^+K^-$$

can be found in reference 29. This analysis is based on a substantially larger data sample. Furthermore, a careful study of systematic effects has increased the precision of the geometrical reconstruction, resulting in an improved mass resolution. This is seen in Fig. 39, where the fitted spectra corresponding to the decay modes listed above are plotted as a function of mass. The $2\pi^+2\pi^-$ and the $\pi^+\pi^-K^+K^-$ spectra now show clear evidence for three peaks centered at 3415 MeV, 3500 MeV and 3550 MeV with an uncertainty of $\pm$ 10 MeV in addition to the peak resulting from the direct decay of the ψ'. The two upper states are not yet resolved in the $3\pi^+3\pi^-$ mode, however, the uniform distribution of the events as a function of mass in this region indicate similar contributions from both. There is a very clear $\pi^+\pi^-$ and K^+K^- signal in the decay of the 3415 MeV state. A significant signal of eight events is also observed in the decay of the 3550 MeV state. The few events with an effective mass around 3500 MeV might result from the decay of the upper state. Note that none of these decay modes shows any evidence for the 3454 MeV state seen in the $\gamma\gamma$ cascade.

The product of the branching ratios for the various decay channels are listed in Table 11, column 4, together with 90% confidence upper limits for the decay of the 3455 MeV state. The $2\pi^+2\pi^-$ and the $\pi^+\pi^-K^+K^-$ branching ratios are nearly the same for all the observed states. These decay modes proceed partly via ρ^0 and K^* production respectively as seen in Fig. 40, where the effective $\pi^+\pi^-$ ($\pi^\mp K^\pm$) mass spectra are plotted for the two decay modes

$$\chi \to \rho^0\pi^+\pi^- \to \pi^+\pi^-\pi^+\pi^-$$
$$\to K^*K^\mp\pi^\pm \to \pi^+\pi^- K^+K^-.$$

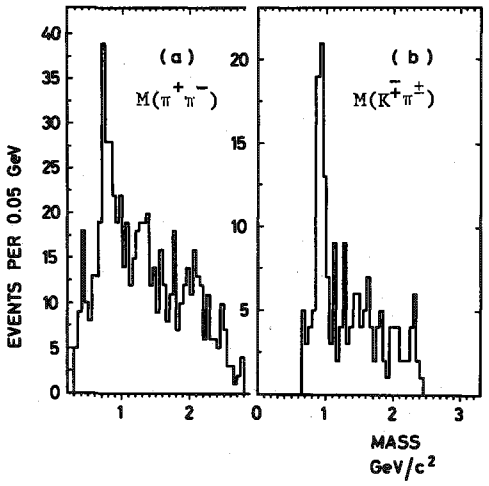

Fig. 40 - Effective mass spectra of $\pi^+\pi^-$(a) and $K^{\mp}\pi^{\pm}$(b) observed in the decay of the $\chi(3.45)$ into $2\pi^+2\pi^-$ and $K^+K^-\ \pi^+\pi^-$.

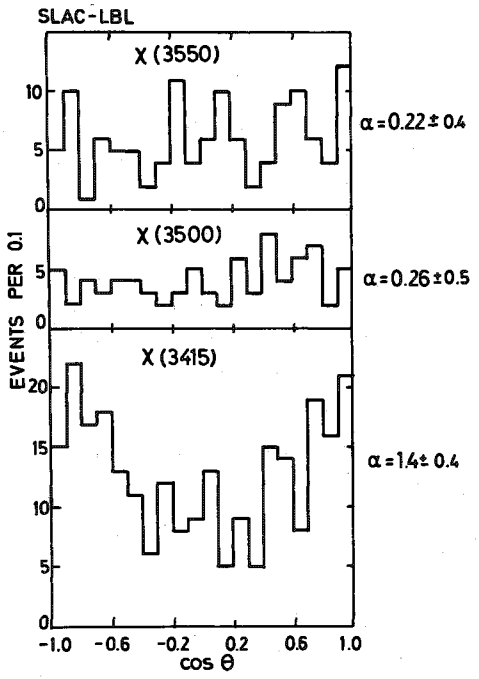

Fig. 41 - The angular distribution with respect to the beam axis of the photon from the decay $\psi' \to \gamma\ P_c/\chi \to \gamma$ charged hadrons. The data were obtained by the SLAC-LBL group.

The fractional contributions are listed in Table 11 column 5.

A ratio of $\rho^0\pi^+\pi^-/K^{*0}K^{\mp}\pi^{\pm} = 9/8$ is predicted assuming the intermediate states to be SU(3) singlets and neglecting effects arising from the mass difference. The experimental results, obtained by multiplying column 4 and 5, are in agreement with this prediction.

The distribution in θ, the angle of the photon with respect to the beam axis, has been obtained by summing over the various decay channels. The result is shown in Fig. 41. Only spin 0 leads to a unique angular distribution $1 + \cos^2\theta$. Higher spins could lead to a more isotropic distribution. The values of the coefficient α determined from fitting the data to $1 + \alpha\cos^2\theta$ are listed in Table 11, column 2. Note that the value of α obtained for the decay to $P_c(3.51)$ disagrees with the value found by the DESY-Heidelberg group.

In the level scheme depicted in Fig. 25 there are four levels with even charge conjugation between the J/ψ and the ψ', one pseudoscalar $^1S_0$ with $J^{PC} = 0^{-+}$ and three ^3P states with $J^{PC} = 2^{++}$, 1^{++}, 0^{++}. Are the levels found consistent with such quantum numbers ?

3.414 GeV It follows from the observed decay into both $\pi^+\pi^-$ and K^+K^- that the state must have natural spin-parity and be an isoscalar. The angular distribution is consistent with J = 0. We can therefore safely assign this state to $J^{PC} = 0^{++}$.

3.454 GeV Presumably for real, but needs to be confirmed.

3.508 GeV The absence of $\pi^+\pi^-$ and K^+K^- decays are consistent with the state belonging to an unnatural spin-parity sequence. 0^-, 1^+ ..... . The SLAC-LBL group and the DESY-Heidelberg group disagree on the value for α. However, they both require $J \neq 0$.

3.552 GeV This level must belong to an natural spin

parity sequence (based on the $\pi^+\pi^-$+K^+K^- events), and the observed value of α indicate J ≠ 0.

This is all that can be deduced from the data alone. However, comparing the available information with the levels available according to Fig. 25, one is lead to a unique assignment by the following reasoning. The 3.414 GeV level must be the 0^{++} state. This leaves only one natural spin parity level, the $^3P_2(2^{++})$ which then must be associated with the 3.552 GeV level. The 3.508 GeV level has J = 0 and must therefore be the $^3P_1(1^{++})$ level. This assignment is also consistent with the fact that it is not seen to decay into $\pi^+\pi^-$ or K^+K^- pairs. The only level left according to Fig. 25 is the pseudoscalar 0^{-+} which then must be identified with the 3.454 GeV level. This assignment has been suggested earlier by Chanowitz and Gilman[42].

Does this level assignment lead to contradictions? For the P.levels the situation seems to be rather satisfactory. If the matrix elements are independent of J then the relative rates for E1 transitions are given by $\Gamma(E1) \sim k^3(2J + 1)$. This leads to:

$$\Gamma(2^3S_1 \to \gamma^3P_0) : \Gamma(2^3S_1 \to \gamma^3P_1) : \Gamma(2^3S_1 \to \gamma^3P_2) =$$
$$1 : 0.9 : 0.6$$

in good agreement with the data listed in Table 10. Recent calculations[43] of the absolute rates are also in agreement with the experimental values.

Define the relative mass splitting R between P levels with even charge conjugation as

$$R = \frac{M(2^{++}) - M(1^{++})}{M(1^{++}) - M(0^{++})}$$

General bounds on R have been derived [44] by Schnitzer for the potential listed in Eq. 18. He finds $0.8 \leq R \leq 1.4$, where the lower limit applies for a pure Coulomb potential and the upper limit for a linear term only. Experimentally R is 0.47. However, agreement can be obtained by including the long-range spin dependent force [33] which was used to obtain a large $^3S_1$, $^1S_0$ splitting.

The short range picture of the decays of the $Q\bar{Q}$ state predicts that the total widths of the 0^{++} and the 2^{++} states should be larger than the total width of the 1^{++} state. This is in qualitative agreement with the data as evidenced by the large branching ratio observed for the decay

$P_c(3.51) \to \gamma\, J/\psi$.

However, identifying the 3.454 GeV level with the 2^1S_0 state leads to a serious contradiction with the expectations based on the charmonium model and the standard short range picture of the decays. According to standard lore, the $^3S_1$ and $^1S_0$ states have similar wave functions while those for 2^3S_1 and 1^3S_1 or 2^1S_0 and 1^1S_0 should be nearly orthogonal. This is certainly consistent with $BR(\psi' \to \gamma X(2.8)) < 1.1\%$ despite the large phase space. Naively, we therefore expect $2^1S_0 \to 1^3S_1 + \gamma$ to be similarly suppressed, contradicting the lower limit $BR(3.454 \to J/\psi + \gamma) > 24\%$. Furthermore, using this limit and the relation $\Gamma(2^1S_0 \to 1^3S_1 + \gamma) \lesssim \Gamma(2^3S_1 \to 1^1S_0 + \gamma) < 2.5$ keV we find $\Gamma(2^1S_0 \to \text{all}) < 10$ keV. This is in strong disagreement with the standard short range picture which predicts a width of about 2 MeV.

It is important to note that the level assignments are based on the assumption that there are only four levels with even charge conjugation between J/ψ and the ψ'. Recently [45] it has been pointed out that the large singlet-triplet splitting obtained by identifying 1^1S_0 with the X(2.8) could also lead to the $^1D_2(J^{PC} = 2^{-+})$ level being located below the ψ'. Then we expect five levels with (C+1) between the J/ψ and the ψ', and a complete assignment of levels in the framework of a $Q\bar{Q}$ model is no longer possible with present information.

The observed spectrum of new states is in good agreement with the predictions based on the charmonium model. This strongly suggests the existence of a new quark. The size of the step in the total cross section observed around 4 GeV makes it likely that the new quark has charge 2/3 e.

The properties of the new quark can be determined by observing the decays of a new class of hadrons made by combining old and new quarks. These hadrons, since they posess a new quantum number which is conserved by the strong and electromagnetic interaction, can decay only weakly into normal hadrons. Their signature would therefore be to observe either mixed lepton and hadron final states resulting from their semileptonic decays or very narrow resonances. The charm hypothesis can be identified by the preferred decay of a charmed quark into a strange quark; $c \to -d \cdot \sin\theta_c + s \cdot \cos\theta$. This leads to properties specific to charm like eK correlation

and apparently exotic decays.

Very recent results obtained by the SLAC-LBL group at SPEAR show that new narrow hadrons with exotic decays exist. The DASP[47] and the PLUTO group[48] at DORIS have observed the semileptonic decays of the new hadrons. They further observe a strong correlation between electrons and kaons. These results very strongly suggest that the new quark indeed is the charmed quark postulated by S.L. Glashow, J.Iliopoulos and L.Maiani[9].

VI) Anomalous lepton events

The pair production in e^+e^- annihilation of new objects with large leptonic or semileptonic decay modes will lead to mixed final states containing electrons and muons or leptons and hadrons. The observation of such final states at a level above the background expected from higher order electroamgnetic interactions and semileptonic pion or kaon decays is direct evidence for the production of new particles. A heavy sequential[49] lepton or a hadron with a new quantum number conserved by the strong and the electromagnetic interactions are two examples of such particles. The anticipated features of a new lepton and a new hadron are summarized in Table 12.

The low multiplicity expected for the decay of a pair of heavy leptons into a final state with an electron (muon) plus hadrons arises as follows. In the decay $L \to \nu_L$ + hadrons, the hadrons come from a low mass current. If the multiplicity is comparable to that from a virtual photon of the same mass, it will be small. Specific calculations[50] support this conjecture. The leptonic decay of its partner L contributes only one charged track. Inelastic production i.e. $e^+e^- \to L\bar{L}$ + hadrons is negligible. The high multiplicity expected in the decay of a pair of heavy hadrons arises as follows: the weak decay of the new hadron into ordinary hadrons will presumably lead to a multiplicity comparable to that observed in the decay of an ordinary hadron of the same mass i.e. on the average 2 to 3 charged particles plus 2 to 3 photons. From the semileptonic decay of its partner we expect roughly 2 charged particles and 2 photons. At higher energies inelastic production is expected to be dominant, contributing additional hadrons.

Table 12 - Properties of heavy sequential leptons and new hadrons

	L	H
Production	$e^+e^- \to L\bar{L}$ (point cross section)	$e^+e^- \to H\bar{H}$ (damped by form factor)
	$e^+e^- \to L\bar{L}$+hadrons (Negligible. Less than α^2 of elastic production)	$e^+e^- \to H\bar{H}$+hadrons (Dominant at higher energies)
Decay modes:	$L \to \ell\, \bar{\nu}_\ell \nu_L$	$H \to \ell\, \bar{\nu}_e$ (suppressed if H has spin = 0)
	$\to \nu_L$ + hadrons	$\to \ell\, \bar{\nu}_e$ + hadrons
		$\to$ hadrons
Final states:		
eμ + neutrino	important, clear signature (e(μ) from three-body decay)	negligible (e(μ) from two-body decay)
eμ+neutrino +hadrons	negligible (order α^2)	large, (e(μ) from a multibody decay)
e(μ)+neutrino + hadron	large, lepton spectrum computable and "hard" low multiplicity $\langle n_{ch}\rangle \sim \langle n_\gamma\rangle \sim 2\text{-}3$	large, lepton spectrum might be soft high multiplicity $\langle n_{ch}\rangle \sim \langle n_\gamma\rangle \sim 4\text{-}6$

VI.1 eμ-events as evidence for a new lepton

As is well known the SLAC-LBL group at SPEAR has found [49] events of the type

$$e^+e^- \to e^\mp\mu^\pm + \text{"nothing"}.$$

These events were selected using the following criteria:

1) Only two charged tracks with opposite charge and no photons.
2) Each track should have a momentum greater than 650 MeV/c.
3) One prong is identified as an electron by the pulseheight in the shower counter, the other as a muon by range. The probability of misidentifying a hadron as an electron or as a muon is respectively 18% or 20%.
4) The coplanarity angle between the planes defined by the electron and beam direction and the muon and the beam direction must be greater than 20°.

A total of 139 events produced at cms energies between 3.8 GeV and 7.8 GeV satisfied these criteria with an estimated background of 34 events. The signal of 105 events is statistically significant and might represent the production and decay of new particles. To verify the production of new particles and to study their properties the SLAC-LBL group has investigated the following geatures:

1) Threshold behaviour.
2) Angular correlation between the e and the μ.
3) Does the e(μ) result from a threebody or a twobody decay ?
4) Mass of undetected particles.
5) Limits on unseen hadrons accompanying the eμ events.

Their findings are:

1) The cross section plotted in Fig. 42

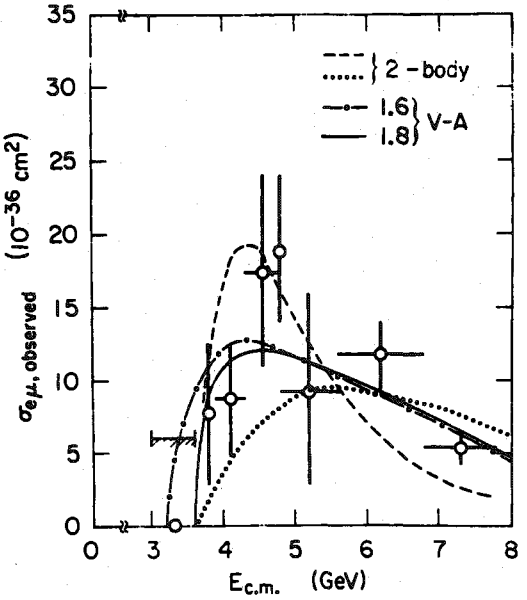

Fig. 42 - The observed cross section for eμ production, corrected for background. The cross hatched line indicate the 90% confidence upper limit for the background. The solid and dash-dot curves are the expected cross section for the production of heavy leptons of mass 1.6 GeV/c^2 and 1.8 GeV/c^2. The dashed and the dotted curve are for a boson of mass 1.8 GeV with a two-body leptonic decay mode. These latter curves are strongly model dependent.

as a function of energy suggests a threshold for eμ production at or below 4 GeV. This would seem to limit the mass of the new particle to 2 GeV or less. A stringent mass limit is difficult to derive from these data because of the background and the small number of events observed below 4.4 GeV. The energy dependence of the cross section is consistent with the behaviour expected for a heavy lepton. However, a reasonable fit can also be obtained assuming production of new hadrons.

2) At high cms energies the electron and the muon are preferentially emitted in opposite directions since they result from the decay of heavy particles produced back to back. From the threshold behaviour and the collinearity distribution the SLAC-LBL group determines the mass of the new particles to be between 1.6 GeV/c^2 and 2.0 GeV/c^2.

They argue that the observation of a threshold and the strong angular correlations between the electron and the muon demonstrates that new particles are produced.

3) The observed momentum distribution of the electrons (muons) exclude a two-body decay mode as the sole source. The three-body decay mode required by the data is necessary for a heavy lepton, but might also be the preferred mode for the semileptonic decay of a heavy hadron.

Note that the experimental observations discussed above cannot be used to disentangle the production of a heavy lepton from the production of new hadrons. These possibilities might be separated either by a measurement of the mass of the third particle in the decay or by excluding unobserved hadrons.

4) The electron (muon) spectrum is plotted in Fig. 43 as a function of the normalized momentum

$$\rho = \left(\frac{P - 0.65\ GeV/c}{P_{max} - 0.65\ GeV/c} \right) .$$

The momentum distribution of the electron (muon) expected from the decay of a heavy particle into 3 particles, two of which are massless, is also plotted as a function of the mass of the third particle. The curves - all except one - are evaluated for a V-A current. A particle with the mass of the neutron is clearly excluded. However, an acceptable fit is obtained if the third particle has a mass of 0.5 GeV or less.

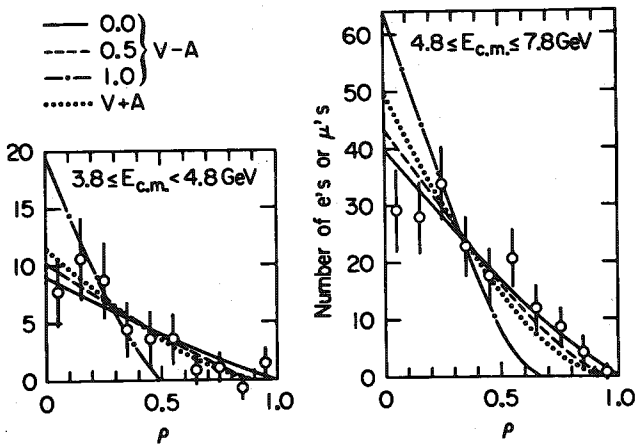

Number of e's or μ's

Fig. 43 - The electron and the muons plotted as a function of the normalized momentum ρ. The solid, the dashed and the dashed-dotted curve show the distribution expected from the (V-A) decay of a lepton with mass 1.8 GeV for various values of the neutrino mass. The dotted curves are for a massless neutrino, and a (V+a) current.

5) The SLAC-LBL group has made a careful evaluation of the possibility that the eμ events are accompanied by undetected hadrons. They conclude with 90% confidence that no more than 39% of all the eμ-events can contain additional charged particles or photons.

They argue that if the eμ events are to be explained by a single source they must arise from the production and the leptonic decay of a new sequential lepton. From the observed eμ cross section and the production cross section for a pair of point particles with a mass of 1.8 GeV/c^2 they find

$$BR\ (\ U \to \nu_U\ \ell\ \bar{\nu}_e\ ) = (0.17\ ^{+\ 0.06}_{-\ 0.03}\ )$$

This was derived assuming equal decay rates to be the e and the μ modes, V-A coupling and a massless neutrino.

All the data published by the SLAC-LBL group point to a new heavy lepton as the source of the observed eμ-events. However, it seems crucial and prudent to verify such an important discovery by an independent method, for example by a measurement of the hadronic decay modes of the heavy lepton. Such information might be obtained from a measurement of single electrons or muons produced in $e^+e^- \to U\bar{U} \to \ell$ + anything. The observed lepton originating in the leptonic or the semileptonic decay of one of the pairproduced new objects is used to tag the event, imposing no constraint on the other member of the pair. Thus heavy leptons and new hadrons might be identified by the momentum distribution of the observed lepton and the observed multiplicity. Present data on inclusive lepton spectra are as yet not conclusive.

References:

1) No attempt is made to give a complete set of references. Review talks which cover this area in great detail can be found in the Proceedings of the 7th International Symposium on Lepton and Photon Interactions at High Energies, Stanford, USA, 21-27 August 1975 and in the Proceedings of the XVIII International Conference on High Energy Physics, Tbilisi, USSR, 15-21 July 1976

2) J.J.Aubert et al., Phys.Rev.Lett. 33, 1404 (1974)

3) J.E.Augustin et al., Phys.Rev.Lett. 33, 1406 (1974)

4) G.S.Abrams et al., Phys.Rev.Lett. 33, 1453 (1974)

5) J.E.Augustin et al., Phys.Rev.Lett. 34, 764 (1975)
J.Siegrist et al., Phys.Rev.Lett. 36, 700 (1975)

6) T.Appelquist and H.D.Politzer, Phys.Rev.Lett. 34, 43 (1975

7) S.L.Glashow and A.De Rujula, Phys.Rev.Lett. 34, 46 (1975)
T.Appelquist et al., Phys.Rev.Lett.34, 365 (1975)
E.Eichten et al., Phys.Rev.Lett. 34, 369 (1975)

8) Y.Hara, Phys.Rev. B 134, 701 (1964)
J.D.Bjorken and S.L.Glashow, Phys.Lett. 11, 255 (1964)

9) S.L.Glashow, J.Iliopoulos and L.Maiani, Phys.Rev.D2, 1285 (1970)

10) A good description on the physics of electron storage rings can be found in M.Sands - SLAC-121 and H.Wiedemann "Herbstschule für Hochenergiephysik" Maria Laach 13-22 September, 1973

11) For a more complete discussion see T.Walsh in "Herbstschule für Hochenergiephysik" Maria Laach 13-22 September 1973

12) A.M.Boyarski et al., Phys.Rev.Lett.34,1357 (1957)
V.Lüth et al., Phys.Rev.Lett. 35, 1124 (1975)

13) This is a rather technical subject. A clear discussion can be found in J.D.Jackson Nucl.Inst. and Methods

14) S.Okubo, Phys.Lett. 5, 105 (1963)

G.Zweig, CERN-Report TH 401, 412 (1964)

J.Iizuka, K.Okada and O.Shito, Prog. Theo.Physics 35, 1061 (1966)

15) B.H.Wiik in the Proceedings of the 7th International Symposium on Lepton and Photon Interactions at High Energies, Stanford, USA, August 21-27, 1975

16) E.B.Hughes et al., Phys.Rev.Lett. 36,76 (1976)

17) W.Braunschweig et al., Phys.Lett.63B,487 (1975)

18) B.Jean-Marie et al., Phys.Rev.Lett. 36, 291 (1976)

19) J.Burmester et al., Contribution to the 18th International Conference on High Energy Physics, Tbilisi USSR, July 15-21, 1976

20) G.S.Abrams et al., Phys.Rev.Lett. 34, 1181 (1975)

21) W.Tannenbaum et al., Phys.Rev.Lett. 36, 402 (1976)

22) V.Gupta and R.Kögerler,Phys.Lett. 56B, 473 (1975,

F.Gilman, Invited paper to the VI International Conference on High Energy Physics and Nuclear Structure, Santa Fe, New Mexico, June 9-13,1975 AIP Conference Proceedings No. 26, 33, 1975

23) F.Vannucci et al., SLAC-PUB-1724 (1976)

24) F.Vannucci et al., to be published

25) T.Appelquist and H.D.Politzer, Phys.Rev.Lett. 34, 43 (1975)

26) B.Esposito et al., Phys.Lett.58B, 478 (1975)

M.E.Biagini, LNF-76/3a CP) 1976

27) For a recent status report see H.L.Lynch, Invited paper at the Conference on the Production of Particles with New Quantum Number, Madison Wise

28) W.Braunschweig et al., Phys.Lett.57B, 407 (1975)

29) G.J.Feldman et al.,Phys.Rev.Lett.35, 821 (1975)

30) J.Heintze in the Proceedings of the 7th International Symposium on Lepton and Photon Interactions at High Energies, Stanford, USA, August 21-27, 1975

31) H.Fritzsch and P.Minkowski, Nuovo Cimento 30A 393 (1975)

E.Pelaquier and F.M.Renard, Nuovo Cimento 32A, 421 (1976)

32) F.A.Berends and R.Gastman, Nucl.Phys.B 61, 414 (1973)

33) H.J.Schnitzer, Preprint Brandeis University, Waltham, Massachusetts 02159, July 1976

34) D.H.Badtke et al., Contribution to the 18th International Conference on High Energy Physics, Tbilisi, USSR, July 15-21, 1976

W.Vernon private communication

35) J.S.Whitaker, W.Tannenbaum et al., to be published.

36) G.Goldhaber, LBL report LBL-4884 (1976)

37) W.Bartel et al., Contribution to the 18th International Conference on High Energy Physics, Tbilisi, USSR, July 15-21, 1976

W.Bartel et al., DESY-Report 76/40

38) T.F.Walsh, Nuovo Cimento Lett. 14, 290 (1975) R.N.Cahn and M.S.Chanowitz, Phys.Lett. 59B, 277 (1975)

J.Ellis, Schladming Lectures 1975, CERN TH 1996 (1975)

A.Kazi, G.Kramer and D.H.Schiller, Nuovo Cimento Lett. 15, 120 (1976)

39) H.Harari, Phys.Lett. 60B, 172 (1976)

40) W.Tannenbaum et al., Phys.Rev.Lett.35,1323 (1975)

41) F.M.Pierre, Contribution to the 18th International Conference on High Energy Physics, Tbilisi, USSR, July 15-21, 1976

G.H.Trilling et al., to be published

42) M.S.Chanowitz and F.J.Gilman, SLAC-PUB 1746, 1976

43) A.B.Henriques, B.H.Kellett, R.G.Moorhouse, Phys.Lett. 64B, 85 (1976)

44) E.Eichten et al., Phys.Rev.Lett.36, 500 (1976)

H.J.Schnitzer, Phys.Rev.Lett. 35, 1540 (1975)

45) H.Harari, CERN-Preprint TH-2222

G.Goldhaber et al.,Phys.Rev.Lett.37,255(1976)

I.Peruzzi et al.,Phys.Rev.Lett 37, 569 (1976)

46) F.M.Pierre et al., Contribution to the 18th International Conference on High Energy Physics, Tbilisi, USSR, July 15-21, 1976

47) W.Braunschweig et al., Phys.Lett.64B, 471 (1976)

48) J.Burmester et al., DESY Report 76/50

49) M.L.Perl, Phys.Rev.Lett. 35, 1489 (1975)

M.L.Perl, Phys.Lett. 63B, 466 (1976)

50) Y.S.Tsai, Phys.Rev. D4, 2821 (1971)

J.D.Bjorken and C.H.Llewellyn-Smith, Phys.Rev. D7, 887 (1973)

K.Fujikawa and N.Kawamoto, DESY Preprint 76/01

K.J.F.Gaemers and R.Raito, SLAC-PUB-1727 (1976)

For a nice discussion on the properties of heavy leptons and how to observe them in e^+e^- collisions see Ya.I.Azimov, L.L.Frankfurt and V.A.Khoze, Leningrad Nuclear Physics Institute, Preprint 245, June 1976

Social life at the School

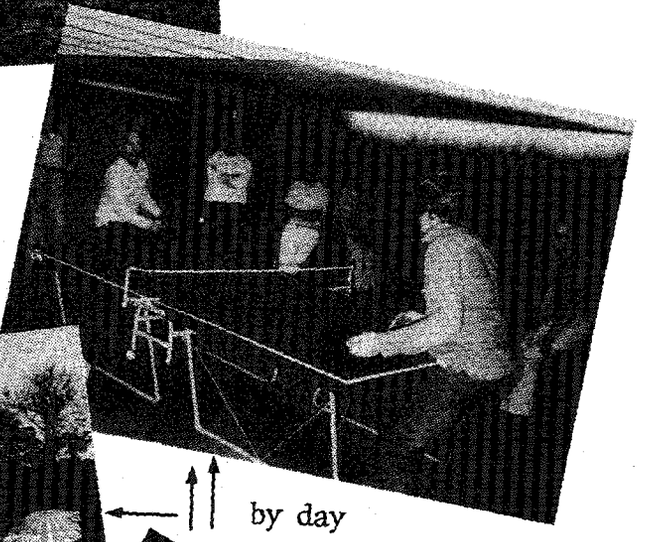

by day

by night

Photos by F. Cerulus

ORGANIZING COMMITTEE

AMALDI, U. *CERN, Geneva, Switzerland*

CERULUS, F. *Inst. voor Theoretische Fysika, Heverlee, Belgium (Chairman)*

GOLDSCHMIDT-CLERMONT, Y. *CERN, Geneva, Switzerland*

GRARD, F. *Faculté des Sciences, Université de l'Etat à Mons, Belgium*

LEMONNE, J. *Inter-University Inst. for High Energies, Brussels, Belgium*

LOCK, W.O. *CERN, Geneva, Switzerland*

SACTON, J. *Inter-University Inst. for High Energies, Brussels, Belgium*

WEYERS, J. *CERN, Geneva, Switzerland*

CATON, D.A. *CERN, Geneva, Switzerland (Organizing Secretary)*

Secretariat

NARTUS, R. *Inst. voor Theoretische Fysika, Heverlee, Belgium*

LIST OF PARTICIPANTS

SPEAKERS

CLOSE, F.E. *Rutherford Laboratory, Chilton, Didcot, U.K.*

ELLIS, J. *CERN, Geneva, Switzerland*

KISS, D. *JINR, Dubna, USSR*

MAIANI, L. *Istituto Superiore di Sanità, and INFN, Rome, Italy*

SCHOPPER, H. *DESY, Hamburg, Federal Republic of Germany*

STEINBERGER, J. *CERN, Geneva, Switzerland*

TYURIN, N. *IHEP, Serpukhov, USSR*

VAN HOVE, L. *CERN, Geneva, Switzerland*

WIIK, B.H. *DESY, Hamburg, Federal Republic of Germany*

WILSON, E.J.N. *CERN, Geneva, Switzerland*

TUTORS

DE WIT, B. *Inst. Lorentz voor Theoretische Natuurkunde, Leiden, Netherlands*

ELLIS, J. *CERN, Geneva, Switzerland*

HEY, A.J.G. *Department of Physics, University of Southampton, U.K.*

SEHGAL, L.M. *III. Physikalisches Inst. der TH Aachen, Federal Republic of Germany*

BARONCELLI, A. *Istituto Superiore di Sanità, Rome, Italy*

BERGSTROM, L. *Royal Institute of Technology, Stockholm, Sweden*

BEST, C. *Physics Department, University of Liverpool, U.K.*

BHARADWAJ, V. *Nuclear Physics Department, University of Oxford, U.K.*

BIRSA, R. *Institute for Experimental Physics, University of Trieste, Italy*

BRUNO, R. *Institute of Physics, University of Bari, Italy*

BURNHAM, A. *Physics Department, University of Bristol, U.K.*

BUST, P. *Cavendish Laboratory, University of Cambridge, U.K.*

CANZLER, T. *DESY, Hamburg, Federal Republic of Germany*

CARPATHOPOULOS, S. *N.R.C. Democritos, Aghia Paraskevi, Greece*

CHAFF, J. *Physics Department, Imperial College, London, U.K.*

COMBER, C. *Rutherford Laboratory, Chilton, Didcot, U.K.*

CONBOY, J. *Department of Physics and Astronomy, University College, London, U.K.*

CORDIER, A. *Laboratoire de l'Accélérateur Linéaire, University of Paris, France*

DE CLERCQ, C. *Dienst Elementaire Deeltjes, Vrije Universiteit Brussel, Belgium*

DEWIT, M. *Service de Physique des Particules Elémentaires, University of Brussels, Belgium*

DEY, W. *ETH Zurich, c/o S.I.N. Villigen, Switzerland*

DORENBOSCH, J. *CERN, Geneva, Switzerland*

DORSAZ, P.-A. *Département de Physique Nucléaire et Corpusculaire, University of Geneva, Switzerland*

EASON, R. *Department of Physics, Imperial College, London, U.K.*

EICHLER, R. *ETH, Zurich, c/o S.I.N., Villigen, Switzerland*

ELVERHAUG, N. *Institute of Physics, University of Bergen, Norway*

FERNOW, R. *Randall Laboratory, University of Michigan, U.S.A.*

FRANCOIS, T. *LPNHE, Ecole Polytechnique, Palaiseau, France*

FROST, G. *Department of Physics, University of Lancaster, U.K.*

GAY, M. *H.H. Wills Physics Laboratory, University of Bristol, U.K.*

GEBERT, W. *II. Institut für Experimentalphysik, University of Hamburg, Federal Republic of Germany*

GENTILE, S. *Institute of Physics, University of Rome, Italy*

GORDON, J. *Department of Nat. Phil., University of Glasgow, U.K.*

HASSALL, J. *Cavendish Laboratory, University of Cambridge, U.K.*

HAUSAMMANN, R. *S.I.N., Villigen, Switzerland*

HILL, S. *Department of Physics, University of Manchester, U.K.*

KÖNIGSMANN, K. *Physics Institute, University of Bonn, Federal Republic of Germany*

LESCEUX, J.-M. *Service de Physique Expérimental, Université de l'Etat à Mons, Belgium*

LEVY, J.-M. *LPNHE, University of Paris, France*

MAGON, V. *Rutherford Laboratory, Chilton, Didcot, U.K.*

MATTEUZZI, C. *CERN, Geneva, Switzerland*

McDOWELL, L. *Department of Nuclear Physics, University of Oxford, U.K.*

MEINKE, R. *Max-Planck-Institut für Physik, Munich, Federal Republic of Germany*

MEYER, H.-J. *Institut für Reine und Angewandte Kernphysik, Kiel, Federal Republic of Germany*

MOUNT, R. *CERN, Geneva, Switzerland*

NANDI, A. *Cavendish Laboratory, University of Cambridge, U.K.*

PAYRE, P. *CERN, Geneva, Switzerland*

PIREDDA, G. *Institute of Physics, University of Rome, Italy*

RINGEL, J. *II. Institut für Experimentalphysik, University of Hamburg, Federal Republic of Germany*

SEEBRUNNER, H. *Department of Physics, University of Munich, Garching, Federal Republic of Germany*

SEVER, R. *Department of Physics, Middle East Technical University, Ankara, Turkey*

SPIERING, C. *JINR, Dubna, USSR*

STORR, M. *Department of Physics, University of Lancaster, U.K.*

UHLIG, S. *Max-Planck-Institut für Physik und Astrophysik, Munich, Federal Republic of Germany*

VAN DEN BOGAERT, F. *University of Antwerp, Wilrijk, Belgium*

VERGEEST, J. *Physics Laboratory, University of Nijmegen, Netherlands*

VIRDEE, J. *Physics Department, Imperial College, London, U.K.*

VOTANO, L. *CNEN, Frascati, Italy*

VRBA, V. *JINR, Dubna, USSR*

WACKER, K. *II. Institut für Experimentalphysik, Hamburg, Federal Republic of Germany*

WILKES, P. *Department of Physics, University of Sheffield, U.K.*

WILLIAMS, W. *Physics Department, Oliver Lodge Labs., Liverpool University, U.K.*

WINNIK, M. *Physics Department, Technion, Haifa, Israel*

WRIEDT, H. *DESY, Hamburg, Federal Republic of Germany*

Part-time students

FAVART, D. *University of Louvain, Belgium*

LAURENT, J. *Université de l'Etat à Mons, Belgium*

PRIEELS, R. *University of Louvain, Belgium*

RENTON, P. *Inter-University Institute for High Energies, Brussels, Belgium*

ROLIN, N. *University of Louvain, Belgium*

VAN ELMBT, L. *University of Louvain, Belgium*

VAN OYSTAEYEN, B. *University of Louvain, Belgium*